

Microwave Electronics

**DESIGN AND DEVELOPMENT OF COMPACT
MULTIBAND DUAL POLARIZED PATCH ANTENNAS
USING TRUNCATION AND SLIT LOADING TECHNIQUES**

A thesis submitted by

SUMITHA MATHEW

*in partial fulfillment of the
requirements for the degree of*

DOCTOR OF PHILOSOPHY

Under the guidance of

Prof. K.VASUDEVAN



**DEPARTMENT OF ELECTRONICS
FACULTY OF TECHNOLOGY
COCHIN UNIVERSITY OF SCIENCE AND TECHNOLOGY
KOCHI-22, INDIA**

June 2017

**Design and Development of Compact
Multiband Dual Polarized Patch Antennas
Using Truncation and Slit Loading Techniques**

Ph.D. Thesis under the Faculty of Technology

Author

Sumitha Mathew

Research Scholar
Department of Electronics
Cochin University of Science and Technology
Kochi - 682022
Email: sumithamathew@gmail.com

Supervising Guide

Dr. K. Vasudevan

Professor Emeritus
Department of Electronics
Cochin University of Science and Technology
Kochi - 682022
Email: vasudevankdr@gmail.com

Department of Electronics
Cochin University of Science and Technology
Kochi - 682022

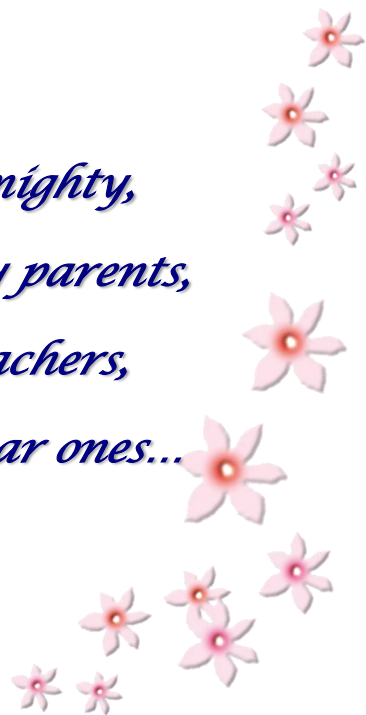
June 2017

Dedicated to the Almighty,

My parents,

Teachers,

Dear ones...





**DEPARTMENT OF ELECTRONICS
COCHIN UNIVERSITY OF SCIENCE AND TECHNOLOGY,
KOCHI – 682 022**

Dr. K. Vasudevan
Professor Emeritus

Email: vasudevankdr@cusat.ac.in
Ph: 0484 2576418

Certificate

This is to certify that this thesis entitled “**Design and Development of Compact Multiband Dual Polarized Patch Antennas Using Truncation and Slit Loading Techniques**” is an authentic record of research work carried out by **Mrs. Sumitha Mathew** under my supervision in the Department of Electronics, Cochin University of Science and Technology. The results embodied in this thesis or parts of it have not been presented for any other degree. All the relevant corrections and modifications suggested by the audience and recommended by the doctoral committee of the candidate during the presynopsis seminar have been incorporated in the thesis.

Kochi-22
June 2017

Dr. K. Vasudevan
(Supervising Teacher)

Declaration

I hereby declare that the work presented in this thesis entitled “**Design and Development of Compact Multiband Dual Polarized Patch Antennas Using Truncation and Slit Loading Techniques**” is a bonafide record of the research work done by me under the supervision of Dr. K. Vasudevan, Professor Emeritus, Department of Electronics, Cochin University of Science and Technology, India and that no part thereof has been presented for the award of any other degree.

Kochi-22
June 2017

Sumitha Mathew

Words of Gratitude...

I remember with utmost gratefulness.....

My supervisor and guide Prof. K. Vasudevan for his constant encouragement and excellent guidance all throughout the tenure of the work. His positive attitude to life has had a profound influence on me. I consider it a great honour and fortune to have worked under his supervision.

Prof. P. Mohanan, UGC-BSR Professor, Dept. of Electronics for his timely and special care and concern and great encouragement all throughout my years at the research lab.

Prof. C. K. Anandan, Dept. of Electronics for his timely advice and valuable suggestions.

Prof. Supriya M.H., Head, Dept. of Electronics for her great support and help during the writing and timely completion of the thesis.

Prof. James Kurian, for his encouragement and cooperation.

Prof. P. R. S. Pillai, Prof. K. T. Mathew and Prof. Tessamma Thomas former professors, Dept. of Electronics for their support and blessings.

All Faculty members of the department of Electronics for their goodwill and assistance. I thank all the technical, administrative and non-teaching staff of the department for the warm and cordial relations shared and invaluable helps.

My senior researchers Dr. Sarin V.P, Dr. Nishamol M.S., Dr. Sujith R and Dr. Nijas C.M. for sharing their sound technical and scientific knowledge with me.

Dr. Shameena V.A., Post-Doctoral Fellow, Queens University, U.K., for the wholehearted support during the documentation. Her precious friendship and good humour has had a significant impact on me.

My fellow researchers and best friends at the CREMA lab, Mr. Prakash K.C., Mrs. Anitha R, Mr. Vinesh P.V, Mr. Vivek R, Kurup, Mr. Mohammad Ameen, Mr. Manoj M, Ms Remsha M, Ms. Vinisha C.V, Mr. Deepak U, Mrs. Roshna T.K, Mrs. Sajitha V. R and Mrs. Anila P.V., and for all the immemorable times we spent together.

Mr. Jayakrishnan M.P, and Ms. Nimisha S., Research Fellows, Grenoble University, France for all their untiring support and help during the wee period of my research work.

My research colleagues from the RCS lab, Sreenath S, Lindo A.O, Anju Mathews, Sreekgala P.S, Libimol V. A, and Dibin Mary Pulickal for their encouragement.

My colleagues at Centre for Ocean Electronics (CUCENTOL), Microwave Tomography and Material Research Laboratory (MTMR) and Audio and Image Research Lab (AIRL), Department of Electronics, Cochin University of Science and Technology for the supreme cooperation and excellent rapport.

Prof. P. Sureshkumar, Director, Institute of at Resources Development (IHRD) for the sponsorship, financial assistance and prompt advices.

The Principal and staff of College of Engineering Cherthala for all the timely administrative help. The financial support provided by the Technical Education Quality Improvement Programme (TEQIP), Govt. of India is also gratefully acknowledged.

All my colleagues and friends in Model Engineering College, Kochi and College of Engineering Cherthala for their support and prayers.

My colleagues and close friends Dr. Bindu C.J., Dr. Laila D and Dr. Sarah Jacob for being the pillars of support in difficult times.

My good friend Dr. Rekhia Lakshamanan for all the concern and support.

All my girlfriends of NSS College of Engg., Palakkad '93 batch for keeping my spirits up and their undying loyalty and precious friendship.

My in-laws for their unwavering support, prayers and blessings.

Achachan and Amma who always gave the highest priority to my education in spite of all hardships.

My brother Suman, sister Susan and their families for all the concern and prayers.

My Husband Dr. Vinu Thomas for his love, support and care.

My kids Joel, Jerry and Aleena for being patient and adorable and letting their mother persevere.

Above all there is that supreme power whose blessings and kindness without which one single step would not have been possible.

Sumitha Mathew

Abstract

Modern life has become so dependent on mobile communication that one cannot picture a world devoid of it. In recent years, the communication scenario has shown a visible trend for the demand of products/services which employ compact, lightweight, multifunction, and multiband antennas. Commercial frequency services like GPS, UMTS, and WLAN coexist on several devices to meet various needs. These services operate on different frequency bands and polarizations which mean the system requires separate antennas in order to support all of them. In this context, compact multiband microstrip antennas play a significant role in the integration of multiple services in a single structure thereby considerably reducing the bulk of the device.

In this thesis, the design and development of compact multi band antennas with different polarizations for multi frequency applications using two different patch geometries 1) sectoral and 2) circular are investigated. The main aim of the designs is to achieve circular polarization in the fundamental resonance band and linear polarization in the rest. The geometrical parameters, upon which the various aspects of design are centered, are investigated. The dependence of the reflection and polarization characteristics on these dimensions was studied using standard simulation tools and was experimentally confirmed. Mathematical relations were also deduced which would enable the antenna to be designed on any chosen substrate for any desired frequency range of operation. The design also incorporates techniques within the structure to effectively reduce cross polarization. Different patch geometry modifications have been utilized which results in not only reducing the ground plane dimensions by a good margin, but also produces a high axial ratio bandwidth by lowering the Q factor. One major contribution of the work is the analysis of the higher order modes and subsequent higher gain obtained.

Contents

Chapter 1

INTRODUCTION	01 - 27
1.1 Introduction.....	02
1.2 Modern wireless communication systems.....	04
1.3 Microstrip antennas	06
1.3.1 Radiation from the microstrip antenna	07
1.3.2 Microstrip patch antenna	08
1.3.3 Printed slot antenna	09
1.3.4 Feeding techniques	10
1.3.4.1 Coaxial probe feed.....	10
1.3.4.2 Microstrip line feed	11
1.3.4.3 Proximity coupled feed.....	11
1.3.4.4 Aperture coupled feed	11
1.3.5 Polarization of an antenna.....	12
1.4 Models of analysis	13
1.4.1 Transmission line model.....	13
1.4.2 Cavity model.....	14
1.4.3 The multiport network model	14
1.4.4 Method of moments.....	14
1.4.5 Finite element method	15
1.4.6 Spectral domain analysis	15
1.4.7 Finite Difference Time Domain (FDTD) method	16
1.5 Compactness of patch antennas	16
1.5.1 Compact circularly polarized microstrip antennas	17
1.5.2 Compact dual and triple band patch antennas	18
1.6 Motivation behind the current research work.....	19
1.7 Thesis organization	21
References.....	24

Chapter 2

LITERATURE REVIEW	29 - 67
2.1 Microstrip radiators – A review	30
2.2 Compact microstrip antennas	33
2.3 Multi band and dual polarized microstrip antennas	41
References.....	50

Chapter 3

METHODOLOGY	69 - 84
3.1 Simulation tool: Ansys HFSS	70
3.2 Antenna fabrication procedure.....	71

3.2.1	Substrate selection.....	71
3.2.2	Photolithography.....	72
3.3	Excitation technique.....	74
3.4	Antenna measurement facilities.....	75
3.4.1	Performance Network analyzer PNAE 8362B.....	75
3.4.2	Anechoic Chamber.....	77
3.4.3	Automated Turn table assembly and software for far field radiation pattern measurement.....	78
3.5	Experimental procedures.....	78
3.5.1	Measurement of S parameters, resonance frequency and bandwidth.....	79
3.5.2	Radiation pattern.....	80
3.5.3	Antenna gain and efficiency.....	81
3.5.4	Polarization.....	82
3.5.5	Axial Ratio.....	83
	References.....	83

Chapter 4

DESIGN AND ANALYSIS OF DUAL BAND SECTORAL PATCH ANTENNA WITH CORNER TRUNCATIONS 85 - 136

4.1	Introduction to compact dual polarized multiband antennas.....	86
4.2	Coaxial probe fed circularly polarized circular disc sector patch antenna.....	87
4.3	Corner truncated circular disc sector patch antenna.....	90
4.3.1	Dual band dual polarized circular disc sector patch antenna.....	90
4.3.2	Parametric analysis.....	95
4.3.2.1	Effect of corner truncation r_1	95
4.3.2.2	Effect of corner truncation r_2	98
4.3.3	Design.....	100
4.3.4	Validation of the design.....	103
4.3.5	Experimental measurement.....	104
4.3.5.1	Reflection characteristics.....	105
4.3.5.2	Radiation pattern of Antenna1.....	106
4.3.5.3	Radiation pattern of Antenna2.....	108
4.3.5.4	Gain and efficiency of Antenna 1 and Antenna 2.....	109
4.4	Circularly polarized sectoral patch antenna for WLAN application.....	109
4.5	Circularly polarized sectoral patch antenna for WiMAX applications.....	114
4.6	Dual band corner truncated sectoral patch antenna with dual slits for GPS and WLAN.....	119

4.6.1	Antenna evolution and geometry	119
4.6.2	Design.....	122
4.6.3	Simulated current distributions	122
4.6.4	Effect of the patch modifications	123
4.6.4.1	Effect of varying corner truncation r_1	124
4.6.4.2	Effect of varying corner truncation r_2	125
4.6.4.3	Effect of varying corner truncation r_3	126
4.6.4.4	Effect of the left slit (slit 1)	126
4.6.4.4.1	Effect of varying slit position	128
4.6.4.4.2	Effect of varying slit length	128
4.6.4.4.3	Effect of varying slit width	128
4.6.4.5	Effect of the right slit (slit 1)	129
4.6.4.5.1	Effect of varying slit position	129
4.6.4.5.2	Effect of varying slit length	129
4.6.4.5.3	Effect of varying slit width	131
4.6.4.6	Effect of the left and right slits combined.....	131
4.6.5	Experimental measurement.....	132
4.7	Summary of the chapter	135
	References.....	136

Chapter 5

INVESTIGATIONS ON COMPACT TRIBAND DUAL POLARIZED CORNER TRUNCATED SECTORAL

PATCH ANTENNA 137 - 174

5.1	Introduction.....	138
5.2	Triband dual polarized sectoral patch antenna	139
5.2.1	Evolution and geometry of the antenna	139
5.2.2	Antenna1 characteristics	140
5.2.3	Antenna2 characteristics	141
5.2.4	Antenna3 characteristics	142
5.2.5	Antenna4 characteristics	143
5.2.6	Parametric analysis of the triband sectoral patch Antenna	144
5.2.6.1	Effect of truncation length r_1 on reflection coefficient and CP characteristics.....	144
5.2.6.2	Effect of truncation length r_1 on ground plane dimensions.....	145
5.2.6.3	Effect of truncation length r_2 on reflection coefficient and CP characteristics.....	145
5.2.6.4	Effect of truncation length r_3 on reflection coefficient and CP characteristics.....	146
5.2.6.5	Effect of sectoral notch at edge L_4 on reflection and CP characteristics.....	148
5.2.7	Analysis of modes excited in the three bands	150
5.2.7.1	Mode at Band 1	151

5.2.7.2	Mode at Band 2	152
5.2.7.3	Mode at Band 3	152
5.2.8	3D radiation plots of Antenna4	154
5.2.9	Experimental measurements	155
5.3	Slotted ground triband dual polarized sectoral patch antenna for low cross polarization and enhanced gain.....	161
5.3.1	Antenna geometry	161
5.3.2	Parametric study of the slotted ground triband sectoral patch antenna.....	163
5.3.2.1	Effect of variation of radius d_1 of slot 1	164
5.3.2.2	Effect of variation of centre point D of slot 1	165
5.3.2.3	Effect of variation of radii d_2 and d_3 of slots 2 & 3	165
5.3.3	Experimental measurements	167
5.4	Summary of the chapter	171
	References.....	172

Chapter 6

INVESTIGATIONS ON COMPACT TRI BAND DUAL

POLARIZED CIRCULAR PATCH ANTENNA.....175 - 227

6.1	Introduction.....	176
6.2	Coaxial probe fed circular disc printed antenna	176
6.2.1	Circular patch antenna for circular polarization.....	178
6.2.2	Parametric study of the circular patch antennas for CP.....	183
6.2.2.1	Effect of slit length and width on Antenna A	183
6.2.2.2	Effect of slot length and width on Antenna B	184
6.2.2.3	Effect of the length and width of tuning stub on Antenna C.....	185
6.2.3	Experimental results	186
6.3	Slit embedded annular ring dual band patch antenna.....	189
6.3.1	Antenna geometry	190
6.3.2	Resonance modes	192
6.3.3	Parametric study of the slit embedded annular ring patch antenna.....	193
6.3.3.1	Effect of slot radius variation on the annular ring patch antenna	193
6.3.3.2	Effect of rectangular slit length variation on the annular ring patch antenna.....	195
6.3.3.3	Effect of rectangular slit width variation on the annular ring patch antenna.....	196
6.3.3.4	Effect of rectangular slit position on the annular ring patch antenna	197
6.3.4	3D radiation patterns	199
6.3.5	Experimental results	200

6.4	Slit, slot and stub embedded circular triband patch antenna	202
6.4.1	Antenna evolution and geometry	203
6.4.2	Antenna 1 characteristics	204
6.4.3	Antenna 2 characteristics	205
6.4.4	Antenna 3 characteristics	207
6.4.5	Antenna 4 characteristics	208
6.4.6	Simulated current distributions and radiation plots on Antenna4.....	210
6.4.7	Parametric analysis on Antenna4	212
6.4.7.1	Effect of inner circular slot radius (r) variation	212
6.4.7.2	Effect of length of y directed slits l_{y1}	213
6.4.7.3	Effect of length of x directed slits l_{x1}	214
6.4.7.4	Effect of width of y and x directed slits w_1	214
6.4.7.5	Effect of length of y directed stubs l_{y2}	215
6.4.7.6	Effect of length of x directed stubs l_{x2}	216
6.4.7.7	Effect of width of x and y directed stubs w_2	217
6.4.7.8	Effect of angle of rotation of the inner slot α	217
6.4.8	Design.....	219
6.4.9	Validation of the design.....	220
6.4.10	Experimental measurements.....	222
6.5	Summary of the chapter	225
	References.....	226

Chapter 7

CONCLUSIONS AND FUTURE PERSPECTIVE.....229 - 235

7.1	Thesis Summary.....	230
7.2	Inferences from the investigations on the antennas described.....	231
7.2.1	Dual band sectoral patch antenna with corner truncations	231
7.2.2	Triband dual polarized corner truncated sectoral patch antenna.....	232
7.2.3	Triband dual polarized circular patch antenna	232
7.3	Suggestions for future work	234

Appendix A

TRIBAND DUAL POLARIZED SECTORAL PATCH

ANTENNA FOR LOW CROSS POLARIZATION237 - 250

A.1	Introduction.....	238
A.2	Antenna design and simulations	238
A.3	Parametric study of sectoral slots	241
A.4	Experimental results.....	244
A.5	Conclusion.....	248

Appendix B
**COMPACT GAP LOADED DUAL BAND
ANNULAR RING PATCH ANTENNA FOR
WIMAX/WLAN APPLICATIONS251 - 261**
 B.1 Introduction.....252
 B.2 Antenna geometry and simulations253
 B.3 Experimental results258
 B.4 Conclusion261

PUBLICATIONS 263 - 266
RESUME OF AUTHOR..... 267 - 268
INDEX..... 269 - 270

Chapter 1

INTRODUCTION

C o n t e n t s	1.1 <i>Introduction</i>
	1.2 <i>Modern wireless communication systems</i>
	1.3 <i>Microstrip antennas</i>
	1.4 <i>Models of analysis</i>
	1.5 <i>Compactness of patch antennas</i>
	1.6 <i>Motivation behind the current research</i>
	1.7 <i>Thesis organization</i>

This chapter describes the history of modern wireless communication scenario with an emphasis on the role of antennas in the field. The significance of microstrip antennas in the modern day research field has been highlighted. An explanation of the principles associated with this class of antennas is presented followed by a description about the importance of compact patch antennas and techniques to achieve it. The motivation behind undertaking this current investigation is rendered next. The chapter concludes with a brief account on how the thesis is organized.

1.1 Introduction

The Webster's dictionary describes the word antenna as a usually metallic device such as a rod or a wire for radiating or receiving radio waves whereas the *IEEE Standard for Definitions of Terms for Antennas* (IEEE Standard 145-2013) defines the word as that part of a transmitting or receiving system that is designed to radiate or to receive electromagnetic waves. However, the origin of the word antenna relative to wireless apparatus is attributed to the Italian radio pioneer Guglielmo Marconi, who in 1895, while testing his wireless system with long wire "aerials" discovered that by raising the aerial wire above the ground and connecting the other side of his transmitter to ground, the transmission range was increased [1]. In Italian language, a pole with a wire was simply called l'antenna. Until then wireless radiating transmitting and receiving elements were known simply as aerials or terminals. Marconi's prominent use of the word antenna led to its spread among wireless researchers and to the general public. Nowadays the technology has progressed so much that antennas have become our electronic eyes and ears to the outer world.

The prominent milestones in the journey of antenna from the days of its inception to the 21st century can be highlighted as follows.

- Proposal of "Dynamical Theory of the Electromagnetic Field", in 1864 by James Clerk Maxwell wherein he observed theoretically that an electromagnetic disturbance travels in free space with the velocity of light [2].
- The construction of the first radio antennas by Heinrich Hertz, in 1886, where he assembled an apparatus that can be described as a

complete radio system operating at meter wavelength with an end-loaded dipole as the transmitting antenna and a resonant square-loop antenna as receiver. This structure that he built became popularly known as dipole antenna or hertz antenna [3].

- Guglielmo Marconi proceeded to add tuning circuits, big antenna and ground systems for longer wavelengths, to the apparatus originally built by Hertz and in 1901, he astounded the world by receiving signals at St. Johns, Newfoundland, from a transmitting station he had constructed at Poldhu in Cornwall, England. He promptly became the Wizard of wireless [4].
- The invention of Yagi-Uda antenna in 1926 by Hidetsugu Yagi and Shintaro Uda from Tohoku Imperial University which became immensely popular due to its simplicity and directionality [5].
- The discovery of extra-terrestrial radio waves by Karl Jansky [6] of Bell Laboratories in 1932 using huge antennas designed by him, rightly earned him the title ‘Father of Astronomy’.
- The eruption of World War II in 1939 played a significant role in the flourishing of antenna research, where necessity became the mother of invention. To keep ahead of the enemy and win, the airplanes and battle ships had to be spotted well in advance. This led to the invention of RADAR and a variety of antennas suitable for the associated communication. The following five decades saw the birth and development of different types antennas like dipole/monopoles, slots, horns, lenses, reflectors, log periodic antennas, helical antennas and microstrip antennas [7].

- The introduction of microstrip antennas by Deschamps in 1953 which took another 30 years to emerge as a vibrant area for want of low loss substrates and proper photolithographic techniques. Although the original concept was proposed by Deschamps, the first practical microstrip antenna was patented by Munson and Howell [8]-[11].

1.2 Modern wireless communication systems

Mobile Communication is one single technology that has had an astounding effect on human life than all the other technologies. It has grown globally over the past fifteen years according to the trace shown in Fig. 1.1 [12].

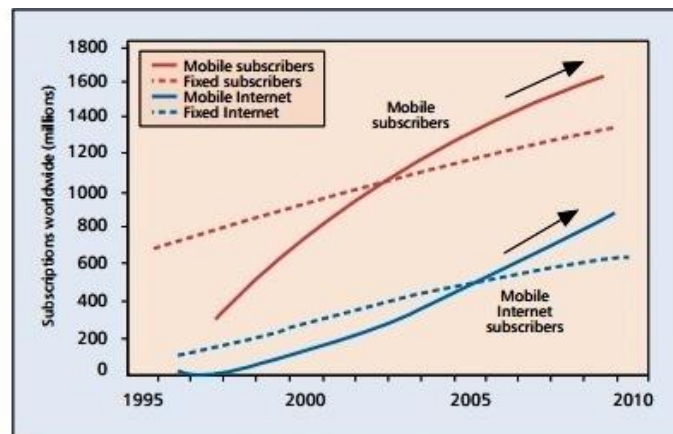


Fig. 1.1. Global growth of mobile and fixed subscribers [12]

About two decades ago no one possessed a mobile phone, while today the population of smartphone users alone comes to around 2 billion, which is expected to cross 7 billion in another three years. Apart from mobile telephone communications, Wireless Local Area Networks (WLAN), which entered the scene around fifteen years ago, has also experienced phenomenal

growth. The spread of Wi-fi enabled public hotspots such as airports and bus terminals has been amazing. They have made their ways into our homes, riding on the back of xDSL and cable access modems, and are now integrated with WLAN Radio Access Points. As a result, the number of wireless internet subscribers has overtaken the number of wired internet users by 2015. The different commercial wireless standards and frequency bands used for the transmission and reception of data has continued to evolve from the first 1G, through 2G and 3G, to the current 4G and to the future 5G levels.

Table 1.1. Frequency Band Allocation

Designation	Service	Allocated Band
GSM 900 GSM 1800 GSM 1900	Global System for Mobile communication	890-960 MHz 1710-1880 MHz 1850-1990 MHz
DCS 1800	Digital Communication System	1710-1880MHz
PCS 1900	Personal Communication System	1850-1990 MHz
GPS L1 GPS L2	Global Positioning System	1227-1575MHz 1565-1585MHz
DVB-H	Digital Video Broadcasting	470-702MHz
UMTS 2000	Universal Mobile Telecommunication Systems	1920-2170MHz
3G IMT 2000	International Mobile Telecommunication	1885-2200MHz
W-LAN ISM2.4(Bluetooth™) ISM5.2 ISM5.8	Wireless Local area Network Industrial, Scientific, Medical	2400-2485MHz 5150-5350MHz 5725-5850MHz
RFID	Radio Frequency Identification	865-868MHz 2.446-2.454MHz
UWB	Ultra Wide Band	3.1-10.6 GHz
WiMax	Worldwide Interoperability for Microwave Access	3.3-3.7GHz
LTE 2300 LTE 2500	Long Term Evolution	2300-2400 MHz 2500-2690 MHz

The varied applications of the antennas range from telegraphy to broadcasting to radio astronomy. The personal and data communication field saw the market being flooded with a variety of mobile and wireless devices. Other important spheres of application include air, maritime and space navigation, search for extra-terrestrial intelligence, military, medicine and disaster management. Wireless gadgets ranging from pagers, cell phones, RF enabled toys, car locks, PC locks, GPS and Radiofrequency identification (RFID) to bio chips are some of the commercial applications. The general frequency allocation bands for modern wireless communication systems are illustrated in Table 1.1[13]-[16].

1.3 Microstrip antennas

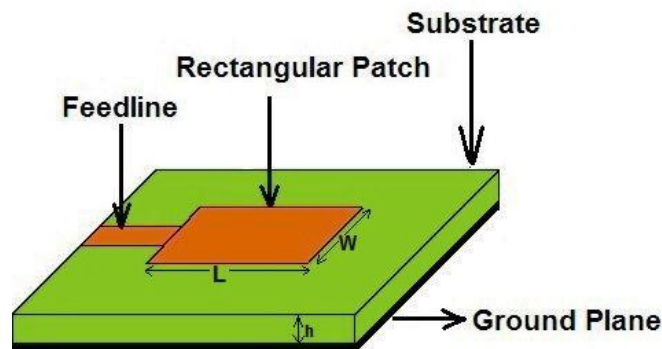


Fig. 1.2. Fundamental configuration of a microstrip antenna

The basic microstrip antenna configuration consists of a dielectric substrate of uniform thickness, on whose one side the radiating metallic patch of any desired geometrical shape is printed as shown in Figure 1.2. The ground plane lies on the other side of the substrate. The conducting patch is made of gold or copper. Although any convenient shape can be chosen for the patch, the common geometries employed are rectangular or

circular. The advantages of microstrip antenna are light weight, low volume, low profile configuration, low cost, easy amenability to mass production, easy integration with MMIC's, capability to produce linear and circular polarization with broadside radiation patterns, dual polarization structures can be easily constructed, dual or multi frequency operation possible, ease of simultaneous fabrication of feed lines and matching circuits with antenna structure. However, the drawbacks include narrow bandwidth, low gain, and low power handling capability, poor end fire radiation, and ohmic loss from the feed and excitation of surface waves when thick substrates are used. Various techniques have been devised to overcome these disadvantages.

1.3.1 Radiation from the microstrip antenna

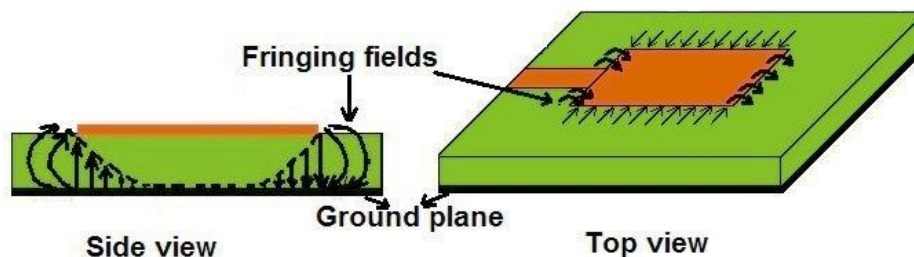


Fig. 1.3. Field radiation in a rectangular patch antenna

The radiation from the microstrip antenna can be attributed to the fringing fields that occur between the patch conductor edges and the ground plane. The electric field radiation from a rectangular patch is shown in Figure 1.3 which shows that the fields are constant along the width and thickness. The field variation occurs only along the length of the patch which is about one half-wavelength long. The fringing fields at the open circuited edges can be resolved into normal and tangential components with respect to the ground plane.

The far field due to the normal components cancel with each other owing to the phase difference of 180° (half-wavelength), while the tangential components add up to give maximum radiation in the broadside direction.

The choice of the substrate material influences the size and bandwidth of the microstrip antenna to a large extent. With respect to the microwave frequency band applications, the height h of the substrate is usually taken as $0.003 \lambda_0 \leq h \leq 0.05 \lambda_0$ where λ_0 is the free space wavelength. The patch thickness t is selected to be so thin such that $t \ll \lambda_0$. The dielectric constant value range for the substrate is typically $2.2 \leq \epsilon_r \leq 12$.

A thick dielectric substrate with low dielectric constant provides better efficiency, larger bandwidth and better radiation for good performance while, such a configuration makes the antenna larger in size. A higher value of dielectric constant decreases the size but also lowers the bandwidth and efficiency of the antenna. Hence a compromise must be made between the dimensions and optimum performance of the antenna [11].

1.3.2 Microstrip patch antenna

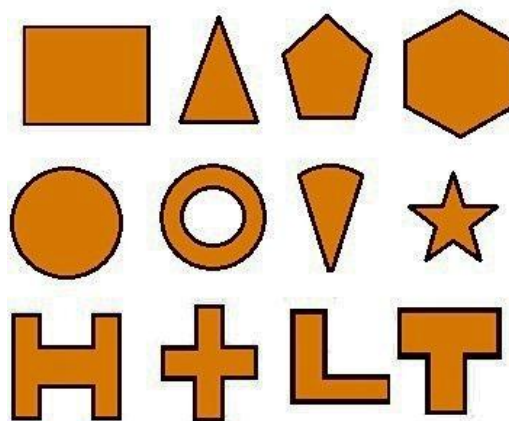


Fig. 1.4. Common patch shapes in microstrip antenna

Microstrip patch antenna also called Patch antenna is a standard configuration of the microstrip antenna in which a planar or nonplanar patch of any geometry is printed on one side of the substrate and the ground plane is printed on the opposite side. The common shapes of patches in practice are shown in Fig.1.4. A patch antenna has radiation characteristics similar to that of a dipole because it behaves like a dipole. Typical gain of a patch antenna is between 5 and 6dB and exhibits a typical 3dB beam width between 70° and 90° [9].

1.3.3 Printed slot antenna

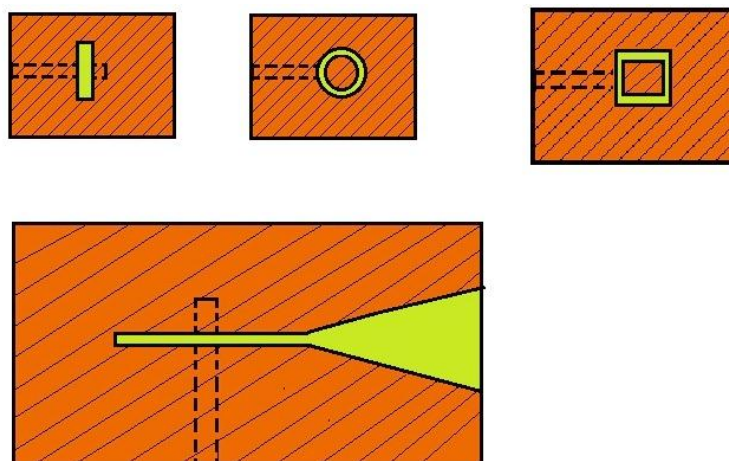


Fig. 1.5. Common printed slot antennas

Printed slot antennas comprise another important configuration where a slot of any suitable shape is etched in the ground plane of a grounded substrate. A slot antenna generally exhibits a bidirectional radiation pattern since they radiate on both sides of the slot. A unidirectional pattern is obtained when a reflector plate is placed on one side of the slot. The common slot shapes used are rectangular, circular, elliptical, annular ring, L shape, T shape etc. Some typical slot shapes are shown in Fig. 1.5.

1.3.4 Feeding Techniques

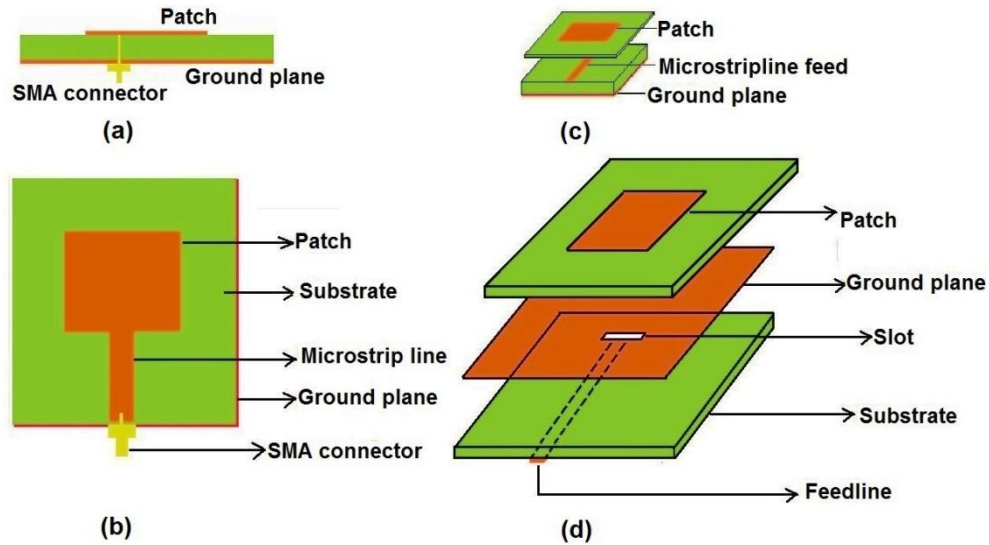


Fig. 1.6. Feeding techniques. a) Coaxial probe feed b) Microstrip line feed c) Proximity coupled feed d) Aperture coupled feed

The efficient coupling of the energy from the transmission line takes place through the feed and the manner in which this task is carried out. The popular feeding techniques used to excite the antenna are coaxial probe feed & microstrip line feed (contacting type) and aperture coupling & proximity fed coupling (non contacting type) [9] and are shown in Fig.1.6.

1.3.4.1 Coaxial probe feed

This is the conventional feeding technique, where the inner conductor of the Sub Miniature Amphenol (SMA) connector passes through the dielectric and is soldered to the patch on top while the outer conductor is affixed to the ground plane on bottom (Fig.1.6a). Using this scheme, the feed can be conveniently placed on any point of best impedance matching on the patch. Ease of fabrication and low spurious radiation are two

advantages. The disadvantages include narrow bandwidth, tougher feed modelling and the structure being not completely planar for thick substrates as the connector protrudes outside the ground plane.

1.3.4.2 Microstrip line feed

This is the simplest feeding scheme and also known as edge feed where the conducting strip is connected to an edge of the feed (Fig.1.6b). The patch and the feedline can be fabricated simultaneously and the structure is planar. The drawback of this feeding mechanism is the occurrence of spurious radiations from the transitions, bends and junctions which has a negative effect on the side-lobe and cross-polarization levels of the antenna.

1.3.4.3 Proximity coupled feed

In this technique (also known as electromagnetically coupled feed), the substrate is of two layers with the microstrip line on the lower substrate. The patch is fabricated on the upper layer (Fig.1.6c). This type of feeding technique rejects spurious feed radiation and provides very high bandwidth of the order of 13%, due to the overall increase in the thickness of the microstrip patch antenna. Two different dielectric media, one for the patch and one for the feed line can also be incorporated in order to optimize the individual performances. However, this leads to complications in the alignment of the patch and the feedline, hence making the fabrication more difficult [11].

1.3.4.4 Aperture coupled feed

This scheme uses two substrates that are separated by a common ground plane. A microstrip line on the lower substrate is electromagnetically coupled to the patch through a slot or aperture in the ground plane. The slot

should be aligned correctly under the patch and far enough from the edge of the patch to avoid backward radiations (Fig.1.6d). As the feed is physically separated from the patch by the ground plane, spurious radiations are very much minimized. The demerits of this method are the difficulty in manufacturing due to the presence of multiple layers and narrow bandwidth.

1.3.5 Polarization of an antenna

Polarization of an antenna is defined as the polarity of the transmitted wave by the antenna in the maximum gain direction. Polarization of a radiated wave then is the curve traced by the end point of the arrow (vector) representing the instantaneous electric field. The field must be observed along the direction of propagation. At far field of an antenna, the radiated wave can be represented by a plane wave whose electric-field strength is the same as that of the wave and whose direction of propagation is in the radial direction from the antenna. Polarization may be classified into three types as linear, circular, or elliptical. If the electric field vector at a point in space as a function of time is directed along a line always, the field is said to be linearly polarized. In general, however, if the figure that the electric field traces is an ellipse, the field is said to be elliptically polarized, with the polarization sense being designated as right-hand polarization for clockwise rotation and left hand polarization for counter clockwise rotation [17]. Circular polarization (CP) is a special case of elliptical, and is obtained when the ellipse becomes a circle. Co-polarization represents the polarization the antenna is intended to radiate (receive) while Cross polarization represents the polarization orthogonal to a specified polarization which is usually the co-polarization.

1.4 Models of analysis

The analysis of the antenna can provide an understanding of the operating principles that could be useful for developing a new design or new configuration and also for modifying an already existing design. Through the analysis, different radiation characteristics of the antenna such as radiation pattern, gain, polarization, input impedance, impedance bandwidth, mutual coupling, antenna efficiency etc. can be predicted. The important analytical methods used are [9], [18]

- The Transmission line model
- The Cavity model
- The Multiport network model

These methods are best suited for simple geometries with regular patch shapes. They provide simplicity at the expense of accuracy. On the other hand, full wave methods based on numerical techniques are highly accurate but rigorous in procedure. The prominent numerical techniques are

- Method of Moments (MoM)
- Finite Element method (FEM)
- Spectral domain method (SDT)
- Finite Difference Time Domain (FDTD) method

1.4.1 Transmission line model

This technique developed by Munson [19] was the earliest to analyze a rectangular microstrip antenna. The interior region of the antenna is modelled as a section of transmission line. The radiator element is treated as two narrow slots, one at each end of the line resonator. The interaction between the two slots is considered by defining a mutual conductance. The

open circuited ends are the main sites for the occurrence of fringing fields. The drawback of the method is that it is not applicable to all types of geometries.

1.4.2 The cavity model

In this model the inside of the patch is modelled as a cavity confined by electric walls on top and bottom and a magnetic wall along the boundary. The field in the interior region does not vary with thickness [20]. For regular patch shapes such as rectangular, circular, triangular, and sectoral the fields underneath the patch can be expressed as a summation of the various resonant modes of the two-dimensional resonator. For irregular geometries the patch is divided into a number of regular shapes. The radiated field is accounted for by defining an effective loss tangent.

1.4.3 The multiport network model

This method is an extension of the cavity model. The electromagnetic fields underneath the patch and those outside the patch are separately patterned. The patch is modelled as a two-dimensional planar network, with a large number of ports arranged around the edges. The external fields are represented by equivalent networks connected to these ports [21]. The overall impedance matrix is evaluated via the segmentation method. The radiated fields are calculated from the voltage distribution around the periphery.

1.4.4 Method of moments

The method of moments is used to analyze microstrip antennas of rectangular and nonrectangular shape. Surface currents are used to model the polarization currents along the microstrip patch and volume of the dielectric slab. The method requires unusually precise computation of the impedance matrix but is capable of accurately predicting currents, impedance,

and resonant frequency of the antenna. The method is based upon a boundary condition, or integral equation formulation, with the unknown being the currents on microstrip patches and wire feed lines and their images in the ground plane. The integral equation is solved using the method of moments [22].

1.4.5 Finite element method

Finite element method (FEM) is a numerical method for solving a differential or integral equation. The method essentially consists of assuming the piecewise continuous function for the solution and obtaining the parameters of the functions in a manner that reduces the error in the solution. In a microstrip antenna, the interior fields of the antenna cavity can be determined where the region of interest is subdivided into small areas or volumes depending upon the dimensions of the region. The small regions can be chosen as polygons such as triangles and rectangles for two dimensional problems and tetrahedral elements for three dimensional problems. The problem of solving wave equations with inhomogeneous boundary conditions is achieved by splitting it into two boundary value problems, one being Laplace's equation with an inhomogeneous boundary and the other corresponding to an inhomogeneous wave equation with a homogeneous boundary condition [23]. This method is applicable to arbitrary shaped patches also.

1.4.6 Spectral domain analysis

In this method, the 2-D Fourier transforms along the two orthogonal patch dimensions in the plane of substrate are computed. Then the Fourier transform plane is applied with the boundary conditions. The current

distribution on the conducting patch is then expanded in terms of basis functions chosen. The resulting matrix equation is then solved for the electric current distribution on the conducting patch and the equivalent magnetic current distribution on the surrounding substrate. The different antenna are then evaluated [24].

1.4.7 Finite difference time domain (FDTD) method

The FDTD is a highly powerful electromagnetic tool capable of addressing complex antenna structures by providing a direct solution to Maxwell's equations in differential form. The formulation was originally proposed by Yee [25] and was further refined and reinvented by Taflove, [26]. In FDTD, microstrip antennas are treated in the time domain for the analysis. The frequency dependence of the different parameters is determined from the Fourier transform of the transient current. However, this method is computationally costly and requires vast amounts of memory for complex structures.

1.5 Compactness of patch antennas

Applications that require physical smallness of antennas are NFC (Near Field Communication) systems, RFID (Radio Frequency Identification), UWB (Ultra-Wideband) systems, and wireless broadband systems such as WLAN (Wireless Local Area Network) systems WiMAX (Worldwide Interoperability for Microwave Access) systems and UMTS Mobile communication. Compactness is an important design challenge, which has been tackled by novel methods such as use of edge-shortened patch, shorting pins and shorting walls, meandered patch, slots, parallel resonant circuits, chip resistor loading and Electronic band gap (EBG) materials[9].

1.5.1 Compact circularly polarized microstrip antennas

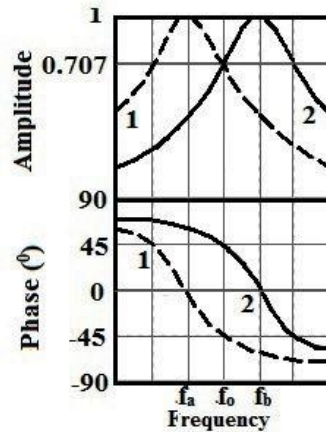


Fig. 1.7. Amplitude and phase of orthogonal modes

Circularly polarized (CP) antennas are attractive for wireless communication applications, because no strict orientations between the base station and the mobile unit are required. Compactness is also a desirable feature for such cases.

The basic principle of the single feed CP patch antenna is that a perturbation of the dimensions be introduced such that, by feeding the patch at the appropriate location, two modes with orthogonal polarizations are generated with resonant frequencies which are slightly different. Perturbation has been introduced in the square patch and the circular patch using the technique of corner truncation thereby making one of the dimensions slightly different from the other [27].

Fig.1.7 illustrates the amplitudes and phases of the radiated fields of the two orthogonal modes of resonant frequency f_a and f_b respectively. CP is produced at the frequency f_0 , located midway between f_a and f_b , where the amplitudes of the two modes are equal and the phases differ by 90° [28].

Different techniques have been proposed for the realization of compact circularly polarized printed antennas. These include embedding suitable slots or slits in the radiating patch or ground plane and use of a dual-orthogonal feed with an external power divider network. Another important scheme is using a single-point feed for which an external power divider is not required [9].

1.5.2 Compact dual and triple band patch antennas

Most wireless communication applications require the operation in two or more discrete yet closely spaced and arbitrarily separated bands than that in a continuous wide band. Mobile phones operable in two or more different bands without raising issues pertaining to the different technologies are a typical case. Similarly, for applications of large array cases where considerable saving in space, weight, material and cost are the main considerations it is highly desirable to employ a thin patch capable of operating in multiple bands [29]. Dual frequency patch antennas also provide an alternative to large bandwidth planar antennas, where it is needed to operate at two separate transmit- receive bands and/or with different polarizations. A dual-frequency patch structure can be employed to avoid the use of separate antennas when the two operating frequencies are far apart or the complicated deployment of a dual feed network for obtaining opposite polarizations.

With the short-range radio communication scenario undergoing an explosive change, it required the utilization of triple band frequencies to be simultaneously incorporated into the same device. Much research effort has been concentrated in the development of compact triple band

operation in the UMTS, WiMAX and WLAN ranges of frequency. 3G mobile communication systems must also be 2G compatible. This means the concurrent support of GSM and UMTS bands while being HiperLAN compatible [30].

Several techniques have been proposed to achieve dual and multiple band performance in microstrip antennas. These include the insertion of shorting pins [31], etching of slots [32], stacking of patches [33] etc. Many designs for producing linear orthogonal [34] and circularly polarized radiations have also been described [27].

1.6 Motivation behind the current research work

Mobile communication has become an indispensable part of the modern life. Different communication systems like GPS, UMTS, and WLAN have been implemented to meet various needs. These applications do not utilize the same frequency bands or polarizations and the system requires separate antennas in order to support different applications. In recent years, many problems arise since the number of systems on individual platforms grows, such as: co-site interference, cost, maintainability, reliability and weight. Therefore, the design of multifunctional antennas for newly developed systems is of practical interest. In almost all multiple functionality systems that can simultaneously support devices operating at any of or combinations of these different frequency bands, the patch or printed antennas have become an integral part. The printed antenna technology has gained the attention of mobile wireless system designer due to its attractive features like light weight, ease of fabrication and low cost of production. The fast development in the field of communication systems demands

compact microstrip antennas suitable for use in MMIC's, satellite mobile communication systems, personal communication systems, etc.

In all these wireless communication systems, circularly polarized antennas are preferred as they can provide better mobility and weather penetration than linear polarization. CP antennas are less sensitive to orientation of the mobile device and can reduce multi path loss. CP operation can be implemented using single and double feed schemes. Single feed systems have the advantage of requiring no external polarizers or power divider networks as compared to double feed systems. Circular polarization and polarization diversity has been achieved by suitably altering the antenna dimensions in these configurations.

The patch shapes commonly employed in CP antennas are square, rectangular and circular even though a wide variety of geometries have been proposed in the recent years. The circular disc sector patch is a simple geometry that can be employed to generate CP radiation using a single probe feed. It is well known that the disc sector patch antenna has the advantage of being physically smaller at a fixed frequency, compared to square or circular patch antennas. However, very few designs for achieving CP operation using disc sector shaped antennas are found in the literature, which motivated this study.

A broadband microstrip antenna can cover the frequencies of interest when multi band operation is desired. However, the disadvantage of using a broadband antenna is that it also receives non-desired frequencies unless some kind of filtering network is introduced to reject such frequencies. On the other hand, the advantage of a dual- and multiband frequency design is

that it focuses only on the frequencies of interest and is thus more desirable and more efficient [27].

The techniques of corner truncation and slit loading at the patch boundary have been established as two prime methods to obtain circularly polarized radiation and multi band performance for the last decade[35]-[39]. Use of slits at the patch boundary has also been deployed to attain frequency tuning and bandwidth improvement. Tuning stubs is also reported to be a simple yet convenient method to attain compact CP radiation [40]. Consequently a combination of all these three methods were experimented upon a basic circular patch with the aim of compactness, better axial ratio bandwidth (ARBW) and maximum impedance matching of the resonances in mind. Probe fed patches are known to suffer from the disadvantage of increased cross polarization which is also a major area of concern for researchers. A significant volume of work has occurred in the direction of overcoming this demerit. Taking all the above points into consideration, the main inspiration of this research work was to devise and analyze compact multi band polarization diverse microstrip antenna using simple and efficient modification of the geometry. Ground plane was also reduced making the antenna smaller in size. Slots have been applied to the ground plane to reduce the level of cross polarized radiation significantly.

1.7 Thesis organization

The prime aim of this research work is the design and development of different multi band microstrip antennas employing various patch modification techniques. The design, fabrication, characterization and theoretical analysis of two different patch geometries for use at different

operating frequencies and polarizations, thus reducing the complexity of implementing several antennas and circuitry for different applications is presented in this thesis. Investigations on the effects that the modifications bring about on the performances of the antennas are examined in detail. Parametric analyses are carried out for optimizing the dimensions and are experimentally verified.

A brief introduction on the history and technology of microstrip antennas, the different feeding mechanisms, methods of analysis, polarizations and multiband techniques are explained in Chapter 1.

Chapter 2 presents a detailed account of the earlier works related to microstrip antennas with an emphasis on dual and triple band designs which preserve compactness.

Chapter 3 deals with the methodology relevant to the development of the microstrip antennas described in this thesis. The simulation tool used for the initial design has been explained. Measurements in the frequency domain such as return loss, radiation pattern, axial ratio, polarization and gain are described. The fabrication procedure has been outlined in this chapter.

Chapter 4 investigates the compact dual band antenna based on the circular disc sectoral patch shape. The technique applied here is corner truncation and the effects of all these truncations on the antenna characteristics are studied. The proposed antenna design is simulated and the resonant modes are identified by examining the surface current and field distributions on the antenna at the resonant modes. The etching of slits in the patch boundary has been effectively used to tune the resonance frequency to the desired band and is demonstrated.

Chapter 5 concerns with the simulated and experimental observations on the compact triple band sectoral patch antenna. The techniques of truncation and notch are applied here. The different polarizations in the three bands have been illustrated and verified through experiment. Excitations of higher order degenerate modes are analyzed. The chapter also explains the reduction of cross polarization by the technique of etching slits of different shapes in the ground plane.

Chapter 6 elucidates a novel triple band microstrip antenna based on the circular shaped patch. A combination of slits, slots and stubs have been employed in this design to attain optimum triple band operation in the desired bands. The parametric simulation studies have been utilized to deduce the design equations and design methodologies on any substrate for the desired operating frequencies. The simulations are experimentally verified.

A summarized account of all the works presented in the previous chapters is highlighted in Chapter 7 along with some directions on the scope for future work in this area.

Other major works carried out during the research period is given in Appendix. Appendix 1 gives the design of a Triband Dual Polarized Sectoral Patch Antenna for Low Cross Polarization. Appendix B describes a Compact Gap Loaded Dual Band Annular Ring Patch Antenna for WiMAX/WLAN Applications.

References

- [1] Marconi, “Wireless Telegraphic Communication: Nobel Lecture, 11 December 1909.” Nobel Lectures. Physics 1901–1921. Amsterdam: Elsevier Publishing Company, 196–222. p. 206, 1967.
- [2] Maxwell, “A Treatise on Electricity and Magnetism”. Macmillan and Co., Oxford University, 1873.
- [3] J. D. Kraus, “Antennas: Our Electronic eyes and ears,” Microwave journal, January 1989.
- [4] J.D. Kraus, “Antennas since Hertz and Marconi”, IEEE Trans. Ants. Prop, AP-33, 131-137, 1985
- [5] S. Uda, “Wireless Beam of short electric waves,” J. IEE (Japan), pp. 273-282, March 1926.
- [6] Jansky, K.G, “Electrical disturbances apparently of extraterrestrial origin” in Proc. IRE in 1933 (Reprinted in Proc. IEEE, vol. 86, no. 7, pp. 1510-1515, July 1998.
- [7] David M. Pozar, “An overview of wireless systems and antennas, ”IEEEA ntennas Propagat. Soc. Int. Symp.,Salt lakecity, vol.2, pp.566-569, July 2000.
- [8] Deschamps G. A., “Microstrip Microwave Antennas”, III rd USAF symposium on Antennas, 1953.
- [9] Ramesh Garg, Prakash Bhartia and Inder Bahl, “Microstrip Antenna Design Handbook”, 1st ed. MA Artech House, 2001.
- [10] Pozar, D.M, “Microstrip antennas”, Proceedings of the IEEE Volume 80, Issue 1, pp 79 – 91, Jan. 1992.
- [11] J.R. James and P.S.Hall, Handbook of Microstrip antennas-volume I, Peter Peregrinus Ltd., U.K.
- [12] Y. Kim, B. J. Jeong, J. Chung, C.-S. Hwang, J. S. Ryu, K.-H.Kim and Y. K. Kim, “Beyond 3G: vision, requirements, and enabling technologies”, IEEE Communications Magazine, pages 120–124, March, 2003.
- [13] Harold Sobol and Kiyo Tomiasu, “Milestones of Microwaves”, IEEE Trans. Microwave Theory Tech.,YoI.MTT-50(3),pp.594-611, March 2002.

-
- [14] B. Z. Ying, "Antennas in Cellular Phones for Mobile Communications," Proceedings of the IEEE, vol. 100, no. 7, 2012.
- [15] <http://www.itu.int/>
- [16] <http://www.fcc.gov/>
- [17] C.A.Balanis(ed.),Modern Antenna Handbook, John Wiley and Sons, 2008.
- [18] K. R. Carver and J. M. Mink, "Microstrip antenna technology," IEEE Antennas and Propagation, Vol.29, No.1, 1981.
- [19] R.E Munson, "Conformal Microstrip Antennas and Phased Arrays," IEEE Trans. Antennas & Propagation, Ap-22, pp. 74-77, 1974.
- [20] Y. T. Lo, D. Solomon and W. F. Richards, "Theory and experiments on microstrip antennas," IEEE Transactions on Antennas and propagation, vol-AP-27, 137-145, 1979.
- [21] Abdelaziz Benella and K.C.Gupta, "Multiport Network Model and Transmission Characteristics of Two-Port Rectangular Microstrip patch antennas," IEEE Transactions on Antennas and propagation, vol-36, no.10, pp. 1337–1342, October 1988.
- [22] E. H. Newman, "Analysis of Microstrip Antennas Using Moment Methods," IEEE Transactions on Antennas and propagation, vol-AP-29, no. 1, pp. 47–53, January 1981.
- [23] P. Silvester, "Finite Element Analysis of Planar Microwave Network," IEEE Trans. Microwave Theory Tech., Vol. MTT-21, pp.104–108, 1973.
- [24] T. Itoh and W. Menzel, "A Full-Wave Analysis Method for Open Microstrip Structure," IEEE Trans. Antennas Propagation, Vol. AP-29, 63–68, 1981.
- [25] K.S. Yee, "Numerical solution of initial boundary value problems involving Maxwell's equations in isotropic media," IEEE Trans. Antennas Propagat., vol.14, pp.302-307, May 1966.
- [26] A. Taflove, Computational electrodynamics, Finite difference time domain method, Artech house, MA, 1995.
- [27] K. F. Lee and K. Tong, "Microstrip Patch Antennas -Basic Characteristics and Some Recent Advances," Proceedings of the IEEE, vol. 100, no. 7, pp. 2169–2180, 2012.

- [28] Stutzman W.L., “Polarization in electromagnetic systems”, Artech House, Norwood MA, 1993.
- [29] F. Bao, “Microstrip Antennas for Dual-Frequency Operation,” IEEE Transactions on Antennas and Propagation, vol. 32, no. 9, pp. 938–943, 1984.
- [30] Anil Kumar Gautam, Lalit Kumar, Binod Kumar Kanaujia, and Karumudi Rambabu, “Design of Compact F-Shaped Slot Triple-Band Antenna for WLAN/WiMAX Applications”, IEEE Transactions On Antennas and Propagation, Vol. 64, No. 3, pp.1101-1105, March 2016.
- [31] K. L.Wong, C. L. Tang, and H. T. Chen, “A compact meandered circular microstrip antenna with a shorting pin,” Microwave Opt. Technol. Lett.15, pp. 147–149, 1997.
- [32] H. Iwasaki, “A circularly polarized small-size microstrip antenna with a cross slot,” IEEE Trans. Antennas Propagat., vol.44, pp. 1399–1401, 1996.
- [33] Q. Kewei, F. Chanjuan, and W. Bin, “Compact Perturbed Hexagonal Microstrip Antenna for Dual-Band Circular Polarization,” Electromagnetics, vol. 33, no. 8, pp. 583–590, Nov. 2013.
- [34] M. S. Nisha, V. P. Sarin, Augustin Gijo, V. Deepu, C. K. Anandan, P. Mohanan, and Kesavath Vasudevan, “Compact Dual Frequency Dual polarized Cross Patch Antenna with an X-Slot”, Microwave And Optical Technology Letters / Vol. 50, No. 12, pp.3198-3201, December 2008.
- [35] V. V Reddy and N. V. S. N. Sarma, “Triband Circularly Polarized Koch Fractal Boundary Microstrip Antenna,” IEEE Antennas and Wireless Propagation Letters, vol. 13, pp. 1057–1060, 2014.
- [36] W. Chen, C. Wu, and K. Wong, “Novel Compact Circularly Polarized Square Microstrip Antenna,” IEEE Transactions on Antennas And Propagation vol. 49, no. 3, pp. 1998–2000, 2001.
- [37] C. Sim, J. Row, and S. Chen, “A Dual-Band Antenna Design For GPS and UMTS Applications”, Microwave And Optical Technology Letters vol. 49, no. 8, pp. 1935–1939, 2007.
- [38] C.-L. Tang, J.-H. Lu and K.-L. Wong, “Circularly polarized equilateral-triangular microstrip antenna with truncated tip,” Electronics Letters, vol. 34, no. 13, p. 1277, 1998.

- [39] J. Lu, C. Tang, and K. Wong, "Novel Dual-Frequency and Broad-Band Designs of Slot-Loaded Equilateral Triangular Microstrip," *IEEE Transactions on Antennas and Propagation*, vol. 48, no. 7, pp. 1048–1054, 2000.
- [40] Wong, K. L., and Lin, Y, "Circularly polarized microstrip antenna with a tuning stub", *Electron Lett.*, 34, (9), pp. 8–9, 1998.

.....✂.....

Chapter 2

LITERATURE REVIEW

Contents

- 2.1 *Microstrip radiators –A review*
- 2.2 *Compact microstrip antennas*
- 2.3 *Multi band and dual polarized microstrip antennas*

This chapter deals with a comprehensive review of literature associated with the development of multi band microstrip antennas. The pioneer research works in microstrip antenna are presented. With an emphasis to compactness, numerous significant works in the area of printed microstrip antenna are covered. The varied techniques and methodologies employed by different researchers for achieving diverse polarizations and multi band performances are briefed. The recent works in the field of triband microstrip antennas are finally described.

2.1 Microstrip Radiators - A review

The invention of microstrip printed structures revolutionized the microwave engineering field by replacing the heavy, bulky and hard to manufacture waveguide structures. Although the microstrip geometries which radiated electromagnetic geometries were originally contemplated in the 1950s, it is Deschamps [1] who is credited with the successful realization of a microstrip printed antenna. In 1955, Bassinot and Gutton came up with the patent for a microstrip antenna design [2]. The radiation from the discontinuities in a stripline was studied by Lewin [3]. Nearly a decade later in 1969, Denlinger [4] noted that rectangular and circular microstrip resonators could radiate efficiently where the radiation mechanism of a rectangular microstrip resonator was attributed to the discontinuities at each end of a truncated microstrip transmission line. The fields and currents of the resonant modes of circular microstrip geometries were described by Watkins by the end of the same year [5]. The next year Byron [6] described a conducting strip radiator separated from the ground plane by a dielectric substrate. Munson patented [7] a microstrip element shortly thereafter. His early works resulted in the practical application of these low profile structures on many flush-mounted antenna systems like rockets and missiles.

Work on basic rectangular and circular patch elements were reported by Howell [8]. His design consisted of a low profile antenna in which the planar resonating element is separated from the ground plane by a dielectric substrate whose thickness was very small compared to the wavelength. The design methods for linearly and circularly polarized and dual band antennas in UHF to C band were described in this paper. The bandwidth depended upon the permittivity and thickness of the substrate and was found to be very narrow.

A microstrip line slot antenna and a two-dimensional X-band Dolph-Chebyshev slot-array antenna were designed and fabricated by Yoshimura [9] as an application of this type of slot. The deployment of antenna arrays in aircrafts rockets and missiles became prevalent with the typical works on a cylindrical S band array by Weinschel [10]. The conformal L band array for communication from KC-135 aircraft to ATS-6 satellite by Sanford [11] and flush mounted low profile antennas by Garvin et al. [12] were reported later. IEEE Transactions on Antennas and Propagation dedicated a special issue to microstrip antennas [13] in 1981 since by this time the term had received a global acceptance. Carver and Mink [14] presented a concise picture of the theoretical and practical design techniques in microstrip antenna technology till 1981.

The choice of an appropriate substrate is a decisive factor in the design of a microstrip antenna, where dielectric constant, loss tangent, thermal coefficient, homogeneity, isotropicity and temperature range are the parameters of selection. Nowicki [15] had done an early elaborate survey on the different dielectric materials. Traut [16] reported Polytetraflouroethylene substrates reinforced with glass random fiber where the filler materials occupy preferred orientations in the polymer matrix during the manufacture. Murphy reported lighter substrate materials for specialized applications such as aircraft [17]. Carver [18] described two thin layers of PTFE bonded on both sides of a hex cell honeycomb structure and Das and Choudhary reported microstrip antenna on Ferrite substrates [19].

Mathematical modelling of microstrip antennas developed into a key area where different approaches were employed for the modelling.

Transmission line analogies to simple rectangular patches fed at the centre of a radiating wall was first proposed independently by Munson [20] and Derneryd [21-22]. James and Wilson studied the radiation mechanism of an open circuited microstrip termination [23]. Lo et.al developed a more accurate method in their cavity model [24-26], Agarwal and Bailey [27] suggested the wire grid model for evaluating the microstrip antenna characteristics. Alexopoulose [28] et al. reported a dyadic Green's function technique to calculate the fields radiated by a Hertzian dipole printed on a ground substrate. The modal expansion model similar to cavity model was formulated by Carver and Coffey [29-31] where the patch is considered as a thin cavity with leaky magnetic walls. The wall admittance calculations have been given by Hammerstad [32] and more accurately by Alexopoulose et al. [33]. A vector potential approach to evaluate the fields produced by any microstrip antenna of any shape was developed by Mosig and Gardiol [34]. Newman and Pozar [35] developed the method of moments for the numerical analysis of the patch antennas. Carver and Coffey [36] explained a finite element approach for the numerical analysis of the fields interior to the microstrip antenna cavity. Chadha and Gupta [37] developed Green's function of circular sector annular ring and annular sector shaped segments in microwave planar circuits and microstrip antennas. An electrically short omni microstrip antenna which is a microstrip-shortened quarter-wave resonator wrapped around a cylinder was developed by Krali [38].

Different feed techniques which influence the input impedance and antenna characteristics were developed for applying the excitation currents [39-42]. These include giving the feed coaxially, electromagnetically coupling the feed, aperture coupled and coplanar waveguide feed.

Microstrip antennas enjoy numerous advantages such as low weight, small volume, low fabrication cost, ease of fabrication using printed-circuit technology, thin profile configuration which easily conforms to the surface of wireless gadgets and ready amenability to mass production. However, they suffer from some inherent demerits like narrow band width and low gain, uni polar radiation, lower capacity to handle power, inferior end fire radiation and surface wave excitation when thick substrates are employed. Advances in microstrip antenna design has progressed to such an extent that ways have been devised to mitigate or eliminate the effect of these limitations. Sizeable amount of literature has appeared which deals with the broad banding of microstrip antennas such as stacking parasitic radiators and reducing the Q of the microstrip radiators by employing thick air or foam substrates [43-47]. Use of a high-permittivity dielectric superstrate [48] and an amplifier-type active circuitry [49] to obtain an enhanced antenna gain, have been demonstrated. Meandering technique has been applied in [50-52] to lower the fundamental resonant frequency. The limitations associated with surface waves such as low efficiency, greater mutual coupling, reduced gain and degradation of radiation pattern can be minimized by using photonic band gap structures [53].

Conventional patch shapes were replaced with new geometries like rectangular ring and H shaped, annular ring and U shaped slots were etched into the patch for enhancement of bandwidth [54-57].

2.2 Compact microstrip antennas

Although the commonly used compact patch shapes were rectangular and circular, varying geometrical shapes were developed depending on the

application. Advancements in the different communication bands placed more stringent demands on compactness. New techniques were invented and attempted for minimizing the size of the microstrip antennas.

The H-shaped patch antenna reported by Palanisamy et al. [54] required very less area compared to the rectangular patch antenna and was found to be attractive for UHF applications.

A compact broadband antenna system in which a driven patch is gap coupled with a number of parasitic elements was developed by C.K. Aanandan and K.G. Nair [58] which achieved a bandwidth of 6% without any pattern deterioration.

A C-shaped microstrip radiating element operating in the UHF and L-bands was reported by Kossiavas et al. [59] whose dimensions were found to be smaller than those of conventional square or circular elements.

Simple schemes for lowering the resonant frequency of the rectangular patch antenna without changing the size by placing a perturbation below the patch was proposed by Volakis and Jin [60] and it obtained as much as 30 % reduction in resonant frequency.

Supriyo Dey et al. [61] proposed a compact, low-cost wideband circularly polarized antenna for personal communication applications which consists of four shorted rectangular patches.

Jacob George et al. [62] developed a compact drum shaped microstrip antenna with significant amount of reduction in size and radiation properties similar to those of an equivalent rectangular patch antenna.

H.T. Chen [63] experimentally studied the characteristics of compact microstrip antennas through the placement of shorting pin and meandering and compared them with those of conventional microstrip antennas.

Lo et al. [64] used a high permittivity substrate to design a miniature microstrip antenna. The patch size was found to be reduced to one fifth of that of the conventional microstrip antenna.

Loading the patch antenna with a dielectric resonator to obtain frequency reduction was implemented by Yung et al. [65]. It was observed that the resonant frequency of a circular microstrip antenna decreases with the position of the DR on the antenna.

Supriyo Dey et al. [66] obtained a 19 % reduced resonant frequency by modifying the geometry of an ordinary microstrip circular patch antenna by putting two sectoral slots shunted by conducting strips. A wide variation in input impedance along the circumference of the modified structure was noted and it could be matched directly with a microstripline.

Three thin shorting posts instead of a complete short circuit were used by Sanad [67] who showed that the size of a quarter wavelength antenna could be reduced considerably without degrading the gain of the antenna.

The U patch antenna which may be used as an alternative to the half wave square patch antenna was demonstrated by Douglas and Johnston [68]. It requires only about one third of the surface area of the square half wave antenna.

A probe-fed circular patch featuring a single shorting post was compared by Waterhouse [69] with larger area patches and circular patches of the same size as the shorted patch, and designed on the same substrate.

A compact microstrip antenna for cellular phone applications consisting of a driven element and five small parasitic patches distributed in two stacked layers was proposed by Sanad [70].

The two main issues of resonant microstrip antennas namely miniaturization and frequency tuning have been explored in detail by Bokhari [71]. A basic circular geometry with slits cut into, allows considerable size reduction over a limited range.

K.L.Wong et al. introduced a wideband cylindrical monopole antenna for mobile phone applications [72] which consists of an upper hollow conducting cylinder and a lower conducting cone, with a volume comparable to that of the conventional helical monopole antenna.

K.L.Wong and S. C. Pan [73] showed that a triangular microstrip antenna loaded with a shorting pin can significantly reduce the antenna size at a given operating frequency. The resonant frequency variations with variations in the shorting pin positions are studied in this paper.

A chip-resistor loaded rectangular microstrip antenna with probe feed and inset microstrip line feed are demonstrated by K. L. Wong and Y.F. Lin [74].The antenna has a small size and wide bandwidth.

K. L.Wong and K. P.Yang [75] demonstrated a modified planar inverted F antenna with antenna length less than $\lambda/8$ and bandwidth higher than that of a simple PIFA by a decade. The reduction in length is achieved by meandering the radiating patch and wider bandwidth is obtained by replacing the shorting post by a chip resistor.

K. L. Wong has also published considerable amount of literature on compact circularly polarized microstrip antennas using different techniques. A rectangular microstrip with a cross slot and an inclined slot coupled feed had a 40% reduction in size [76]. Bent slots placed in the centre of the rectangular patch achieved 32% size reduction [77]. Circular patch was embedded with cross slot and tuning stubs [78]. Lowering of resonant frequency was attained by the insertion of spur lines at the edges of an equilateral triangular patch [79]. Size reduction of 20% using cross slots and peripheral cuts on a circular patch antenna was proposed [80]. A square microstrip patch antenna with four slits and a pair of truncated corners achieved a 36% size reduction [85]. These are some of the prominent works by K.L. Wong.

C.Y. Huang has described an aperture coupled square ring microstrip antenna with a cross strip which achieved a 24~30% size reduction [81].

Experimental studies of an equilateral triangular microstrip antenna embedded with cross slots of unequal slot lengths to produce circularly polarized radiation and achieve size reduction when compared to an equivalent triangular microstrip antenna at a fixed operating frequency were performed by J.H. Liu [82].

Waterhouse et al. have proposed a printed antenna consisting of a synchronous subarray of shorted patches. The feed network is etched on a high dielectric constant substrate below the ground plane. The antenna exhibits compact dimensions of $0.195\lambda \times 0.195\lambda \times 0.052\lambda$ [83].

K.M. Luk et al. [84] have presented the theoretical analysis and calculated results of achieving compactness by the application of shorting walls to an L probe wideband patch antenna.

H.D. Chen [86] presented a reduced size two corners truncated square patch antenna with a group of four bent slots embedded in the ground plane.

Hao chun Tung [87] demonstrated that an inverted U shaped patch on an air substrate can achieve 50% size reduction. Y. Qin [88] has described a circularly polarized compact patch antenna with embedded star shaped slots and offset planar feed with size reduction of 38%.

An ultra-compact printed antenna with connective and concentric double split rings (CCDSR) with tuning arms and dimensions $9 \times 24 \times 1 \text{ mm}^3$ is presented by Gao et al. [89].

Kan reported a concentric shorted annular ring printed antenna with a small size resonating at 2.1 GHz [90]. A square ring patch antenna with a coupling strip located inside the patch and a compact single feed circularly polarized patch antenna realized by cutting cross slots in the patch and the ground plane were explained by Row [91-92].

A compact hybrid rat race coupler embedded with a defected ground structure achieving size reduction and harmonic suppression has been reported by Y.J.Sung et al. in [93].

Binu Paul et al. [94] presented a high permittivity multiband dielectric-eye resonator antenna operating at 1.9 GHz and 2.4 GHz with significant size reduction in comparison with rectangular and circular patch antennas at the same frequencies.

Rohith K. Raj [95] proposed a planar antenna with a very compact size and resonating in four frequency bands.

An E shaped patch in which the bandwidth is increased by cutting a pair of tapered slots and using the even mode symmetry of the E shape to achieve compactness is proposed by Deshmukh and Kumar [96].

Amman [97-98] has described single and dual frequency compact circularly polarized circular patch antennas which are inscribed in an annular ring and have unequal cross slotted ground planes resulting in size reductions of about 55%.

The analysis using equivalent circuit model of an H shaped patch antenna has been carried out in [99] by Ansari et al.

Eleftheriades [100] has employed a defected ground plane by cutting an L slot in the ground plane of a circular disc monopole antenna with dual wideband resonances and having a size of $24 \times 28.3 \text{ mm}^2$.

Nageswara Rao has [101] proposed the use of a fractal curve as boundary to a square patch which can reduce the size by more than 50% while keeping the gain unchanged.

A simple and effective mobile unit antenna operating in the 2.4 GHz and 5 GHz bands with a small form factor and compact size of $8 \text{ mm} \times 25 \text{ mm}$ is proposed by Fa Shian Chang [102].

Compactness is achieved by the use of four asymmetric slits on a square microstrip patch by Nasimuddin [103]. A square slot, a pair of L strips and a monopole radiator were employed in the work by Wei Hu et al. [104]. Simple crescent shaped pair of patches was implemented by Chao Liu [105].

Baohua Sun et al. [106] proposed a novel triple frequency antenna for the WLAN/WiMAX bands which employs a meandered split ring slot and a pair of inverted L strips on a monopole radiator.

The modal cavity model of the corner truncated square microstrip antenna with four slits and achieving 39 % size reduction has been analyzed by A.K. Gautham in [107].

Stacked patch configuration has been employed in a hexagonal shaped patch with truncated corner and pair of inserted slits to achieve a small radiating area of $15.6 \times 16 \text{ mm}^2$ by Qian Kewei [108].

Unequal rectangular slots have been cut at the edge of a rectangular patch to reduce the antenna size by 73% making it suitable for mobile communication applications by Chatterjee et al. [109]

Compact printed antennas for the WLAN/WiMAX networks have been proposed by Liang in [110] and Y.N. Lai in [111].

A rectangular microstrip antenna for IEEE 802.11a with two single slots and slotted ground plane which achieved a 53% size reduction compared to the standard unslotted rectangular microstrip antenna has been realized by Chakraborty et al. [112]

Recently Wu Di et al. [113] have developed a compact antenna of size $21 \times 15 \text{ mm}^2$ using S shaped and inverted L shaped shorted strips which is highly suitable for 4G mobile applications.

Another recent work on compact microstrip antenna is the structure reported by Khandelwal [114] where low cross polarization is achieved by the use of triangular and square shaped defects in the ground plane.

An excellent comprehensive review on the most popular and significant miniaturization techniques on microstrip antennas has been presented by Sharawi et al. [115].

2.3 Multi band and dual polarized microstrip antennas

With the advent of advanced multi standard mobile communication devices and equipments, the necessity and growing demand to incorporate multiple frequency bands into the single system also was on the rise. Dual, triple and quad or in general multi band antennas were integrated within a given volume without any possibility of interference between any two bands. Keeping the polarizations different in the operating bands proved to be a challenging field for the designer. Moreover, circular polarization was preferred in one or more bands owing to its insensitivity to transmitter-receiver orientation and resistance to multipath fading. This section reviews the major techniques adopted by researchers to develop multi band patch antennas with diverse polarizations.

An intensive description of all the major techniques to attain dual frequency operation of microstrip patch antennas has been presented by S.Maci and Biffi Gentili [116]. A novel frequency array using piggyback elements operating at 401.8 and 468.8 MHz with a gain of 12dB and employed as a link from Buoy or Ship to a satellite was reported by Weinschel and Carver [117]. Stacking technique was applied to circular disc and its dual frequency properties were studied very early by Long and Walton [118] in 1979. A dual frequency microstrip antenna with a dish feed consisting of a microstrip element that resonates at one frequency embedded within another element which resonates at a different lower frequency was

suggested by Kerr et al. [119]. Schaubert et al. [120] used two trapezoidal shaped patches stacked one over the other to implement a piggyback antenna for dual frequency operation. Dual frequency operation of a circular patch antenna was attained by McIlvenna et al. [121] by etching two ears separated by an angle of 60° (named bunny antenna) on the patch. Itoh and Goto [122] described the dual frequency circularly polarized nature of a printed antenna with slots and strips which was excited by a microstrip feed. Shorting pins were placed along the patch at appropriate locations and the frequency ratio was varied from 3 to 1.8 in the dual frequency microstrip antennas proposed by Wang and Lo [123]. A dual frequency circularly polarized microstrip antenna with optimum feed location method was reported by Suzuki and Chiba [124]. A single feed dual frequency microstrip antenna where the two frequencies can be independently impedance matched at centre frequencies of 2.32 and 9.42 GHz over a wide bandwidth was discussed by Garg and Rao [125].

K. L. Wong has implemented dual frequency microstrip antennas on various geometrical patch shapes. These include single feed rectangular patch resonating at 1.42 and 1.54 GHz with the polarization planes being perpendicular to each other at the two frequencies [126] and a bow-tie antenna loaded with slots and frequency ratio varied by varying the flare angle of the patch [127]. A circular patch embedded with two pairs of arc shaped slots with circular polarization in both bands [128], shorting pin loaded triangular [73] and circular microstrip antenna [129] with tunable frequency ratios are prominent works by the same author. Wen Shyang Chen [130] has developed a rectangular patch loaded with square slot and linear polarization in the two operating bands. Equilateral triangular patch

loaded with bent slots [131-132] having tunable frequency ratio and same polarization planes at the two bands was proposed by Jui Han Lu.

Triple band antennas began to gain widespread popularity by the early twenty-first century and several papers appeared in the open literature. K.H. Lee et al. had put forward the triband spiral microstrip antenna operating at 900, 1800 and 2000 MHz with probe feed and wideband balun [133]. A triple band antenna for cellular phone, GPS and PCS systems which consists of three stacked patches with a slot coupling the first patch to the third one was explained by Park et al. [134]. Brissos [135] designed a small triple band rectangular patch antenna with a pair of slots and five shorting pins for use in the GSM800, UMTS and HiperLAN2 frequency bands.

Shun Yun Lin [136] has described the dual band design of a compact antenna consisting of a corner truncated square patch and an annular ring patch with four slits in the ground plane, operating in the GPS and DCS frequency bands. Jeen Sheen Row et al. have published the dual frequency work on square patch producing two different radiation patterns [137]. An annular ring patch with circular polarization in the dual bands and tunable frequency ratio was proposed by Amman [98].

Deshmukh and Ray [138] etched rectangular and half U slots inside a rectangular microstrip patch antenna to yield the dual band and triple band configurations. The multiport network models of these multiband microstrip antennas were also proposed, which expressed the voltage distribution at all frequencies. Du et al. [139] proposed a stacked square patch triple band configuration in which circular polarization in all bands are achieved by etching two pairs of narrow slots parallel to the top square edge along with a

slit cut in the bottom square. The resonances are at 1.57, 1.69 and 2.49 GHz. Xiao-Hua Wu et al. [140] explored the dual and triple band operation of an asymmetric M shaped patch where vias are utilized to achieve compactness of the structure. Radiation patterns were found to be distorted with large cross polarization level due to the increased substrate thickness.

T.K.Geok [141] implemented a dual band printed dipole antenna by combining a rectangular and two L shaped radiating elements, embedded on a single layer. This structure produced an omnidirectional radiation pattern in the two bands of WLAN. The simple technique of etching two or three U slots in a rectangular patch to yield dual band and triple band operations respectively was demonstrated by K.F. Lee [142-143]. The designs by Lee was implemented using stacked patches with U slots, to generate dual band circularly polarized operation in the WiMAX and Hiper LAN bands by Payam Nayeri [144].

Several triple band antennas for the WLAN/WiMAX bands were proposed. Wei Hu [104] employed L strips, square slot and a monopole radiator, W.H. Wang [145] used T shaped strips pair and staircase pattern in a wide rectangular slot, B.Sun portrayed a Y shaped monopole radiator with inverted L strips [106] and C. Liang developed an ear shaped patch using three circular arc shaped strips [110]. A.K. Gautham [146] very recently put forward an F shaped planar prototype which consists of two similar F shaped slots etched on a rectangular patch and a circular shaped patch printed on the ground plane. Three circularly polarized bands were realized by etching three different shaped geometries consisting of 1) an inverted-U-shaped 45° rotated radiator 2) an I-shaped strip on the right side of the radiator and 3) an inverted-L-shaped strip at the end of the I-shaped strip [147].

R.Sujith et al. [148] have implemented a multi band CPW fed uniplanar antenna where a modified T shaped radiating element is imposed with different current paths for a quad frequency resonance.

The self-similarity property of fractal antennas naturally leads to a multi band behavior. Dual and Triple band configurations adopting the fractal geometry have appeared in the open literature in the recent years. An L shaped series step impedance microstripline fed concentric annular slot antenna [149] and an asymmetrical Koch fractal boundary square patch [150] generate circular polarization in all the three bands. The Sierpinski fractal geometry has been incorporated in the multiband antenna for operation in the WiFi, WiMAX and Public Safety Standard frequency bands [151]. Dual frequency resonances at the WLAN/WiMAX bands are obtained by the complementary Minkowski Island fractal geometry based square patch with aperture coupled feed [152].

Falade [153] proposed a stacked patch antenna with triple resonances in the L1, L2 and L5 GPS bands having circularly polarized radiation in all three bands. He used three square patches mounted one on top of each other. The antenna exhibits broad beam width with good axial ratio.

The realization of different or orthogonal polarizations in the various bands of single feed multiband microstrip antennas is a popular sphere of research. Researchers have succeeded in attaining this objective through wide variety of techniques. J. Kaiser [154] had described a two wire spiral antenna as early as 1960, where the two senses of circular polarization could be separately selected without any difference in the radiation patterns. Wolfson [155] proposed a C band radiator in an 8×8 element test array

where linear and circular polarizations could be obtained. Adrian and Schaubert [156] proposed a new method to generate dual or circular polarization where a square microstrip patch with a microstrip line is fed through an aperture. Two orthogonally placed rectangular slots beneath the patch excite the x and y directed linear polarizations respectively. Exciting the two apertures in quadrature produces circular polarization. A lightweight microstrip antenna radiating right hand circularly polarized (RHCP) and left hand circularly polarized (LHCP) patterns, consisting of a four element patch array with two polarizing feed networks, was reported by Upshur et al. [157]. A square patch intended with a rectangular notch, generates dual frequency responses at 3.69 and 4.49 GHz where the polarization planes are perpendicular to each other by Vichien et al. was implemented [158]. Dual frequency patch antennas with dual linear polarizations in the two bands have been developed using polarizing grid technique on a cross shaped patch with etched bars on the sides and dual slot coupling of a circular patch antenna [159-160].

A novel structure applicable as a data communicator for terrestrial and satellite systems constructed by integrating two different antenna modes into dual-band, dual polarized antenna where linear and circular polarization are realized has been implemented by Gardner et al. [161].

Some typical designs for dual frequency rectangular patch antennas with orthogonal polarization planes at the two frequencies include the proper selection of feed point [162], inclined slot coupling [163] and etching of a cross slot in the patch [164].

A dual band stacked patch antenna operating in the L and C bands centered at 1.275 and 5.3 GHz and dual linearly polarization was discussed

by Shafai [165]. The L-band elements were chosen as perforated patches and the C-band elements were placed within them.

Binoy et al. [166] have introduced a placard shaped slot embedded square patch antenna, having two extensions as tuning stubs suitable for application in the GSM and CDS 1800 frequency ranges. The two operating modes have orthogonal polarization planes and broadside radiation patterns. This topology was later reworked by C.H. Chen [167] and et al. with a nearly square patch with the placard shaped slot alone and a different substrate. The lengths of the bar slots and the patch sides, the frequency ratio of the two bands which are in orthogonal polarization planes could be varied.

Jeen Sheen Row [168] presented an equilateral patch incorporated with two shorting screws which excited two resonant modes. The two modes are linearly polarized with omnidirectional radiation pattern and circularly polarized with broadside radiation pattern respectively. The frequency ratio of the two bands is 1.71.

Shynu et al. [169] have reported a square microstrip antenna with an embedded hexagonal slot which resonates at dual frequencies. The frequency ratio can be tuned in the range 1.06 to 1.09. The resonant modes have linear orthogonal polarization planes.

Wong implemented a dual circularly polarized annular ring with microstrip feed and ring slot coupling [170]. The sense of polarization is left handed at the lower frequency of 2.075 GHz and right handed at the upper frequency of 2.735 GHz.

Serra et al. [171] demonstrated a wide-band stacked patch antenna with dual linear polarization operating in the UMTS 1, ISM band and in the new UMTS extension bands.

Bao and Amman [172] described a dual frequency annular slot antenna with microstrip feed. Four unequal linear slots which enhance the annular slot provide the dual sense circular polarizations of RHCP and LHCP at 1.5 GHz and 2.6 GHz respectively.

Sarin V.P [173] proposed a novel design of an electromagnetically coupled square patch with slot loading for dual frequency application in the WLAN 5.2 GHz and 5.8 GHz bands. The first band has elliptical polarization while the second one is linearly polarized.

A cross patch antenna, embedded with a cross slot and resonating at 1.42 GHz and 1.79 GHz was investigated by Nisha M.S. in [174]. The antenna offers size reductions of 74% and 59% respectively at the two frequencies and are orthogonally linearly polarized.

Shafai focused on investigating the polarization characteristics of loaded and unloaded microstrip square ring [175] and annular ring [176] patches. Stub notch, gap and shorting pin loadings were experimented upon and the change in polarization characteristics were thoroughly observed.

A microstripline fed circular patch is inserted with orthogonally placed rectangular slots to produce right hand and left hand senses of circular polarization with CP bandwidth greater than 40 % by Rezaeieh [177]. The antenna resonates in the GPS and WLAN bands.

Liang [178] has proposed a quad sense circularly polarized annular patch etched with an X shaped slit and a ground plane inscribed with a T shaped slit. The antenna has a broad bandwidth of 3.1 to 22.2 GHz and covers the WiMAX, WLAN, X band and Ku band ranges.

Li-Ting Wang [179] reported an omnidirectional antenna for the 2G, 3G and LTE applications which consists of two modified asymmetric cones and six concentrically printed dipoles. A six way power splitter is used to feed the dipoles. Vertically polarized radiation with a bandwidth of 17.4% in the 806 ~960 MHz band and horizontally polarized radiation with a bandwidth of 35% in the 1880~2700 MHz were obtained.

Falade [180] succeeded in designing a triple band antenna with stacked patches applicable for surveying and geo informatics in handheld terminals with linear and circular polarizations. The antenna has good impedance bandwidth and axial ratio in the GPS L1, L2, and GSM 1800 bands.

A compact novel microstrip fed omnidirectional antenna with two circularly polarized bands for the WLAN band and linearly polarized radiation for the WiMAX band has been implemented by Hao Bai et al. [181].

A conventional square patch antenna etched with a square slot which is further loaded with a mushroom unit cell embedded with a CSRR has been explored for both dual and triple band operations in [182]. The antenna has orthogonally linearly polarized modes in the lower bands and circular polarization in the upper band.

Recently Tao Zhang et al. [183] developed a triple band antenna using two triangular rings of different sizes with each ring working as a dual

frequency dual polarized radiating element. The resonances are at 8.33, 9.6, and 10.78 GHz with bandwidths of 3.1%, 1.4% and 2.1% respectively. The three respective bands have horizontal polarization, 45° polarization, and vertical-polarization.

W.Q. Cao [184] proposed a novel probe-feed circular patch antenna with dual-band dual polarization lately. The antenna has broad bandwidth and unidirectional linearly polarized characteristics at the higher band of 5.74 GHz and omnidirectional circularly polarized radiation at the lower frequency band of 4.42 GHz. A modified mushroom structure enables dual-band dual-mode characteristics. Bandwidth is broadened by a loading structure consisting of four curved patches around the circular patch.

The literature reviewed in this chapter obviously indicates that the design and development of multi band patch antennas is an active and relevant topic for research in the contemporary communication scenario. Numerous techniques are available for achieving compactness and broad bandwidth. The main objective of this thesis is the description of a few novel antennas applicable for different commercial frequency bands.

References

- [1] G.A. Deschamps, Microstrip Microwave Antennas, 3rdUSAF symposium on Antennas, 1953.
- [2] H. Gutton and G. Bassinot, Flat Aerial for Ultra high Frequencies, French Patent No. 703113,1955.
- [3] L. Lewin, "Radiation from Discontinuities in Strip Lines", Proc. IEE, vol.107, pp 163-170, 1960.
- [4] Edgar J. Denlinger, "Radiation from Microstrip Radiators," IEEE Trans Microwave Theory Tech., pp. 235-236, April 1969.

- [5] J.Watkins, "Circular Resonant Structures in Microstrip," *Electron Lett.*, vol.5, no.21, pp.524-525, October 16, 1969.
- [6] E.V Byron, "A new Flush Mounted Antenna Element for Phased Array Applications", *Proc. Phased Array Antenna Symp.*, pp.187-192, 1970.
- [7] R.E Munson, *Single Slot Cavity Antennas*, US patent no-3713162, January 22, 1973.
- [8] J.Q Howell, "Microstrip Antennas", *IEEE Trans. Antennas Propagat.*, vol.AP-23, pp.90-93, 1975.
- [9] Y. Yoshimura, "A microstrip line slot antenna", *IEEE Transactions on Microwave theory and techniques*, November 1972, pp. 760-762.
- [10] H.D Weinschel, "Progress report on Development of Microstrip Cylindrical Arrays for Sounding Rockets", *Phys. & Sci. Lab.*, New Mexico State Univ., Las Cruces, 1973.
- [11] G.G Sanford, "Conformal Microstrip Phased Array for Aircraft Tests with ATS-6", *Proc. Nat. Electronic Conf.*, vol.29, pp. 252-257, 1974.
- [12] G.W Garvin, R.E Munson, L.T Ostwald and K.G Schroeder, "Low Profile Electrically Small Missile Base Mounted Microstrip Antennas", *Dig. Int. Symp. Antennas Propagat. Soc.*, Urbana, IL, pp-244-247, 1975.
- [13] *IEEE Transactions on Antennas and Propagation*, January 1981.
- [14] K.R.Carver and J.W.Mink, "Microstrip Antenna Technology", *IEEE Trans. Antennas & Propagation*, AP-29;p. 2-24, 1981.
- [15] T.E. Nowicki. "Microwave Substrates, Present and Future" in *Workshop on Printed CircuitAntennaTech.1979*. Las Cruces.
- [16] G.R. Traut, "Clad Laminates of PTFE composites for Microwave Antennas," *ibid*, 27, p.1-17, 1979.
- [17] L.R Murphy, "SEASAT and SIR-A Microstrip Antennas", *ibid.*, pp. 18/1-20, 1979.
- [18] K.R Carver, "Description of a Composite Hex cell Microstrip Antenna", *Private Communication to J.W. Mink*, 1979.

- [19] S.N Das and S.K Choudhary, "Rectangular Microstrip Antenna on a Ferrite Substrate", IEEE Trans. Antennas Propagat., vol.AP-30, pp.499-502, 1982.
- [20] R.E.Munson, "Conformal microstrip antennas and phased arrays," IEEE Trans. Antennas Propagat., vol. AP-22, pp. 74-77, 1974.
- [21] A.G.Demeryd, "Linear microstrip array antenna," Chalmer Univ. Technol., Goteborge, Sweden, Tech. Report.,TR 7505, 1975.
- [22] A.G.Demeryd, "Linearly polarized microstrip antennas," IEEE Trans. Antennas Propagat., vol.AP-24, pp.846-851, 1976.
- [23] J.R James and C.J Wilson, "Microstrip Antennas and Arrays Part I Fundamental Action and Limitations", IEE Proc. Microwaves, opt. & Antennas, Vol.1, pp. 165-174, 1977.
- [24] Y.T Lo, D. Solomon and W.F Richards, "Theory and Experiment on Microstrip Antennas", IEEE AP-S Symposium (Japan), pp.53-55, 1978.
- [25] W.F Richards, Y.T Lo and D.D Harrison, "Improved Theory for Microstrip Antennas", Electron. Lett., Vol.15, pp.42-44, 1979.
- [26] Y.T Lo, D. Solomon and W.F Richards, "Theory and Experiment on Microstrip Antennas", IEEE Trans. Antennas Propagat., vol. AP-27, pp.137-145, 1979.
- [27] P.K Agarwal and M.C Bailey, "An Analysis Technique for Microstrip Antennas", IEEE Trans. Antennas Propagat., vol. AP-25, pp.756-759, 1977.
- [28] N.G Alexopoulose, N.K Uzunoglu and I.E Rana, "Radiation by Microstrip Patches", Dig. Int. Symp. Antennas Propagat., pp.722-727, 1979.
- [29] K.R Carver, "A Modal Expansion Theory for the Microstrip Antenna", Dig.Int.Symp.Antennas Propagat.Soc., Seattle, WA, pp.101-104, 1979.
- [30] K.R Carver and E.L Coffey, "Theoretical Investigations of the Microstrip Antenna", Tech.Rept. PT 00929, Physical Science Lab., New Mexico Science Univ., Las Cruces, 1979.
- [31] E.L Coffey and T.H Lehman, "A New Analysis Technique for Calculating the Self and Mutual Impedance of Microstrip Antennas", Proc. Workshop on Printed Circuit Antennas, New Mexico State Univ., pp.31/1-21, 1979.

-
- [32] E.O Hammerstad, "Equations for Microstrip Circuit Design", Proc. 5th European Microwave Conf., Hamburg, pp.268-272, 1975.
- [33] N.G Alexopoulou and I.E Rana, "Mutual Impedance Computation between Printed Dipoles", IEEE Trans. Antennas Propagat., vol. AP-27, pp.137-145, 1979.
- [34] J.R Mosig and F.E Gardiol, "The near Field of an Open Microstrip Structure", IEEE AP-S, Int.Symp. Digest, pp.379-381, 1979.
- [35] E.L Newman and D.M Pozar, "Electromagnetic Modeling of Composite Wire and Surface geometries", IEEE Trans. Antennas Propagat., vol. AP-26, pp.784-787, 1978.
- [36] K.R Carver and E.L Coffey, "Theoretical Investigations of the Microstrip Antenna", Physical and Science Lab., New Mexico State Univ., Las Cruces, pp.3/1-20, 1979.
- [37] R. Chadha and K.C.Gupta, "Green's functions for circular sectors, annular rings, and annular sectors in planar microwave circuits", IEEE Trans. Microwave Theory Tech., vol. MTT-29, pp. 68-71, Jan 1981.
- [38] A. D. Krali, J. M. McCorkle, J. F. Scarzello and A. M. Syeles, "The omni microstrip antenna: A new small antenna," IEEE transactions on antennas and propagation," Vol. Ap-27, No.6, pp.850-853, Nov.1979.
- [39] J. S. Roy, et al., "Some Experimental Investigations on Electromagnetically Coupled Microstrip Antennas on Two Layer Substrate," Microwave Optical Tech. Letters, Vol. 4, No. 9, pp. 236-238, 1991.
- [40] D. M. Pozar, and S. D. Targonski, "Improved Coupling for Aperture-Coupled Microstrip Antennas," Electronics Letters, Vol. 27, No. 13, pp. 1129-1131, 1991.
- [41] W. Menzel and W. Grabherr, "Microstrip Patch Antenna with Coplanar Feed Line," IEEE Microwave and Guided Wave Letters, Vol. 1, No. 11, pp. 340-342, 1991.
- [42] R. L. Smith, and J. T. Williams, "Coplanar Waveguide Feed for Microstrip Patch Antenna," Electronics Letters, Vol. 28, No. 25, pp. 2272-2274, 1992.

- [43] Pozar D.M., “A review of bandwidth Enhancement techniques for microstrip antennas,” in *Microstrip antennas, The Analysis and Design of* IEEE press, New York, pp 157-166, 1995.
- [44] J. R. James, P. S. Hall and C. Wood, *Microstrip antennas: Theory and design*, Peter Peregrinus, London, UK, 1981.
- [45] J. R. James and P. S. Hall, *Handbook of Microstrip Antennas*, Vol. 1, London: Peter Peregrinus Ltd., 1989.
- [46] Sanchez-Hernandez D, and I.D Robertson, “A survey of Broadband Microstrip Patch Antennas,” *Microwave Journal*, pp 60-84, September 1996.
- [47] Zurcher, J.F and F.E Gardiol, “Broadband Patch Antennas” , Artech House, Norwood, MA, 1995.
- [48] C. Y. Huang, J. Y. Wu, C. F. Yang, and K. L. Wong, “Gain-enhanced compact broadband microstrip antenna,” *Electron. Lett.* 34, 138–139, Jan. 22, 1998.
- [49] B. Robert, T. Razban, and A. Papiernik, “Compact amplifier integration in square patch antenna,” *Electron. Lett.* 28, 1808–1810, Sept. 10, 1992.
- [50] K. L. Wong, C. L. Tang, and H. T. Chen, “A compact meandered circular microstrip antenna with a shorting pin,” *Microwave Opt. Technol. Lett.* 15, 147–149, June 20, 1997.
- [51] C. K. Wu, K. L. Wong, and W. S. Chen, “Slot-coupled meandered microstrip antenna for compact dual-frequency operation,” *Electron. Lett.* 34, 1047–1048, May 28, 1998.
- [52] J. H. Lu and K. L. Wong, “Slot-loaded, meandered rectangular microstrip antenna with compact dual-frequency operation,” *Electron. Lett.* 34, 1048–1050, May 28, 1998.
- [53] Qian Y., et al. “Microstrip patch Antenna using Novel Photonic Band Gap Structures”, *Microwave Journal*, vol.42, pp 66-76, Jan 1999.
- [54] Palanisamy, V., and R. Garg, “Rectangular Ring and H-Shaped Microstrip Antennas Alternative to Rectangular Patch Antennas”, *Electronics Letters*, Vol. 21, No. 19, pp. 874–876, 1985.

- [55] Chew, W. C., "A Broadband Annular Ring Microstrip Antenna," IEEE Trans. Antennas Propagation, Vol. AP-30, pp. 918–922, 1982.
- [56] Luk, K. M., K. F. Lee, and W. L. Tam, "Circular U-Slot Patch with Dielectric Superstrate," Electronics Letters, Vol. 33, No. 12, pp. 1001–1002, 1997.
- [57] Wong, K. L., and Hsu W. H., "Broadband Triangular Microstrip Antenna with U-Shaped Slot", Electronics Letters, Vol. 33, No. 25, pp. 2085–2087, 1997.
- [58] C.K. Aanandan and K.G. Nair, "Compact broadband microstrip antenna", Electron. Lett., vol.22, no.20, pp.1064-1065, 1986.
- [59] G. Kossiavas, A. Papiemik, LP. Boisset, and M. Sauvan, "The C-Patch: A Small Microstrip Element," Electron. Lett., vol.25, no.4, pp.253-254, 1989.
- [60] J.L. Volakis and I.M. Jin, "A scheme to lower the resonant frequency of the microstrip patch antenna," IEEE Microwave and Guided Wave Lett., vol. 2, pp.292-293, Jul. 1992.
- [61] S. Dey, S. Chebolu, R. Mittra, I. Park, T. Kobayashi and M. Itoh, "A Compact Microstrip Antenna for CP," IEEE Antennas Propagat. Soc. Int. Symp., California, pp.982-985, June 1995.
- [62] J. George, M. Deepukumar, C.K. Aanandan, P. Mohanan and K. G. Nair, "New compact microstrip antenna," Electron. Lett., vol.32, no.6, pp.508-509, March 1996.
- [63] H.T. Chen, "Experimental results of compact microstrip antennas," IEEE Antennas Propagat. Soc. Int. Symp., Montreal, pp.932-935, 14-17 April 1997.
- [64] T. K. Lo, C. O. Ho, Y. Hwang, E. K. W. Lam, and B. Lee, "Miniature aperture-coupled microstrip antenna of very high permittivity," Electron. Lett., vol.33, no.1, pp.9-10, 1997
- [65] E. K. N.Yung, W. W. S. Lee, and K. M. Luk, "A dielectric resonator on a microstrip antenna," IEEE Antennas Propagat. Soc. Int. Symp., Michigan, pp. 1504-1507, June 1993.
- [66] SupriyoDey, C.K.Aanandan, P.Mohanan and K. G.Nair, "A new compact circular patch antenna," IEEE Antennas Propagat. Soc. Int. Symp., Washington, pp. 822-825, June 1994.

- [67] M.Sanad, "Effect of the shorting posts on short circuit microstrip antennas," IEEE Antennas Propagat. Soc. Int.Symp., Washington, pp.794-797, June1994.
- [68] M. G.Douglas and R.H.Johnston, "A compact two way diversity microstrip U-patch antenna," IEEE Antennas Propagat. Soc.Int. Symp., California, pp.978-981, June 1995.
- [69] R.B.Waterhouse, "Performance of microstrip patches incorporating a single shorting post," IEEE Antennas Propagat.Soc. Int.Symp., Maryland, pp. 29 - 32, July 1996.
- [70] M. Sanad, "A compact dual-broadband microstrip antenna having both stacked and planar parasitic elements", IEEE Antennas Propagat. Soc. Int. Symp.,Maryland,pp. 6- 9, July 1996.
- [71] S. A. Bokhari, J. Zurcher, J. R. Mosig, S. Member, and F. E. Gardiol, "A Small microstrip Patch Antenna with a Convenient Tuning Option," IEEE Transactions on Antennas and Propagation, vol. 44, no. 11, pp. 1521–1528, 1996.
- [72] Kin-Lu Wong and Shao-Lun Chien, "Wide-Band Cylindrical Monopole Antenna for Mobile Phone", IEEE Transactions on Antennas and Propagation, Vol. 53, No. 8, pp. 2756-2758, August 2005.
- [73] K. L.Wong and S.C.Pan, "Compact triangular microstrip antenna," Electron. Lett., vol. 33, no. 6, pp. 433-434, 1997.
- [74] K.L.Wong and Y. F. Lin, "Small broad band rectangular microstrip antenna with chip-resistor loading", Electron. Lett., vol. 33, no. 9, pp. 11593-1594, 1997.
- [75] K L. Wong and K. P. Yang, "Modified planar inverted F antenna," Electron. Lett.,vol. 34, no. 1, pp. 7-8, 1998.
- [76] Kai-Ping Yang and Kin-Lu Wong, "Inclined-slot-coupled compact dual-frequency microstrip antenna with cross-slot," Electronics Letters vol. 34, no. 4, pp.321-322, 1998.
- [77] Kai-Ping Yang and Kin-Lu Wong, "Compact dual frequency microstrip antenna with a pair of bent slots," Electronics Letters vol. 34, no. 3, pp.225-226,1998.

- [78] Kin-Lu Wong and Yi-Fang Lin, "Circularly polarized microstrip antenna with a tuning stub", *Electronics Letters*, Vol. 34 No. 9, pp. 831-832, 1998.
- [79] J. Lu, H. Yu, and K. Wong, "Compact circular polarization design for equilateral-triangular microstrip antenna with spur lines," *Electronics Letters*, vol. 34, no. 21, pp. 1989–1990, 1998.
- [80] W.-S. Chen, C.-K Wu, and K.-L. Wong, "Compact Circularly-Polarized Circular Microstrip Antenna with Cross-Slot and Peripheral Cuts," *Electron. Lett.*, vol. 34, no. 11, pp. 1040–1041, 1998.
- [81] C. -Y. Huang, "Designs for an aperture-coupled compact circularly polarized microstrip antenna," *IEE Proc. - Microwaves, Antennas Propag.*, vol. 146, no. 1, p. 13, 1999.
- [82] J. Lu, C. Tang, and K. Wong, "Single-Feed Slotted Equilateral-Triangular Microstrip Antenna for Circular Polarization," *IEEE Transactions on Antennas and Propagation*, vol. 47, no. 7, pp. 1174–1178, 1999.
- [83] H. Kan and R.B. Waterhouse, "Small circularly polarized printed antenna", *Electronics Letters*, vol. 36 no. 5, pp.393-394, 2000.
- [84] K. F. Lee, Y. X. Guo, J. A. Hawkins, R. Chair, and K. M. Luk, "Theory and experiment on microstrip patch antennas with shorting walls," *IEE Proc. - Microwaves, Antennas Propag.*, vol. 147, no. 6, p. 521, 2000.
- [85] W. Chen, C. Wu, and K. Wong, "Novel Compact Circularly Polarized Square Microstrip Antenna," *IEEE Transactions on Antennas and Propagation*, vol. 49, no. 3, pp. 1998–2000, 2001.
- [86] H.-D. Chen, "Compact circularly polarized microstrip antenna with slotted ground plane", *Electronics Letters*, Vol. 38, No. 13, pp.616-617, 2002.
- [87] K. L. Wong and H. C. Tung, "An inverted U-shaped patch antenna for compact operation," *IEEE Trans. Antennas Propag.*, vol. 51, no.7, pp. 1647–1648, 2003.
- [88] M. Elsdon, A. Sambell, S. C. Gao, and Y. Qin, "Compact circular polarized patch antenna with relaxed manufacturing tolerance and improved axial ratio bandwidth," *Electronics Letters*, vol. 39, no. 18, pp. 1–2, 2003.

- [89] H.-S. Ding, Z.-Q. Li, and P.Gao, "An ultra-compact dual-band antenna with tuning arms for WLAN applications," *Progress In Electromagnetics Research Letters*, Vol. 21, 109-117, 2011.
- [90] H.K. Kan, R.B. Waterhouse and D. Pavlickovski, "Compact dual concentric ring printed antennas", *IEE Proc.-Microw. Antennas Propag.*, Vol. 151, No. 1, pp.37-42,2004.
- [91] J.S. Row, "Design of Square-Ring Microstrip Antenna for Circular Polarization", *Electronics Letters*, pp.93-95, vol. 40, no. 2, 2004.
- [92] J. Row and C. Ai, "Compact design of single-feed circularly polarized microstrip antenna," *Electronics Letters*, vol. 40, no. 18, pp. 4–5, 2004.
- [93] Y. J. Sung, C. S. Ahn, and Y. S. Kim, "Size Reduction and Harmonic Suppression of Rat-Race Hybrid Coupler Using Defected Ground Structure," *IEEE Microw. Wirel. Components Lett.*, vol. 14, no. 1, pp. 7–9, 2004.
- [94] Binu Paul, S. Mridula, P. Mohanan, P.V. Bijumon and M.T. Sebastian, "A compact very high permittivity Dielectric-eye Resonator Antenna for multiband wireless applications," *Microwave and Optical Technology letters*, Vol. 43, No.2, pp.118-121, October 20, 2004.
- [95] Rohith. K. Raj, Manoj Joseph, Binu Paul and P. Mohanan, "Compact planar multiband antenna for GPS,DCS,2.4/5.8GHz WLAN applications," *IEE Electronics Letters*, Vol. 41, No.6,pp.290-291, 2005.
- [96] A.A. Deshmukh and G. Kumar, "Compact broadband E-shaped microstrip antennas", *Electronics Letters*, Vol. 41, No. 18, pp.989, 2005.
- [97] X. L. Bao and M. J. Ammann, "Compact concentric annular-ring patch antenna for triple-frequency operation," *Electronics Letters*, vol. 42, no. 20, pp. 9–10, 2006.
- [98] X. L. Bao and M. J. Ammann, "Dual-frequency circularly-polarized patch antenna with compact size and small frequency ratio," *IEEE Trans. Antennas Propag.*, vol. 55, no. 7, pp. 2104–2107, 2007.
- [99] J. A. Ansari, Satya Kesh Dubey, Prabhakar Singh, R. U. Khan, and Babau R. Vishvakarma, "Analysis Of Compact H-Shaped Microstrip Antenna", *Microwave and Optical Technology letters*, Vol. 50, No.7,pp.1779-1784,July, 2008

- [100] M. A. Antoniadis, and G. V Eleftheriades, “A Compact Multiband Monopole Antenna with a Defected Ground Plane,” *IEEE Antennas Wirel. Propag. Lett.*, vol. 7, pp. 652–655, 2009.
- [101] P. Nageswara Rao and N. V. S. N. Sarma “Compact Single Feed Circularly Polarized Fractal Boundary Microstrip Antenna,” *Microwave and Optical Technology letters*, Vol. 52, No.1,pp.141-147,January 2010.
- [102] Saou-Wen Su, and Fa-Shian Chang, “Compact, Printed Mobile-Unit Antenna For 2.4 and 5 GHz WLAN Applications”, *Microwave and Optical Technology letters*, Vol. 52, No.12, pp.2648-2653, Dec, 2010.
- [103] Nasimuddin, X. Qing, and Z. N. Chen, “Compact asymmetric-slit microstrip antennas for circular polarization,” *IEEE Trans. Antennas Propag.*, vol. 59, no. 1, pp. 285–288, 2011.
- [104] Wei Hu, Ying-Zeng Yin, Peng Fei, and Xi Yang, “Compact Triband Square-Slot Antenna with Symmetrical L-Strips for WLAN/WiMAX Applications,” *IEEE Antennas Wirel. Propag. Lett.*, vol. 10, pp. 462–465, 2011.
- [105] J. Guo, Y. Zou, and C. Liu, “Compact broadband crescent moon-shape patch-pair antenna,” *IEEE Antennas Wireless. Propag. Lett.*, vol. 10, pp. 435–437, 2011.
- [106] P. Liu, Y. Zou, B. Xie, X. Liu, and B. Sun, “Compact CPW-Fed Tri-Band Printed Antenna with Meandering Split-Ring Slot for WLAN / WiMAX Applications,” *IEEE Antennas Wireless. Propag. Lett*, vol. 11, pp. 1242–1244, 2012.
- [107] A. K. Gautam, Pramod Benjwal, and B. K. Kanaujia , “A Compact Square Microstrip Antenna For Circular Polarization,” *Microwave and Optical Technology letters*, Vol. 54, No.4,pp.897-900, April, 2012.
- [108] Q. Kewei, F. Chanjuan, and W. Bin, “Compact perturbed hexagonal microstrip antenna for dual-band circular polarization,” *Electromagnetics*, vol. 33, no. 8, pp. 583–590, 2013.
- [109] Samiran Chatterjee, Kalyanbrata Ghosh, Joydeep Paul, S. K. Chowdhury, Debasree Chanda Sarkar, and P.P. Sarkar , “Compact Microstrip Antenna For Mobile Communication”, *Microwave And Optical Technology Letters* , Vol. 55, No. 5, pp.954-957, May 2013.

- [110] Zhai, H., Ma, Z., Han, Y., and Liang, C, “A Compact Printed Antenna for Triple-Band WLAN/WiMAX applications,” *IEEE Antennas Wireless. Propag. Lett*, vol. 12, no. 1, pp. 65–68, 2013.
- [111] C. Y. D. Sim and Y. N. Lai, “An inverted-F antenna design for WLAN/WiMAX dual-network applications,” *Int. J. RF Microw. Comput. Eng.*, vol. 24, no. 5, pp. 523–528, 2014.
- [112] U. Chakraborty, A. Kundu, S. K. Chowdhury, and A. K. Bhattacharjee, “Compact Dual-Band Microstrip Antenna for IEEE 802.11a WLAN Application”, *IEEE Antennas Wireless. Propag. Lett* vol. 13, pp. 407–410, 2014.
- [113] Li Jiu-Sheng and Wu Di, “A Compact Antenna For 4G Mobile Handset”, *Microwave And Optical Technology Letters* , vol. 56, no. 9, pp. 2199 - 2203,September 2014.
- [114] Mukesh Kumar Khandelwal, Binod Kumar Kanaujia, Santanu Dwari, Sachin Kumar and A. K. Gautam “Bandwidth Enhancement And Cross-Polarization Suppression in Ultra-wide band Microstrip Antenna with Defected Ground Plane”, *Microwave And Optical Technology Letters* , vol. 56, no. 9, pp. 2141 -2146,September 2014.
- [115] M. S. Sharawi, M. U. Khan, and R. Mittra, “Microstrip patch antenna miniaturization techniques: a review,” *IET Microwaves, Antennas Propag.*, vol. 9, pp. 913–922, 2015.
- [116] S. Maci and G. Biffi Gentili, “Dual-Frequency Patch Antennas,” *IEEE Antennas and Propagation Magazine*, Vol. 39, No. 6, pp.13-20, December 1997.
- [117] H.Weinschel and K.Carver, “A Medium Gain Circularly Polarized Microstrip VHF Antenna for Marine DCP Communication to the GOES satellite System”.in *IEEE AP-S International Symposium Antennas & Propagation*, 1976.
- [118] S. Long and M. Walton, “A dual-frequency stacked circular-disc antenna,” *IEEE Trans. Antennas Propagation*, vol. 27, no. 2, pp. 270–273, 1979.
- [119] J.L.Kerr, *Microstrip Antenna Developments.in Workshop on Printed Circuit Antenna Tech.*1979, New Mexico State University, Las Cruces.

- [120] D.H.Schaubert and F.G.Farrar. "Some Conformal Printed Circuit Antenna Designs in Workshop on Printed Circuit Antenna" Tech.1979, New Mexico State Univ, Las Cruces.
- [121] J.McIlvenna and N.Kemweis. "Variations on the Circular Microstrip Antenna Calculations" in Workshop on Printed Circuit Antenna Tech.1979, New Mexico State Univ. Las Cruces.
- [122] K.Itoh and N.Goto, "Dual Frequency Circularly Polarized Microstrip Antennas Composed of Strips and Slots," IEE Proc. Pt.H, 130, pp. 170-174, 1983.
- [123] B.F.Wang and Y.T.Lo, "Microstrip Antennas for Dual-Frequency Operation," IEEProc. Pt.H.132:p. 938-943, 1985.
- [124] Y.Suzuki and T.Chiba, "Improved Theory for Single fed Circularly Polarized Microstrip Antenna", Trans. Inst. Electron. and Commn Engg, Japan Sect.E, E-68: p. 76-82, 1985.
- [125] Ramesh Garg and K.V.S. Rao,"Dual Frequency Microstrip Antenna", Electronics Letters, Vol.19, No.10, pp.357-358, 1983.
- [126] Jin-Sen Chen and Kin-Lu Wong "A Single-Layer Dual Frequency Rectangular Microstrip Patch Antenna Using A Single Probe Feed", Microwave And Optical Technology Letters", vol. 11, no. 2, pp. 83-84, 1996.
- [127] Kin-Lu Wong and Wen-Shan Chen, "Slot-loaded bow-tie microstrip antenna for dual-frequency operation", Electronics Letters, vol.34, no.18, pp.1713-1714, 1998.
- [128] Gui-Bin Hsieh, Ming-Huang Chen and Kin-Lu Wong, "Single feed dual band circularly polarized microstrip antenna", Electronics Letters, vol.34 , no.12, pp.1170-1171, 1998.
- [129] Chia-Luan Tang, Hong-Twu Chen and Kin-Lu Wong, "Small circular microstrip antenna with dual- frequency operation", Electronics Letters, vol.33, no.13, pp.1112-1113, 1997.
- [130] W.-S. Chen, "Single-feed dual-frequency rectangular microstrip antenna with square slot," Electron. Lett., vol. 34, no. 3, p. 231, 1998.

- [131] Jui-Han Lu, “Novel Dual-Frequency Design of Single-Feed Equilateral-Triangular Microstrip Antenna” *Microwave and Optical Technology Letters*, vol. 22, no. 2, pp. 133-136, 1999.
- [132] J. Lu, C. Tang, and K. Wong, “Novel Dual-Frequency and Broad-Band Designs of Slot-Loaded Equilateral Triangular Microstrip,” *IEEE Trans. Antennas Propag* , vol. 48, no. 7, pp. 1048–1054, 2000.
- [133] K. H. Lee, S. A. Hamilton and M. S. Bong, “A Tri-Band Circular Polarized Microstrip Antenna”, *IEEE Antennas and Propagation Society International Symposium*, 2002.
- [134] Han-Cheol Ryu, Hee-Ran Ahn, Sang-Hwa Lee and Wee Sang Park, “Triple-stacked microstrip patch antenna for multiband system,” *Electron. Lett.*, vol. 38, no. 24, pp. 1496–1497, 2002.
- [135] J. Brissos and C. Peixeiro, “Compact triple-band microstrip patch antenna element for cellular and WLAN systems,” *IEEE Int. Symp. Pers. Indoor Mob. Radio Commun. PIMRC*, vol. 1, pp. 916–920, 2003.
- [136] S. Y. Lin and K. C. Huang, “A compact microstrip antenna for GPS and DCS application,” *IEEE Trans. Antennas Propag.*, vol. 53, no. 3, pp. 1227–1229, 2005.
- [137] Shing-Hau Chen, Jeen-Sheen Row, and Chow-Yen-Desmond Sim “Single-Feed Square-Ring Patch Antenna with Dual-Frequency Operation” *Microwave And Optical Technology Letters*, vol. 49, no. 4, pp. 991-994,2007.
- [138] A. A. Deshmukh and K. P. Ray, “Multi-Band Rectangular Microstrip Antennas,” *Microwave and Optical Technology Letters*, vol. 49, no.11, pp.2757-2761, 2007.
- [139] W. Liao, Q. Chu, and S. Du, “Tri-band Circularly Polarized Stacked Microstrip Antenna for GPS and CNSS Applications,” *Proc. International Conference on Microwave and Millimeter Wave Technology* pp. 252–255, 2010.
- [140] Lin Peng, Cheng-Li Ruan, and Xiao-Hua Wu, “Design and Operation of Dual / Triple-Band Asymmetric M-Shaped Microstrip Patch Antennas,” *IEEE Antennas and Wireless Propagation Letters*, vol. 9, pp. 1069–1072, 2010.

- [141] O.Tze-Meng and T. K. Geok, "A Dual-Band Omni-Directional Microstrip Antenna," *Progress In Electromagnetics Research*, vol. 106, no. May, pp. 363–376, 2010.
- [142] K. F. Lee, K. M. Luk, K. M. Mak, and S. L. S. Yang, "On the use of U-slots in the design of dual-and triple-band patch antennas," *IEEE Antennas Propag. Mag.*, vol. 53, no. 3, pp. 60–74, 2011.
- [143] W. C. Mok, S. H. Wong, K. M. Luk, and K. F. Lee, "Single-Layer single-patch dual-band and triple-band patch antennas," *IEEE Trans. Antennas Propag.*, vol. 61, no. 8, pp. 4341–4344, 2013.
- [144] P. Nayeri, S. Member, K. Lee, A. Z. Elsherbeni, F. Yang, and S. Member, "Dual-Band Circularly Polarized Antennas Using Stacked Patches With Asymmetric U-Slots," *IEEE Antennas Wireless Propag. Lett.*, vol. 10, pp. 492–495, 2011.
- [145] X. Q. Zhang, Y. C. Jiao, and W. H. Wang, "Compact wide tri-band slot antenna for WLAN/WiMAX applications," *Electron. Lett.*, vol. 48, no. 2, p. 64, 2012.
- [146] A. K. Gautam, L. Kumar, and B. K. Kanaujia, "Design of Compact F-Shaped Slot Triple-Band Antenna for WLAN / WiMAX Applications," *IEEE Trans. Antennas Propag.*, vol. 64, no. 3, pp. 1101–1105, 2016.
- [147] H. C. Park and T. V. Hoang, "Very simple 2.45/3.5/5.8 GHz triple-band circularly polarized printed monopole antenna with bandwidth enhancement," *Electron. Lett.*, vol. 50, no. 24, pp. 1792–1793, 2014.
- [148] R. Sujith, V. Deepu, S. Mridula, B. Paul, D. Laila, and P. Mohanan, "Compact CPW-fed uniplanar antenna for multiband wireless applications," *AEU - Int. J. Electron. Commun.*, vol. 65, no. 6, pp. 553–559, 2011.
- [149] Wang, L.; Guo, Y.-X.; Sheng, W.X., "Tri-band circularly polarized annular slot antenna for GPS and CNSS applications", *Journal of Electromagnetic Waves and Applications*, Volume 26, Issue 14-15, pp. 1820-1827, 2012.
- [150] V. V. Reddy and N. V. S. N. Sarma, "Triband Circularly Polarized Koch Fractal Boundary Microstrip Antenna," *IEEE Antennas Wireless Propag. Lett.*, vol. 13, pp. 1057–1060, 2014.

- [151] L. Lizzi, R. Azaro, G. Oliveri, and a. Massa, “Multiband Fractal Antenna for Wireless Communication Systems for Emergency Management,” *J. Electromagn. Waves Appl.*, vol. 26, no. 1, pp. 1–11, Jan. 2012.
- [152] T. Hung, J. Liu, C. Wei, C. Chen, and S. Bor, “Dual-Band Circularly Polarized Aperture-coupled Stack Antenna with Fractal Patch for WLAN and WiMAX Applications,” *International Journal of RF and Microwave Computer-Aided Engineering*, pp. 130–138, 2013.
- [153] O. P. Falade, M. U. Rehman, Y. Gao, X. Chen, and C. G. Parini, “Single feed stacked patch circular polarized antenna for triple band GPS receivers,” *IEEE Trans. Antennas Propag.*, vol. 60, no. 10, pp. 4479–4484, Oct. 2012.
- [154] J. Kaiser, “Dual Operation with the Two-Wire Spiral Antenna,” *IRE Transactions on Antennas and Propagation*, vol.9, Issue 6, pp. 2–3, 1961.
- [155] Ronald I. Wolfson and William G. Sterns, “A High-Performance, Microstrip Dual Polarized Radiating Element”, *Antennas and Propagation Society International Symposium, APS- 15-2*,” pp. 6–9, 1984.
- [156] A. Adrian and D. H. Schaubert, “Dual aperture-coupled microstrip antenna for dual or circular polarization,” *Electron. Lett.*, vol. 23, no. 23, pp. 1226–1228, 1987.
- [157] L. Sichan, R. M. Sorbello, S. Siddiqif and J.I. Upshur, “A Lightweight, C-Band, Dual Circularly Polarized Microstrip Antenna for Satellite Applications,” *Antennas and Propagation Society International Symposium, AP-S. Digest* pp. 909–912, 1989.
- [158] H Nakano and K Vichien, “Dual-Frequency Square Patch Antenna with Rectangular Notch,” *Electronics Letters*, vol. 25, no. 16, pp. 1067–1068, 1989.
- [159] L. Habib, G. Kossias and A. Papiernik, “Cross-Shaped Patch with Etched Bars for Dual Polarization”, *Electron. Lett.*, vol. 29, no. 10, pp. 6–8, 1993.
- [160] Y. Murakami, W. Chujo, I. Chiba, and M. Fujise, “Dual slot-coupled microstrip antenna for dual frequency operation,” *Electron. Lett.*, vol. 29, no. 22, p. 1906, 1993.
- [161] E. Lee, P.S. Hall and P. Gardner, “Compact dual-band dual-polarization microstrip patch antenna,” *Electron. Lett.*, vol. 35, no. 1, pp. 1034–1036, 1999.

- [162] Chen, J.S., and Wong, K.L., "A single-layer dual-frequency rectangular microstrip patch antenna using a single probe feed," *Microw. Opt. Technol. Lett.*, 11, pp. 83-84, 1996.
- [163] Antar, Y.M M., Ittipiboon, A.I., and Bhattacharyya, A. K., "A dual-frequency antenna with a single patch and an inclined slot", *Microw. Opt. Technol. Lett.*, 8, pp. 309-311, 1995.
- [164] Kin-Lu Wong and Kai-Ping Yang, "Small dual frequency microstrip antenna with cross slot," *Electron. Lett*, vol. 33, no. 23, pp. 1916–1917, 1997.
- [165] L. L. Shafai, W. A. Chamma, M. Barakat, P. C. Strickland, and G. Séguin, "Dual-band dual-polarized perforated microstrip antennas for SAR applications," *IEEE Trans. Antennas Propag.*, vol. 48, no. 1, pp. 58–66, Jan.2000.
- [166] G. S. Binoy, C. K. Aanandan, P. Mohanan, and K. Vasudevan, "Dual-frequency dual-polarized slot-coupled compact microstrip antenna for communication systems," *Int. J. Electron.*, vol. 89, no. 3, pp. 191–195, Mar. 2002.
- [167] C. H. Chen, X. L. Wang, and W. Wu, "Compact single-feed dual-frequency dual-polarization microstrip antenna," *Electron. Lett.*, vol. 46, no. 20, p. 1362, 2010.
- [168] J. Row and K. Lin, "Low-profile design of dual-frequency and dual-polarized triangular microstrip antennas", *Electronics Letters*, vol. 40, no. 3, pp. 3–4, 2004.
- [169] S. V. Shynu, R. K. Raj, A. R. Chandran, C. K. Aanandan, P. Mohanan, and K. Vasudevan, "Single-feed dual-frequency dual polarized microstrip antenna with hexagonal slot," *IEEE Antennas Propag. Soc. Symp.*, vol. 4, p. 4380–4383 Vol.4, 2004.
- [170] C. Cai, J. Row, and K. Wong, "Dual-frequency microstrip antenna with dual circular polarisation," *Electronics Letters*, vol. 42, no. 22, pp. 4–5, 2006.
- [171] A. A. Serra, P. Nepa, G. Manara, G. Tribellini, and S. Cioci, "A Wide-Band Dual-Polarized Stacked Patch Antenna," *IEEE Antennas Wirel. Propag. Lett.* , vol. 6, pp. 141–143, 2007.

- [172] X. Bao and M. J. Ammann, "Dual-frequency dual-sense circularly-polarized slot antenna fed by microstrip line," *IEEE Trans. Antennas Propag.*, vol. 56, no. 3, pp. 645–649, 2008.
- [173] Sarin V P, Nishamol M S, Gijo Augustine, C K Aanandan, P Mohanan and K Vasudevan "An Electromagnetically coupled dual band dual polarized microstrip antenna for WLAN applications", *Microwave and optical technology letters*, vol.50,no.7, pp.1867-1870, July 2008.
- [174] Nishamol M S, Sarin V P , G ijo Augustine, Deepu V, C K Aanandan, P Mohanan and K Vasudevan " Compact dual frequency dual polarized cross patch antenna with an X-slot", *Microwave and optical technology letters*, vol. 50, No.12, pp. 3198-3201, December 2008.
- [175] S. S. Oh and L. Shafai, "Investigation into polarization of unloaded and loaded microstrip square-ring antennas," *IEEE Trans. Antennas Propag.*, vol. 56, no. 10, pp. 3129–3135, 2008.
- [176] S. I. Latif and L. Shafai, "Polarization Characteristics of Multiband Loaded Microstrip Annular Ring Antennas," *IEEE Trans. Antennas Propag.*, vol. 57, no. 9, pp. 2788–2793, 2009.
- [177] S. A. Rezaeieh, "Dual band dual sense circularly polarized monopole antenna for GPS and WLAN applications," *Electronics Letters*, vol. 47, no. 22, pp. 5–6, 2011.
- [178] G. Li, H. Zhai, T. Li, L. Li, and C. Liang, "A compact antenna with broad bandwidth and quad-sense circular polarization," *IEEE Antennas Wireless. Propag. Lett.*, vol. 11, pp. 791–794, 2012.
- [179] Xi-Wang Dai, Zhen-Ye Wang, Chang-Hong Liang, Xi Chen, and Li-Ting Wang, "Multiband and Dual-Polarized Omnidirectional Antenna for 2G/3G/LTE Applications," *IEEE Antennas Wireless. Propag Lett.*, vol. 12, pp. 1492–1495, 2013.
- [180] O. P. Falade, Y. Gao, X. Chen, and C. Parini, "Stacked-Patch Dual-Polarized Antenna for Triple-Band Handheld Terminals," *IEEE Antennas Wireless. Propag Lett.*, vol. 12, pp. 202–205, 2013.

- [181] X.-W. Shi, T. Wu, H. Bai, and P. Li, “Tri-band microstrip-fed monopole antenna with dual-polarization characteristics for WLAN and WiMAX applications,” *Electron. Lett.*, vol. 49, no. 25, pp. 1597–1598, Dec. 2013.
- [182] K. Saurav, D. Sarkar and K. V. Srivastava, “Dual-Polarized Dual-Band Patch Antenna Loaded With Modified Mushroom Unit Cell,” *IEEE Antennas Wireless. Propag Lett.* vol. 13, pp. 1357–1360, 2014.
- [183] T. Zhang, W. Hong, and K. Wu, “A Low-Profile Triple-Band Triple-Polarization Antenna with Two Triangular Rings,” *IEEE Antennas Wireless. Propag Lett.*, vol. 14, pp. 378–381, 2015.
- [184] W.-Q. Cao, “Compact dual-band dual-mode circular patch antenna with broadband unidirectional linearly polarized and omnidirectional circularly polarized characteristics,” *IET Microwaves, Antennas Propag.*, vol. 10, no. 2, pp. 223–229, Jan. 2016.

.....✂.....

Chapter **3**

METHODOLOGY

<i>Contents</i>	3.1 <i>Simulation tool: Ansys HFSS</i>
	3.2 <i>Antenna fabrication procedure</i>
	3.3 <i>Excitation technique</i>
	3.4 <i>Antenna measurement facilities</i>
	3.5 <i>Experimental procedures</i>

This chapter deals with the basic facilities employed for carrying out the investigations. The simulation, fabrication measurement tools and procedures utilized in the current research work are explained. Simulation and parametric studies were carried out using the FEM based simulation software Ansoft HFSS. The antenna prototypes were fabricated using the photolithographic procedure. Experimental measurements and observations were conducted using the Vector Network analyzer and Anechoic Chamber. A comprehensive description of the methodology adopted for each entity is described.

3.1 Simulation tool: Ansys HFSS

The use of efficient simulation software is essential for the successful achievement of our goals. The software used should facilitate the calculation of the location of the antenna's feed point, the optimization of the various dimensions as well as the theoretical behavior of the structure. The initial design and parametric studies of the antennas presented in this thesis prior to their actual fabrication and measurement are performed using the commercial software Ansys High Frequency Structure Simulator (HFSS) [1]. HFSS is a high-performance full-wave electromagnetic (EM) field simulator for arbitrary 3D volumetric device modeling based on the Finite Element Method (FEM). Simulation, modelling, visualization and automation have been integrated into an easy learn by yourself environment. The optimization of the location and dimensions of the structure and their parametric variation studies were performed with HFSS.

Simulating a structure in HFSS begins with the definition of the geometry of the system. This includes assigning the material properties and 3D or 2D boundary elements available in the HFSS windows. The suitable port excitation is selected from among wave port, lumped port incident wave scheme etc. An air filled radiation boundary of appropriate volume is defined around the system. The frequency sweep range and number of frequency points are then selected. Now the simulation engine is invoked. The results of simulation such as scattering parameters, radiation patterns and field distributions can be displayed on completion of the simulation. Optimization tools are available with the HFSS package which are very helpful for the designer to optimize the parameters and performance. The

scalar and vector representation of the E, H and J fields provide a better insight into the structure being designed [2].

The accuracy of the antenna dimension is very critical at microwave frequencies. Therefore photolithographic technique is used to fabricate the antenna. Photolithography is the process of transferring geometrical shapes from a photo-mask to a surface.

The CAD drawing of the antenna is printed on a high quality butter paper with a high resolution laser printer. The copper clad of suitable dimension is cleaned with a suitable chemical like acetone to remove any impurities. A thin layer of photo resist material is then applied over the copper clad using a high speed spinner. The antenna mask is carefully aligned over the photo resist coated clad and exposed to UV. Extreme care must be taken to ensure that no dust or impurities are present in between the mask and copper clad. The layer of photo resist material in the exposed portions hardens, while the unexposed region remains unaffected and it can be removed by carefully rinsing with a suitable developer solution. The unwanted copper over the copper clad can be removed by processing the copper clad in a ferric chloride (FeCl_3) solution. The laminate is then cleaned to remove the hardened photo resist using acetone solution.

3.2 Antenna fabrication procedure

A brief account of the steps in the fabrication of the prototypes of the different antennas is presented in this section.

3.2.1 Substrate selection

The initial and important step in the fabrication process is the selection of the suitable substrate. There is no ideal substrate but it should be selected

such that its electrical and material properties match with the required application. Material parameters like dielectric constant and loss tangent are critical. In this work, since the feed is coaxial probe, a double sided substrate is required. Materials like Polytetrafluoroethylene (PTFE), polystyrene, polyolefin, polyphenylene, alumina, sapphire, quartz, ferromagnetic, rutile, RT Duroid and semiconductor substrates present a wide range for commercially available substrates. PTFE and quartz possess good radiation efficiency and excellent electrical performance, but these substrate materials are often expensive. Flexible substrate materials are also available, so that the antenna can be mounted on curved surfaces. Surface waves will be excited in high dielectric constant substrates which will cause spurious radiations in unwanted directions from the antenna. A low relative permittivity, low dielectric loss material is essential to reduce the propagation delay and to increase the signal speed. In addition the material should have high thermal conductivity for dissipating heat. Other important substrate characteristics include the thickness, homogeneity, isotropicity and dimensional strength. In this work, FR4 a low cost, easily available and widely used substrate material for microwave applications was chosen for effortless fabrication of the antenna prototype [3-7].

3.2.2 Photolithography

Photolithography or Optical Lithography is the process of transferring geometric shapes from a photo-mask to the surface of a substrate. Once the proper selection of the suitable substrate has been made, the actual printing and fabrication of the prototype is performed using photolithography. The major procedures involved in this technique are explained below. The first step is the computer aided design generation of the geometry to be

generated. A negative mask of the geometry so designed is then printed on a transparent butter paper.

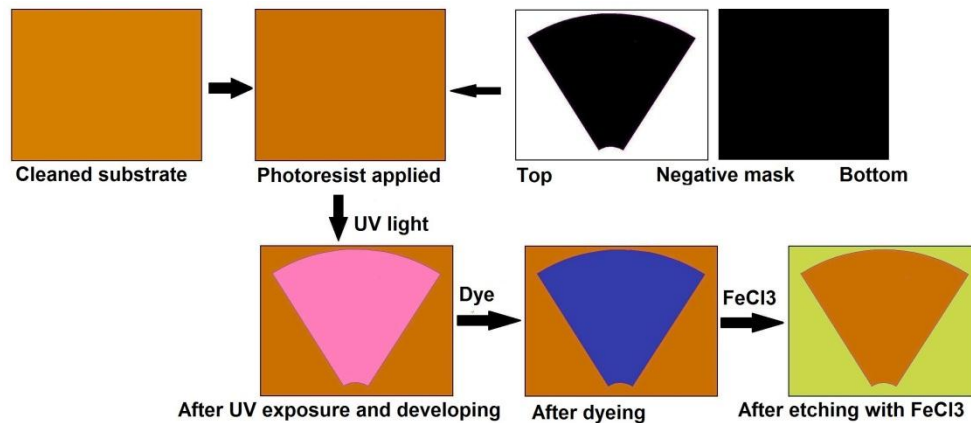


Fig. 3.1. Different steps in the prototype fabrication

A double sided copper clad substrate piece of suitable dimension is thoroughly cleaned and dried so as to remove any dust or impurities whose presence might produce small discontinuities on the copper traces etched on the substrate. Any disparity in the etched structure will shift the resonant frequency from the predicted values, especially when the operating frequency is very high. A thin layer of negative photo resist which is a 1:1 mix of negative photoresist solution and thinner is coated using spinning technique on the substrate surface and is dried. The mask is placed onto the photo resist-coated substrate. The substrate is exposed to ultraviolet (UV) light through the mask for an appropriate time interval. After the proper UV exposure the layer of photo-resist material on the exposed portions hardens. The board is immersed in developer solution for a few minutes and then washed with water. The hardened portions will not be washed out by the developer solution. The board is then dipped in dye ink solution in order to

clearly view the hardened photo resist portions on the copper coating. After this developing phase is over, the unwanted copper portions are etched off by dipping the substrate in Ferric Chloride (FeCl_3) solution for a few minutes. The desired antenna geometry is now clearly printed on the substrate. The etched board is rinsed in running water to remove any etchant. The laminate is then cleaned carefully to remove any hardened photo resist using acetone solution. The various steps involved in the fabrication process are illustrated in Fig. 3.1.

3.3 Excitation technique

In this research work, a coaxial probe feed was used to excite the dominant resonant modes of the patch. The feed point with optimum matching was located on the patch using the simulation software. A via hole was drilled and the SMA connector was soldered into position with the central conductor to the patch on top and the outer conductor to the ground plane on the bottom side as shown in Fig. 3.2.

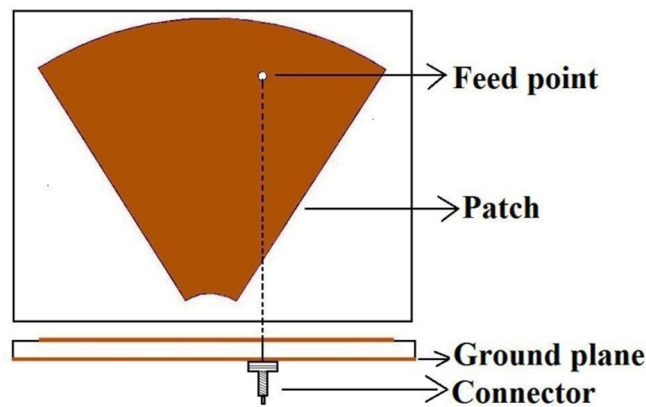


Fig. 3.2. Coaxial probe feed

3.4 Antenna measurement facilities

The measurement setup for antenna characteristics such as return loss, radiation pattern and gain is briefly explained in this section along with the measurement procedure description. The important mechanical systems used for the antenna characterization are the Vector network Analyzer (VNA), Anechoic Chamber and Automated turn table etc. The indigenously developed CREMA SOFT is used for the automatic measurement of the radiation properties of the antenna.

3.4.1 Performance network analyzer PNA E8362B

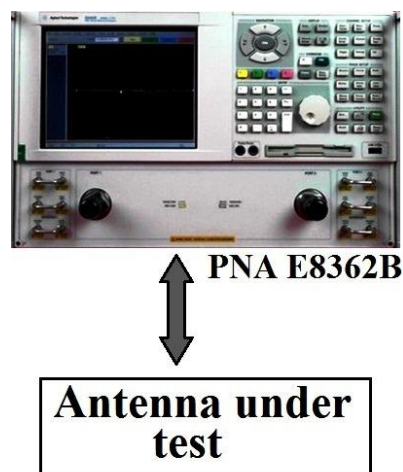


Fig. 3.3. E8362B performance Network Analyzer

The Agilent (currently known as Keysight Technologies) E8362B PNA (Performance Network Analyzer) provides excellent performance, advanced automation features, flexible connectivity and is easy to use [8]. The PNA E8362B is widely preferred by antenna designers and engineers owing to its fast sweep speed, wide dynamic range, and low trace noise and flexible connectivity options for testing high performance components.

The important specifications and features of the network analyzer are:

- 10 MHz to 20 GHz operating frequency range
- IF Bandwidth 1Hz to 40KHz
- 123 dB dynamic range and <0.006 dB trace noise
- Display range of ± 200 dB magnitude
- Intel Pentium 1.1 GHz Processor with 1 GB RAM
- USB, LAN, GPIB I/O ports
- Windows XP operating system
- Measurement speed of <26 μ s/point
- 32 channels, 16,001 points
- Operating temperature range of 0 to 40⁰C
- RF Connector 3.5mm, 50 Ω
- TRL/LRM calibration, on-wafer, in-fixture, waveguide, and antenna measurements
- Log or linear magnitude, SWR, phase, group delay, real and imaginary, Smith chart, polar formats
- Mixer conversion loss, return loss, isolation, and absolute group delay
- Amplifier gain compression, harmonic, IMD, and pulsed-RF
- Measurement Automation Software CREMA Soft

The analyzer works on Windows operating system with a user interface mouse. This provides a user friendly and easy measurement procedure for the designer. The measurement setup with the PNA is shown

in Fig.3.3. In this work, this network analyzer is used to measure the all the scattering parameters, axial ratio and radiation patterns.

3.4.2 Anechoic chamber

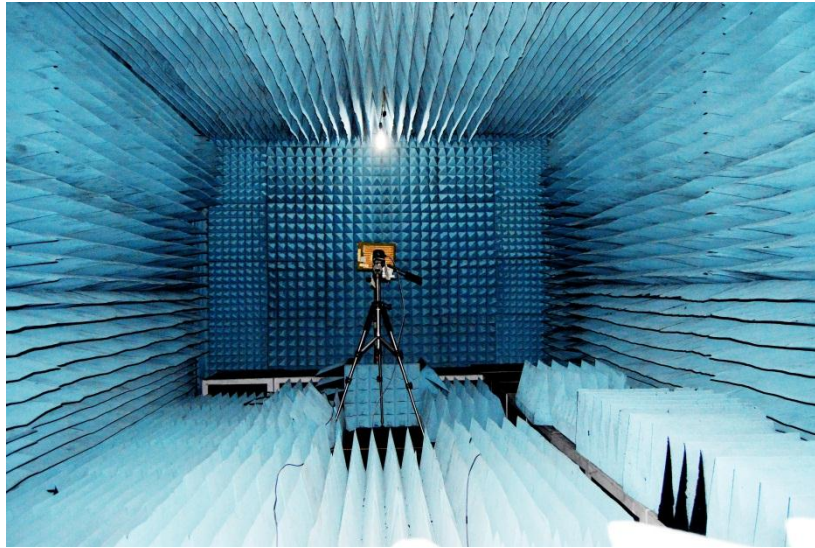


Fig. 3.4. Anechoic Chamber

Anechoic chamber provides the indoor free space environment required for antenna pattern measurements. It forms a “quiet zone” free from all types of electromagnetic interferences [9]. It is a large room compared to the wave length of operation, whose walls, roof and floor are lined with microwave absorbers to suppress the electromagnetic reflections. The absorbers are made of high quality low density carbon black impregnated polyurethane foam. The tapered pyramidal shape of the absorbers provide good impedance matching for the microwave power impinging upon it while the dispersed carbon provides the required attenuation, for a wide frequency range of 1GHz to 18GHz. The chamber is surrounded by aluminum sheet on all the sides to prevent external electromagnetic interferences. All

the antenna characterizations in this study are carried out in this chamber whose photograph is shown in Fig.3.4.

3.4.3 Automated Turn table assembly and software for far field radiation pattern measurement

The turn table assembly kept inside the anechoic chamber at the far field region consists of a stepper motor driven rotating platform on which the Antenna under Test (AUT) is mounted. The AUT is rotated by the indigenously developed, microcontroller based antenna positioner STIC 310C for radiation pattern and antenna gain measurement. The AUT is the receiver while a standard wideband horn (1-18GHz) is used as the transmitter for radiation pattern measurements. All the measurements are synchronized and coordinated by the MATLAB based in-house automation software 'Crema Soft'. Through the general purpose interface bus (GPIB), the robust instrument control toolbox of the package communicates with the stepper motor control and Network Analyzer. Calibration, antenna measurements and material characterization of the substrate used can be performed using this automated software.

3.5 Experimental procedures

The antenna characteristics like resonant frequency, S-parameters, bandwidth, gain, polarization, and radiation pattern are experimentally measured through a set of predefined procedures which are discussed in the following sections. The network analyzer need to be calibrated against losses associated with the different cables and connectors accompanying the equipment. Known standards of open, short and matched loads are used for this calibration in order to maintain accuracy of measurement. Common

calibration procedures used are single port, full two port and TRL calibration methods. Single port calibration is best suited for measurement of reflection coefficient, VSWR and input impedance, while the two port S parameters can be accurately measured using TRL calibration method. To ensure that the reference plane for all measurements in the desired band is actually at 0°, proper phase delay is introduced while calibrating.

3.5.1 Measurement of S parameters, resonance frequency and bandwidth

The Scattering parameter S11 or Reflection coefficient (Γ) at the antenna input is the ratio of the reflected voltage or current to the incident voltage or current with the antenna connected at the port 1 of the network analyzer. It expresses the degree of impedance mismatch between the antenna and the source line in terms of the input VSWR or return loss. The return loss (RL) expressed as $RL = -20\log(|\Gamma|) = -20\log(|S_{11}|) = -|S_{11}|$ (dB) is the ratio of the reflected power to the incident power. The antenna is connected to any one port of the network analyzer and the VNA is operated in the S11/S22 mode to measure the return loss characteristic. Using the short, open and matched load the port is calibrated for the required frequency range. The AUT is now connected to the calibrated port of the VNA. The magnitude and phase of the measured S11 versus frequency is then stored on the computer using the 'Crema Soft' automation software in comma separated variable (.csv) format. While S11 or S22 indicate the return loss at port 1 or port 2, S21 indicates transmission coefficient or the isolation between the ports 1 and 2 of the antenna. The frequency at which the curve shows the maximum dip (minimum value of return loss) gives the resonant frequency (f_r) of the antenna.

The range of frequencies for which the return loss value is within the -10dB points is usually treated as the 2:1 VSWR bandwidth of the antenna. This is because $VSWR = 2$ corresponds to reflection coefficient $\Gamma = \frac{VSWR+1}{VSWR-1} = \frac{1}{3}$ which gives $RL = -20 \log (1/3) = -10$ dB. Thus the 2:1 VSWR bandwidths at the two ports are calculated by observing the range of frequencies (Δf_r) for which the return loss remains ≤ -10 dB. The fractional bandwidth is calculated as $\frac{\Delta f_r}{f_r}$. Expressed as a percentage, it is given by % band width = $\frac{\text{bandwidth}}{\text{centre frequency}} * 100$. The input impedance of the AUT at the resonant frequencies can be determined directly from the Smith Chart display in the network analyzer in which, after the calibration the centre corresponds to 50Ω .

3.5.2 Radiation pattern

The setup inside the anechoic chamber as shown in Fig.3.4 is used for determining the radiation pattern. The AUT connected as receiver to one port of the VNA is placed in the quiet zone of the chamber on the automated turn table. The transmitter is a standard wideband horn antenna connected to the other port of the network analyzer. A STIC positioner controller controls the turn table. The Crema Soft software coordinates the automated radiation pattern measurement.

The principal E and H-plane radiation patterns (with both co and cross polar pattern) of the AUT are measured by keeping the network analyzer kept in S21/S12 mode with the frequency range within the -10dB return loss bandwidth. The number of frequency points, start stop and step angles of the motor can be conveniently configured in Crema Soft. The antennas are

aligned at boresight for maximum reception by manual adjustment of the positioner. Now a THRU calibration for the frequency band of interest is performed and saved in the CAL set. In order to avoid any spurious reflections that might corrupt the measured data, suitable gate parameters are provided in the time domain. Crema Soft automatically performs the radiation pattern measurement and stores it as a file in comma separated variable (.csv) format in the remote computer.

3.5.3 Antenna gain and efficiency

Gain of an antenna is defined as the ratio of the intensity of its radiation in the direction in which it is strongest, to that of a reference antenna, when both antennas are fed with the same input power. If an isotropic antenna is the reference, the gain is expressed in units of dBi. The gain of an antenna is a passive phenomenon. Power is not added by the antenna, but simply redistributed to provide more radiated power in a certain direction than would be transmitted by an isotropic antenna.

The gain comparison method [10-11] is used to measure the absolute gain of the AUT where the experimental setup is identical to that of the radiation pattern measurement. A standard wideband horn antenna, whose gain chart is available, is used as the reference antenna. The reference antenna is bore sighted using the antenna positioner and THRU calibrated for the frequency range of interest. The horn antenna is then replaced by the AUT aligned in the main beam direction and the transmission coefficient S_{21} (dB) is measured. This gives the value of the relative gain of the antenna with respect to the reference antenna. This relative gain is added to the original gain of the standard antenna, provided by the manufacturer in the gain chart to get the absolute gain.

Antenna efficiency as per IEEE definition is the ratio of the total power radiated by the antenna to the net power accepted by the antenna at its terminals during the radiation process [12]. The Wheeler cap method is the conventional technique used to measure the efficiency of narrowband antennas [13-14] which involves making two impedance measurements: one with the conducting cap enclosing the antenna and the other without the cap. A conducting cylindrical box is used for the Wheeler cap, whose radius is the radius of the antenna and which completely encloses it. The input impedance of the AUT is measured with and without the cap using network analyzer. As the test antenna behaves like a series resonant RLC circuit near its resonance, the efficiency is calculated by the following expression:

$$\text{Efficiency, } \eta = \frac{R_{\text{nocap}} - R_{\text{cap}}}{R_{\text{nocap}}}$$

where, R_{nocap} denotes the input resistance without the cap and R_{cap} is the resistance with the cap.

3.5.4 Polarization

The experimental setup for polarization measurement is similar to that of the radiation pattern. The AUT is arranged in the transmitting mode and the wide band horn is kept as receiver. RF signal input is applied to the AUT and the power received by the wide band horn in the vertical plane is stored as a function of frequency. The transmitting antenna is then rotated through 90° and the received power as a function of frequency in the horizontal plane is measured. The measured data in both the planes is analyzed to find the polarization of the test antenna throughout the entire band of operation.

3.5.5 Axial ratio

The experimental set up is identical to that for radiation pattern measurement. The AUT is connected to port 2 and is kept stationary. The standard horn connected to port 1 as transmitting antenna is rotated on its own axis and the maximum and the minimum values of power received at port 2 are noted. For any particular frequency, the difference between the two values of power gives the axial ratio i.e., Axial Ratio (AR) = Maximum Power in dB – Minimum Power in dB. The procedure is repeated for all the frequency points at regular intervals in the frequency band of interest. A graph is plotted between the frequency and difference power in dB. The 3dB axial ratio bandwidth (ARBW) can be calculated from the graph as the range of frequencies for which the power is below 3dB. The frequency where the minimum axial ratio value is obtained is defined as the CP centre frequency.

References

- [1] <http://www.entuple.com/product/ansys-hfss-hf-bundle>.
- [2] HFSS User's manual, version 13, Ansoft Corporation.
- [3] J Youngs, G. C. Stevens and A. S. Voughan, "Trends in dielectric research: an international review from 1980-2004," J.Phys. D: Appl. Phys, pp 1267-1276, 2006.
- [4] M.G.Pecht, G.R Agarwal, P.McCluskey, T.Dishongh, S. Javadpour and R.Mahajan, "Electronic Packaging Materials and there properties", CRC Press, London, 1999.
- [5] T.Hu,J, Juuti, H. Jantunen and T. Vilkmán, "Dielectric properties of BST/Polymer composites", J.Eur.Ceram.Soc, pp 3997-4001, 2007.
- [6] D.D.L.Chung, "Materials for Electronic Packaging," Butterworth Heinemann, Washington, 1995.

- [7] M.T. Sebastian, “Dielectric materials for wireless communications”, Elsevier Publishers., UK, 2008.
- [8] <http://www.keysight.com>.
- [9] E. J.Zachariah, K. Vasudevan, P. A. Praveen Kumar, P. Mohanan and K. G.Nair, “Design, Development and Performance Evaluation of an Anechoic Chamber for Microwave Antennas Studies”, Indian Journal of Radio and Space Physics, Vol. 13, pp. 29-31, February 1984.
- [10] C. A. Balanis, “Antenna Theory: Analysis and Design”, Second Edition, John Wiley & Sons Inc. 1982.
- [11] John D. Kraus, “Antennas”, McGraw Hill International, second edition, 1988.
- [12] IEEE standard test procedures for antennas (IEEE Std 149{1979}). New York: IEEE. 22.
- [13] H.A Wheeler, “The Radiansphere around a small antenna”, in Proc. IRE, , pp 1325-1331, August 1959
- [14] Hosung Choo, Rogers, R., Hao Ling, “On the Wheeler cap measurement of the efficiency of microstrip antennas”, IEEE Transactions on Antennas and Propag., Volume 53, Issue 7, pp:2328 – 2332, July 2005.

.....❧.....

DESIGN AND ANALYSIS OF DUAL BAND SECTORAL PATCH ANTENNA WITH CORNER TRUNCATIONS

<i>Contents</i>	4.1 <i>Introduction to compact dual polarized multiband antennas</i>
	4.2 <i>Coaxial probe fed circularly polarized circular disc sector patch antenna</i>
	4.3 <i>Corner truncated circular disc sector patch antenna</i>
	4.4 <i>Circularly polarized sectoral patch antenna for WLAN application</i>
	4.5 <i>Wideband circularly polarized circular disc sector patch antenna for WiMAX applications</i>
	4.6 <i>Dual band corner truncated sectoral patch antennas with dual slits for GPS and WLAN</i>
	4.7 <i>Chapter summary</i>

The design procedure of a dual band sectoral patch antenna with different polarizations in the two resonance bands is portrayed in this chapter. Corner truncation method has been employed to achieve compactness and improvement of the circular polarization characteristics. The design equations derived have been validated with different substrates and at several fundamental frequencies of operation. Extensive parametric analysis has been carried out to investigate the various antenna characteristics. The technique of etching slits in the patch boundary has been successfully utilized to conveniently tune the operating frequency to the desired band. All the designs have been simulated and verified experimentally.

4.1 Introduction to compact dual polarized multiband antennas

Wireless Communication scenario has attained steady advancement along with the progress in antenna design and technology. The operating frequencies have also gradually been raised to higher regions; from MF and HF bands to VHF, UHF, and SHF in recent years. A major trend in the recent antenna technology is the miniaturization of antenna systems, which can function with greater intricacy and sophistication. The newly deployed wireless communication systems, especially the mobile communication devices saw the utilization of a wide variety of compact antennas. The mobile phone technology has reached the fifth generation where smart phones, palmtops and handy tablets have become indispensable in our day to day life. The antennas used in such devices are also required to operate in two or more frequency bands which may or may not be close to each other. For example, multiple functionality devices like smart phones and handheld tablets operate at different commercial frequency bands like UMTS, WiMAX and WLAN simultaneously. Microstrip patch antennas are in great demand for such applications due to its characteristics of low profile, lightweight, ease of integration and fabrication. A single microstrip antenna can provide compactness and dual or triple band performances. The polarizations in these frequency bands can also be preferably diverse i.e., a combination of linear or circular polarizations. Circular polarization (CP) is more preferred in mobile communication antennas as such CP antennas can minimize the multipath effect and are insensitive to the transmitter-receiver orientation. Hence it is much desirable to have circular polarization in at least one of the bands in a single multi band antenna. In this chapter, the main concern is to develop a compact dual polarized dual band patch antenna for the various commercial frequency bands.

4.2 Coaxial probe fed circularly polarized circular disc sector patch antenna

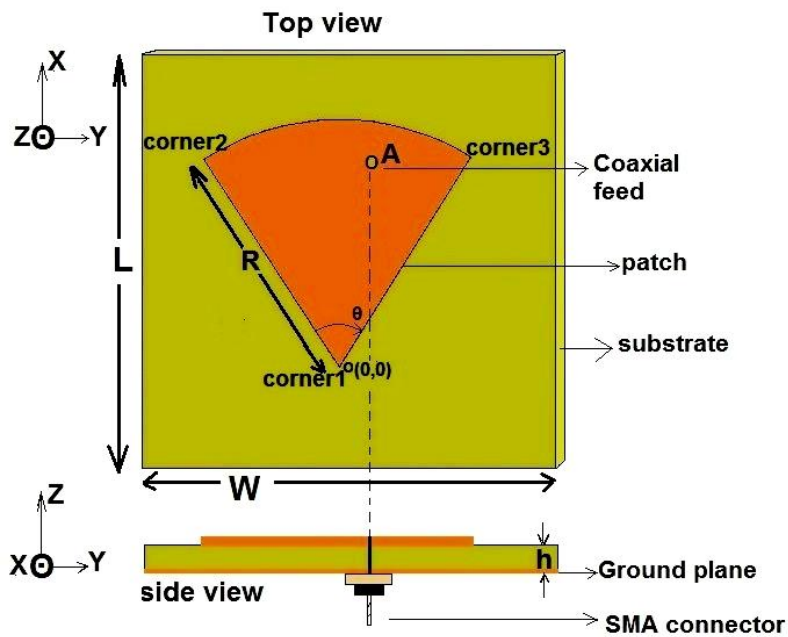


Fig. 4.1. Coaxial probe fed circular disc sector patch antenna
 ($L=W=75$, $R=45$, $h=1.6$ (all in mm), $\theta = 65^\circ$, $A (37.4, 6.27)$, $\epsilon_r=4.4$)

Although the microstrip patch can assume any contour with square, ring and circular shapes being the most common, the circular disc sector geometry is chosen as the theme of this work owing to its suitability as a simple geometry that can generate CP radiation using a single probe feed. The circular disc sector patch shape is a specific fraction of a complete circular disc i.e.; a circular disc patch with a specific flare angle [1]. Though the coaxial probe feed point can be chosen anywhere along the patch area, it was positioned at a point where the two orthogonal modes TM_{10} and TM_{01} at near degenerate frequencies are excited around 2 GHz. The specific flare angle at which these modes are excited was obtained through software simulation.

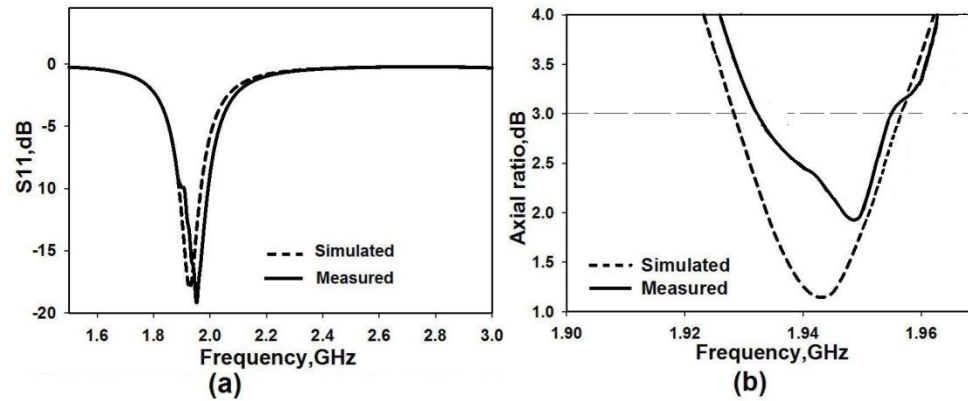


Fig. 4.2. Simulated and Measured a) S_{11} b) Axial ratio characteristics of the coaxial probe fed circular disc sector patch antenna ($L=W=75$, $R=45$, $h=1.6$ (all in mm), $\theta = 65^\circ$, $A (37.4, 6.27)$, $\epsilon_r=4.4$)

The geometry of the sectoral patch antenna with single coaxial probe feed is shown in Fig.4.1. The patch is printed on a FR4 dielectric substrate of $\epsilon_r = 4.4$ and thickness $h = 1.6$ mm. The ground plane of size W mm x L mm covers the opposite side. The simulated and measured reflection coefficient, and axial ratio characteristics are shown in Fig.4.2. A 2:1 VSWR bandwidth of 1.89 – 1.97 GHz (80 MHz) is obtained. The axial ratio characteristics show a CP bandwidth of 1.2% (25MHz). The simulated and measured characteristics show good agreement. The feed is given coaxially at point A, which is adjusted through simulation to get the optimum impedance for CP. The impedance plot shown as smith chart in Fig.4.3 is a simple way to recognize whether the feed position is the optimal one for good CP radiation. The small ‘kink’ or dip in the plot corresponds to the excitation of two orthogonal modes, yielding the best minimum axial ratio at this CP centre frequency (f_c). The presence of a small loop instead of the kink indicates an inferior axial ratio value. In this antenna the feed position of A (37.4, 6.2) offers the best CP performance as seen from Fig.4.3.

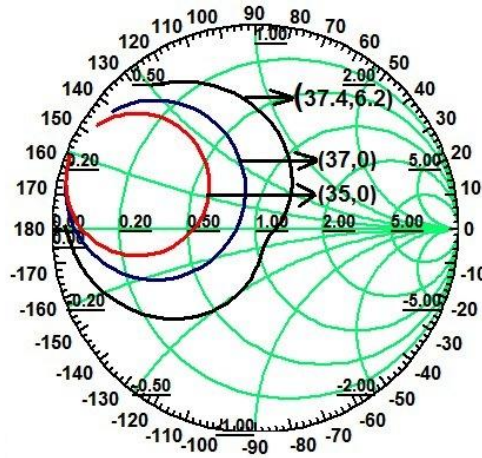


Fig. 4.3. Simulated input impedance variation of the coaxial probe fed circular disc sector patch antenna for different feed positions. ($L=W=75$, $R=45$, $h=1.6$ (all in mm), $\theta = 65^\circ$, $\epsilon_r=4.4$)

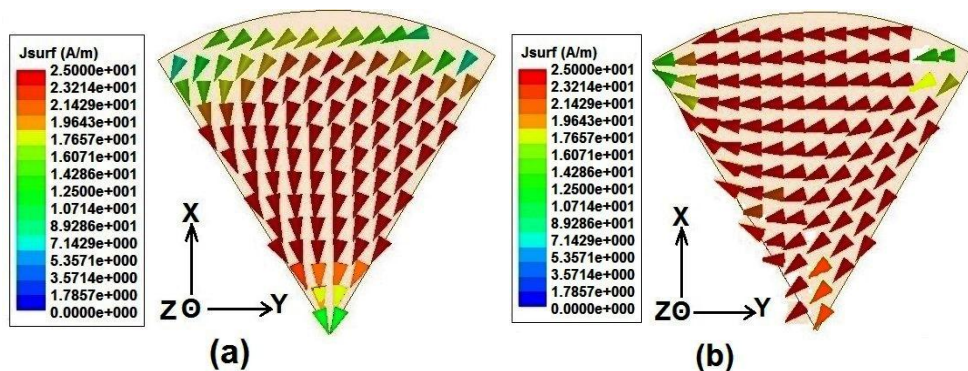


Fig. 4.4. Surface current distribution on the coaxial probe fed circular disc sector patch antenna at a) 1.92 GHz b) 2.1 GHz. ($L=W=75$, $R=45$, $h=1.6$ (all in mm), $\theta = 65^\circ$, $A (37.4, 6.27)$, $\epsilon_r=4.4$)

The simulated surface current distribution on the patch in Fig. 4.4 shows that the CP radiation is the result of the excitation of two orthogonal near-degenerate modes at 1.92 GHz and 2.1 GHz respectively. The polarization is along Y axis for 1.92 GHz and along X axis at 2.1 GHz. The flare angle theta (θ) is varied to obtain the best performance of CP with respect to the < 3 dB axial ratio characteristic as shown in Fig. 4.5.

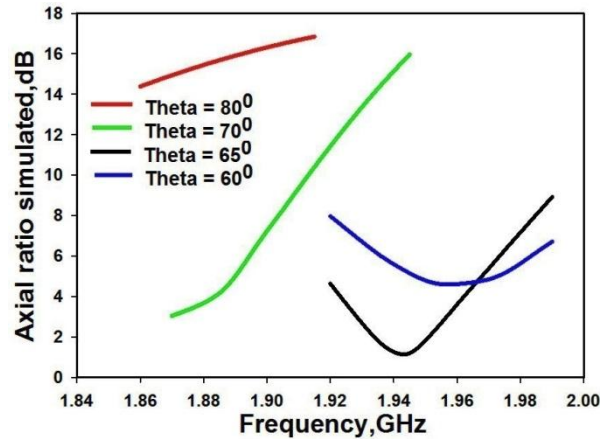


Fig. 4.5. Axial ratio variation of the coaxial probe fed circular disc sector patch antenna for different flare angles. ($L=W=75$, $R=45$, $h=1.6$ (all in mm), $\theta = 65^\circ$, $\epsilon_r=4.4$)

4.3 Corner truncated circular disc sector patch antenna

Dual frequency operation being of utmost importance in wireless communication, this aspect of the sectoral patch antenna is studied in detail in the following section.

4.3.1 Dual band dual polarized circular disc sector patch antenna

The geometry of the disc sector patch antenna with two corner truncations is shown in Fig.4.6. The effects of the two corner truncations are separately studied. Resonances are obtained at the centre frequencies of 1.995 GHz and 3.545 GHz. The feed point is adjusted to obtain perfect matching and minimum axial ratio value. Orthogonal modes of TM_{10} are excited at two near-degenerate frequencies of 1.98 GHz and 2 GHz for circularly polarized radiation at the UMTS (1.92-2.17 GHz) band. The second resonance at 3.545 GHz is due to the excitation of the higher order TM_{20} mode. At the WiMAX (3.3-3.7 GHz) band, the radiation is linearly polarized and directed along the Y axis.

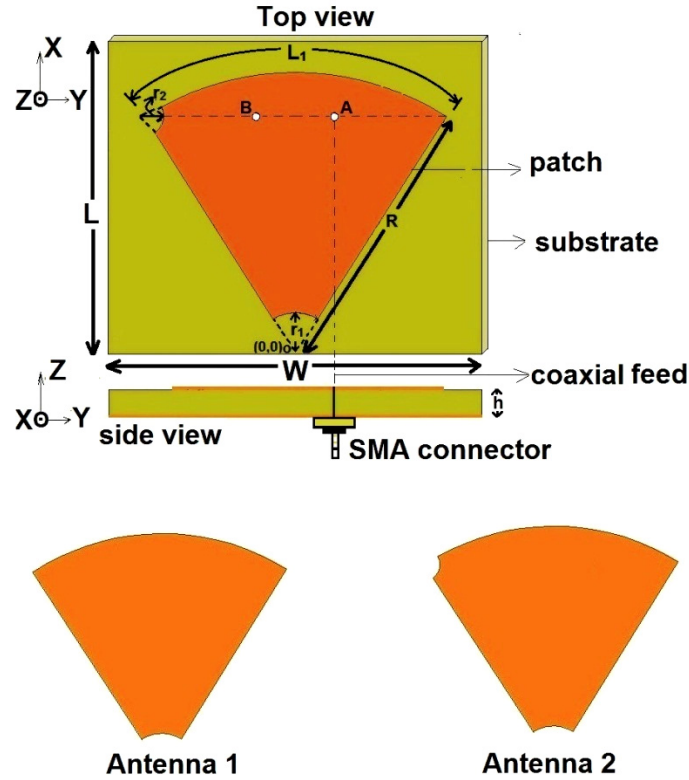


Fig. 4.6. Geometry of the two corners truncated disc sector patch antenna ($L=W=50$, $R=45$, $L_1=51$, $r_1=7$, $r_2=3$, $h=1.6$ (all in mm), $A(37,7)$, $\epsilon_r=4.4$)

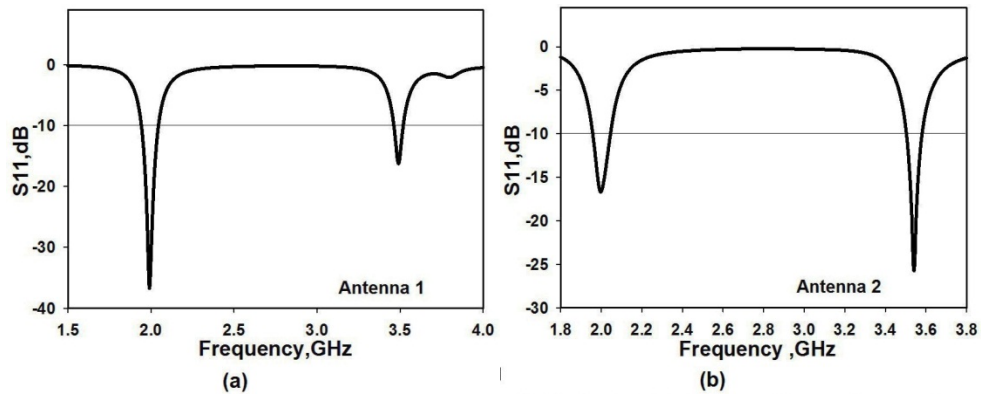


Fig. 4.7. Simulated reflection coefficients of Antenna 1 and Antenna 2 ($L=W=50$, $R=45$, $L_1=51$, $h=1.6$, $r_1=7$, $r_2=3$, $h=1.6$ (all in mm), $A(37,7)$, $\epsilon_r=4.4$)

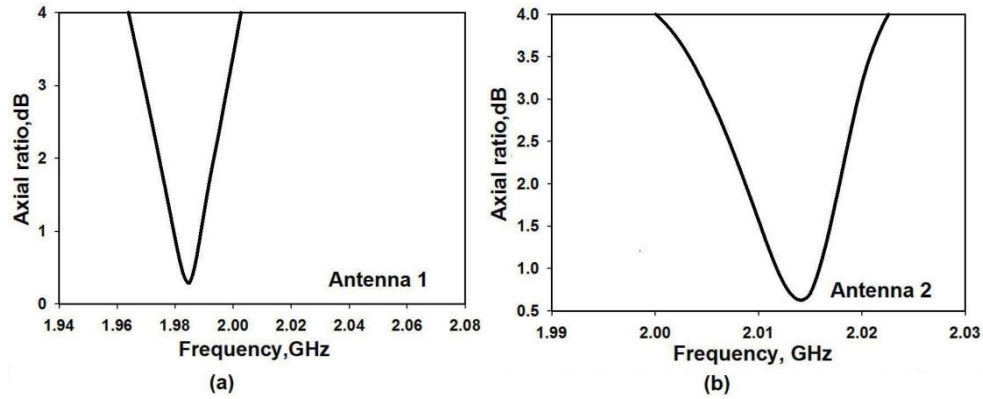


Fig. 4.8. Simulated axial ratio characteristics of Antenna 1 and Antenna 2
($L=W=50$, $R=45$, $L_1=51$, $r_1=7$, $r_2=3$, $h=1.6$ (all in mm), $A(37,7)$, $\epsilon_r=4.4$)

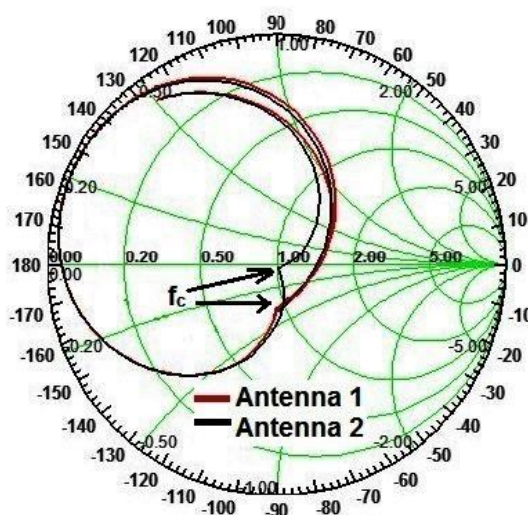


Fig. 4.9. Input impedance characteristics of Antenna 1 and Antenna 2
($L=W=50$, $R=45$, $L_1=65^\circ$, $r_1=7$, $r_2=3$, $h=1.6$ (all in mm), $\epsilon_r=4.4$)

The simulated reflection coefficient and axial ratio characteristics of the structures designated Antenna 1 and Antenna 2 are illustrated in Figs. 4.7 and 4.8 respectively. The input impedance characteristics of these two structures depicted in Fig. 4.9 exhibit the kink in the curves indicating the merger of two near-degenerate modes at the centre frequencies of 1.995 GHz and 2.005 GHz respectively. The simulated current distributions

and the three dimensional radiation patterns of the two structures at the two centre frequencies are shown in Figs. 4.10 and 4.11 respectively.

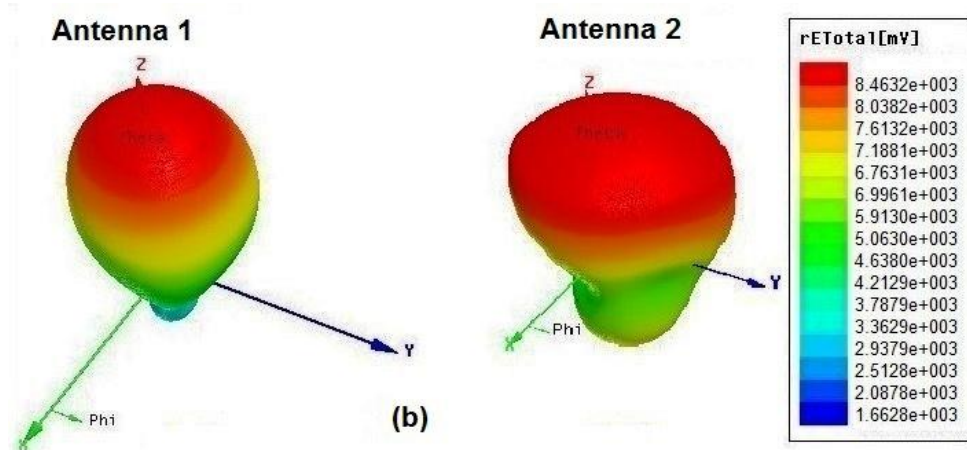
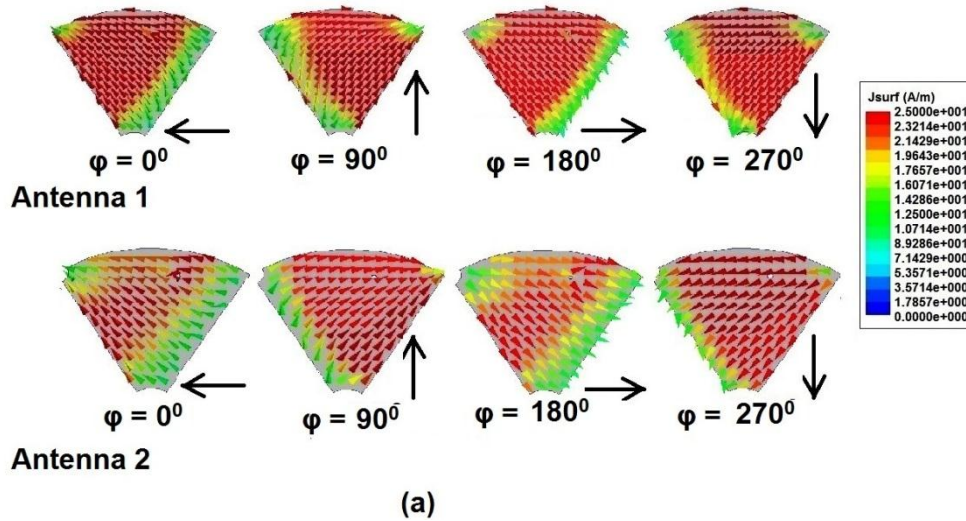


Fig. 4.10. a) Surface current distribution on the corner truncated sectoral patch antenna on Antenna 1 and Antenna 2 at 1.99 GHz b) 3D radiation pattern on Antenna 1 and Antenna 2 at 1.99 GHz ($L=W=50$, $R=45$, $L_1=51$, $r_1=7$, $r_2=3$, $h=1.6$ (all in mm), $\epsilon_r=4.4$)

The sector shaped truncations at the corners improve the compactness of the structures Antenna 1 and Antenna 2, as compared to the original unmodified circular disc sector patch. The ground plane size is optimized and the overall size reduction is 55%. The truncations modify the current paths so that the CP radiation is not affected, except for a slight shift in the frequency towards the upper side of the band. This is expected since the patch area is reduced by 2.755%. The two resonances still remain within the respective frequency ranges as seen from Figs.4.7 and 4.8.

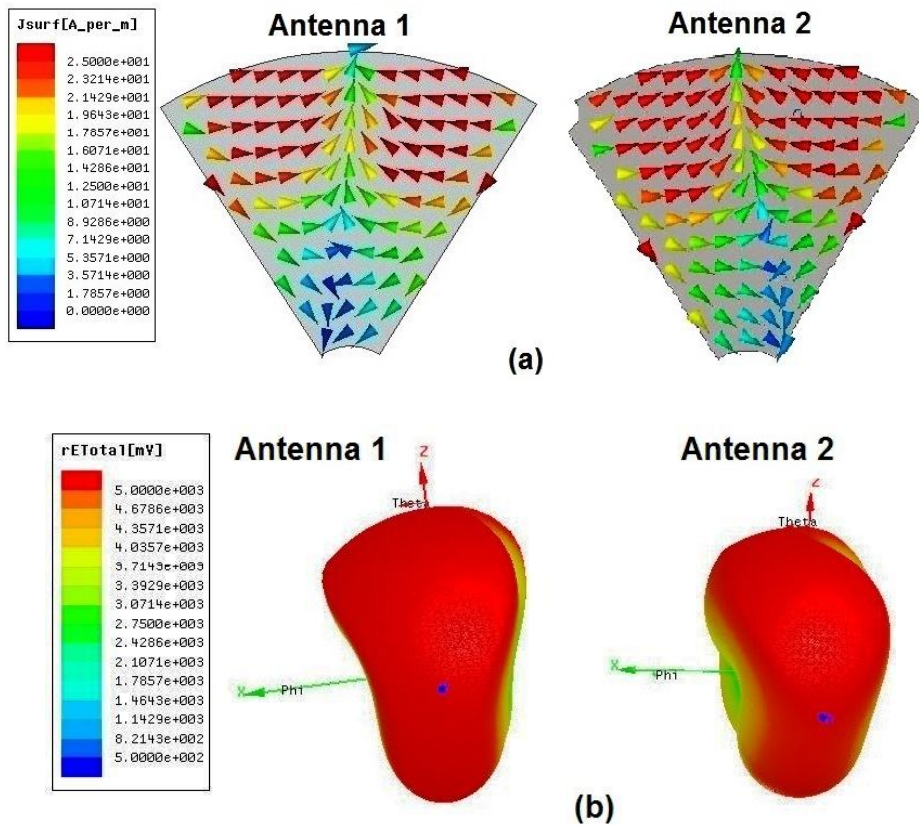


Fig. 4.11.a) Surface current distribution on the corner truncated sectoral patch antenna on Antenna1 and Antenna2 at 3.5 GHz **b)** 3D radiation pattern on Antenna1 and Antenna2 at 3.5 GHz ($L=W=50$, $R=45$, $L_1=51$, $r_1=7$, $r_2=3$, $h=1.6$ (all in mm), $\epsilon_r=4.4$)

4.3.2 Parametric analysis

4.3.2.1 Effect of corner truncation r_1

The effect of the corner truncation r_1 at corner 1 was studied in detail. The truncation r_1 modifies the current paths such that the near degenerate orthogonal modes of TM_{10} produce circularly polarized radiation without any deterioration in the characteristics. The resonance frequencies f_{c1} and f_{c2} are shifted from 1.95 GHz and 3.45 GHz to 1.99 GHz and 3.5 GHz respectively in the two bands, as is obvious from the reflection and axial ratio characteristics before and after the truncation in Figs.4.12a and 4.12b.

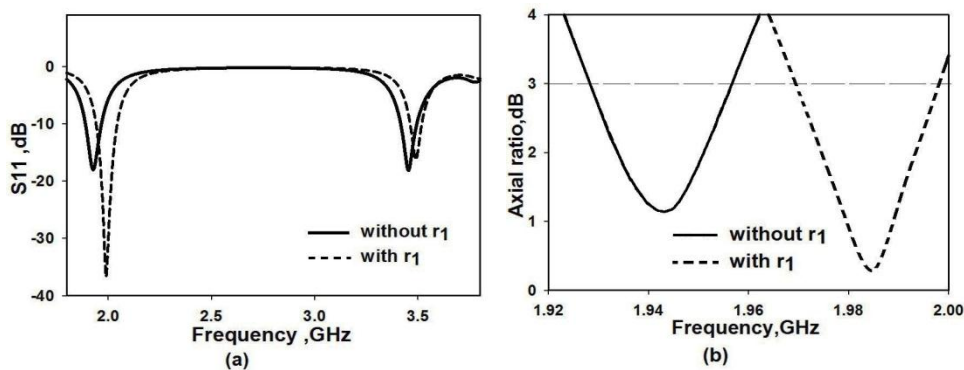


Fig. 4.12. a) Reflection coefficients and b) axial ratio of Antenna 1 with and without truncation r_1 ($L=W=50$, $R=45$, $L_1=51$, $h=1.6$, $r_1=7$ (all in mm), $\epsilon_r=4.4$)

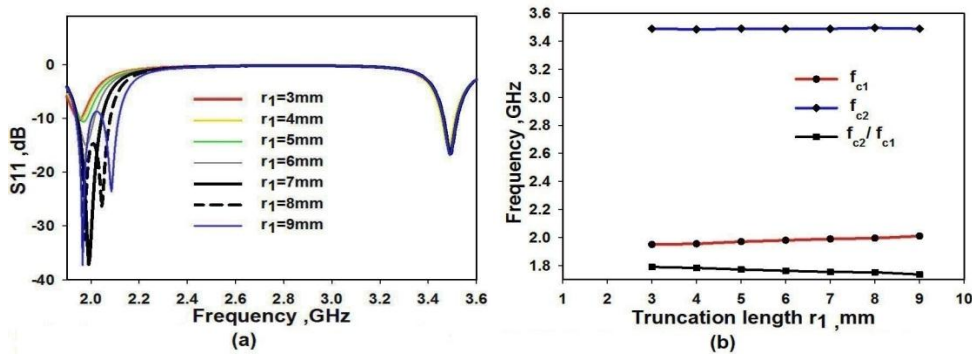


Fig. 4.13. Variation of a) reflection coefficients and b) frequency ratio with truncation length r_1 of Antenna 1 ($L=W=50$, $R=45$, $L_1=51$, $h=1.6$, $r_1=7$ (all in mm), $\epsilon_r=4.4$)

An axial ratio bandwidth of 1.3% was obtained with $r_1=7\text{mm}$. To enable a clear view of the effect of the truncation r_1 on the antenna performance, the antenna design is carried out for varying dimensions of r_1 in terms of its length and flare angle. The results are tabulated in Table 4.1.

The truncation length r_1 is varied from 3mm to 9mm and the impacts on the two resonance bands are analyzed. The variations in the S11 characteristics and the resonance frequencies of the two bands are shown in Fig. 4.13a and 4.13b. There is very small shift in the centre frequency (f_{c1}) of Band 1 while the second band centre frequency (f_{c2}) remains unaffected by this truncation. As a result, the frequency ratio remains almost constant as seen in Fig. 4.13b. The reason for this little or no change in both resonance frequencies is the occurrence of a minimum or null at the region near corner 1 in Antenna 1 for all phase angles ϕ as observed from the simulated current distribution plots in Fig. 4.10 and 4.11.

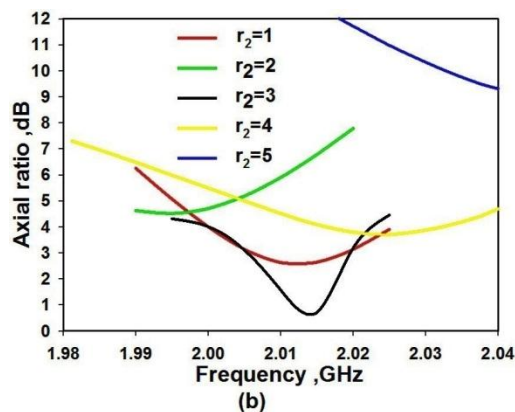


Fig. 4.14. Variation of axial ratio characteristics with truncation length r_1 of Antenna 1 ($L=W=50$, $R=45$, $L_1=51$, $h=1.6$, $r_1=7$ (all in mm), $\epsilon_r=4.4$)

It is also seen that at smaller values of r_1 , the impedance matching of Band 1 is poor but improves to optimum value with increase in r_1 . However;

the impedance matching and bandwidth at Band2 is hardly affected by the truncation r_1 . Impedance bandwidths of 5.5% and 1.86% respectively are obtained in the two bands. This is a salient feature of the proposed design.

The orthogonal dimensions of the patch are changed such that the CP performance in Band 1 is significantly affected by this truncation as seen from the Fig. 4.14. The CP bandwidth (ARBW) falls above the standard 3dB level for r_1 values below 7 mm. The maximum ARBW of 1.2 % and the minimum axial ratio value (ARmin) of 1.3 dB are obtained at $r_1 = 7$ mm as can be noted from Table 4.1. For values of r_1 above 7mm, the band breaks up into two linear orthogonally polarized resonances as can be seen from Fig. 4.13a. The proposed antenna is also compared to standard circular and equilateral patches with the same fundamental operating frequency in Table 4.1. Area reductions of 26% and 37% are obtained at $r_1=7$ mm.

Table 4.1. Performance of Antenna1 for varying truncation lengths of r_1

r_1 (mm)	f_{c1} (GHz)	f_{c2} (GHz)	Input impedance(Ω)				Imped. BW (%)		3dB ARBW (%)	ARmin	Area reduction (%)	
			Band1		Band2		Band1	Band2			Circular patch	Triangular patch
			Re	Im	Re	Im						
3	1.95	3.49	88	-12	50	-19	1	1.86	-----	10.0	24.7	35.5
4	1.955	3.485	86	5	51	-20	1.1	1.86	-----	17.5	25	35.7
5	1.97	3.49	80	-4	49	-18	2	1.86	-----	9.6	25.3	36
6	1.98	3.49	72	-1	51	-17	3.5	1.86	-----	12.8	25.7	36.3
7	1.99	3.49	60	1	51	-16	5.5	1.86	1.3	1.3	26	37
8	1.995	3.495	57	2	52	-17	7	1.86	1.1	2.2	26.8	37.2
9	2.01	3.49	56	10	55	1	3.8	1.86	-----	4.4	27.5	38

4.3.2.2 Effect of corner truncation r_2

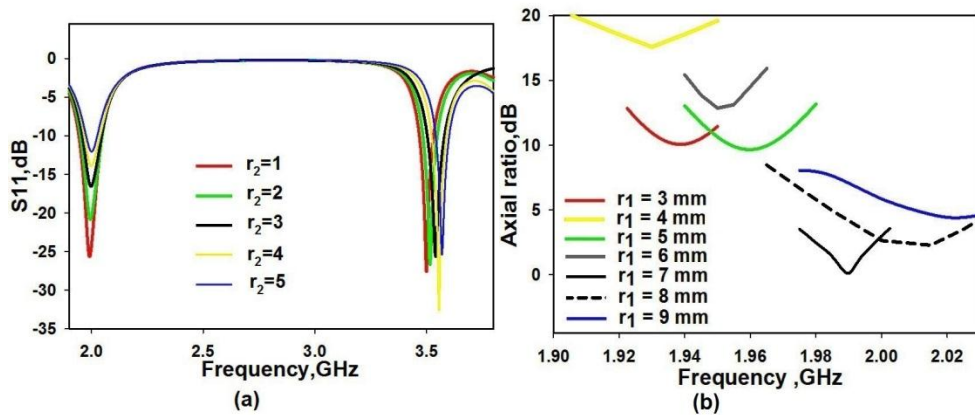


Fig. 4.15. Variation of a) reflection coefficients and b) axial ratio with truncation length r_2 of Antenna 2 ($L=W=50$, $R=45$, $L_1=51$, $h=1.6$, $r_1=7$ (all in mm), $\epsilon_r=4.4$)

The truncation at corner 2 denoted as r_2 is varied from 1mm to 5mm and its effect on the two bands is analyzed. Fig.4.15a depicts the variation of the reflection characteristics of Antenna2 with r_2 . While there is no variation at all in f_{c1} , the Band2 resonance frequency undergoes small shift towards the right. This is because the truncation r_2 modifies the patch dimension in the y direction. The axial ratio graph in Fig.4.15b illustrates that adequate CP performance is obtained at $r_2 = 3$ mm only.

A clear picture of the electromagnetic performance of the antenna at the two bands can be visualized in the simulated current distribution in Fig.4.16a and the 3D radiation patterns in Fig.4.16b. Two half wave variations can be seen in the Y direction, in Fig.4.16b at the Band2 resonance frequency, which means that the mode excited in Band 2 is TM_{20} .

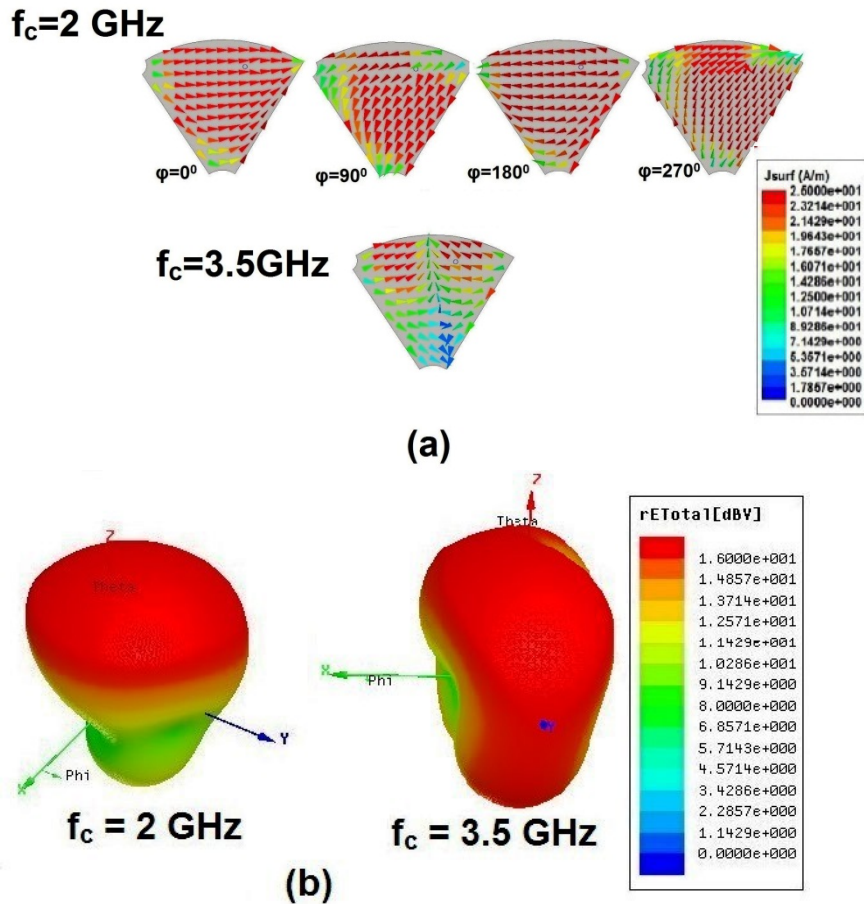


Fig. 4.16. a) Surface current distribution and b) 3D radiation pattern on the corner truncated sectoral patch Antenna2 ($L=W=50$, $R=45$, $L_1 = 51$, $r_1=7$, $r_2=3$, $h=1.6$ (all in mm), $\epsilon_r=4.4$)

The performance results of Antenna 2 with dimension of r_1 fixed at 7 mm are tabulated in Table 4.2. It is inferred from the Table 4.2 that the impedance matchings in both bands are not affected by this truncation. The impedance bandwidth decreases only slightly in Band1 while that in Band2 shows an improvement. Good CP performance is obtained at only $r_2 = 3$ mm, although the ARBW is slightly lower. Area reductions of 27% and 36% respectively are obtained with respect to circular and triangular patches.

Table 4.2. Performance of Antenna2 for varying truncation lengths of r_2 ($r_1=7\text{mm}$)

r_2 (mm)	f_{c1} (GHz)	f_{c2} (GHz)	Input impedance(Ω)				Imped. BW (%)		3dB ARBW (%)	ARmin (dB)	Area reduction (%)	
			Band1		Band2		Band1	Band2			Circular patch	Triangular patch
			Re	Im	Re	Im						
1	1.99	3.5	54	-6	60	12	5.35	2.14	1.47	2.6	26.3	36.8
2	1.99	3.51	55	-7	61	13	5.2	2.1	-----	4.5	26.5	37
3	2.01	3.54	64	-10	59	-1	5.1	2.2	1.1	1	26.8	37.2
4	2.02	3.55	68	-16	56	3	4.2	2.2	-----	3.7	27.1	37.5
5	2.02	3.56	79	-14	62	6	3.1	1.9	-----	9.1	27.6	38

4.3.3 Design

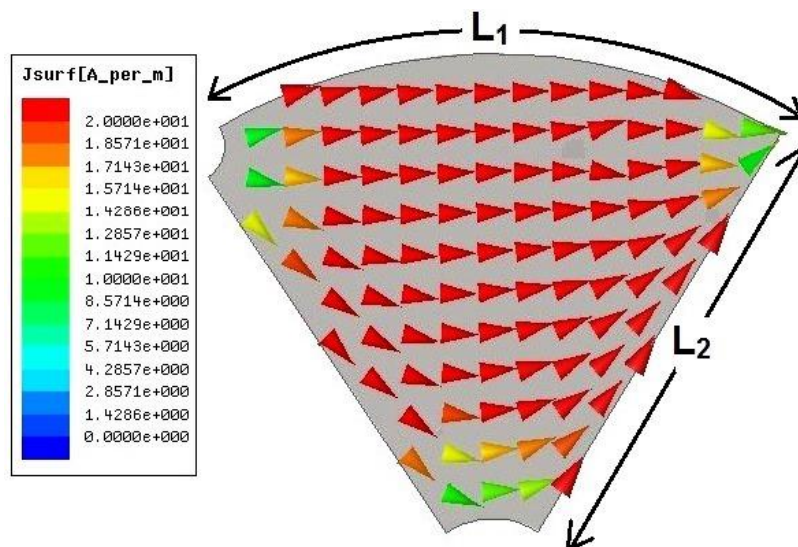


Fig. 4.17. Surface current distribution on the corner truncated sectoral patch Antenna2 at Band 1 resonance frequency ($L=W=50$, $R=45$, $L_1=51$, $r_1=7$, $r_2=3$, $h=1.6$ (all in mm), $\epsilon_r=4.4$)

The simulation and parametric studies described in the previous section provide an insight into the radiation mechanism of the structure and the effect of the different parameters on the radiation characteristics. These observations form the basis for deriving the design equations of the antenna which are the key factors in extending the implementation on other substrates. The design equations are summed up in the following steps.

1. The corner truncated circular disc geometry can be approximated to that of a triangular patch for simplicity and ease of design. Accordingly, the equation for the fundamental frequency (f_{10}) of TM_{10} mode of the triangular patch [2] given by

$$f_{10} = \frac{2c}{3a_e\sqrt{\epsilon_r}} \dots\dots\dots (3.1)$$

where a_e is the effective side length of the patch is applied to the above antenna and is given by

$$a_e = a + \frac{h}{\sqrt{\epsilon_r}} \dots\dots\dots (3.2)$$

Taking f_{10} as the centre frequency of the fundamental mode TM_{10} in the circular disc sectoral antenna, the dimensions of the patch are calculated.

The surface current distribution plot of the Band1 resonance frequency shown in Fig.4.17 shows a half wave variation along the patch periphery ($L_1 + L_2$). Therefore,

$$\frac{L_1 + L_2}{K} = \frac{\lambda_g}{2} \dots\dots\dots (3.3)$$

Where K is a parameter that takes into account the effect of the substrate and λ_g is the guide wavelength in the substrate. The free space wavelength λ_0 corresponding to the fundamental frequency f_{10} is related to λ_g by the relation

$$\lambda_g = \frac{\lambda_0}{\sqrt{\epsilon_{eff}}} \dots\dots\dots (3.4)$$

where ϵ_{eff} is the effective dielectric constant of the substrate given by

$$\epsilon_{eff} = \frac{\epsilon_r + 1}{2} \dots\dots\dots (3.5)$$

2. The dimensions L_1 (arc length) and L_2 are calculated as

$$L_1 = 0.55\lambda_g \dots\dots\dots (3.6)$$

$$L_2 = 0.48\lambda_g \dots\dots\dots (3.7)$$

3. The truncation lengths are calculated as

$$r_1 = 0.07\lambda_g \dots\dots\dots (3.8)$$

$$r_2 = 0.03\lambda_g \dots\dots\dots (3.9)$$

4. The 50 ohm matched impedance point is located on the patch. The approximate coordinates of this point are

$$x_p = 0.4\lambda_g \dots\dots\dots(3.10)$$

$$y_p = 0.08\lambda_g \dots\dots\dots(3.11)$$

with the corner 1 (O in Fig.4.1) of the untruncated circular disc sector patch as the origin.

4.3.4 Validation of the design

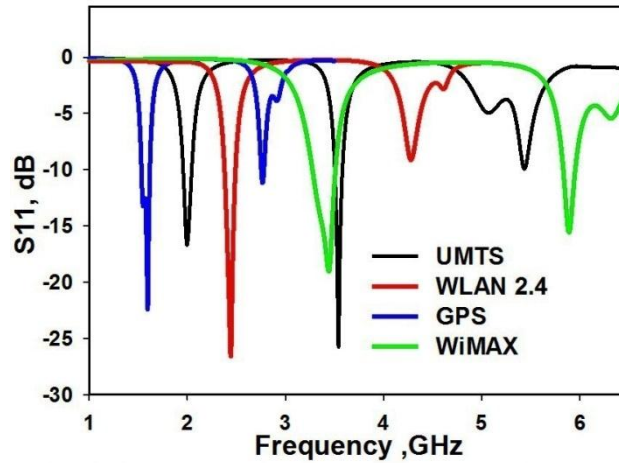


Fig. 4.18. Simulated reflection coefficients of Antenna2 operating in different frequency bands

The design equations derived in the above section were applied to substrates of different permittivity and were validated. The structures with these computed dimensions were simulated using Ansys HFSS and the results so obtained along with their resonance frequencies are tabulated in Table 4.3. The validity of the above design equations were further confirmed by implementing the equations to three other important communication bands. The reflection characteristics of the Antenna 2 operating in other bands of interest shown in Fig. 4.18 indicate good impedance bandwidth in their respective bands. This proves the suitability of the design equations to other frequency bands. The simulated characteristics and parameter values of the prototype on an FR4 substrate in different frequency bands are summarized in Table 4.4. It is understood that the antenna performances are consistent in all the frequency bands.

Table 4.3. Validation on different substrates and comparison with simulation

Laminate	ϵ_r	h(mm)	R(mm)	L ₁ (mm)	r ₁ (mm)	r ₂ (mm)	Centre frequency f _{c1} (GHz)	
							Computed	Simulated
FR4	4.4	1.6	45	51	7	3	2.08	2.01
Rogers RO4003	3.38	1.57	49	56	7.2	3.1	2.13	2.07
Rogers RO3006	6.15	1.25	47	53	6.8	2.91	2.07	2.05
Rogers 6010LM	10.2	0.635	30.7	35	4.5	1.9	2.02	1.98

Table 4.4. Validation of Antenna 2 for different communication bands

Communication Band	Antenna parameters(mm)				Centre frequency (GHz)		% Bandwidth		Axial ratio	
	R	L ₁	r ₁	r ₂	f _{c1}	f _{c2}	Band1	Band2	%ARBW	AR _{min} (dB)
GPSL1 1.5 GHz	56	64	8.1	3.5	1.56	2.8	3.8	1	1.3	1.2
WLAN 2.4 GHz	36	41	5.2	2.2	2.45	4.25	4.1	2	1.3	1.5
WiMax 3.3 GHz	25	28.7	3.6	1.6	3.5	5.8	7.3	2.8	2.2	1.78
UMTS 2 GHz	45	51	7	3	2.01	3.54	5.1	2.2	1.1	0.98

4.3.5 Experimental measurement

Conventional photolithographic process was employed to fabricate a prototype of the designed structures with dimensions R = 45mm, L₁ = 51mm, r₁ = 7 mm, r₂ = 3 mm and W = L = 50 mm on an FR4 substrate of $\epsilon_r = 4.4$ and thickness h = 1.6 mm. The S₁₁ characteristics, 3D radiation patterns and gain were measured using the PNA E8362B network analyzer. The measured and simulated characteristics are compared and are found to be in good agreement with each other.

4.3.5.1 Reflection characteristics

The measured and simulated reflection coefficients of Antenna1 and Antenna 2 are shown compared in Fig.4.19a and Fig.4.19b respectively.

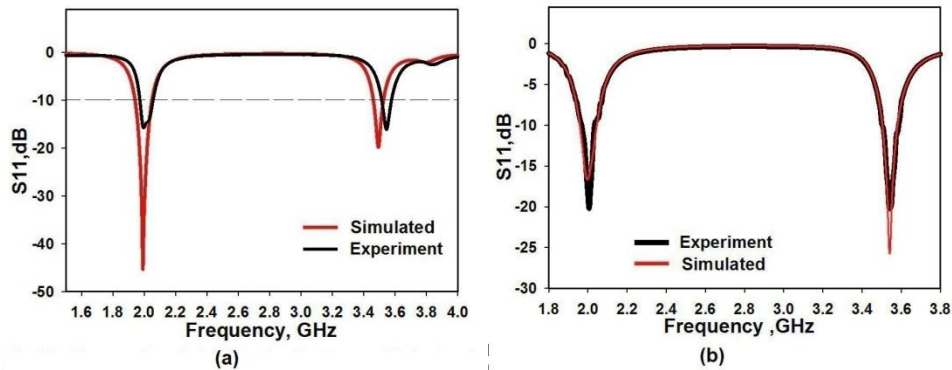


Fig. 4.19. Measured and simulated reflection coefficients of the dual band dual polarized circular disc sector patch antenna a) Antenna1 b) Antenna2 ($L=W=50$, $R=45$, $L_1=51$, $h=1.6$, $r_1=7$ (all in mm), $\epsilon_r=4.4$)

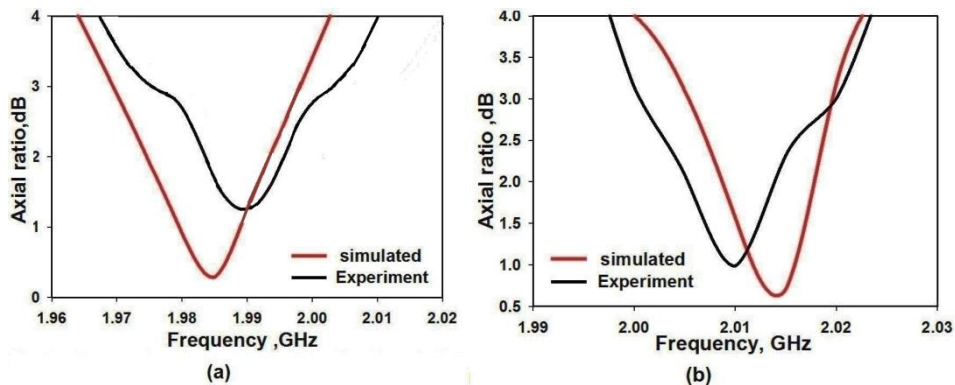


Fig. 4.20. Measured and simulated axial ratio characteristics of the dual band dual polarized circular disc sector patch antenna a) Antenna1 b) Antenna2 ($L=W=50$, $R=45$, $L_1=51$, $h=1.6$, $r_1=7$ (all in mm), $\epsilon_r=4.4$)

Two resonances are excited in the UMTS band and WiMAX band. Antenna 1 exhibits 2:1 VSWR bandwidths of 1.96 - 2.06 GHz (5%) at centre frequency 1.99 GHz and 3.51-3.57 GHz (1.7%) at centre frequency 3.54 GHz respectively. Antenna 2 exhibits a 2:1 VSWR bandwidth of

1.98-2.08 GHz (4.9%) at a centre frequency of 2.03 GHz and a 2:1 VSWR bandwidth of 3.51-3.59 GHz (2.5%) at a centre frequency of 3.54 GHz. The impedance bandwidth in Band 2 is slightly increased which is due to the lowering of the Q factor by the truncation r_2 at this frequency. The axial ratio characteristics were also experimentally measured and are depicted in Figs. 4.20a and 4.20b. Measured ARBW's of 1.3 % (1.97-2.01GHz) in Antenna1 and 1.1% (2.0-2.02GHz) in Antenna2 were obtained.

The experimental and simulated characteristics of Antenna 1 and Antenna 2 are compared in Table 4.5. It is observed that the simulated and experimental values agree to a great extent with each other in both structures.

Table 4.5. Comparison of experimental and simulated characteristics of Antenna1 and Antenna 2

Parameter		Antenna 1		Antenna 2	
		simulated	expt	simulated	expt
Band 1	f_{c1}(GHz)	1.99	1.99	2.01	2.03
	3 dB ARBW(%)	1.3	1.3	1.1	1.1
	ARmin (dB)	1.3	1.1	1	1.
	Imp.Bandwidth (%)	5.5	5	5.1	4.9
Band 2	f_{c2}(GHz)	3.49	3.54	3.54	3.54
	Imp.Bandwidth (%)	1.86	1.7	2.2	2.5

4.3.5.2 Radiation pattern of Antenna1

The radiation pattern of Antenna1 was measured inside the Anechoic Chamber with the standard horn antenna as transmitter. The 2D radiation patterns in two orthogonal planes i.e., y-z plane and x-z plane were experimentally measured and are shown in Fig.4.21 for the centre frequencies of the two bands.

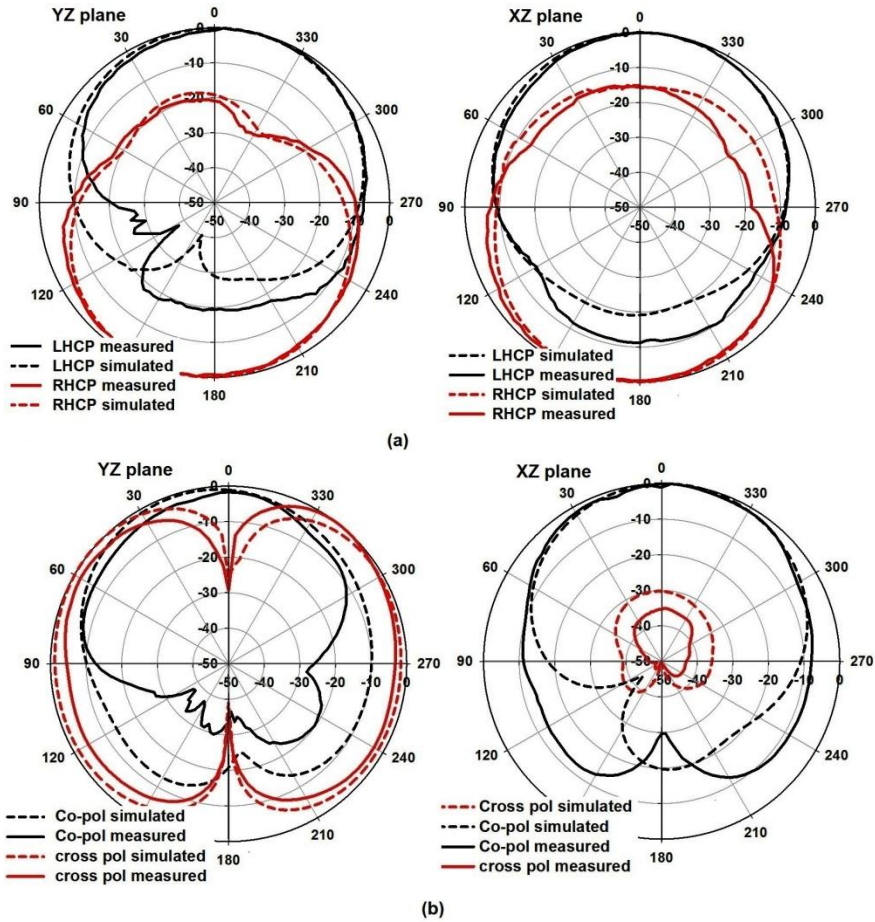


Fig. 4.21. Measured and simulated radiation pattern in orthogonal planes of the dual band dual polarized circular disc sector patch antenna Antenna1 at a) 1.99 GHz b) 3.54 GHz ($L=W=50$, $R=45$, $L_1=51$, $h=1.6$, $r_1=7$ (all in mm), $\epsilon_r=4.4$)

The simulated 2D radiation patterns are compared with the experimental patterns and are found to be in agreement. In Band1, far field radiation patterns in two orthogonal planes of LHCP and RHCP mode are obtained. The patterns are broadside and similar in both the modes with good LHCP in the boresight direction. The cross polarization level i.e., RHCP, here is lower by 20dB in the main beam direction. Half power beam width of 90° is

obtained in both planes. In Band 2 nearly omnidirectional linearly polarized pattern is observed, with cross polarization level better than 20 dB in both principal planes which means good isolation between co and cross polarization. Half power beam width is 100° in YZ plane and 80° in XZ plane.

4.3.5.3 Radiation pattern of Antenna 2

The measured radiation pattern of Antenna 2 is shown compared to the simulated pattern in two orthogonal planes YZ and XZ planes in Fig.4.22.

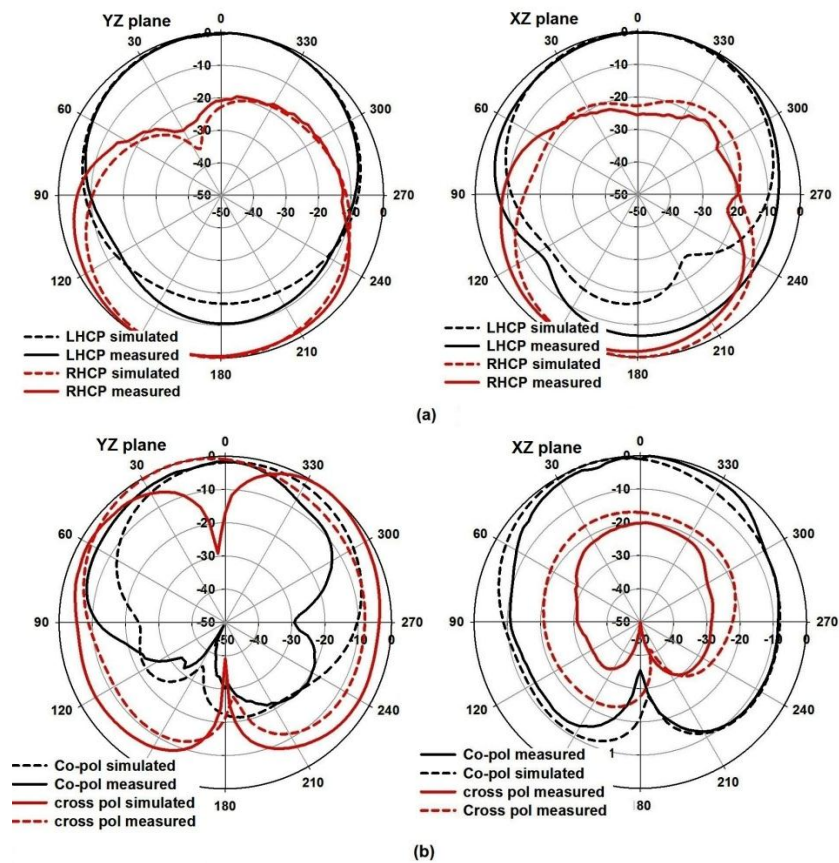


Fig. 4.22. Measured and simulated radiation patterns in orthogonal planes of the dual band dual polarized circular disc sector patch antenna Antenna2 at a) 1.99 GHz b) 3.54 GHz ($L=W=50$, $R=45$, $L_1=51$, $h=1.6$, $r_1=7$ (all in mm), $\epsilon_r=4.4$)

It is observed that the patterns are not much different from that of Antenna 1. In band 1, good LHCP radiation is obtained in the boresight direction with an isolation of more than 20 dB from the orthogonal RHCP radiation. Half power beam width is 96° and 100° in the two planes respectively in Band 1. In Band 2, half power beam widths are 60° and 80° respectively in the two planes. The nearly omnidirectional pattern is observed in Band 2 with an isolation of more than 20 dB between the co and cross polarization levels in the two principal planes.

4.3.5.4 Gain and efficiency of Antenna 1 and Antenna 2

The gain comparison method was utilized to measure the gain of the antennas, with the standard ridged horn antenna as the reference. Antenna 1 measured peak gains of 1.5 dBi and 1.4 dBi in Bands 1 & 2 respectively and Antenna 2 measured peak gains of 1.4 dBi and 1.3 dBi in Band 1 and Band 2 respectively. Radiation efficiency measured through the Wheeler Cap method yielded 73% and 78% in the two bands respectively for Antenna 1 and 60% and 76% respectively in the two bands for Antenna 2.

4.4 Circularly polarized sectoral patch antenna for WLAN application

The general design equations developed in the previous section were put into application to develop the sectoral patch antenna for 2.4 GHz fundamental frequency. Accordingly the dimensions were computed as $R = 36.5\text{mm}$, $L_1 = 41\text{ mm}$, $r_1=5.2\text{ mm}$, $r_2=2.2\text{mm}$ and ground plane size $W= 42\text{ mm}$ and $L= 38\text{ mm}$. The substrate chosen was FR4 with ϵ_r and thickness $h = 1.6\text{mm}$. The feed point coordinates were obtained as A (29, 5) from the design equations and was carefully adjusted for optimum performance in CP. The geometry is shown in Fig.4.23a.

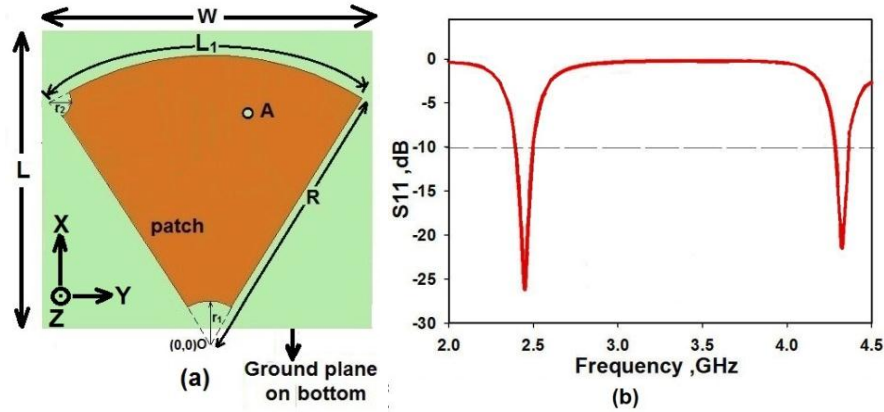


Fig. 4.23. Circularly polarized sectoral patch antenna for WLAN applications
 a) geometry of the antenna b) simulated S11 characteristics
 ($L=38$, $W=42$, $R=36.5$, $L_1=41$, $r_1=5.2$, $r_2=2.2$, $h=1.6$ (all in mm),
 $A(29,5)$, $\epsilon_r=4.4$)

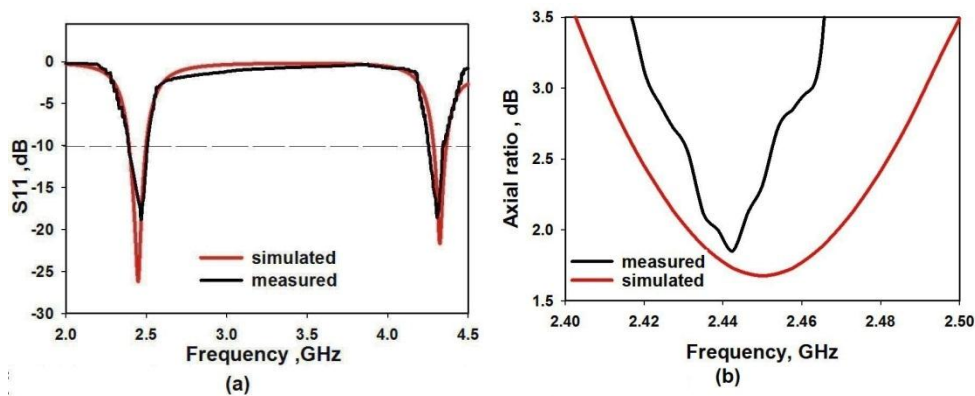


Fig. 4.24. Measured and simulated reflection and axial ratio characteristics of
 the circularly polarized sectoral patch antenna for WLAN applications
 ($L=42$, $W=38$, $R=36$, $L_1=41$, $r_1=5.2$, $r_2=2.2$, $h=1.6$ (all in mm), $\epsilon_r=4.4$)

The reflection and radiation characteristics were simulated and two well matched resonances at 2.4 GHz and 4.2 GHz were obtained (Fig.4.23b). The antenna was experimentally tested for the characteristics using the PNA E8362B network analyzer. The experimental reflection and axial ratio characteristics are shown compared to the simulated results in Fig. 4.24. The graphs indicate an impedance bandwidth of 4 % and 2 % in the two bands

respectively. An axial ratio bandwidth of 1.3% with a minimum AR value 1.7dB at a CP centre frequency of 2.45 GHz is obtained. The simulation and experimental characteristics are in good agreement.

The simulated current distribution plots are examined to infer that the polarization is circular in the first resonance frequency, and linear at the second resonance as shown in Fig.4.25a. The radiation pattern can be better visualized through the simulated 3D radiation plot shown in Fig.4.25b.

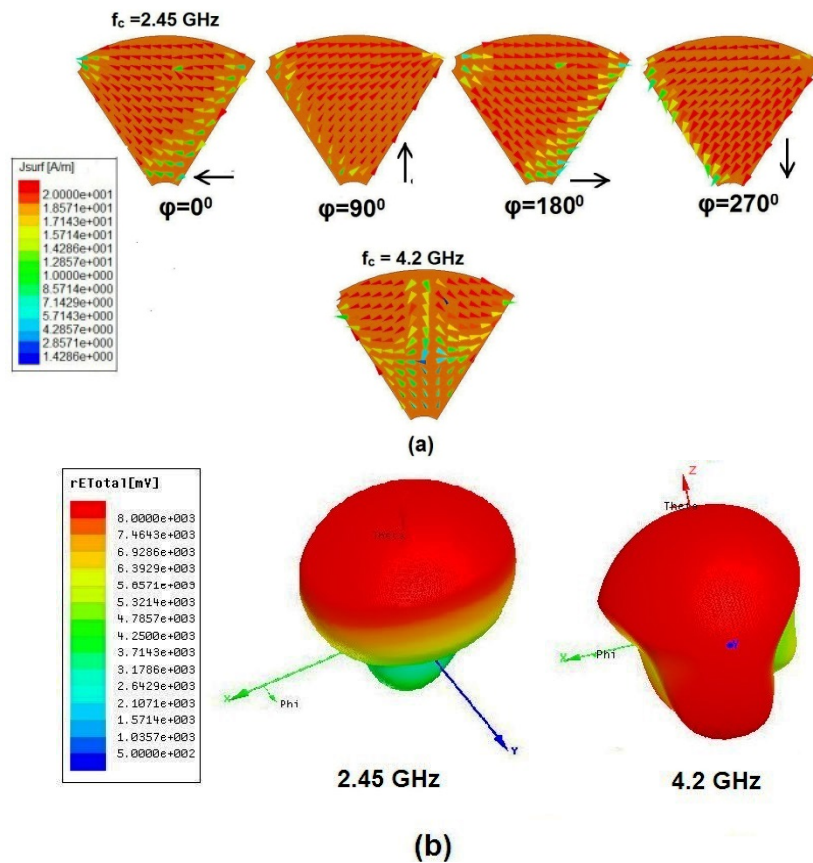


Fig. 4.25. a) Simulated current distribution plot and b) 3D radiation pattern of the circularly polarized sectoral patch antenna for WLAN applications ($L=42$, $W=38$, $R=36$, $L_1=41$, $r_1=5.2$, $r_2=2.2$, $h=1.6$ (all in mm), $\epsilon_r=4.4$)

The radiation pattern characteristics in Fig.4.26 show good LHCP in the boresight direction with an isolation of more than 20dB from RHCP at 2.45 GHz. The radiation is linearly polarized in the second band at 4.2 GHz. The pattern at 4.2 GHz is non directional in the YZ plane and figure of eight in the XZ plane. Nearly omnidirectional patterns with cross polarization level greater than 20dB down are observed. Half power beam width is around 100°

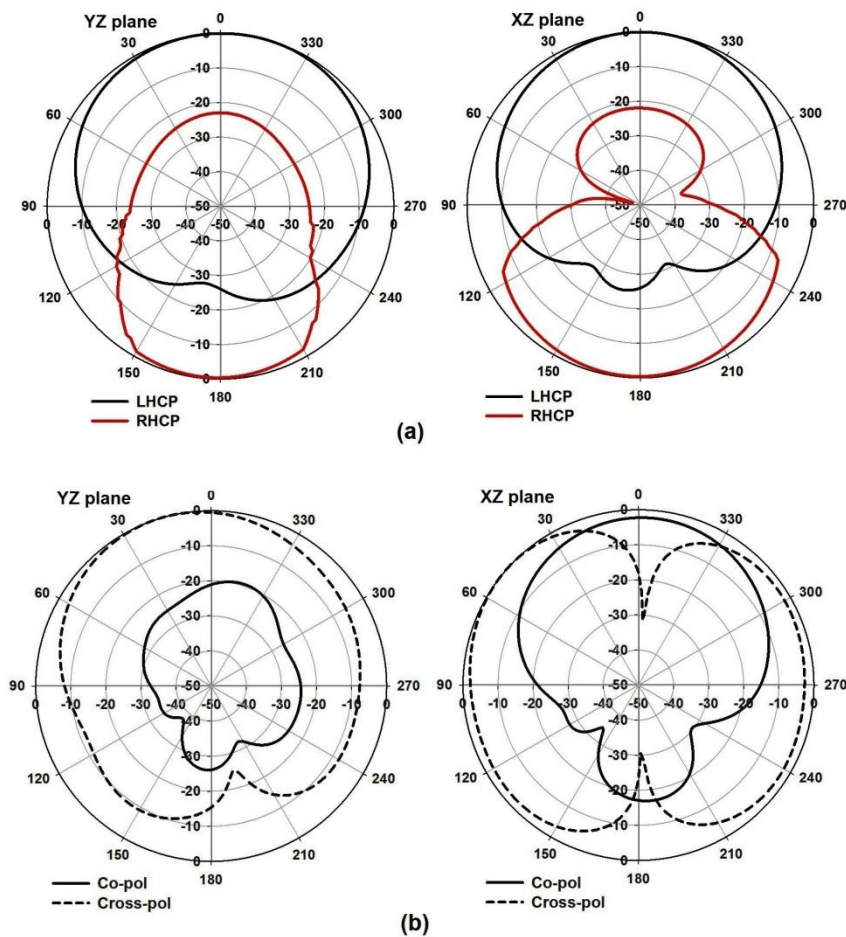


Fig. 4.26. Measured radiation pattern characteristics of the circularly polarized sectoral patch antenna for WLAN applications in two orthogonal planes at a) 2.45 GHz b) 4.2 GHz ($L=42$, $W=38$, $R=36$, $L_1=41$, $r_1=5.2$, $r_2=2.2$, $h=1.6$ (all in mm), $\epsilon_r=4.4$)

in both the principal planes at 2.45 GHz and 100° & 80° respectively in the two orthogonal planes at 4.2 GHz. Gain measurement using the gain comparison method yielded peak gains of 2.2 dBi and 1.2 dBi in the two bands respectively. Efficiencies of 75% and 52% were experimentally obtained for the sectoral patch antenna for WLAN applications. The measured characteristics of this proposed antenna for WLAN frequency band are tabulated in Table 4.6.

Table 4.6. Characteristics of circularly polarized sectoral patch antenna for WLAN applications

f_{c1} (GHz)		2.4
f_{c2} (GHz)		4.2
Imp bandwidth (%)	Band1	4
	Band2	2
ARBW (%)		1.3
ARmin (dB)		1.7
% area reduction w.r.t.	Circular patch	14
	Triangular patch	35
Peak gain (dBi)	Band 1	2.2
	Band 2	1.2

The design equations derived in the earlier section are applied here, with 2.4 GHz WLAN frequency as the dominant mode frequency. The antenna is compact and has a sizeable reduction in patch area when compared to standard patch geometries as shown in Table 4.6. The polarization characteristics are preserved in the two bands of operation. Broadside radiations are obtained with good LHCP in the boresight direction. The pattern shapes also bear consistency with those obtained for the Antenna2 described in the earlier section.

4.5 Circularly polarized sectoral patch antenna for WiMAX applications

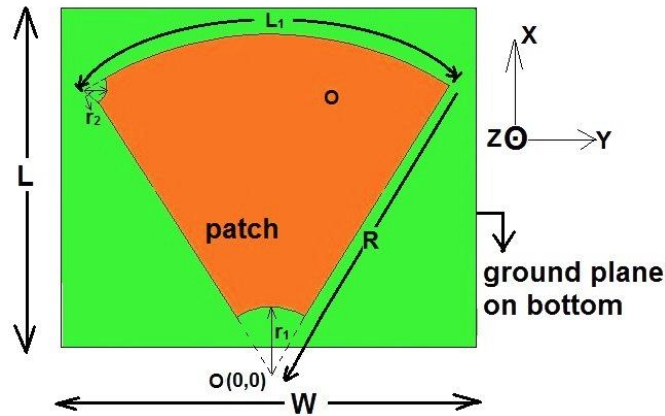


Fig. 4.27. Geometry of the circularly polarized sectoral patch antenna for WiMAX applications ($L=25$, $W=30$, $R=26$, $L_1=29.5$, $r_1=5$, $r_2=1.4$, $h=1.6$ (all in mm), $A(21,5)$, $\epsilon_r=4.4$)

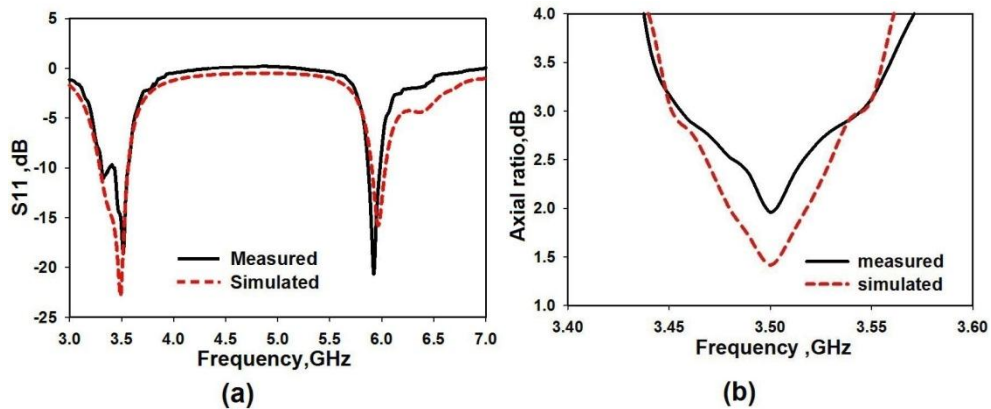


Fig. 4.28. Measured and simulated reflection coefficient and axial ratio characteristics of the circularly polarized sectoral patch antenna for WiMAX applications ($L=30$, $W=25$, $R=26$, $L_1=29.5$, $r_1=5$, $r_2=1.4$, $h=1.6$ (all in mm), $\epsilon_r=4.4$)

The design equations developed for circular disc sector patch antenna were exploited to develop a dual frequency antenna with a wider bandwidth in the WiMAX 3.5 range and narrowband resonance in the WLAN 5.8 range. The antenna was designed and fabricated with patch dimensions $R= 26\text{mm}$, $L_1=29.5\text{mm}$, $r_1= 5\text{mm}$, $r_2 =1.4\text{mm}$ and ground plane size $W= 30\text{ mm}$ and $L= 25\text{ mm}$ on an FR4 substrate with $\epsilon_r =4.4$ and $h= 1.6\text{mm}$. The feed position for maximum impedance matching and optimum CP performance was located as A (21, 5). The antenna geometry is depicted in Fig. 4.27. Dual band resonance at 3.5GHz and 5.8 GHz are observed with circular polarization at the first band and linear polarization in the second.

The simulated reflection and axial ratio characteristics of the structure are shown in Fig.4.28a and Fig.4.28b. The two resonances are well matched and fall in the WIMAX and WLAN 5.8 frequency bands respectively. The simulated current distribution on the patch at both centre frequencies are illustrated in Fig.4.29. At the Band1 centre frequency, the polarization is circular in the left hand sense. Two resonances at near degenerate frequencies of 3.31 GHz and 3.59 GHz are combined to generate the circularly polarized radiation in the first band. The second band has the TM_{20} mode excited and is linearly polarized in the y direction. The 3D radiation patterns are shown at both the centre frequencies in Fig.29b. It can be seen that the pattern at the higher frequency has deviated from the near omnidirectional pattern in the earlier prototypes. This is due to the increase in electrical length at the higher frequencies.

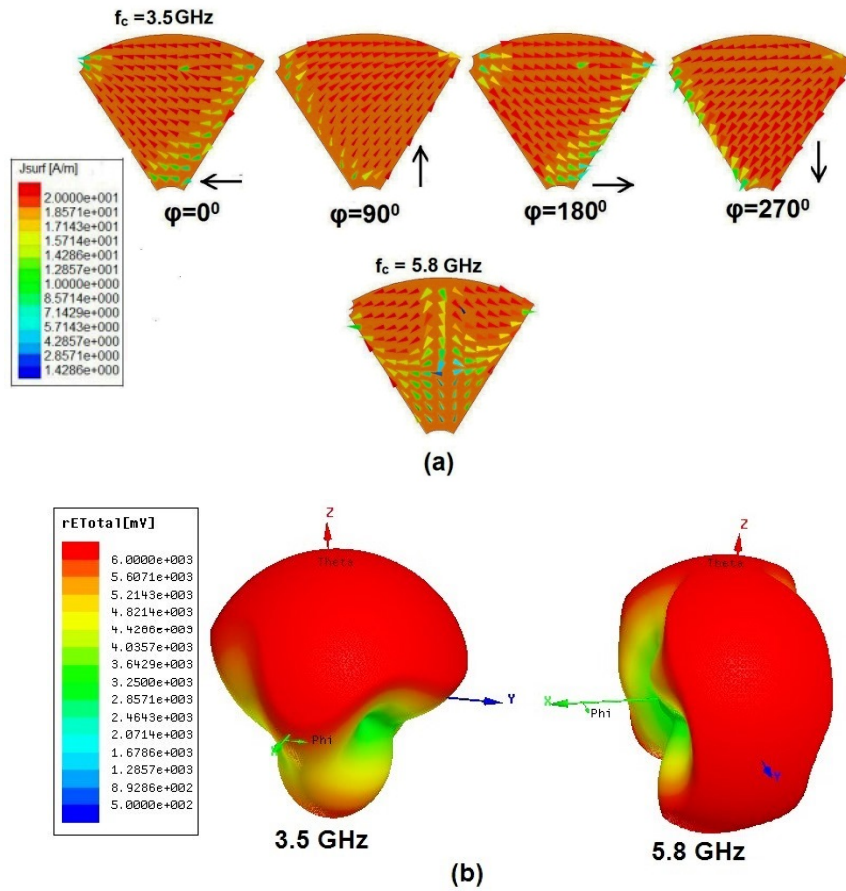


Fig. 4.29. a) Simulated current distribution plot and b) 3D radiation pattern of the circularly polarized sectoral patch antenna for WIMAX applications ($L=30$, $W=25$, $R=26$, $L_1=29.5$, $r_1=5$, $r_2=1.4$, $h=1.6$ (all in mm), $\epsilon_r=4.4$)

Experimental measurements after fabricating the prototype on an FR4 substrate showed 2:1 VSWR bandwidths of 8 % and 3.8% in the two bands respectively as illustrated in Fig.4.28a. The measurement also yielded ARBW of 2.5% at centre frequency 3.54 GHz and minimum AR value 1.9dB. Radiation patterns in two orthogonal planes were measured at the two centre frequencies of 3.54 GHz and 5.8 GHz and are shown in Fig.4.30a and Fig.4.30b.

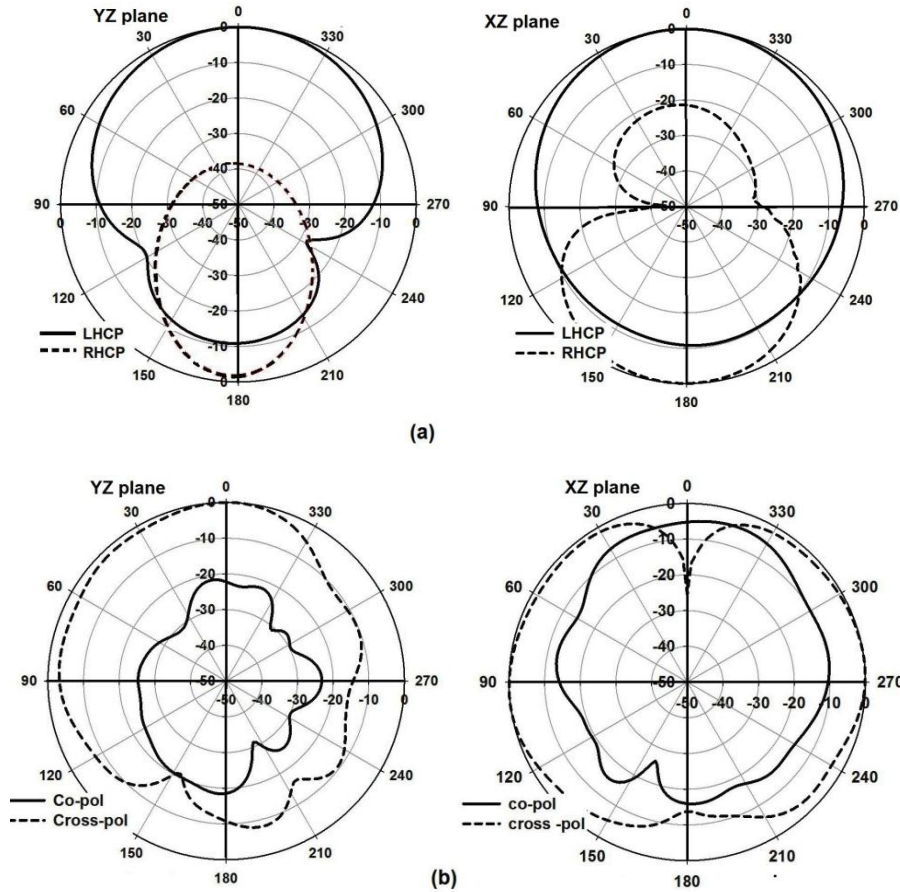


Fig. 4.30. Measured radiation pattern characteristics of the circularly polarized sectoral patch antenna for WIMAX applications in two orthogonal planes at a) 3.5 GHz b) 5.8 GHz ($L=30$, $W=25$, $R=26$, $L_1=29.5$, $r_1=5$, $r_2=1.4$, $h=1.6$ (all in mm), $\epsilon_r=4.4$)

In the first band, good LHCP radiation is observed in the boresight direction, with the isolation between right handed and left handed circular polarization being greater than 20dB. In band 2, broadside radiation with cross polarization level at > 20 dB is observed in the two orthogonal planes. However the pattern has become little distorted due to increase in the effective electrical length at the Band2 frequency and is no longer near omnidirectional. Peak gains of 3.08dBi and 2dBi were obtained in the two

bands respectively using the gain comparison method. Efficiency measured using the Wheeler cap method showed 60% and 52 % at the two bands respectively.

Table 4.7. Characteristics of circularly polarized sectoral patch antenna for WiMAX applications

f_{c1} (GHz)		3.5
f_{c2} (GHz)		5.8
Imp bandwidth (%)	Band1	8
	Band2	3.8
ARBW (%)		2.5
ARmin (dB)		1.9
%area reduction w.r.t.	Circular patch	12
	Triangular patch	34
Peak gain (dBi)	Band 1	3.08
	Band 2	2

The design equations postulated in section 4.3.3 have once more been validated to be applicable in the WiMAX range of frequency through the simulation, fabrication and experimentation of the antenna here. Although the pattern is having distortion at the higher frequency, it possesses good circularly polarized radiation in the lower band. Moderate gain values are also observed in the two bands. Half power beam widths are 80° in both planes at 3.5 GHz and 60° and 80° in the two principal planes at 5.8 GHz. Area reductions of 12% and 34% respectively are obtained for this proposed sectoral patch antenna on comparison with standard circular and triangular patches designed for the same fundamental frequency. The measured characteristics of the sectoral patch antenna for WiMAX applications are tabulated in Table 4.7.

4.6 Dual band corner truncated sectoral patch antenna with dual slits for GPS and WLAN

Majority of the GPS designs integrated with other important wireless communication standards such as WLAN, GSM and DCS are linearly polarized, while the GPS antenna itself needs to be circularly polarized in order to avoid the mismatch loss associated with transceiver polarization. The transmitted signal is right hand circularly polarized in GPS systems, which requires the mobile GPS antenna to be polarized in the right hand sense. In the following section, the corner truncated disc sector patch antenna is designed for dual band operation with the first resonance frequency being right hand circularly polarized in the GPS L2 band (1.565-1.585 GHz) and the second resonance tuned to the WLAN 2.4 GHz band with linear polarization. The geometry, design and characteristics of the antenna are discussed.

4.6.1 Antenna evolution and geometry

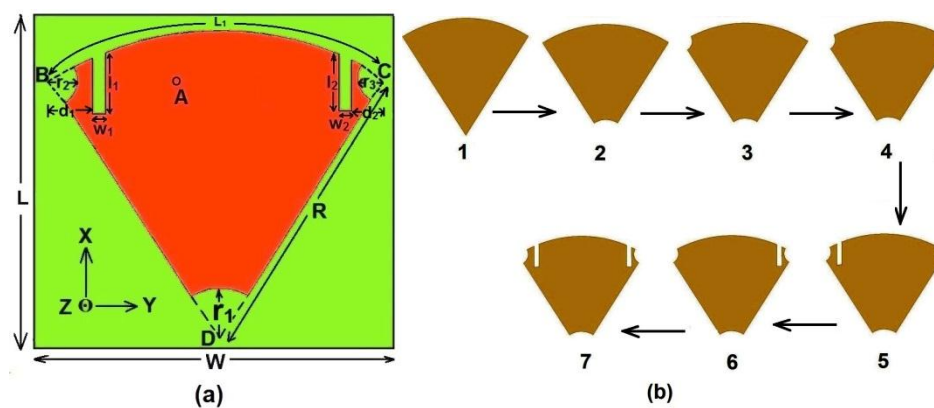


Fig .4.31. a) Geometry and b) evolution of the corner truncated sectoral patch antenna with dual slits for GPS and WLAN ($L=55$ $W=65$, $R=59$, $L_1=64$, $r_1=11$, $r_2=r_3=5$, $l_1=l_2=11.5$, $w_1=w_2=2.5$, $h=1.6$ (all in mm), $A(50,-8)$, $\epsilon_r=4.4$)

The configuration of the proposed dual band corner truncated disc sector patch antenna with dual slits is shown in Fig.4.31a. The patch is designed on an FR4 substrate of size $W \times L = 55 \times 65 \text{ mm}^2$, thickness $h = 1.6 \text{ mm}$ and $\epsilon_r = 4.4$. The evolution of the antenna from the basic sectoral patch is shown in Fig.4.31b. Initially the circular disc sector patch with a radius of $R = 59 \text{ mm}$ with origin $D(0, 0)$ is subjected to truncation of its three corners one by one (steps 1 to 4). In step 5 a rectangular slit (slit 1) is etched on the patch, on the left side of the X axis. Next the slit position is shifted to the right side of X axis (slit 2). Finally, the slit1 is added again to get the proposed structure. The reflection and axial ratio characteristics are observed in each step and based on the observations the final geometry is optimized.

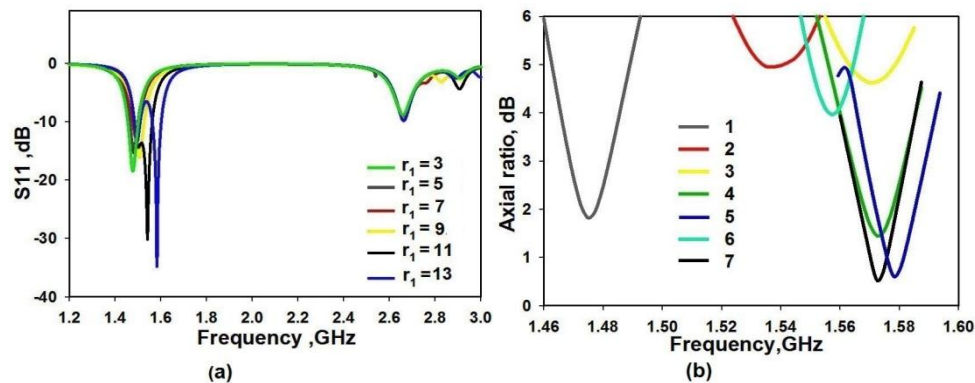


Fig. 4.32. a) Reflection coefficient and b)axial ratio characteristics of the corner truncated sectoral patch antenna with dual slits for GPS and WLAN
($L=55$ $W=65$, $R=59$, $L_1 =64$, $r_1=11$, $r_2 =r_3 =5$, $l_1=l_2=11.5$, $w_1=w_2=2.5$, $h=1.6$ (all in mm), $A(50,-8)$, $\epsilon_r=4.4$)

Fig.4.32a depicts the reflection coefficient graph obtained in each step in the evolution. A dual band response is obtained at step 4, where two near degenerate (TM_{10}) modes of equal amplitude and 90° phase difference are excited to produce circular polarization in the first band at 1.5 GHz and TM_{20} mode with linear polarization is excited in the second band at 2.8GHz.

In step 1, the resonances are at 1.48GHz and 2.8 GHz as seen from the graph. The truncations of the three corners shift the resonance at 1.48 GHz slightly to the right so that it falls in the 1.56 GHz GPS range. This shift towards higher side is expected since the patch area is reduced by the truncation. However, the resonance at 2.8GHz is shifted down in frequency to the WLAN 2.4GHz band by the addition of these slits. The locations of the two slits are carefully determined so that the resonance at the first band remains unaffected by their presence. The technique employed here is the altering of current paths through patch geometry modification. The feed point is located at A (50,-8) to obtain right hand circularly polarized radiation in the GPS band.

The variations in axial ratio in the first band are also simultaneously observed as shown in Fig.4.32b. It is clear from the graph that the CP performance in the first band is affected by the three corner truncations. The etching of the slits significantly improve the CP characteristics so that the axial ratio values fall below the stipulated $< 3\text{dB}$ level. It can be seen that, by the presence of slit1 alone, it is possible to produce good CP characteristics. Hence this case is further investigated by observing the performance at the second band in the next section. At the same time, etching of slit 2 alone degrades the CP performance considerably. When both slits are present, the orthogonal dimensions of the patch are such that the near degenerate TM_{01} and TM_{10} modes are excited. Through extensive parametric study, it is confirmed that both slits 1 and 2 are essential for achieving perfect CP characteristics, impedance matching and tuning of the second resonance to the desired frequency band.

4.6.2 Design

The corner truncated disc sector patch antenna is basically designed according to the design equations explained in section 4.3.3. The dimensions obtained as per the equations are $R = 59$ mm, $L_1 = 67$ mm, $r_1 = 11$ mm and $r_2 = r_3 = 5$ mm. The feed position for right hand sense CP is located at $(x_p, y_p) = (50, -8)$ with point D as the origin. The slits are of dimensions $l_1 = l_2 = 11.5$ mm and $w_1 = w_2 = 2.5$ mm. The dimensions and locations of the slits were determined by extensive parametric studies of the simulated S11 characteristics and the current distributions on the patch.

4.6.3 Simulated current distributions

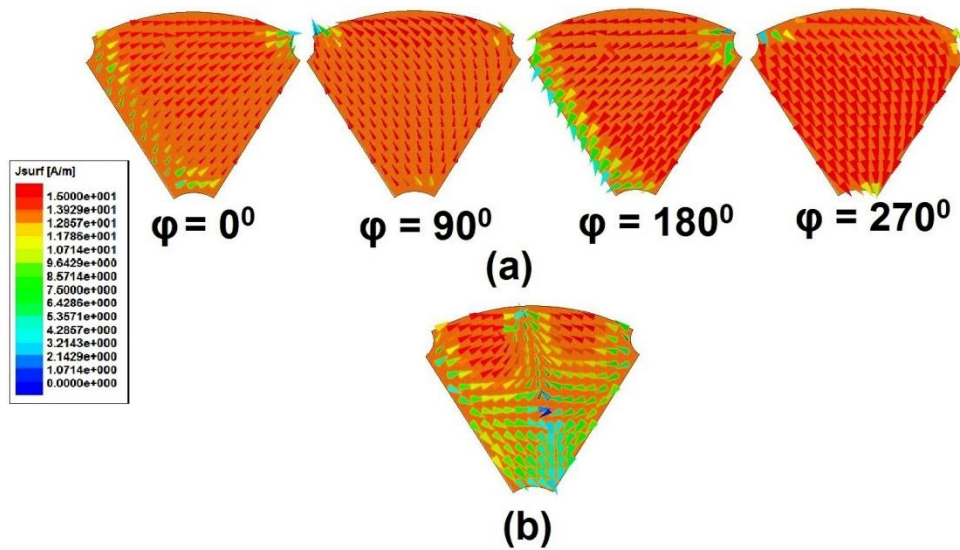


Fig. 4.33. Surface current distribution on the corner truncated sectoral patch antenna without slits at a) 1.57 GHz b) 2.45 GHz ($L=55$ $W=65$, $R=59$, $L_1=64$, $r_1=11$, $r_2=r_3=5$, $h=1.6$ (all in mm), $A(50,-8)$, $\epsilon_r=4.4$)

The current distributions on the patch with the three corners truncated and without the slits at the two centre frequencies of the two resonance bands are shown in Fig. 4.33. In the first band, the polarization sense is of

right hand circular. The current distributions at four different phase intervals are shown in Fig.4.33a. It is observed that at all phase instants, a null is obtained at the patch area near the truncations at corners 2 and 3. The TM_{20} mode is excited at the second resonance band as seen from Fig.4.33b. Two half wave variations are seen along the y direction, which means the resonance at this band is dependent on the patch dimension L_1 . Hence by modifying the patch geometry along this direction, the resonance at the second band can be varied. At the same time, this modification should also not have any effect on the resonance at the first band. Since the occurrence of nulls at the two ends of the patch boundary L_1 was already noted, the most reasonable position to introduce changes in the patch geometry so as to affect only the second resonance frequency is the region near the truncated corners 2 and 3. This assumption is confirmed by etching two slits (slit 1 & slit 2) in these regions and is validated through simulation and later through fabrication and measurement.

4.6.4 Effect of the patch modifications

The effect of the three truncations and the two slits on the reflection coefficient and impedance matching are studied by analyzing the S11 graph in Fig.4.32a once again. In the first step in the unmodified sectoral patch (refer Fig.4.31 b), resonances near 1.49 GHz and 2.8 GHz are obtained. The resonance at 2.8 GHz is not matched. In step 2, when corner D is truncated with a sectoral portion of radius r_1 , the second resonance becomes poorly matched, while the first one shifts to 1.52 GHz. When the corners B and C are truncated with sectoral portions in steps 3 and 4, the two resonances show a shift towards the higher side in frequency. At the same time impedance matching becomes poor at both frequencies as the truncation

lengths are increased. In step 5, the left slit (slit1) is etched. The first resonance shifts to 1.56 GHz while the second resonance moves down to 2.5 GHz. Impedance matching is improved. Step 6 shows the impedance characteristics when right slit (slit 2) alone is given. It can be seen that the resonance at 2.5 GHz loses its matching when the right slit alone is present with the slit 1 being absent. Finally in step 7, when both the slits are embedded in the patch, optimum characteristics in terms of operating bands and impedance matching are obtained. The first band covers the GPS L2 band and the second band falls in the WLAN 2.4 GHz range with adequate impedance matching. Hence it is confirmed that the combined presence of the two slits are responsible for the tuning of the second band to the 2.4 GHz and proper impedance matching.

4.6.4.1 Effect of varying corner truncation r_1

The truncation of corner D is varied in radius from $r_1 = 3$ mm to 13 mm. The effect of this variation on the reflection characteristics and the axial ratio are depicted in Figs.4.34a and 4.34b. It is seen that the first resonance is adequately matched; the second resonance has poor matching. As the length of the truncation is increased from 3 mm, the resonance at 1.49 GHz shifts towards the left and two separate resonances are found to occur in the first band when the length r_1 becomes greater than 11mm. From the axial ratio graph, it is seen that the circular polarization property is lost as the value of r_1 increases from 3 mm to 9mm. However, at $r_1 = 11$ mm it is seen that the axial ratio value falls below 3 dB, indicating CP radiation. At this value of r_1 , the orthogonal dimensions of the patch are such that, it results in the excitation of two near degenerate modes of 90° phase difference. Hence the dimension of r_1 is fixed at 11 mm.

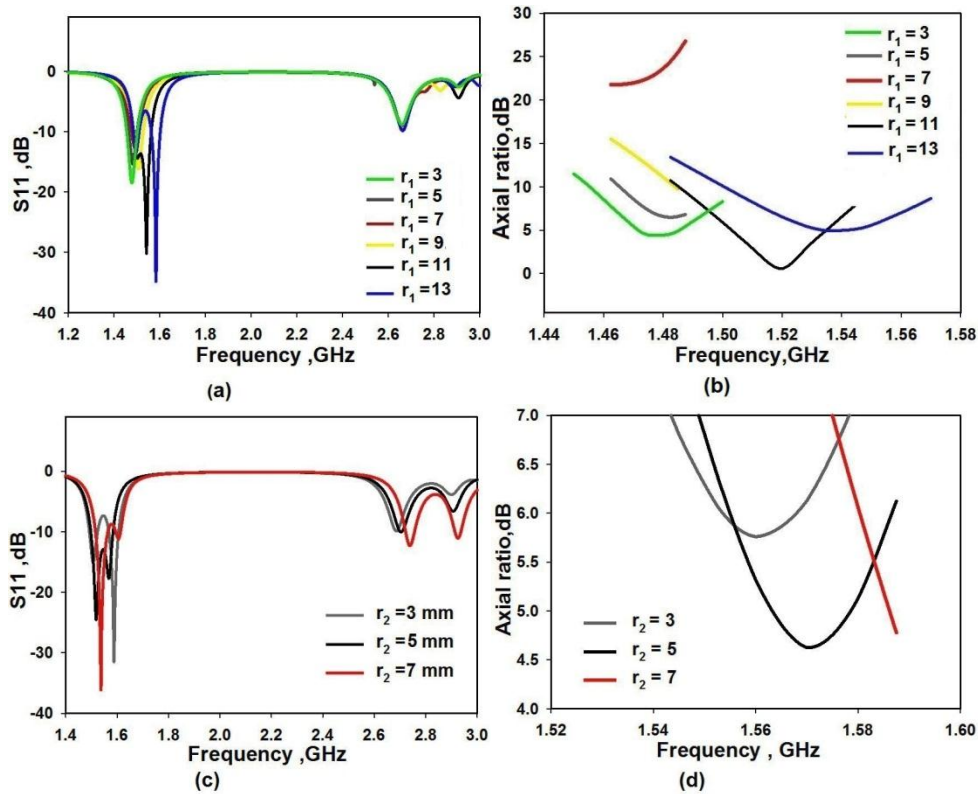


Fig. 4.34. Effect of corner truncation r_1 on a) reflection coefficient b) axial ratio characteristics and corner truncation r_2 on c) reflection characteristics d) axial ratio characteristics ($L=55$ $W=65$, $R=59$, $L_1 =64$, $h=1.6$ (all in mm), $A(50,-8)$, $\epsilon_r=4.4$)

4.6.4.2 Effect of varying corner truncation r_2

The corner B is also truncated with radius r_2 , with the truncation length r_1 fixed as 11 mm. As r_2 is varied from 3 to 7 mm in steps of 2 mm, it is observed that the impedance matching at the first resonance is unchanged, while the second resonance continues to be poorly matched. The axial ratio graphs at these varying values of r_2 indicate that the radiation is no longer circularly polarized. Figs.4.34c and 4.34d depict the effect of corner truncation r_2 . The value of r_2 is fixed as 5 mm.

4.6.4.3 Effect of varying corner truncation r_3

A sector shaped truncation is applied to corner C (Fig.4.31a) also, with the truncation lengths at corners D and B fixed at $r_1=11$ mm and $r_2=5$ mm. The truncation length r_3 is varied from 1mm to 7 mm and the impact on the reflection coefficient and axial ratio characteristics are graphically studied. As observed from the graph shown in Fig.4.35a, the truncation at corner C shifts the two resonances slightly to the higher side of frequency. The matching also becomes poorer when the value of r_3 is greater than 5 mm. Improved CP performance is obtained when the three corners are truncated, than with the case where corners D and B (see Fig.4.31a) alone were truncated as shown in Fig.4.35b. Optimum CP performance in terms of minimum AR value and maximum ARBW are obtained at $r_3 = 5$ mm. Thus the value of r_3 is fixed at 5mm.

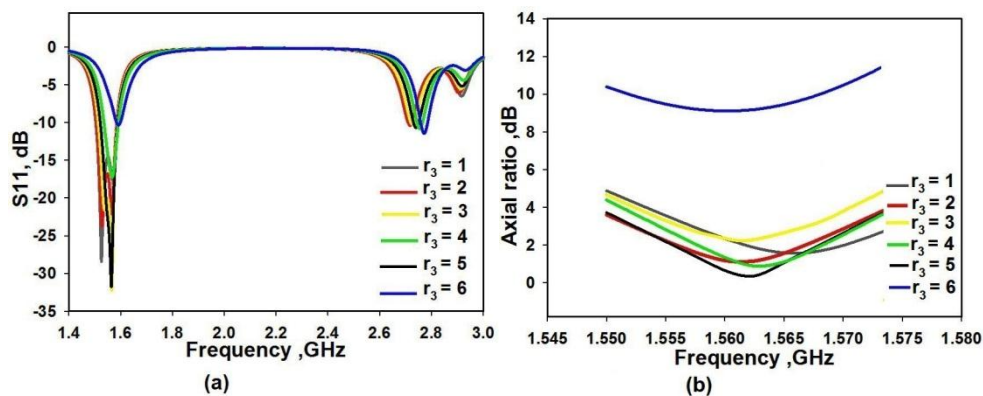


Fig. 4.35. Effect of corner truncation r_3 on a) reflection coefficient b) axial ratio characteristics ($L=55$ $W=65$, $R=59$, $L_1=64$, $h=1.6$ (all in mm), $A(50,-8)$, $\epsilon_r=4.4$)

4.6.4.4 Effect of the left slit (slit 1)

Based on the observation from the simulated current distribution earlier that nulls occur near the two ends of the patch boundary L_1 , a

rectangular slit of length l_1 and width w_1 is etched near the truncated corner B. The position, length and width of this slit were varied and the impacts on the reflection and axial ratio characteristics were parametrically analyzed. The results are depicted in Fig.4.36.

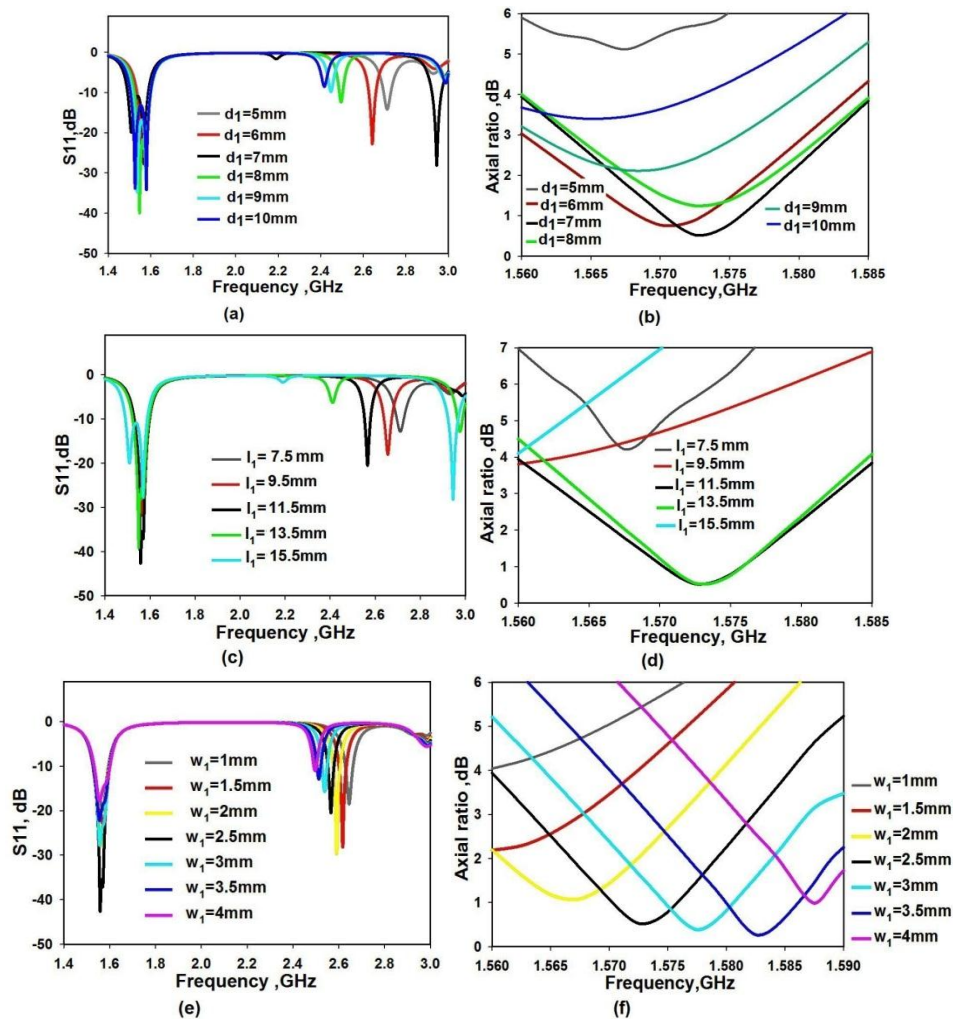


Fig. 4.36. Effect of position of slit1 on a) reflection coefficient b) axial ratio characteristics, length l_1 of slit 1 on c) reflection coefficient d) axial ratio characteristics and width w_1 of slit 1 on e) reflection characteristics f) axial ratio characteristics ($L=55$ $W=65$, $R=59$, $L_1=64$, $r_1=11$, $r_2=r_3=5$, $d_1=7$, $h=1.6$ (all in mm), $A(50,-8)$, $\epsilon_r=4.4$)

4.6.4.4.1 Effect of varying the slit1 position

The position of the slit is critical since it is located at the minimum or null current position. The position can be varied by changing the distance d_1 from corner B shown in Fig.4.31a. Varying d_1 does not affect the impedance matching at the first resonance much, while that at the second resonance is greatly affected (Fig.4.36a). However, change in d_1 has a more pronounced effect on the CP performance in the first band in terms of axial ratio (Fig.4.36b). The impedance matching at the second resonance becomes poor at higher values of d_1 beyond 7mm, while that at the first band has little change. Optimum performance in terms of both impedance matching and axial ratio are obtained at $d_1 = 7\text{mm}$. The second resonance is shifted in frequency because the currents in the Y direction are lengthened by the embedding of the slit.

4.6.4.4.2 Effect of varying the slit length l_1

The length of the slit l_1 is changed from 7.5 mm to 15.5 mm with the width w_1 fixed at 2.5 mm and $d_1=7\text{mm}$. The second resonance shifts in frequency and impedance matching. Little variation in matching is produced at the first band, but axial ratio graph shows considerable change. At longer values of l_1 , the radiation is no longer circularly polarized since axial ratio becomes higher than the 3 dB level. Hence based on all these results, the optimum value of l_1 is found to be 11.5 mm. The impact of l_1 on the reflection and axial ratio characteristics are shown in Figs.4.36c and 4.36d.

4.6.4.4.3 Effect of varying the slit width w_1

The slit width w_1 is varied from 1mm to 4mm with $l_1=11.5\text{mm}$ and $d_1=7\text{mm}$. As the slit becomes wider it reduces the matching at both resonance frequencies and shifts the ARBW to the higher side i.e., above the required

band of GPS L2 range. The best performances in reflection coefficient and axial ratio are observed at $w_1 = 2.5$ mm as seen from Figs.4.36e and 4.36f.

From these parametric studies, it can be understood that the left slit alone is able to produce good CP performance in Band 1. However the main issue is that the second resonance band is not exactly tuned to the 2.4 GHz band. The effect of the right slit on overcoming this problem is explained in the next section.

4.6.4.5 Effect of the right slit (slit 2)

A rectangular slit of length l_2 and width w_2 (slit 2) is etched on the right portion of the sectoral patch near the truncated corner 3. The left slit is removed and the effect of slit 2 on the reflection and CP characteristics are parametrically studied as in the earlier section. The results are depicted in Fig.4.37.

4.6.4.5.1 Effect of varying the slit2 position

The position of the right slit is changed by varying d_2 from 5mm to 10 mm. The presence of this slit affects the second resonance only as seen from Figs.4.37a. The second resonance shifts to the lower side in frequency, as the parameter d_2 is increased. At the same time, the axial ratio value deteriorates from the 3 dB level and falls away from the required band of GPS L2 as seen from Fig.4.37b.

4.6.4.5.2 Effect of varying the slit length l_2

Varying the slit length l_2 of slit2 has little effect on the first resonance, while the second resonance is brought down to near 2 GHz. The CP performance is drastically affected as the axial ratio value goes above the

stipulated 3 dB optimum level. Figs.4.37c and 4.37d show the effect of varying the slit length.

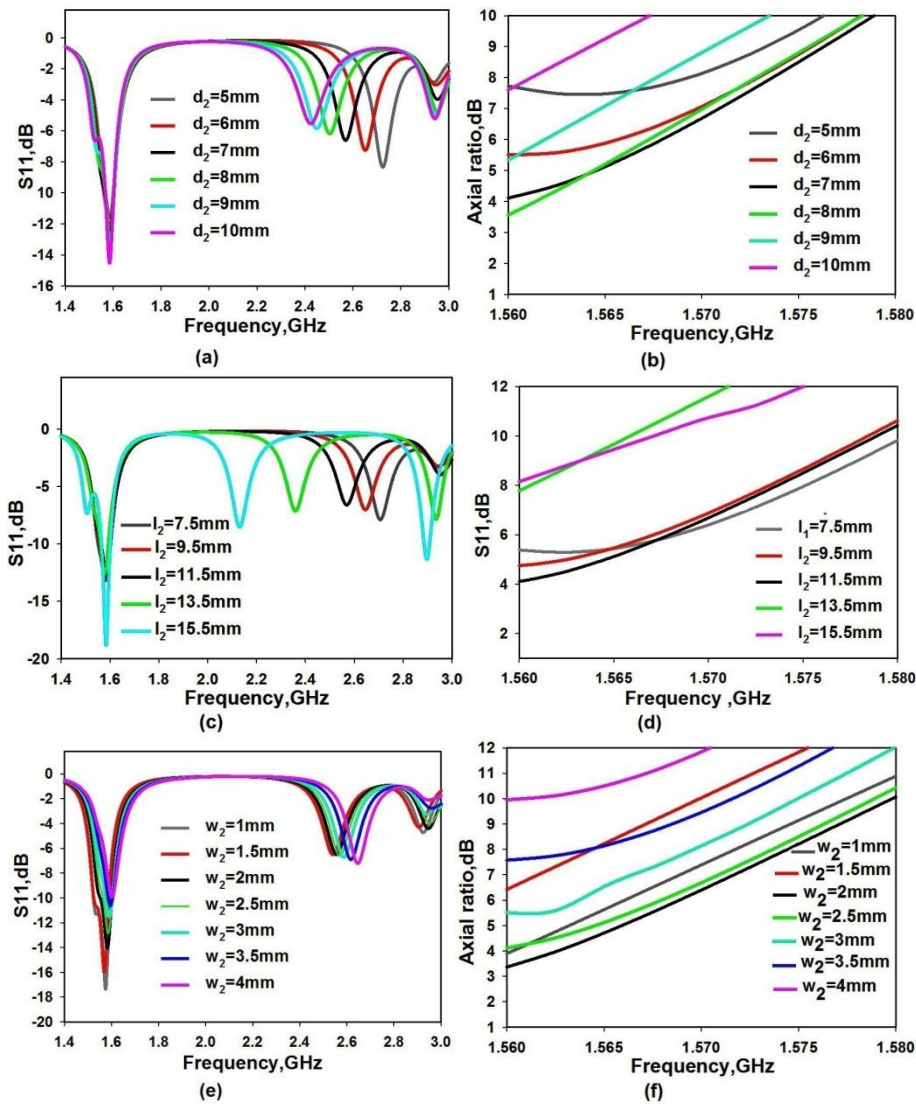


Fig. 4.37. Effect of position of slit2 on a) reflection coefficient b) axial ratio characteristics, length l_2 of slit 2 on c) reflection coefficient d) axial ratio characteristics and width w_2 of slit 2 on e) reflection characteristics f) axial ratio characteristics ($L=55$ $W=65$, $R=59$, $L_1=64$, $r_1=11$, $r_2=r_3=5$, $d_2=7$, $h=1.6$ (all in mm), A (50,-8), $\epsilon_r=4.4$)

4.6.4.5.3 Effect of varying the slit width w_2

The effects of change in the slit width are illustrated in Figs.4.37e and 4.37f. It is observed that as the width w_2 is varied from 1 mm to 4mm, both resonances are affected in impedance matching. The second resonance also shifts to a higher frequency as the y directed currents have to traverse a longer path when the slit width increases.

4.6.4.6 Effect of the left and right slits combined

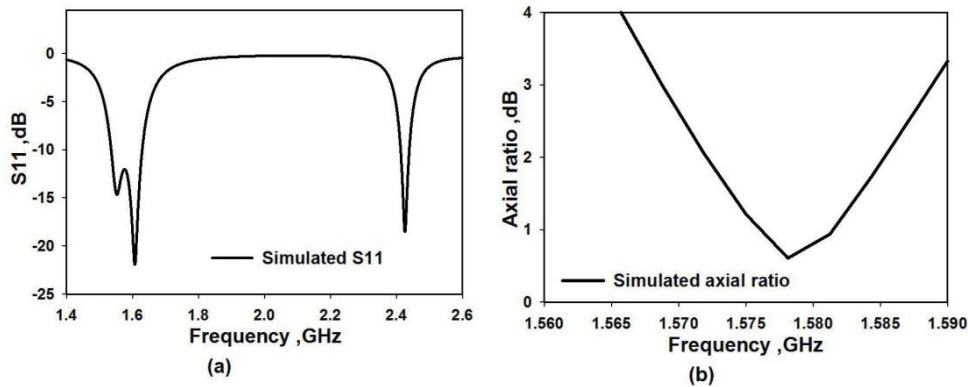


Fig. 4.38. Simulated optimum a) reflection coefficient b) axial ratio characteristics with both the left and right slits present ($L=55$ $W=65$, $R=59$, $L_1=64$, $r_1=11$, $r_2=r_3=5$, $l_1=l_2=11.5$, $w_1=w_2=2.5$, $d_1=d_2=7$, $h=1.6$ (all in mm), $A(50,-8)$, $\epsilon_r=4.4$)

When both the two slits are etched on the patch, the best possible characteristics in terms of ARBW and ARmin in the concerned frequency band of GPS L2 are obtained. This is because, both the x directed and y directed current are modified equally such that near degenerate modes are excited at the dominant mode frequency in the 1.56 GHz range. Moreover, the impedance matching is also proper in both the resonance bands. Fig.4.38 shows the optimum reflection and axial ratio characteristics of the final structure.

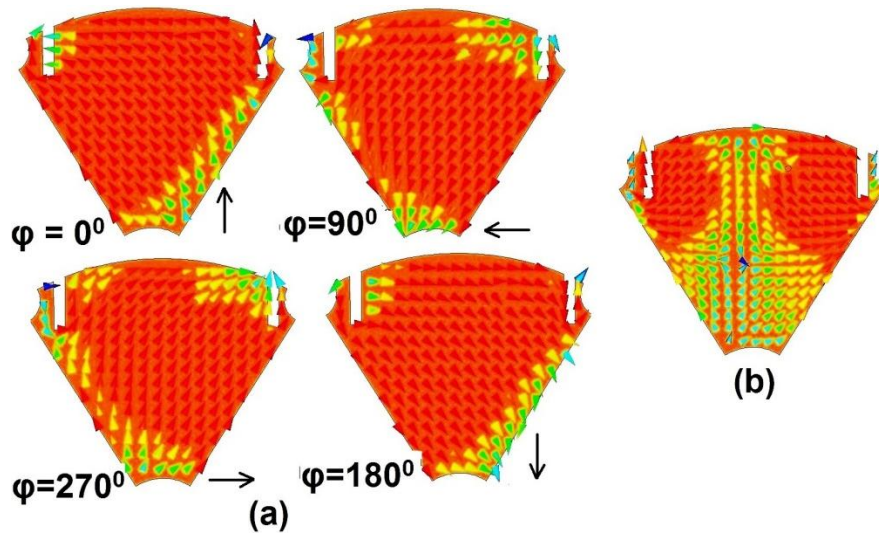


Fig. 4.39. Simulated surface current distributions with both the left and right slits present at a) 1.57 GHz b) 2.45 GHz ($L=55$ $W=65$, $R=59$, $L_1=64$, $r_1=11$, $r_2=r_3=5$, $l_1=l_2=11.5$, $w_1=w_2=2.5$, $d_1=d_2=7$, $h=1.6$ (all in mm), $A(50,-8)$, $\epsilon_r=4.4$)

The simulated current distribution on the patch with the two slits is shown in Fig.4.39. The current path is modified near the slits as is obvious from the distribution. The sense of polarization is right handed in the GPS L2 band. The y directed currents are bent around the edge of the slits traversing a longer path which results in the shifting of the second resonance frequency to 2.4 GHz from 2.8 GHz. At this band, the TM_{20} mode is excited, with the radiation being linearly polarized.

4.6.5 Experimental Measurement

A prototype of the corner truncated sectoral patch antenna with dual slits was fabricated on an FR4 substrate of dielectric constant 4.4 and thickness $h=1.6$ mm. The reflection coefficient measured using PNA E8362B network analyzer was compared with the simulated characteristics and are found to be in good agreement (Fig.4.40a). Orthogonal TM_{10} modes at near

degenerate frequencies are excited to produce RHCP radiation at 1.575 GHz with 4.5% impedance bandwidth. The axial ratio characteristics were also measured and are found to be matching with the simulated ones as shown in Fig.4.40b. ARBW of 1.27% at an AR min of 0.9dB is obtained at a CP centre frequency of 1.575GHz. The second band is due to the excitation of TM_{20} mode and is linearly polarized with a centre frequency of 2.45 GHz and a 2.06% impedance bandwidth.

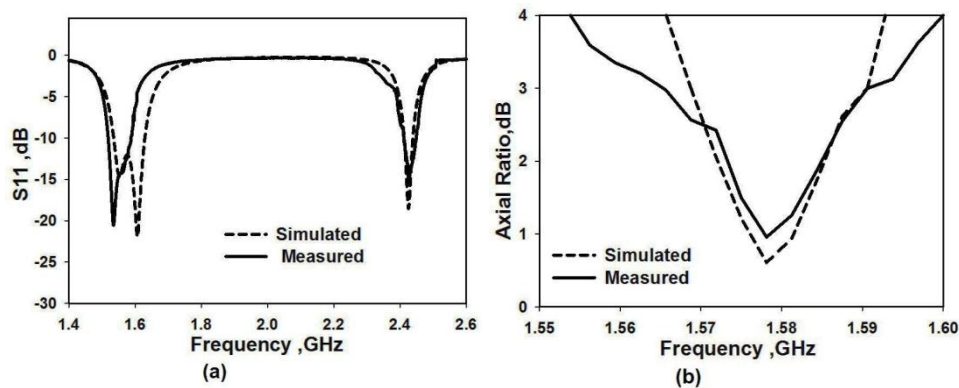


Fig. 4.40. Measured a) reflection coefficient and b) axial ratio characteristics of the corner truncated sectoral patch antenna with dual slits for GPS and WLAN ($L=55$, $W=65$, $R=59$, $L_1=64$, $r_1=11$, $r_2=r_3=5$, $l_1=l_2=11.5$, $w_1=w_2=2.5$, $d_1=d_2=7$, $h=1.6$ (all in mm), $A(50,-8)$, $\epsilon_r=4.4$)

Radiation patterns of the corner truncated sectoral patch antenna with dual slits were measured in two orthogonal planes and are depicted in Fig.4.41. The antenna exhibits good right hand circular polarization in the two planes with an isolation of more than 30 dB with the cross polarized left hand CP. The second band at 2.45 GHz centre frequency shows around 15dB isolation between the co and cross polarizations. All radiation patterns are broadside in nature.

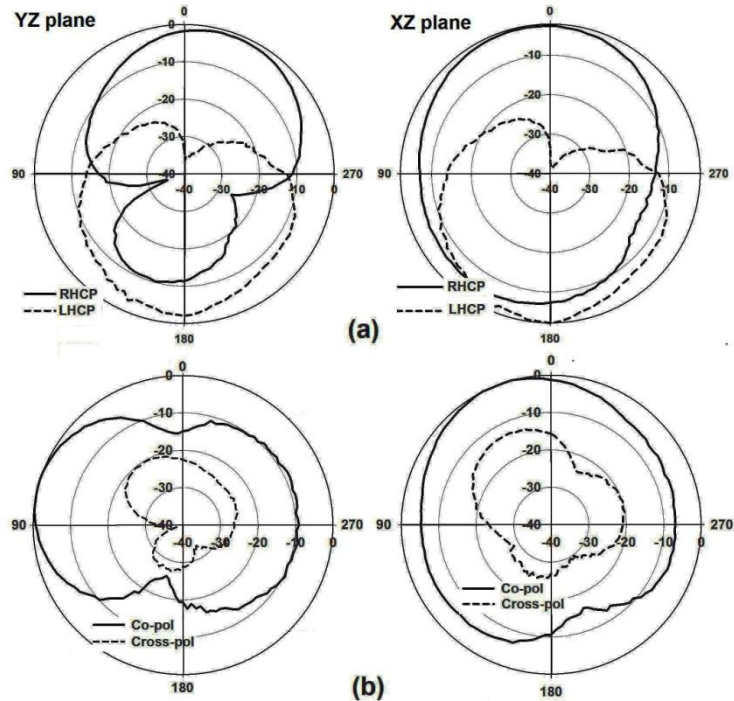


Fig. 4.41. Measured radiation patterns in orthogonal planes of the corner truncated sectoral patch antenna with dual slits for GPS and WLAN at a) 1.57 GHz b) 2.45 GHz ($L=55$ $W=65$, $R=59$, $L_1=64$, $r_1=11$, $r_2=r_3=5$, $l_1=l_2=11.5$, $w_1=w_2=2.5$, $d_1=d_2=7$, $h=1.6$ (all in mm), $A(50,-8)$, $\epsilon_r=4.4$)

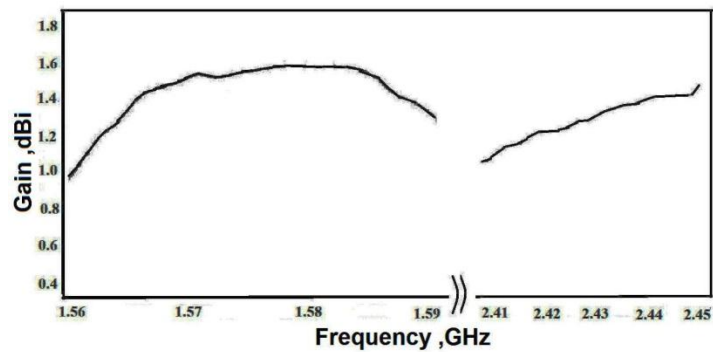


Fig. 4.42. Measured gain in the two operating bands of the corner truncated sectoral patch antenna with dual slits for GPS and WLAN ($L=55$ $W=65$, $R=59$, $L_1=64$, $r_1=11$, $r_2=r_3=5$, $l_1=l_2=11.5$, $w_1=w_2=2.5$, $d_1=d_2=7$, $h=1.6$ (all in mm), $A(50,-8)$, $\epsilon_r=4.4$)

The gain was also measured using the gain comparison method with the double ridged horn antenna as reference. A peak gain of 1.57dB is obtained for the first band. Since the currents have to traverse a path around the edges of the slits, the peak gain at the second band is lower at 1.38dB. The gain plots are illustrated in Fig.4.42.

The detailed study of a single feed sectoral patch antenna with corner truncations and dual slits is presented. A dual band response in the GPS and WLAN bands with dual polarizations is achieved. The etching of the double slits has been conveniently used for tuning of the higher order mode to the WLAN frequency band. Matching and axial ratio characteristics can also be controlled by the slit dimensions and positions. The antenna is well suited for GPS transmitter applications which require the polarization to be right hand circular. The proposed work also shows an area reduction of 8% in comparison with the unmodified circular disc sector. The antenna shows an area reduction of 21% and 31% respectively compared to circular patch antenna and equilateral triangular patch antenna designed for the same fundamental operation frequency.

4.7 Summary of the chapter

The circular disc sector patch antenna has been analyzed in this chapter. The key inferences derived from the studies can be summarized as below.

- The sector shaped patch can be conveniently used to produce a dual band response of different polarizations at the two bands.
- Circularly polarized radiation at the fundamental frequency is produced by the merging of near degenerate TM_{01} and TM_{10} modes.

- The excitation of higher order mode TM_{20} produces linearly polarized radiation at the second resonance.
- Corner truncation can be effectively utilized to reduce the overall size of the patch and the antenna.
- Reduction in patch size through truncation maintains the fundamental frequency within the concerned frequency band.
- Null current positions occur at all three corners of the sectoral patch.
- These null locations can be well utilized to shift the second resonance frequency without affecting the CP performance at the fundamental frequency.
- The presence of two slits combined can control the impedance matching at the two bands and tune the second resonance frequency to the desired band.
- Design equations developed are found to hold good for different substrates and also for various commercial frequency ranges of interest.

References

- [1] Hsu, W.-H. and K. L. Wong “Circularly polarized disk-sector microstrip antenna,” *Electronics Letters*, Vol. 34, No. 23, pp. 2188-2190, 1998.
- [2] Jashwant S. Dahele, and Kai Fong Lee, “On the Resonant Frequencies of the Triangular Patch Antenna”, *IEEE Transactions on Antennas and Propagation*, Vol. AP-35, No. 1, pp. 100-101, January 1987.

.....✂.....

**INVESTIGATIONS ON COMPACT TRI BAND DUAL POLARIZED
CORNER TRUNCATED SECTORAL PATCH ANTENNA**

Contents	5.1 <i>Introduction</i>
	5.2 <i>Tri band dual polarized sectoral patch antenna</i>
	5.3 <i>Triband dual polarized sectoral patch antenna for low cross polarization and enhanced gain</i>
	5.4 <i>Summary of the Chapter</i>

The detailed analysis of the triband performance of the sectoral patch antenna is carried out in this chapter. The evolution, geometry and parametric analyses are explained in detail. The excitations of combined modes have been emphasized. A slotted ground sectoral patch antenna with circular shaped slots has been described with the objective of attaining reduced cross polarization and enhanced gain. Extensive simulation studies along with experimental verifications have been presented here.

5.1 Introduction

Microstrip antenna technology is racing up fast to keep pace and meet the ever growing demands for newer lightweight, compact, multi-function and multi band capability antennas. Multiple functionality devices that simultaneously support individual blocks which operate at different frequency bands prefer the microstrip antenna owing to its properties of low profile, compactness, ease of integration and fabrication. To name a few of these popular frequency bands include the Universal Mobile Telecommunication services (UMTS), Wireless Local area Network (WLAN) and Worldwide Interoperability for Microwave Access (WiMAX). Various techniques have been devised to achieve multi frequency operation of microstrip patch antennas which include use of multiple radiators [1], fractal geometries [2], stubs [3] and coupled resonators [4] at these multiple bands.

Polarization diversity in these different bands is also a highly desirable feature as it can mitigate the effects of fading and improve the isolation between the frequency bands. Frequency ratios between two operating bands can be made tunable on a low or moderate scale by careful modifications of the geometry of the antenna.

The single and dual band operations of the sectoral patch antenna were explored in detail in the previous chapter. The current chapter is concerned with the triple band operation of the patch, achieved by the excitation of higher order hybrid modes. The polarizations in the three bands are different and are examined. The frequency ratio tunability of the second and third bands has been achieved by using a sectoral notch in the truncated boundary of the patch. The chapter also describes a simple and

effective technique to reduce the cross polarization level of the linearly polarized bands.

5.2 Tri band dual polarized sectoral patch antenna

Most triple band patch antenna designs available in literature are based on conventional Euclidian geometries like square, rectangular, triangular and hexagonal. The main idea behind the choice of the circular disc sector patch as the geometry for the work was that although this is a simple and plain patch shape, the coaxial probe fed version has not been explored and analyzed much for the multi band operations and hybrid mode excitations. In this section, the sectoral patch antenna truncated at its three corners is explained and investigated for its triple band operation.

5.2.1 Evolution and geometry of the antenna

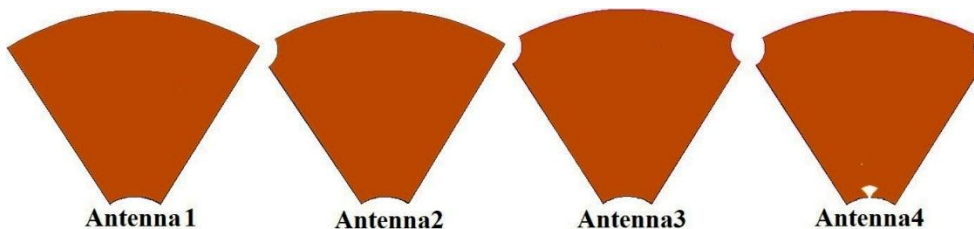


Fig. 5.1. Configurations in the evolution of the triband dual polarized sectoral patch antenna

The basic circular disc sector is subjected to successive truncations of its three corners. A fourth sectoral notch or indentation is etched at the truncated edge at corner 1. The evolution of the geometry is shown in Fig.5.1. The configuration of the proposed antenna as shown in Fig.5.2 consists of a circular disc sector of radius R mm. From the corners 1, 2 and 3, sectoral truncations of indentation radii (IR) r_1 , r_2 and r_3 and indentation

angles (IA) θ_1 , θ_2 , θ_3 respectively are made. The sectoral shaped truncations and the indentation are all actually scaled down versions of the original sectoral patch. The terms IR and IA are analogous to those in [5] and are borrowed from the theory of fractals. On the midpoint of the truncated edge L_4 of the patch, a sectoral notch of radius r_4 and angle θ_4 is carved. This is the proposed structure of Antenna 4.

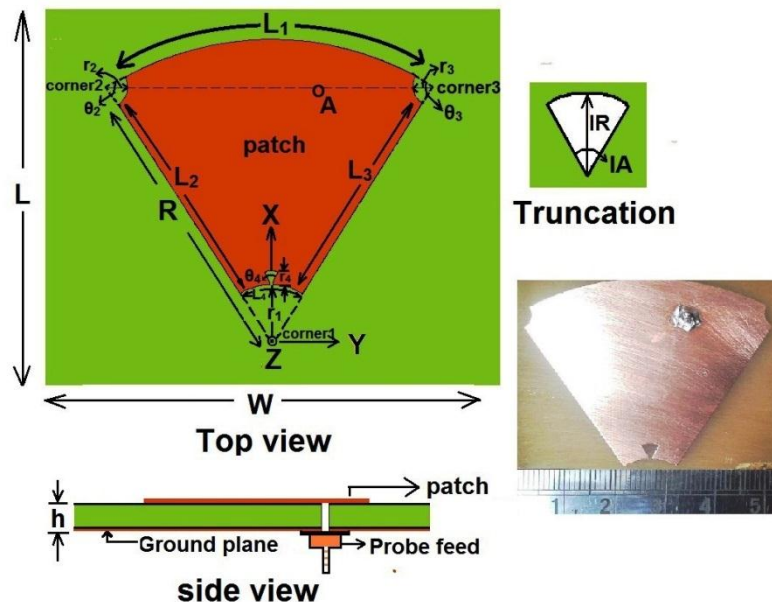


Fig. 5.2. Geometry and photograph of the triband dual polarized sectoral patch antenna ($L=50$, $W=40$, $R=45$, $L_1 = 51$, $h=1.6$ (all in mm), $A(37,7)$, $\epsilon_r=4.4$)

The reflection and CP characteristics of all the intermediate structures shown in Fig.5.1 are analyzed in the next section.

5.2.2 Antennal characteristics

Antenna 1 is the structure that results after the truncation of corner1. By optimizing the ground plane dimensions after this step, it amounts to 64% size reduction of the antenna when compared to the original sectoral patch without

the truncation [6]. Fig.5.3a reveals two independent resonances at 1.9 GHz and 3.5 GHz which are UMTS and WiMAX frequency ranges respectively.

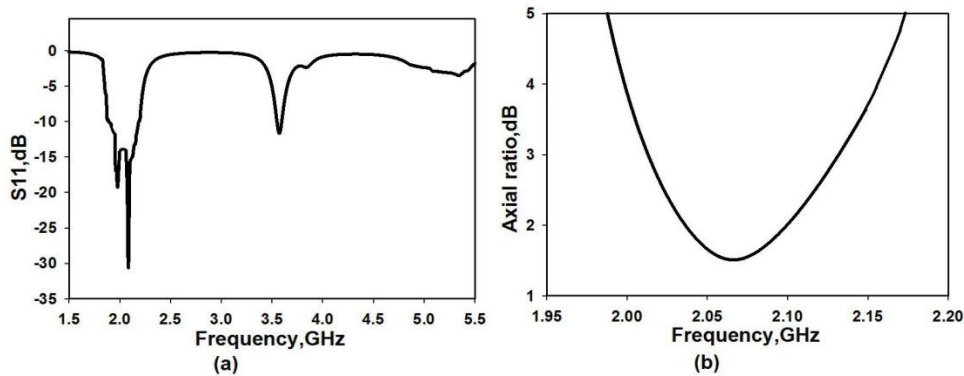


Fig. 5.3. Simulated a) reflection coefficient and b) axial ratio characteristics of Antenna1 ($L=50$, $W=40$, $R=45$, $L_1 = 51$, $r_1=9$, $h=1.6$ (all in mm), $A(37,7)$, $\epsilon_r=4.4$)

A strong discontinuity in Band 1 indicating the possibility of circularly polarized radiation which is confirmed from the simulated axial ratio characteristics in Fig.5.3b. To further reduce the patch size, corner 2 of Antenna 1 is truncated, which is described in the next section.

5.2.3 Antenna2 characteristics

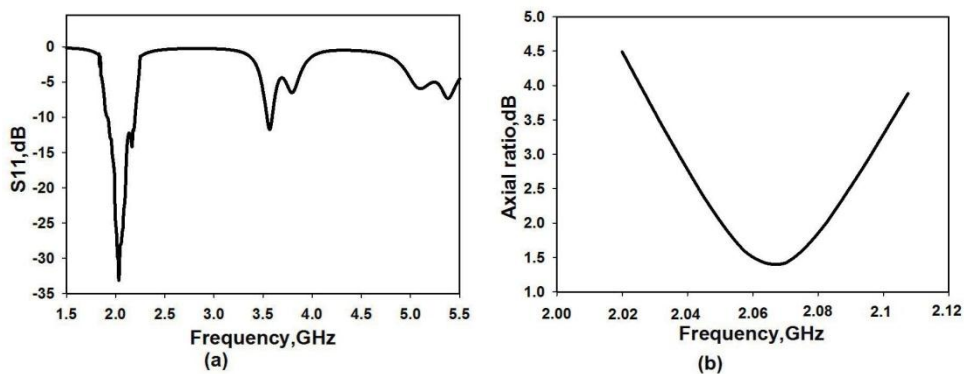


Fig. 5.4. Simulated a) reflection coefficient and b) axial ratio characteristics of Antenna2 ($L=50$, $W=40$, $R=45$, $L_1 = 51$, $r_1=9$, $r_2=3$, $h=1.6$ (all in mm), $A(37,7)$, $\epsilon_r=4.4$)

With the truncations applied at the two corners 1 and 2, the structure is denoted as Antenna2. Reflection coefficient and axial ratio characteristics are again simulated to study the CP performance of the antenna (Fig.5.4). It is observed that the two resonances remain within the respective bands as in those for the previous Antenna1. The polarization is also circular as seen from the axial ratio graph. The occurrence of two new close to each other poorly matched resonances in the vicinity of 5GHz is also noted. With a view to improve the matching and merge the two new close resonances, corner 3 in Antenna2 is truncated and the structure is explained in the next section.

5.2.4 Antenna3 characteristics

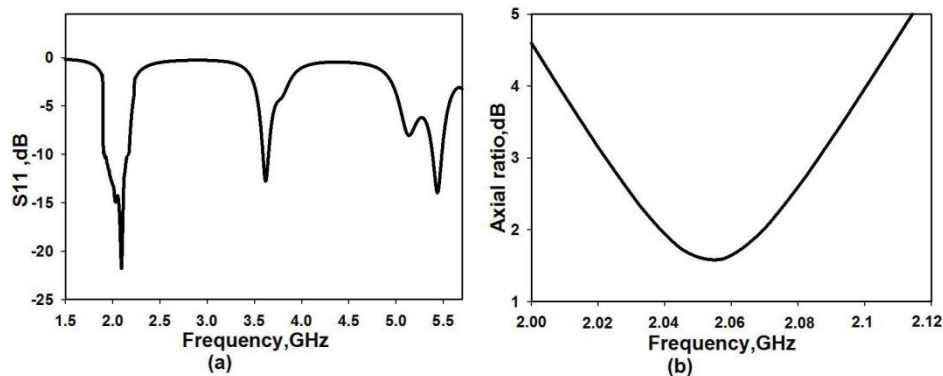


Fig. 5.5. Simulated a) reflection coefficient and b) axial ratio characteristics of Antenna3 ($L=50$, $W=40$, $R=45$, $L_1 = 51$, $r_1=9$, $r_2=3$, $r_3=3$, $h=1.6$ (all in mm), $A(37,7)$, $\epsilon_r=4.4$)

The corner 3 in Antenna2 is truncated with a sectoral portion of radius r_3 . This structure is denoted as Antenna3 and the reflection coefficient and axial ratio characteristics are simulated and examined as in Fig.5.5. The first and second resonances remain in the frequency ranges of UMTS and WiMAX itself while the two close resonances near 5 GHz have not yet merged but have become better matched in impedance. But these two

resonances are not in the ISM 5.2 frequency region of interest. The next step is to introduce further modification of the patch which can result in merger of the two resonances and also tune them to the desired ISM 5.2 band. This is explained in the next section.

5.2.5 Antenna4 characteristics

The evolution of the proposed antenna becomes complete with the carving of a sectoral indentation of radius r_4 and angle θ_4 at the midpoint of the truncated edge L_4 . This is the final structure Antenna4. The reflection coefficient and axial ratio characteristics of Antenna4 are illustrated in Fig.5.6.

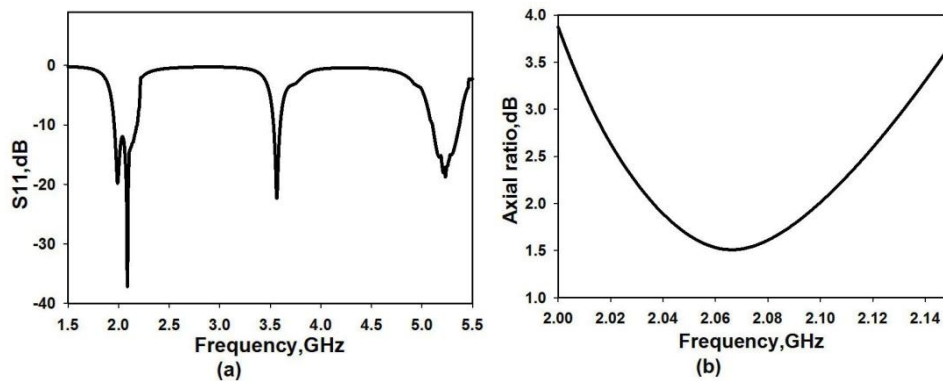


Fig. 5.6. Simulated a) reflection coefficient and b) axial ratio characteristics of Antenna4 ($L=50$, $W=40$, $R=45$, $L_1 = 51$, $r_1=9$, $r_2=3$, $r_3=3$, $r_4=2$, $h=1.6$ (all in mm), $A(37,7)$, $\epsilon_r=4.4$)

It is observed that etching of the small indentation at edge L_4 helps to improve the impedance matching at the third band and merges the two close resonances. The effective length at edge L_4 is increased by this indentation without any change in the physical dimensions of the patch. The current path through L_4 is adjusted and consequently the resonance is tuned to the ISM 5.2 range. The feed point is adjusted to fine tune the reflection and axial ratio characteristics to their best possible values. This point is located

at A (37, 7). The dimensions of the ground plane are also optimized. The effects of all the truncations on the antenna characteristics are examined by parametric variation and through simulated patch surface current distributions in the following sections.

5.2.6 Parametric analysis of the triband sectoral patch antenna

Parametric analysis through simulation helps to gain a better insight into the antenna performance. The manner in which each parameter affects the antenna characteristics is discussed below.

5.2.6.1 Effect of truncation length r_1 on reflection coefficient and CP characteristics

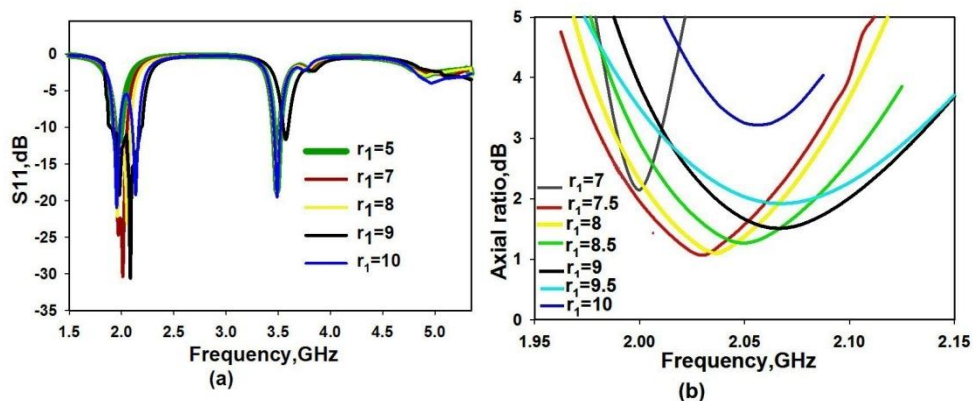


Fig. 5.7. Effect of variation of r_1 on a) reflection coefficient and b) axial ratio characteristics of Antenna1 ($L=50$, $W=40$, $R=45$, $L_1 = 51$, $\theta_1 = 65^\circ$, $h=1.6$ (all in mm), A(37,7), $\epsilon_r=4.4$)

The increase in truncation length r_1 has little effect on the impedance matching in Band 1 while the matching at Band 2 improves as seen from Fig.5.7a. At the same time, the CP characteristic in Band 1 becomes poorer as AR value falls above the 3 dB level (Fig 5.7b). Hence to get adequate impedance matching at both bands and appropriate CP performance in Band 1, optimum value of the truncation length is selected as $r_1=9$ mm.

5.2.6.2 Effect of truncation length r_1 on ground plane dimensions

It is observed that without the truncation, a large ground plane of size $75\text{mm} \times 75\text{mm}$ is required. It is seen that when the corner 1 is truncated, the ground plane area could be optimized to $40\text{mm} \times 50\text{mm}$ which amounts to a 64% reduction in the antenna size. The ARBW is also increased by 100 MHz. This is the major advantage of the corner truncation method. Table 5.1 tabulates the variation of ground plane area with r_1 .

Table 5.1. Effect of r_1 on ground plane size

Truncation length r_1 (mm)	CP characteristics		Ground plane size $W \times L(\text{mm}^2)$	Input impedance in Band1(Ω)	
	ARBW (MHz)	ARmin(dB)		Re	Im
0	25	1.3	75×75	67	47
1	--	4.17	60×60	69	47
3	--	16	55×60	78	49
5	--	12.5	55×55	81	50
7	50	1.73	55×55	56	45
9	125	1.51	40×50	50	40

5.2.6.3 Effect of truncation length r_2 on reflection coefficient and CP characteristics

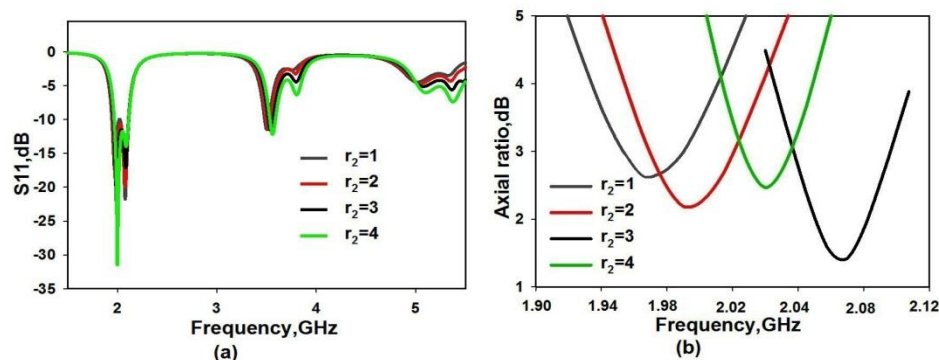


Fig. 5.8. Effect of variation of r_2 on a) reflection coefficient and b) axial ratio characteristics of Antenna2 ($L=50$, $W=40$, $R=45$, $L_1 = 51$, $\theta_1 = 65^\circ$, $\theta_2 = 90^\circ$, $r_1=9$, $h=1.6$ (all in mm), $A(37,7)$, $\epsilon_r=4.4$

Keeping the truncation length r_1 fixed at 9mm, the corner 2 is also truncated by a length r_2 which results in the structure designated Antenna2. The reflection and axial ratio characteristics are depicted in Fig.5.8. From Fig.5.8a it is observed that the matching in Band 1 is not much affected by the variation in r_2 . However, the CP performance is disturbed as seen from Fig.5.8b where the axial ratio characteristics fall above the 3 dB level beyond $r_2=4$ mm. This is because the orthogonal dimensions of the patch are no longer such that the near degenerate TM_{01} and TM_{10} modes are combined. The occurrence of a poorly matched resonance near the 3.5 GHz band is noted. At the same time two poorly matched close resonances in the 5 GHz vicinity is also observed. There is only negligible shift in the frequencies at the Band1 and Band 2, but they still remain within the respective ranges of UMTS and WiMAX. To get optimum CP characteristics with adequate matching in the two bands, the best value of $r_2=3$ mm is selected.

5.2.6.4 Effect of truncation length r_3 on reflection coefficient and CP characteristics

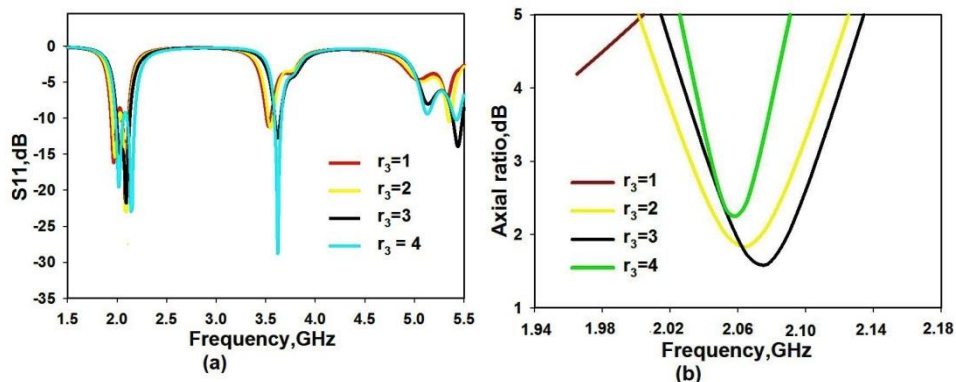


Fig. 5.9A. Effect of variation of r_3 on a) reflection coefficient and b) axial ratio characteristics of Antenna3 with r_2 fixed ($L=50$, $W=40$, $R=45$, $L_1 = 51$, $\theta_1 = 65^\circ$, $\theta_2 = \theta_3 = 90^\circ$, $r_1=9$, $r_2=3$, $h=1.6$ (all in mm), $A(37,7)$, $\epsilon_r=4.4$

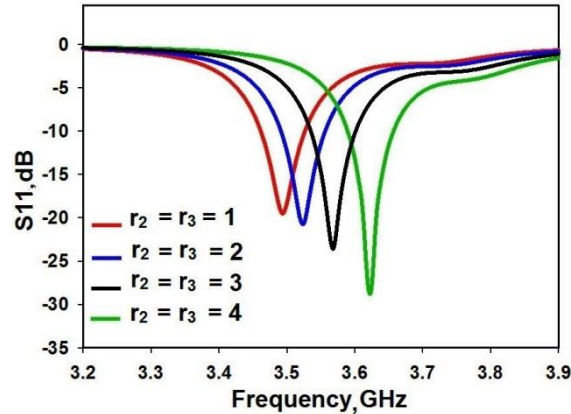


Fig. 5.9B. Effect of variation of r_2 and r_3 on reflection coefficient of Antenna3 in Band 2 ($L=50$, $W=40$, $R=45$, $L_1 = 51$, $\theta_1 = 65^\circ$, $\theta_2 = \theta_3 = 90^\circ$, $r_1=9$, $h=1.6$ (all in mm), $A(37,7)$, $\epsilon_r=4.4$)

Keeping the truncation length r_2 constant at 3mm, the corner 3 truncation length r_3 was varied. The reflection characteristics in Band 1 is not much affected by this truncation, but that at the Band 2 improves with increase in r_3 as is seen from Fig.5.9Aa. The axial ratio characteristics deteriorate beyond $r_3=3$ mm as seen from Fig.5.9Ab. This is again because the truncation changes the orthogonal dimensions of the patch such that they are not in a ratio that can excite near-degenerate orthogonal modes. The two close resonances near 5 GHz are present and have improved in matching but not merged. The optimum value to obtain perfect matching and CP performance is found as $r_3 = 3$ mm.

As the truncation length r_3 has an impact on the impedance matching in Band 2, its effect on this frequency band was further analyzed by varying the truncation length r_2 equally with r_3 . This is shown in Fig.5.9B. It is understood from the graph that although the matching increases with increase in r_2 and r_3 , for values beyond 3mm, the resonance shifts to a

region beyond the desired band of WiMAX frequency. Thus based on all the above observations, the optimum values for r_2 and r_3 are selected as 3 mm where the lowest reflection coefficient value and ideal location within the band of interest (3.3-3.6 GHz) are obtained.

5.2.6.5 Effect of sectoral notch at edge L_4 on reflection and CP characteristics

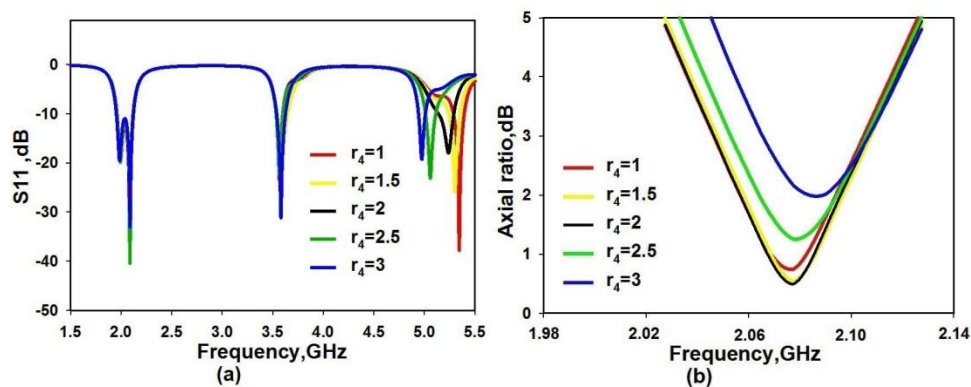


Fig. 5.10. Effect of variation of r_4 on a) reflection coefficient and b) axial ratio characteristics of Antenna4 in the three bands ($L=50$, $W=40$, $R=45$, $L_1 = 51$, $r_1=9$, $r_2=r_3=3$, $\theta_1 = 65^\circ$, $\theta_2 = \theta_3 = \theta_4=90^\circ$, $h=1.6$ (all in mm), $A(37,7)$, $\epsilon_r=4.4$)

In order to merge the two resonances near 5 GHz and to tune the third frequency band to the desired ISM 5.2 band, the sectoral indentation of radius r_4 and angle θ_4 is etched at the centre of the truncated edge L_4 . The dimensions r_4 and θ_4 were varied to study their impacts on the antenna performance. By introducing this indentation, the effective length of edge L_4 is increased without increasing the patch physical length. The current path through L_4 is modified which in turn tunes the third resonance to the desired frequency location. This is carried out by varying the parameters r_4 and θ_4 . This in turn results in controlling the frequency ratio of the second and third frequency bands. Only the third band is tuned by this notch, while the first

and second bands remain unaffected. This can be observed from the reflection and axial ratio characteristics portrayed in Fig.5.10. Here r_4 is varied while keeping θ_4 fixed at 90° . The third band shifts towards the left in frequency as the indentation radius is increased from 1. At $r_4=2$, the band precisely coincides with the desired ISM 5.2 band.

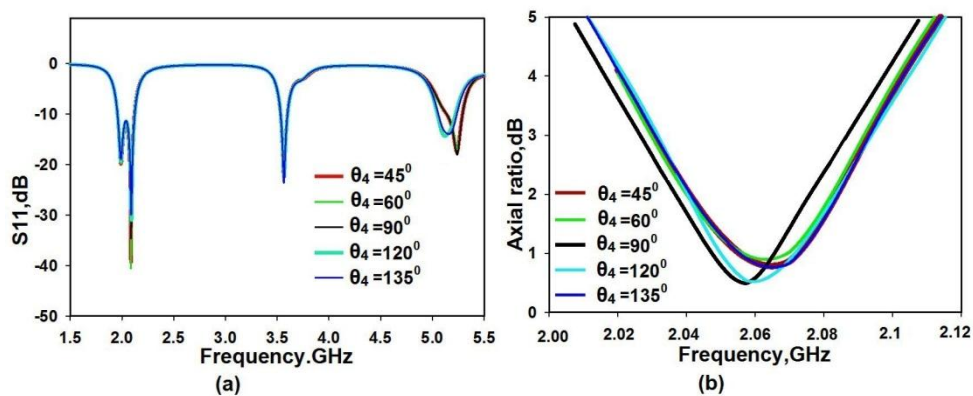


Fig. 5.11. Effect of variation of θ_4 on a) reflection coefficient and b) axial ratio characteristics of Antenna4 in the three bands with r_4 constant ($L=50$, $W=40$, $R=45$, $L_1 = 51$, $r_1=9$, $r_2=r_3=3$, $r_4=2$, $\theta_1 =65^\circ$, $\theta_2 = \theta_3 = 90^\circ$, $h=1.6$ (all in mm), $A(37,7)$, $\epsilon_r=4.4$

The process of varying r_4 is repeated for more values of the indentation angle θ_4 and the results are shown in Fig.5.11. The effect of varying the indentation angle θ_4 is similar to that of varying the indentation radius. The first two bands remain unaffected, while the third band is shifted to the left in frequency. Likewise, the CP characteristics also are not affected.

The effects of varying the indentation parameters on the frequency ratio between Bands 2 and 3 are consolidated in Table 5.2. The variation of θ_4 has no significant effect on the frequency ratio between Band2 and Band3

as can be seen from the table. Hence it is concluded that varying the indentation radius can be conveniently put to use for tuning the third band to the desired frequency range. For the range of values of r_4 and θ_4 selected, the frequency ratio varies in the range 1.39 to 1.51. The optimum values of $r_4 = 2$ and $\theta_4 = 90^\circ$ for locating the third band precisely in the ISM 5.2 range are selected.

Table 5.2 Effect of r_4 and θ_4 on Band2 and Band3 frequency ratio

Angle θ_4	Radius r_4 (mm)	Resonant Frequencies(GHz)		Frequency ratio (f_3/f_2)
		Band 2(f_2)	Band 3(f_3)	
45°	1	3.56	5.35	1.51
	1.5	3.56	5.325	1.49
	2	3.56	5.237	1.47
	2.5	3.56	5.075	1.42
60°	1	3.56	5.34	1.5
	1.5	3.56	5.306	1.49
	2	3.56	5.237	1.47
	2.5	3.56	5.093	1.43
90°	1	3.56	5.331	1.49
	1.5	3.56	5.3	1.48
	2	3.56	5.206	1.46
	2.5	3.56	4.975	1.39

5.2.7 Analysis of modes excited in the three bands

The surface current distribution in the antenna is an efficient tool to analyze the modes that are excited at the different resonance frequencies. The simulated current distributions at the centre frequencies of the three bands were studied.

5.2.7.1 Mode at Band 1

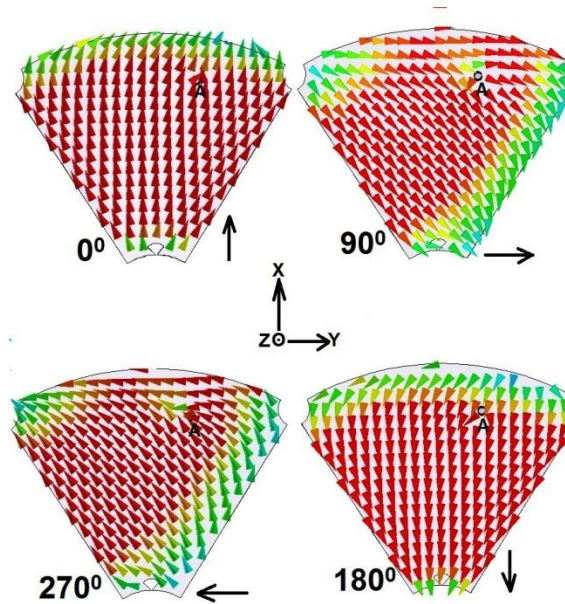


Fig. 5.12. Surface current distribution on Antenna4 in the Band 1 centre frequency ($L=50$, $W=40$, $R=45$, $L_1 = 51$, $r_1=9$, $r_2=r_3=3$, $r_4=2$, $\theta_1 =65^\circ$, $\theta_2 = \theta_3 = \theta_4=90^\circ$ $h=1.6$ (all in mm), $A(37,7)$, $\epsilon_r=4.4$)

The simulated surface current distribution at the Band1 centre frequency (2.06 GHz) is shown in Fig.5.12. The orthogonal dimensions of the patch perturb the fundamental TM_{10} mode so as to split it into two near degenerate modes with equal amplitude and 90° phase difference resulting in the generation of good circularly polarized radiation at the Band1. The current distribution at four different phase instants are shown from which the sense of polarization is inferred as left handed, for the feed point at A. The sense of polarization becomes right handed if the feed is applied at the mirror image point of A with respect to the X axis.

5.2.7.2 Mode at Band 2

The simulated current distribution at the Band 2 centre frequency (3.56 GHz) is illustrated in Fig.5.13. Two half wave variations in surface current can be noticed along the Y direction in the figure.

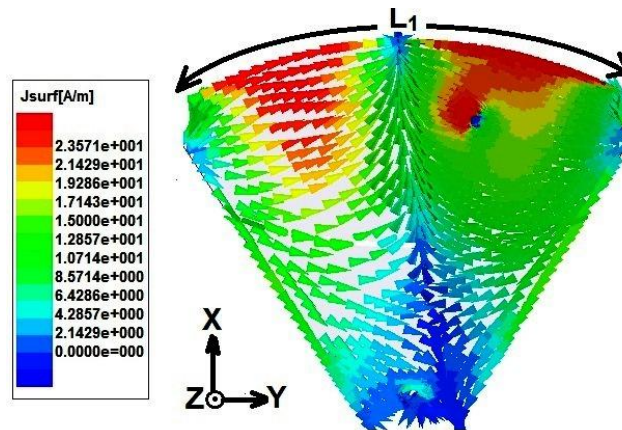


Fig. 5.13. Surface current distribution on Antenna4 in the Band 2 = centre frequency ($L=50$, $W=40$, $R=45$, $L_1 = 51$, $r_1=9$, $r_2=r_3=3$, $r_4=2$, $\theta_1 = 65^\circ$, $\theta_2 = \theta_3 = \theta_4=90^\circ$ $h=1.6$ (all in mm), $A(37,7)$, $\epsilon_r=4.4$)

In the X direction there is no variation. Hence at this resonance the mode generated is the higher order TM_{20} . It can also be inferred from the figure that the strong current distribution along the edge L_1 is responsible for the generation of the Band 2 resonance. The type of polarization is apparently linear and is directed along the Y axis.

5.2.7.3 Mode at Band 3

The simulated current distribution at the Band 3 resonance is shown in Fig.5.14. In the previous section it was explained that the resonance at Band 3 is due to the merger of two close resonances near 5.1 GHz. These two close resonances were found as 5 GHz and 5.4 GHz. The operating modes at these two frequencies were examined and were found to be different. TM_{22}

and TM_{13} modes were excited at these two frequencies respectively, as is obvious from the Fig.5.14.

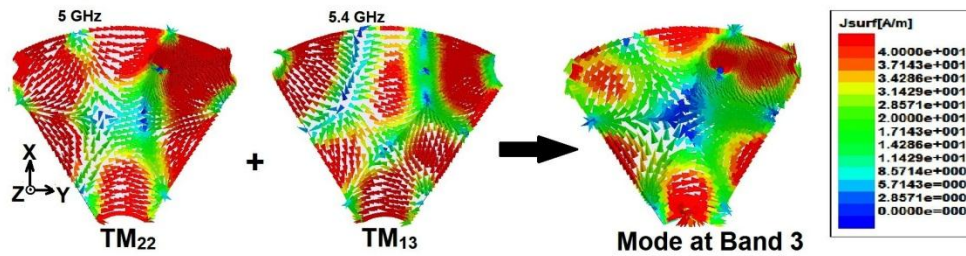


Fig. 5.14. Surface current distribution on Antenna4 in the Band 3 centre frequency ($L=50$, $W=40$, $R=45$, $L_1 = 51$, $r_1=9$, $r_2=r_3=3$, $r_4=2$, $\theta_1 =65^\circ$, $\theta_2 = \theta_3 = \theta_4=90^\circ$ $h=1.6$ (all in mm), $A(37,7)$, $\epsilon_r=4.4$)

Two half wave variations each are observed in the patch along the X and Y directions at 5 GHz. One half wave variation along the X axis and three half wave variations along the Y axis are observed at 5.4 GHz. These TM_{22} and TM_{13} modes combine to produce the degenerate mode at Band 3.

The resonance frequencies at the higher order TM_{22} and TM_{13} can also be theoretically calculated by approximating the patch shape to that of an equilateral triangle of side equal to R mm [7]. Accordingly, the resonance frequency at higher order modes (m, n) is given by,

$$f_{m,n} = \frac{2c}{3a_e\sqrt{\epsilon_r}}\sqrt{m^2 + mn + n^2} \dots\dots\dots (5.1)$$

where a_e is the effective side length of the patch, c is the velocity of light and ϵ_r is the dielectric constant of the substrate. Applying this equation, the resonance frequencies at (m, n) = (2, 2) and (1, 3) approximate to 5 GHz and 5.4 GHz. Thus the modes at Band3 are mathematically verified.

The strong current distribution seen along edge L_4 also further asserts that this dimension is the major contributor for the resonance at Band 3. The type of polarization at this frequency is evidently linear and is directed along the X axis. Thus it can be concluded from the study of the modes that the Band 2 and Band 3 are of orthogonal linear polarizations which is later confirmed experimentally.

5.2.8. 3D radiation plots of Antenna 4

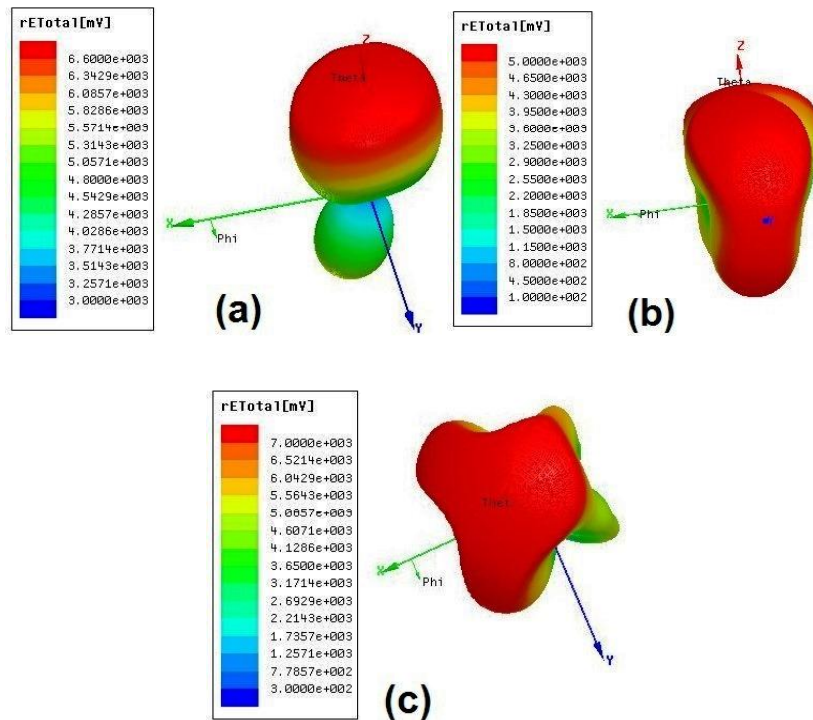


Fig. 5.15. Simulated radiation plots of Antenna4 at a) 2.06 GHz b) 3.56 GHz c) 5.2 GHz ($L=50$, $W=40$, $R=45$, $L_1 = 51$, $r_1=9$, $r_2=r_3=3$, $r_4=2$, $\theta_1 = 65^\circ$, $\theta_2 = \theta_3 = \theta_4=90^\circ$ $h=1.6$ (all in mm), $A(37,7)$, $\epsilon_r=4.4$)

The three dimensional radiation patterns of the proposed triband sectoral patch antenna were observed through simulation to get a picture of

the shape and direction of the radiations at the three centre frequencies. The three plots are depicted in Fig.5.15. It is observed that the pattern is directional at the Band1 frequency. At the Band2 centre frequency, the pattern is almost omnidirectional. Side lobes begin to appear at the higher Band3 centre frequency and the pattern is non-directional.

5.2.9 Experimental Measurements

The prototype of the proposed antenna was fabricated using conventional photolithographic process on an FR4 substrate of $\epsilon_r = 4.4$ and thickness $h=1.6\text{mm}$ with optimum dimensions of $R = 45\text{mm}$, $L_1 = 51\text{mm}$, $r_1=9\text{ mm}$, $r_2 = r_3 =3\text{ mm}$, $W = 40\text{mm}$, $L = 50\text{ mm}$. The antenna was experimentally tested to measure its performances with respect to reflection, transmission, axial ratio, radiation patterns and gain using the PNAE8362B Network Analyzer. The measured results were compared with the simulated characteristics and were verified to be in good agreement.

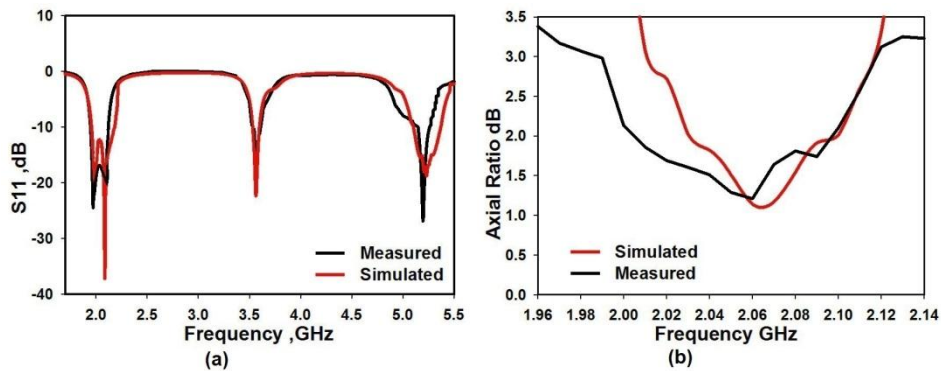


Fig. 5.16. Measured a) reflection coefficient and b) axial ratio characteristics of the proposed antenna ($L=50$, $W=40$, $R=45$, $L_1 = 51$, $r_1=9$, $r_2=r_3=3$, $r_4=2$, $\theta_1 =65^\circ$, $\theta_2 = \theta_3 = \theta_4=90^\circ$ $h=1.6$ (all in mm), $A (37, 7)$, $\epsilon_r=4.4$

Fig.5.16a shows the measured reflection characteristics of the proposed antenna on comparison with the simulated results. The UMTS,

WiMAX and ISM 5.2 frequency bands are covered with 11.2%, 5.14% and 3.9% impedance bandwidths respectively. The axial ratio bandwidth was also experimentally measured and is plotted along with the simulated ARBW in Fig.5.16b.

Table 5.3. Comparison of proposed antenna with other structures

Parameter		Proposed Antenna	Two corners truncated CDSPA[8]	Unmodified CDSPA[6]
Impedance BW (%)		11.2	3	4
ARBW (%)		5.8	1.3	1.2
f_c (GHz)		2.06	2.017	1.944
Ground plane reduction (%)		64	55	--
Input Impedance(Ω)	Re	50	64	67
	Im	41	-10	46

The CP centre frequency defined as the frequency at which minimum axial ratio value is obtained is observed as 2.06 GHz. An ARBW of 5.8% is obtained at this centre frequency. This is a significant improvement in comparison to the original unmodified circular disc sector patch antenna (CDSPA) in [6] and the two corners truncated sectoral patch having two corner truncations in [8]. The combined effect of three factors are accountable for this increase in ARBW. They are selection of the most optimum feed point, reduction in ground plane size and lowering of the Q factor of the patch. The feed point was carefully adjusted so as to reach the point with the best impedance matching and CP characteristics. The input impedance values for structures in [6] and [8] are shown compared with the proposed Antenna4 in Table 5.3 to verify this point. It is understood that the input impedance is equal to 50 Ω in the proposed antenna.

The ground plane size has been optimized in the proposed design, which amounts to a 64% reduction in its area. The Q factor has been lowered by the truncations applied at the three corners and the sectoral notch at edge L₄. In a truncated corner microstrip patch antenna, the inverse relationship between the Q factor and the truncation length L_t is given by [9] as

$$L_t = \frac{L}{\sqrt{2Q}} \dots\dots\dots (5.2)$$

where L is the side length of the patch. According to this relation, the proposed antenna possesses a low value of Q.

In a singly fed circularly polarized patch antenna the best approximation for ARBW % is equal to 35/Q [10]. This in turn means that a lower value of Q factor leads to a higher ARBW. These theoretical explanations account for the achievement of an ARBW value of 5.8% in the proposed antenna.

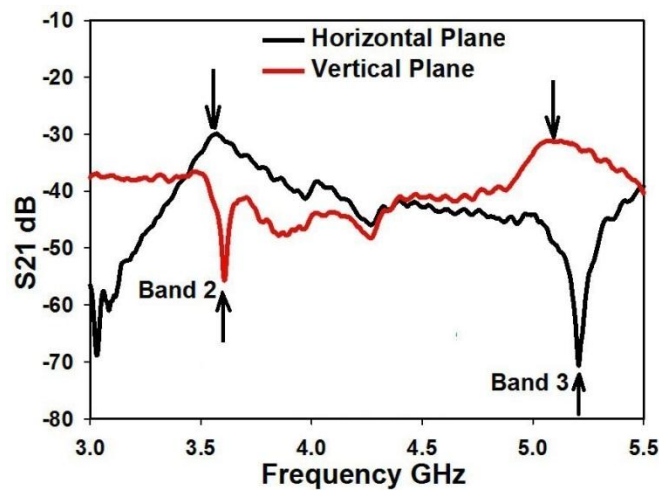


Fig. 5.17. Measured transmission coefficient of the proposed antenna in two orthogonal planes. (L=50, W=40, R=45, L₁ = 51, r₁=9, r₂=r₃=3, r₄=2, θ₁ =65°, θ₂ = θ₃ = θ₄=90° h=1.6 (all in mm), A(37,7), ε_r=4.4

To experimentally verify that the Bands 2 and 3 are orthogonal in polarization, the transmission coefficient S_{21} of the proposed Antenna4 in far field horizontal and vertical planes were measured, with the prototype configured as the receiver at port 1 and standard horn antenna as transmitter at port 2 of the network analyzer. The measured S_{21} characteristics are represented in Fig.5.17. It can be observed from the graph that in the horizontal plane, when Band 2 is at a peak, a dip or minimum is correspondingly observed in Band 3. Similarly in the vertical plane, the Band 2 shows a dip while Band 3 is at its peak value. Thus it is concluded that the polarizations of Band 2 and Band 3 are in orthogonal directions.

The measured 2D radiation patterns in two orthogonal planes provide a better understanding of the cross polar isolation of the proposed antenna as depicted in Fig.5.18. The 2D radiation patterns in the orthogonal y-z and x-z planes at the Band1 centre frequency in Fig.5.18a show that good left handed CP radiation is obtained in both planes. The measured patterns at the Band 2 centre frequency are nearly circular in the y-z plane and figure of eight in the x-z plane as seen from Fig.5.18b. The cross polar level isolation is of the order of 10 dB in the y-z plane, which is not a very high value. This is because the y- directed currents which have mirror image symmetry cancel more at this operating frequency, thus making the co-polarization level lower in the y-z plane. Consequently, the difference between co and cross polar radiations becomes lesser in this plane. However in the x-z plane, this difference is larger and is about 20 dB. The 2D radiation patterns at Band 3 centre frequency in Fig.5.18c indicate that the patterns undergo slight degradation due to the decreased electrical lengths at this frequency. The co-polar to cross polar isolation at this frequency is higher and is about 20

dB. This is because; the x directed currents are in the same direction at the Band 3 frequencies thus reinforcing each other. Hence the co-polarization is at a higher level resulting in a larger difference between the co and cross polar levels.

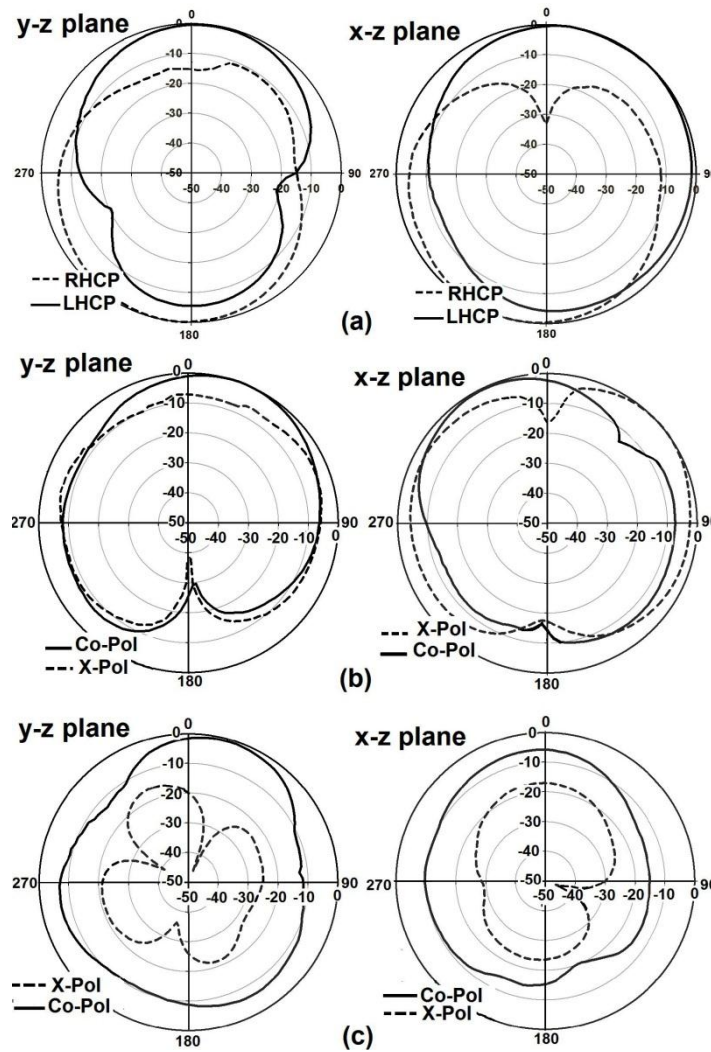


Fig. 5.18. Measured far field radiation patterns of the proposed antenna in two orthogonal planes at a) 2.06 GHz b) 3.56 GHz c) 5.2 GHz ($L=50$, $W=40$, $R=45$, $L_1 = 51$, $r_1 = 9$, $r_2=r_3=3$, $r_4=2$, $\theta_1 = 65^\circ$, $\theta_2 = \theta_3 = \theta_4=90^\circ$ $h=1.6$ (all in mm), $A(37,7)$, $\epsilon_r=4.4$

The gain of the proposed antenna in the boresight direction was measured by the gain comparison method. The gain plot is shown in Fig.5.19. The peak gains obtained in the three bands are 1.7dBi, 1.85dBi and 5.38dBi respectively in Bands 1, 2 and 3. A higher peak gain is obtained in Band 3. This can be attributed to the overlapping of the two higher order modes TM_{22} and TM_{13} at this frequency. The overlapping of the two modes strengthens the current densities in the Y direction which makes the radiation at this frequency more directive. This increased current density causes the higher gain in Band 3.

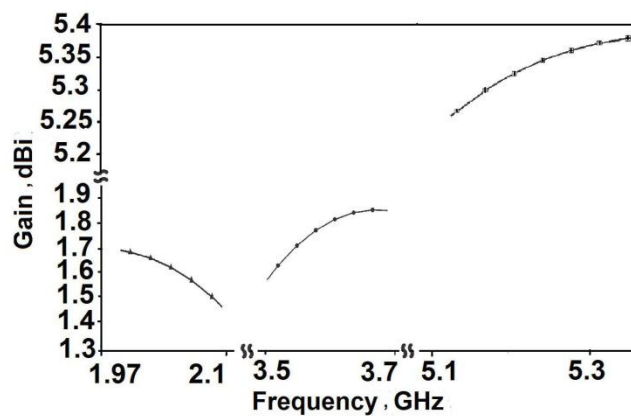


Fig. 5.19. Measured gain plot of the proposed antenna in the three operating bands ($L=50$, $W=40$, $R=45$, $L_1 = 51$, $r_1=9$, $r_2=r_3=3$, $r_4=2$, $\theta_1 =65^\circ$, $\theta_2 = \theta_3 = \theta_4=90^\circ$ $h=1.6$ (all in mm), $A(37,7)$, $\epsilon_r=4.4$

The radiation efficiencies at the centre frequencies were measured using the Wheeler cap method and were obtained as 61%, 54% and 40% respectively at the three bands.

5.3 Slotted ground triband dual polarized sectoral patch antenna for low cross polarization and enhanced gain

In the last section the triband dual polarized corner truncated sectoral patch antenna was analyzed for its properties and performance. One important limitation that was noticed in its characteristics was the higher cross polarization level in the second and third bands of operation. In this section, the antenna is modified by etching slots in the ground and is investigated to reduce the level of cross polarization and improve the gain.

Some of the popular broad banding techniques adopted for bandwidth enhancements of microstrip antenna are using a thick substrate [11], embedding of slots in the patch [12] and stacking of patches [13]. An undesired side effect of these broad banding techniques is the increase in cross polar radiation [14]. Achieving compactness via size reduction methods can also result in increased cross polarization [15]. The triband corner truncated sectoral patch antenna described in the previous section has been modified by etching circular slots in ground plane and the effects on the performance are explored thoroughly.

5.3.1 Antenna geometry

Circle shaped slots are etched at strategic locations in the ground plane of the triband dual polarized corner truncated sectoral patch antenna. Examination of the radiation patterns obtained reveals that this method helps to decrease the cross polarization levels significantly in the third resonance band. The antenna geometry is shown in Fig.5.20.

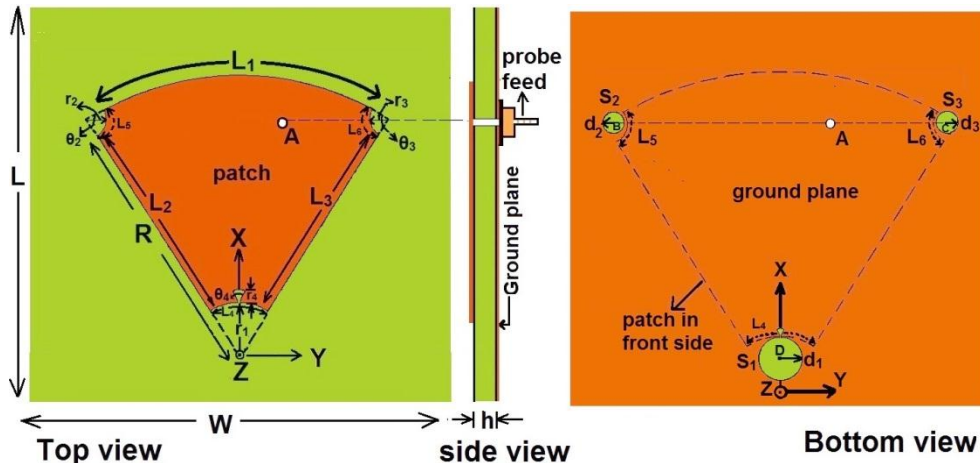


Fig. 5.20. Geometry of the slotted ground triband dual polarized sectoral patch antenna ($L=45$, $W=52$, $R=45$, $L_1 = 51$, $r_1=9$, $r_2= r_3=3$, $d_1=3$, $d_2= d_3=1.5$, $h=1.6$ (all in mm) $\theta_1 =65^\circ$, $\theta_2 = \theta_3 = \theta_4=90^\circ$, $D(5.5,0)$, $A(37,7)$, $\epsilon_r=4.4$)

The prototype of the antenna is designed on an FR4 substrate of $\epsilon_r = 4.4$ and thickness $h=1.6$ mm. The dimensions of the sectoral patch on top of the substrate are kept identical to those in the triband dual polarized sectoral patch antenna described in the previous section. The feed position is also unchanged. A major modification has been made in the ground plane. The bottom side is modified by etching three circular slots s_1 , s_2 and s_3 precisely below the sectoral corner truncations on the patch on top side. These three circular slots are with centers at D , B and C respectively and are of radii d_1 , d_2 and d_3 respectively. They are carefully located so as not to disturb the dominant modes in the patch and keep the backward radiation minimum. The slots are embedded in the ground plane such that their circumferences are exactly aligned with the truncated edges L_4 , L_5 and L_6 respectively above in the Z direction.

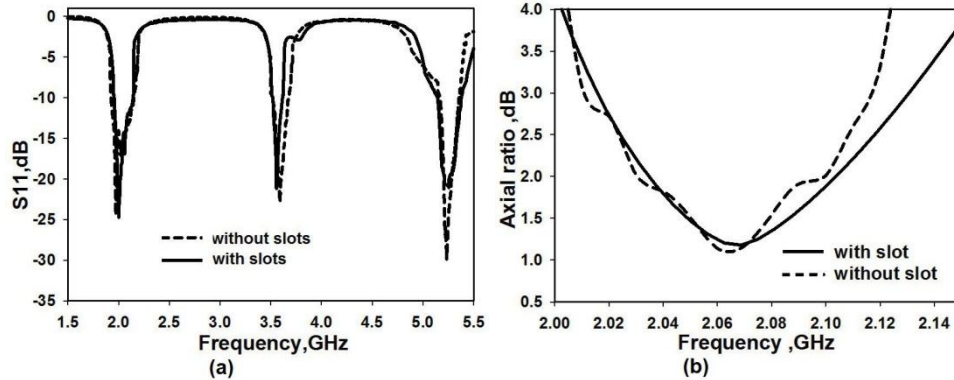


Fig. 5.21. Simulated a)reflection coefficient and b)axial ratio characteristics of the triband sectoral patch antenna with & without circular slots in ground plane ($L=45$, $W=52$, $R=45$, $L_1 = 51$, $r_1=9$, $r_2= r_3=3$, $d_1=3$, $d_2= d_3=1.5$, $h=1.6$ (all in mm) $\theta_1 =65^\circ$, $\theta_2 = \theta_3 = \theta_4=90^\circ$, $D (5.5,0)$, $A(37,7)$, $\epsilon_r=4.4$)

The antenna exhibits circularly polarized radiation in the first band and linear polarization in the second and third bands. The simulated reflection characteristics of the antenna are shown compared with the case without ground slots in Fig.5.21a. The resonances remain unchanged at the same frequency locations. The impedance bandwidth also is unaffected. The axial ratio characteristics are also simulated (Fig.5.21b) and it shows that the CP characteristics in the first band are preserved. The 3dB ARBW however shows a small increase with the slots applied.

5.3.2 Parametric study of the slotted ground triband sectoral patch antenna

As the main aim of the design was the reduction in cross polarization levels in the linearly polarized bands, the effect of these circular slots on the radiation patterns in Band 2 and Band 3 are analyzed parametrically. The performance characteristics that are studied are reflection coefficient, axial ratio and isolation between co polarization and cross polarization.

5.3.2.1 Effect of variation of radius d_1 of slot 1

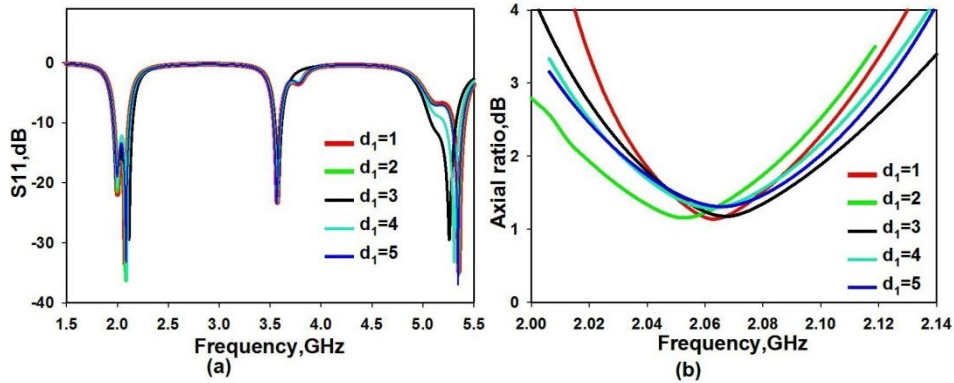


Fig. 5.22. Simulated a) S_{11} and b) axial ratio with radius d_1 of slot 1 varied ($L=45$, $W=52$, $R=45$, $L_1 = 51$, $r_1=9$, $r_2=r_3=3$, $d_2= d_3=1.5$, $h=1.6$ (all in mm) $\theta_1 =65^\circ$, $\theta_2 = \theta_3 = \theta_4=90^\circ$, $D(5.5,0)$, $A(37,7)$, $\epsilon_r=4.4$)

For the patch in Fig. 5.20, the radii d_2 and d_3 of slots s_2 and s_3 are kept fixed at 1.5mm and the radius d_1 of s_1 is varied from 1mm to 5mm and the effects on S_{11} and axial ratio characteristics are observed. The centre point of s_1 is also kept fixed at $D(5.5,0)$. The variation of d_1 does not affect the matching of the bands but the impedance bandwidth in Band 3 shows an increase with d_1 varying from 1 to 3mm. ARBW is also slightly different for different d_1 values. Increasing d_1 beyond 5mm causes the structure to lose its compactness. The best possible matching and minimum ARmin value with maximum ARBW is observed at $d_1=3$ mm. The results are displayed in Fig.5.22.

The levels of isolation between co and cross polarization levels are tabulated in Table 5.4. The slot radius variation has little or no effect on Band 2 while the cross polar level in both planes show marked changes with the variation. The optimum isolation level is found at $d_1=3$ mm.

Table 5.4. Effect of radius d_1 on cross polar level in Band 2 and Band 3

Slot radius(mm)			Cross polar isolation(dB)			
d_1	d_2	d_3	Band 2		Band3	
			YZ plane	XZ plane	YZ plane	XZ plane
1	1.5	1.5	13	12	15	15
2	1.5	1.5	14	13	18	18
3	1.5	1.5	12	13	23	23
4	1.5	1.5	11	12	20	20
5	1.5	1.5	13	14	22	23

5.3.2.2 Effect of variation of centre point D of slot 1

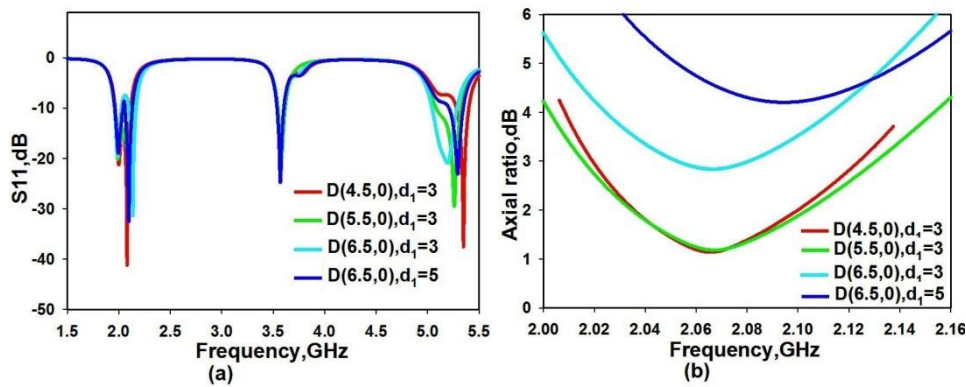


Fig. 5.23. Simulated a) S11 and b) axial ratio with centre point D of slot 1 varied ($L=45$, $W=52$, $R=45$, $L_1 = 51$, $r_1=9$, $r_2= r_3=3$, $d_1=3$, $d_2= d_3=1.5$, $h=1.6$ (all in mm) $\theta_1 =65^\circ$, $\theta_2 = \theta_3 = \theta_4=90^\circ$, $A(37,7)$, $\epsilon_r=4.4$)

Fig.5.23 shows the effect of variation of the centre point D of slot 1 on the S11 and axial ratio characteristics of the proposed antenna. Shifting D changes the alignment between the circumferences of the truncated edge L_4 and that of s_1 . Although this change does not affect the S11 values, the CP radiation in Band 1 is disturbed as seen from Fig.5.23b. Hence to preserve the CP in the dominant mode, D is kept fixed at (5.5,0).

5.3.2.3 Effect of variation of radii d_2 and d_3 of slots 2 & 3

The radius d_1 and the centre point D of slot1 are kept fixed and the radii d_2 and d_3 are varied from 0 to 2mm. Fig.5.24 shows the effect of these variations on the S11 and axial ratio characteristics of the proposed antenna. These variations produce no effect on the S11 characteristics. The axial ratio curves show small variation in terms of the minimum AR value and ARBW.

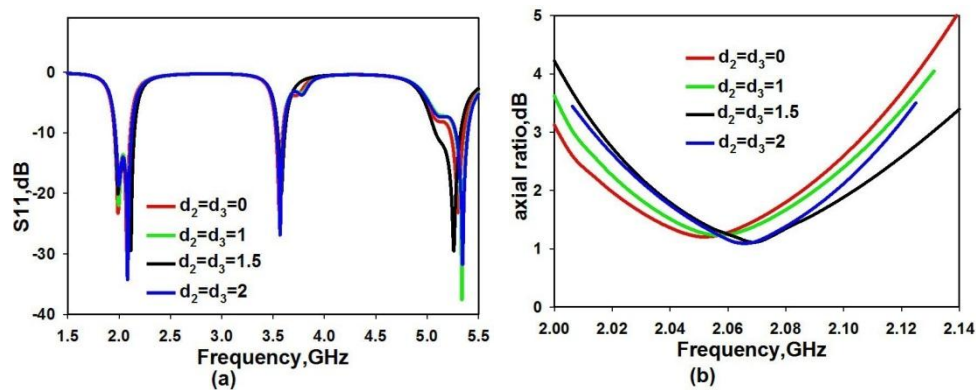


Fig. 5.24. Simulated a) S11 and b) axial ratio with d_2 and d_3 of slots 2 & 3 varied ($L=45$, $W=52$, $R=45$, $L_1 = 51$, $r_1=9$, $r_2= r_3=3$, $d_1=3$, $h=1.6$ (all in mm) $\theta_1 = 65^\circ$, $\theta_2 = \theta_3 = \theta_4=90^\circ$, $D(5.5,0)$, $A(37,7)$, $\epsilon_r=4.4$)

A valid point to be noted from the axial ratio graph is that the CP characteristics remain within the desired range even in the absence of the slots 2 and 3. To further probe into this case, the cross polar isolation in the bands 2 and 3 are tabulated in Table.5.5. It is observed that negligible change is occurring in the cross polar levels at Band 2. But the dimensions d_2 and d_3 have a more significant effect on the cross polar level in Band 3. The cross polar level is found to be high in Band 3 in the absence of the slots 2 and 3. Hence the optimum dimensions of d_2 and d_3 are selected as 1.5 mm.

Table 5.5. Effect of radii d_2 & d_3 on cross polar level in Band 2 and Band 3

Slot radius(mm)			Cross polar isolation(dB)			
d_1	d_2	d_3	Band 2		Band3	
			YZ plane	XZ plane	YZ plane	XZ plane
3	0	0	13	12	15	15
3	1	1.	14	13	18	18
3	1.5	1.5	12	13	23	23
3	2	2	11	12	20	20

5.3.3 Experimental measurements

The antenna prototype was fabricated with optimized dimensions in Table 5.6 on and FR4 substrate of $\epsilon_r = 4.4$ and thickness $h=1.6\text{mm}$ and was tested using the PNAE 8362B network analyzer.

Table 5.6. Optimized dimensions in the Antenna

Radius(mm)	r_1	r_2	r_3	r_4	d_1	d_2	d_3
	9	3	3	2			
Angle	θ_1	θ_2	θ_3	θ_4			
	65^0	90^0	90^0	90^0			

The measured and simulated S11 and axial ratio characteristics are compared with each other and are validated in Figs. 5.25a & 5.25b respectively. The respective graphs without the slots in the ground are also compared. The three resonances remain at the frequency ranges of UMTS, WiMAX and WLAN 5.2 respectively. -10dB return loss bandwidths of 10%, 4.5% and 4.1 % respectively are obtained in the three bands. An ARBW of 6.1% which is 0.3% more than that for the case without the slots is experimentally measured.

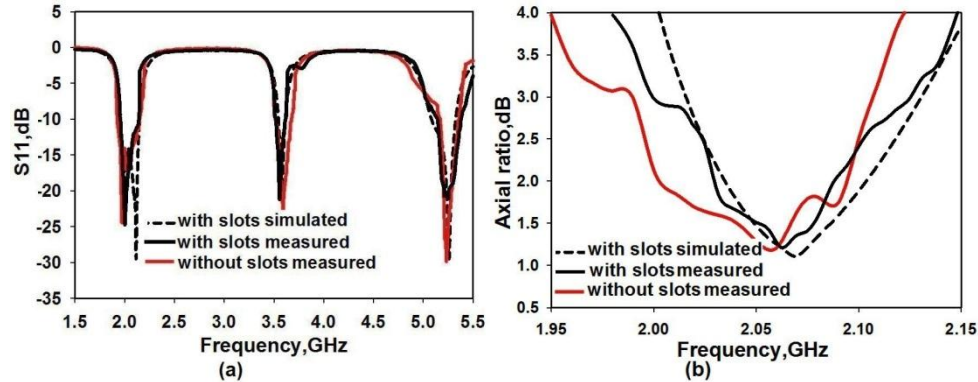


Fig. 5.25. Measured & simulated a) S_{11} and b) axial ratio characteristics for the triband sectoral patch antenna with & without sectoral slots in ground plane ($L=45$, $W=52$, $R=45$, $L_1 = 51$, $r_1=9$, $r_2= r_3=3$, $d_1=3$, $d_2= d_3=1.5$, $h=1.6$ (all in mm) , $\theta_1 =65^\circ$, $\theta_2 = \theta_3 = \theta_4=90^\circ$, $D(5.5,0)$, $A(37,7)$, $\epsilon_r=4.4$)

The radiation patterns were also experimentally measured and are shown plotted in Fig.5.26. In band 1 good LHCP radiation is observed at a centre frequency of 2.07GHz. Band 2 radiation pattern is almost similar to that of the antenna without ground slots. However in Band 3 there is a marked improvement as the cross polarization level is lowered to 23 dB which is 5dB lower than that in the case without the ground slots. The 3D radiation patterns at the three resonance frequencies in Bands 1-3 are also shown in Fig.5.26 which are identical to those for the antenna without the ground slots.

The gain was measured using the gain comparison method and the peak values were obtained as 1.92dBi, 1.8 dBi and 6.8 dBi respectively in the three bands. The radiation efficiencies measured using the Wheeler cap method were obtained as 61%, 54% and 72 % respectively in the three bands. All the measured characteristics of the proposed antenna are compared with those of the antenna without the slots in ground plane and are given in Table 5.7.

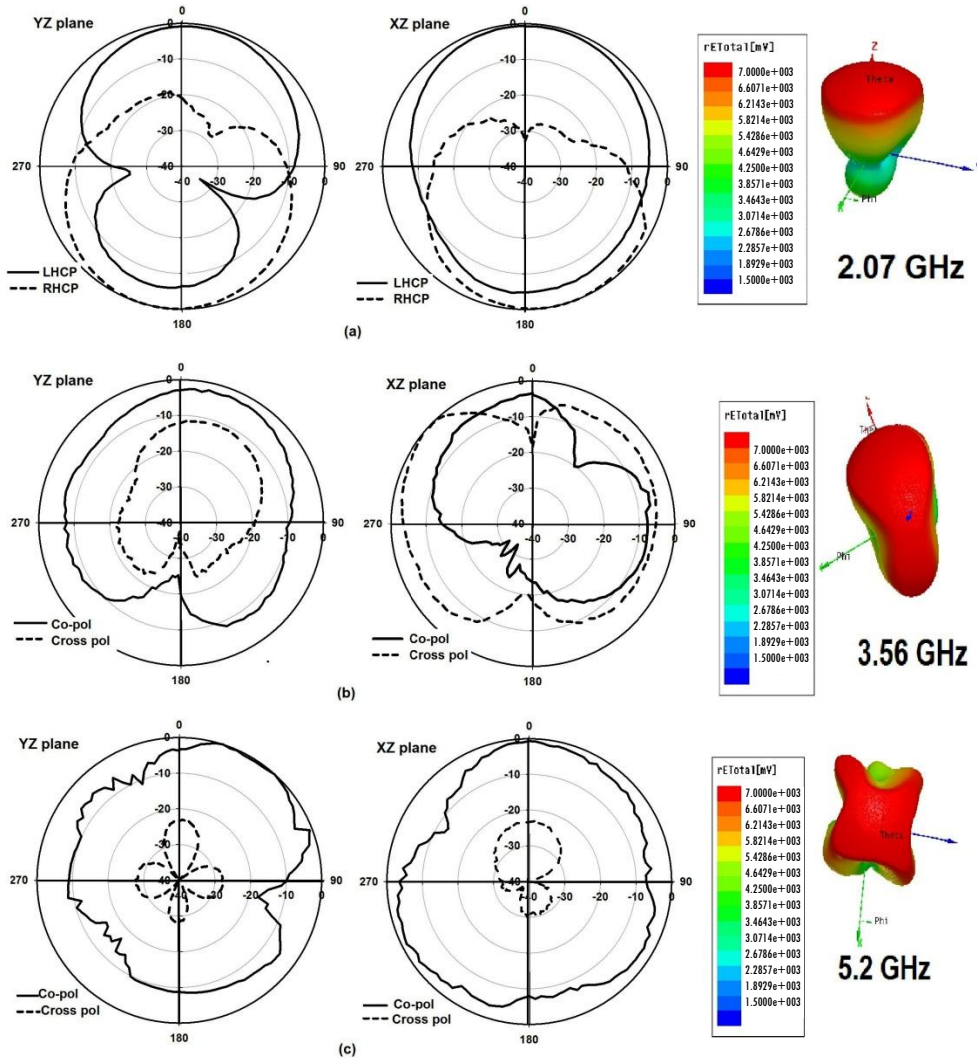


Fig. 5.26. 2D Measured and 3D simulated radiation patterns at a) 2.07 GHz b) 3.56 GHz c) 5.2 GHz for the slotted ground triband dual polarized sectoral patch antenna ($L=45$, $W=52$, $R=45$, $L_1 = 51$, $r_1=9$, $r_2= r_3=3$, $d_1=3$, $d_2= d_3=1.5$, $h=1.6$ (all in mm), $\theta_1 =65^\circ$, $\theta_2 = \theta_3 = \theta_4=90^\circ$, $D(5.5,0)$, $A(37,7)$, $\epsilon_r=4.4$)

The most significant improvements are in the values of peak gain, radiation efficiency and cross polar isolation in Band3. The increase in peak

gain is due to the enhancement of currents in the ground plane at the Band 3 frequency due to the presence of the slots. This can be well understood by visualizing the simulated current distribution in the ground plane at 5.2 GHz as illustrated in Fig.5.27.

Table 5.7. Comparison of Proposed Antenna with and without ground slots

Parameter	Proposed Antenna			Without slots [15]		
	Band1	Band2	Band3	Band1	Band2	Band3
Bandwidth (%)	10	4.5	4.1	11.2	5.1	3.9
ARBW (%)	6.1	---	---	5.8	---	---
ARmin	1.15	---	---	1.2	---	---
Peak gain(dBi)	1.92	1.86	6.8	1.7	1.85	5.38
Rad. efficiency (%)	63	55	72	61	54	40
F/B Ratio(dB)	6	25	9	5	23	7
Cross polar level(dB)	---	12	23	----	10	18

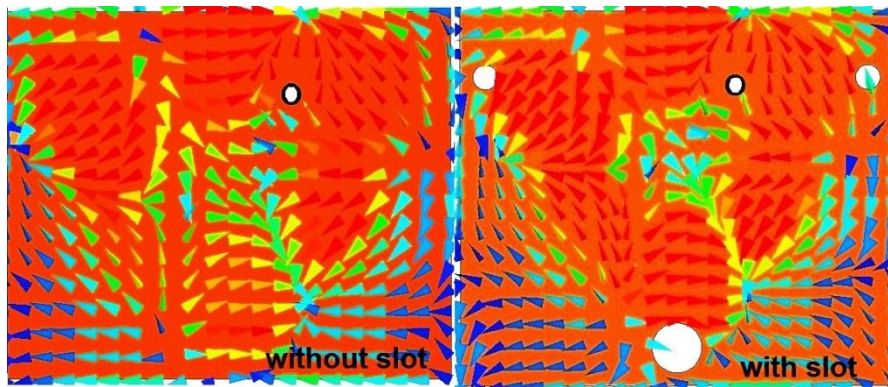


Fig. 5.27. Simulated current distribution on the ground plane at 5.2 GHz for the triband dual polarized sectoral patch antenna with and without slot ($L=45$, $W=52$, $R=45$, $L_1 = 51$, $r_1=9$, $r_2= r_3=3$, $d_1=3$, $d_2= d_3=1.5$, $h=1.6$ (all in mm) , $\theta_1 =65^\circ$, $\theta_2 = \theta_3 = \theta_4=90^\circ$, $D(5.5,0)$, $A(37,7)$, $\epsilon_r=4.4$)

The radiation efficiency measured in the first two bands show very little change in values whereas there is a significant improvement of 32 % in the value in Band 3. This marked improvement in radiation efficiency is attributed to the lowering of quality factor by the embedded circular slots in the ground plane. The surface currents traverse a longer path in the ground plane where the increase in length is equal to the total circumference of the embedded slots. This total circumference corresponds approximately to the guide wavelength λ_g given by

$$\lambda_g = \frac{\lambda}{\sqrt{\frac{\epsilon_r + 1}{2}}} \dots\dots\dots (5.3)$$

at the Band 3 resonance frequency, where λ is the free space wavelength. This could be the reason for the bands 1 and 2 being little affected by the presence of the slots in the ground plane.

A simple technique to reduce the cross polarization level and enhance the gain in the Band 3 without disturbing the CP characteristics in the fundamental mode has been experimentally investigated. The technique has the advantage of preserving the compactness of the structure along with improvement in the radiation efficiency.

5.4 Summary of the chapter

The triple band performance of the circular disc sector patch antenna with corner truncations has been studied in detail in this chapter. The polarization is circular in the first band and linearly orthogonal in the second and third bands. A higher value of CP bandwidth has been obtained by the lowering of Q resulting from the truncations. The indentation at the first

truncated corner is used to control the frequency ratio of the second and third bands. The excitations of degenerate modes have been emphasized. The overlapping of two higher order modes of the patch TM_{22} and TM_{13} in Band 3 strengthens the current density in the patch producing a higher gain at Band 3. The proposed antenna resonates in the UMTS, WiMAX, and the ISM5.2 bands and is appropriate for modern wireless communication systems where diverse polarizations are required.

The corner truncated sectoral patch antenna has been further studied with the objective of attaining reduced cross polarization and enhanced gain. The circle shaped slots etched at strategic locations in the ground plane of the corner truncated sectoral patch antenna helps to decrease the cross polarization levels significantly in the third resonance band. Radiation efficiency shows a marked improvement in the third band, which is attributed to the lowering of Q factor by the ground slots which elongates the current path. This simple technique improves the cross polar isolation level without disturbing the CP performance in the first resonance band.

References

- [1] Anguera, J., G. Font, C. Puente, C. Borja, and J. Soler, "Multifrequency microstrip patch antenna using multiple stacked elements," *IEEE Microwave and Wireless Component Letters*, Vol. 13, No. 3, pp.123-124, Mar. 2003.
- [2] Anguera, J., E. Martinez, C. Puente, C. Borja, and J. Soler, "Broad-band dual-frequency microstrip patch antenna with modified Sierpinski fractal geometry," *IEEE Trans. Antennas Propagat.*, Vol. 52, No. 1, 66-73, Jan. 2004.
- [3] Daniel, A. E. and G. Kumar, "Tuneable dual and triple frequency stub loaded rectangular microstrip antenna," *IEEE Trans. Antennas Propagat.*, Vol. 48, No. 7, 1026-1039, Jul. 2000.

- [4] J. Montero-de-Paz, E. Ugarte-Munoz, F. J. Herraiz-Martinez, V. Gonzalez-Posadas, L. E. Garcia-Munoz, and D. Segovia-Vargas, "Multi frequency self-diplexed single patch antennas loaded with split ring resonators," *Progress In Electromagnetics Research*, Vol. 113, pp. 47-66, 2011.
- [5] K. J. Vinoy, J. K. Abraham, and V. K. Varadan, "On the relationship between fractal dimension and the performance of multiresonant dipole antennas using Koch curves," *IEEE Trans. Antennas Propag.*, vol. 51, pp. 2296–2303, Sep. 2003.
- [6] W.-H. Hsu and K. L. Wong, "Circularly polarized disk-sector microstrip antenna," *Electron. Lett.*, vol. 34, no. 23, pp. 2188–2190, 1998.
- [7] J. R. James and P. S. Hall, *Handbook of Microstrip Antennas*. London, U. K.: Peter Peregrinus, 1989.
- [8] S. Mathew et al., "A fan-shaped circularly polarized patch antenna for UMTS band," *Prog. Electromagn. Res. C*, vol. 52, pp. 101–107, 2014.
- [9] M. Haneishi and S. Yoshida, "A design method of circularly polarized rectangular microstrip antenna by one-feed point," *Electron. Commun. Jpn.*, vol. 64, no. 4, pp. 46–54, Apr. 1981.
- [10] W. F. Richards, Y. T. Lo, and P. Simon, "Design and theory of circularly polarized microstrip antennas," *IEEE APS Int. Symp. Dig.*, vol. 17, pp. 117–120, Jun. 1979.
- [11] Chang E, Long S.A, Richards W.F. "Investigation of electrically thick rectangular microstrip antennas," *IEEE Trans. Antennas Propag.*, 34(6), pp.767-772, 1986.
- [12] Kin-Lu Wong, Jen-Yea Jan., "Broadband circular microstrip antenna with embedded reactive loading," *Electronics Letters*, 34(19), pp.1804-1805, pp.21–26, 1998.
- [13] Coccioli R, Deal W.R, Itoh T. "Radiation characteristics of a patch antenna on a thin PBG substrate," *Proc. IEEE AP-S Int. Symp.*; Atlanta. 1998.
- [14] Lee K.F, Luk K.M, Tong K.F, Shum S, Huynh M.T, Lee R.Q. "Experimental and simulation studies of coaxially fed U-slot rectangular patch antenna," *Microw. Antennas Propag. IEE Proc*; 144(5), pp. 354–358, 1997.

- [15] Iqbal S.S, Siddiqui J.Y, Guha D, “Performance of compact integratable broadband microstrip antenna” *Electromagnetics*, 25(4), pp.317–327, 2005.
- [16] Guha D, Biswas M, Antar Y.M.M., “Microstrip Patch Antenna with Defected Ground Structure for Cross Polarization Suppression,” *IEEE Antennas and Wireless Propagation Letters*, vol. 4, pp. 455-458, 2005.
- [17] Wong K, *Compact and Broadband Microstrip Antennas*. New York: Wiley; 2002.

.....✎.....

**INVESTIGATIONS ON COMPACT TRI BAND
DUAL POLARIZED CIRCULAR PATCH ANTENNA**

<i>Contents</i>	6.1 <i>Introduction</i>
	6.2 <i>Coaxial probe fed circular disc printed antenna</i>
	6.3 <i>Slit embedded annular shaped dual band patch antenna</i>
	6.4 <i>Slit, slot and stub embedded circular triband patch antenna</i>
	6.5 <i>Summary of the Chapter</i>

The detailed analysis of the triband performance of the circular patch antenna is carried out in this chapter. The basic circular and ring shaped patches are initially examined. A novel technique combining the use of slits, slots and stubs in the circular patch for achieving triple band operation is presented here. The evolution, geometry and parametric analyses are elaborated upon. Extensive simulation studies along with experimental validations have been performed.

6.1 Introduction

Smart phones and handheld tablets are typical examples of multiband devices which simultaneously engage the commercial frequency bands such as UMTS, WiMAX and WLAN. A triple band design which can provide compactness along with differing polarizations in the operating bands is a much preferred candidate in such applications. The circular patch is a simple shape that can be modified and manipulated practically to suit the varied requirements. The coaxial probe fed circular patch can be designed to generate circularly polarized radiation in the fundamental mode of operation with a sufficiently high value of axial ratio bandwidth. Techniques devised to achieve compact CP operation of circular patch antenna include slot embedding [1], slit loading of the patch [2] and use of stubs [3]. In the current work, a novel method which combines all these three techniques has been adopted. The design is focused towards developing a compact triple band structure based on the circular patch shape with different polarizations in the different bands. The triple band operation of the truncated corner sectoral patch antenna was explored in detail in the previous chapter. The current chapter deals with the dual and triple band operation of the circular patch where higher order hybrid modes are excited. Both circular and linear polarizations are obtained. Elaborate parametric analysis has been carried out to achieve the optimum impedance matching in all three bands and maximum ARBW.

6.2 Coaxial probe fed circular disc printed antenna

The circular patch shape is more preferred over the rectangular shape owing to its smallness of area and radiates in a direction normal to its plane while it retains its low profile characteristics. Both linear and circular

polarizations can be obtained from this radiating structure. Moreover it is easier to obtain input matching by adjusting the feed position.

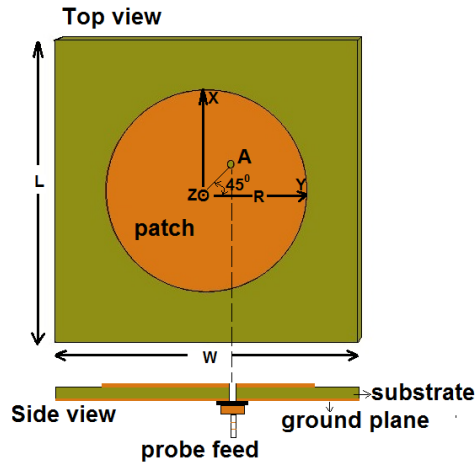


Fig. 6.1. Geometry of the coaxial probe fed circular disc patch antenna ($L=W=50$, $R=21$, $h=1.6$ (all in mm), $A(7,7)$, $\epsilon_r=4.4$)

The configuration of the single coaxial probe fed circular patch antenna is shown in Fig. 6.1. The circular patch of radius R mm is printed on the top side of the FR4 substrate of $\epsilon_r = 4.4$ and thickness $h=1.6$ mm. A ground plane of size W mm x L mm covers the opposite side.

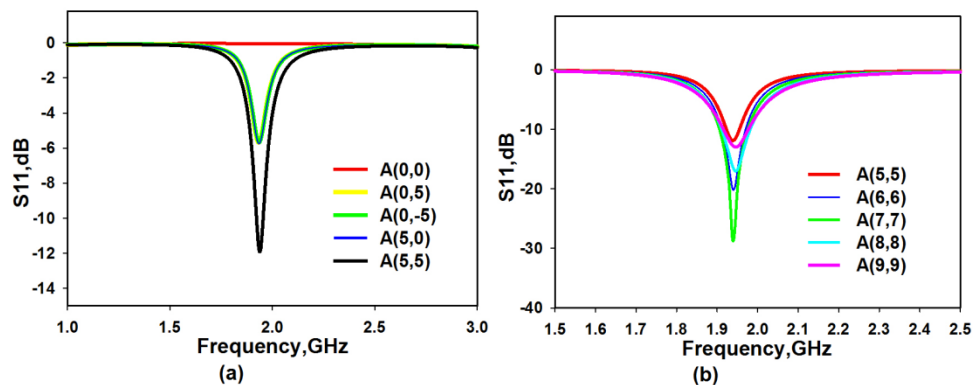


Fig. 6.2. Simulated reflection coefficients of the coaxial probe fed circular disc patch antenna for different feed positions a) along different angles b) along the 45° diagonal ($L=W=50$, $R=21$, $h=1.6$ (all in mm), $\epsilon_r=4.4$)

The simulated reflection coefficient, for different feed positions are shown in Fig.6.2a. A matched resonance at 1.9 GHz is obtained only when the feed point is located along the 45° diagonal. This feed position is again moved along the 45° diagonal line to obtain the maximum impedance matching point. This position is obtained as A(7,7) with the origin at the centre of the circle as seen from Fig.6.2b. The patch was designed for a resonant frequency of 2 GHz using the relation [4],

$$f_{mn} = \frac{\chi_{mn} c}{2\pi a \sqrt{\epsilon_r}} \dots\dots\dots (6.1)$$

where f_{mn} is the resonant frequency in the TM_{mn} mode, χ_{mn} represents the zeroes of the derivatives of the Bessel function $J_m(x)$, c is the velocity of light, ϵ_r is the substrate dielectric constant and a is the radius of the patch.

6.2.1 Circular patch antenna for circular polarization

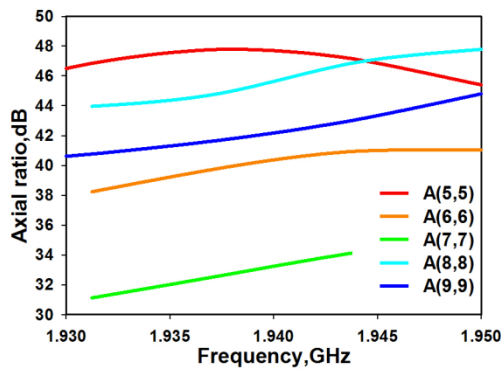


Fig. 6.3. Simulated axial ratio characteristics of the coaxial probe fed circular disc patch antenna for different feed positions along the 45° diagonal (L=W=50, R=21, h=1.6 (all in mm), $\epsilon_r=4.4$)

The radiation obtained from this original circular patch is of linear polarization as seen from the simulated axial ratio graph in Fig.6.3. This is because the orthogonal dimensions of the patch are such that the necessary

perturbation required to excite two near degenerate orthogonal modes is not produced. To introduce the required perturbation without increasing the antenna size, two different rectangular shaped patch modification techniques of 1) slits at the patch boundary and 2) slot at the patch centre are applied. The two new antenna structures in which the compactness of the antennas are preserved, are shown in Fig. 6.4. The simulated reflection coefficient and axial ratio characteristics of these two antennas denoted Antenna A and Antenna B respectively depicted in Fig.6.5 indicate CP radiation with centre frequencies of 1.958 GHz and 1.92 GHz respectively.

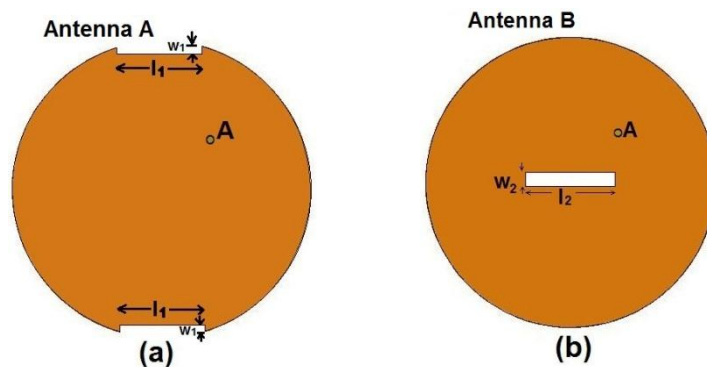


Fig. 6.4. Modified coaxial probe fed circular disc patch antenna for circular polarization a) Antenna A b) Antenna B ($L=W=50$, $R=21$, $w_1=1$, $l_1=12$, $w_2=2$, $l_2=12$, $h=1.6$ (all in mm), $A(7,7)$, $\epsilon_r=4.4$)

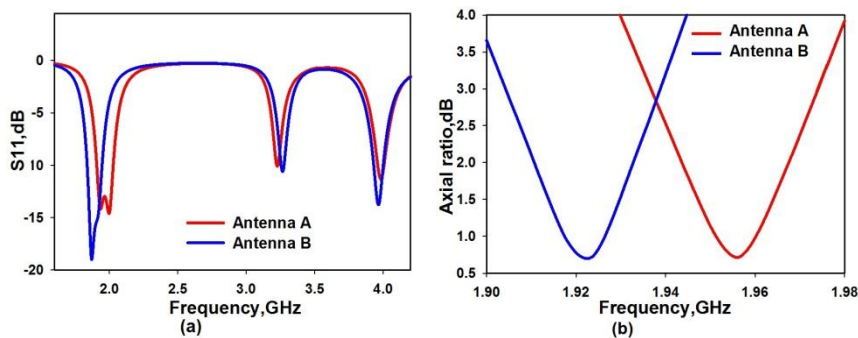


Fig. 6.5. Simulated characteristics of the modified coaxial probe fed circular patch antennas for circular polarization a) S11 b) Axial ratio ($L=W=50$, $R=21$, $w_1=1$, $l_1=12$, $w_2=1$, $l_2=12$, $h=1.6$ (all in mm), $A(7,7)$, $\epsilon_r=4.4$)

In both configurations, the reflection coefficients exhibit a strong discontinuity in the fundamental resonance band, pointing to the occurrence of circularly polarized radiation. This is further verified by plotting the axial ratio graph, where the axial ratio falls below the stipulated 3dB level with a moderate bandwidth of 2.2%. The axial ratio bandwidth also lies within the 10dB impedance bandwidth. The presence of the slots produce the perturbation which causes the excitation of two near degenerate frequencies with orthogonal phases which merge to produce the CP at the centre frequency. On examining the reflection coefficients of the two antennas, these two close lying frequencies were found to be 1.9375 GHz and 2 GHz for Antenna A and 1.8575 GHz and 1.93 GHz for Antenna B.

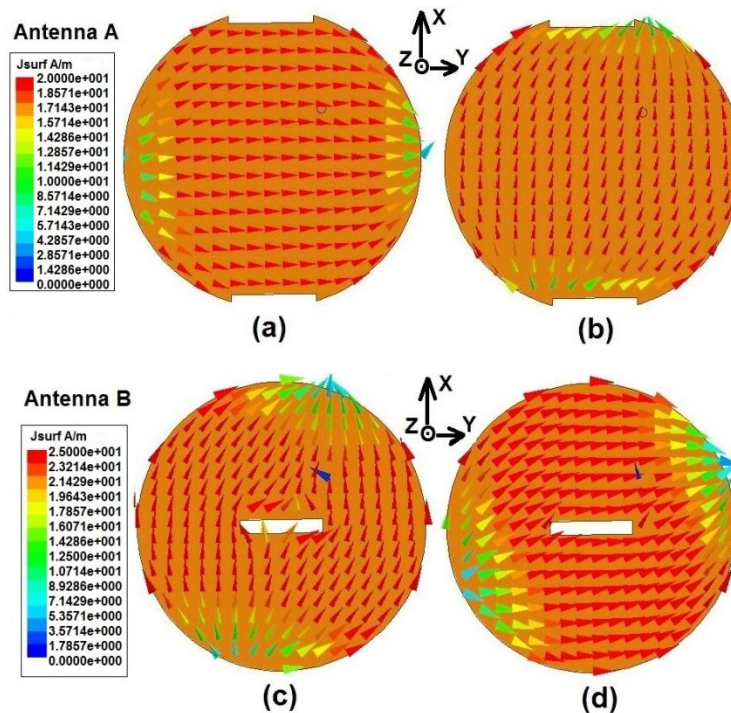


Fig. 6.6. Simulated current distributions on Antenna A a) at 1.9375GHz b) at 2 GHz and Antenna B at c) 1.8575 GHz d) 1.93 GHz ($L=W=50$, $R=21$, $w1=1$, $l1=12$, $w2=1$, $l2=12$, $h=1.6$ (all in mm), $A(7,7)$, $\epsilon_r=4.4$)

The surface current distributions at each of these pairs of frequencies were plotted which further confirmed that the modes are orthogonal. This is illustrated in Fig.6.6. In Antenna A, one half wave variation along the y direction and no variation along the x direction are seen at 1.9375 GHz confirming the TM_{01} mode at this frequency. At 2 GHz, similarly it is inferred that the TM_{10} mode is excited. Likewise for Antenna B, the TM_{10} mode at 1.8575 GHz and TM_{01} mode at 1.93 GHz are observed to be excited. It can be seen that the presence of the slots modify the surface currents so that they bend around the edges of the slots. The central rectangular slot in Antenna B, stretches the current path diagonally also resulting in the occurrence of the maxima and minima along the 45° axis.

In the reflection coefficient graphs of each of the two structures (Fig.6.5), two more poorly matched resonances are also observed at higher frequencies which are due to excitation of higher order resonance modes.

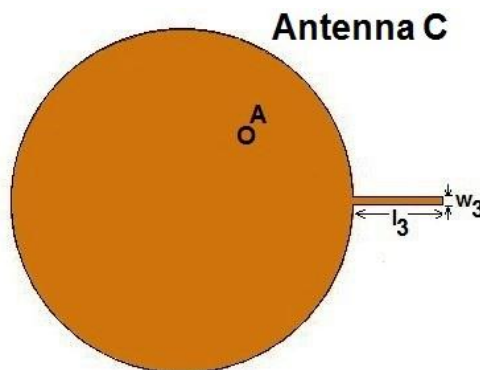


Fig. 6.7. Modified coaxial probe fed circular disc patch antenna for circular polarization with tuning stub (Antenna C) ($L=50$, $W=60$, $R=21$, $w_3=1$, $l_3=11$, $h=1.6$ (all in mm), $A(7,7)$, $\epsilon_r=4.4$)

A third patch modification method which can introduce circular polarization nevertheless making the structure less compact is using a tuning

stub of proper length l_3 and width w_3 in the horizontal direction as shown in Fig.6.7. In this structure denoted as Antenna C, two near degenerate modes are excited thereby achieving CP performance. The reflection coefficient and axial ratio characteristics are shown in Fig.6.8.

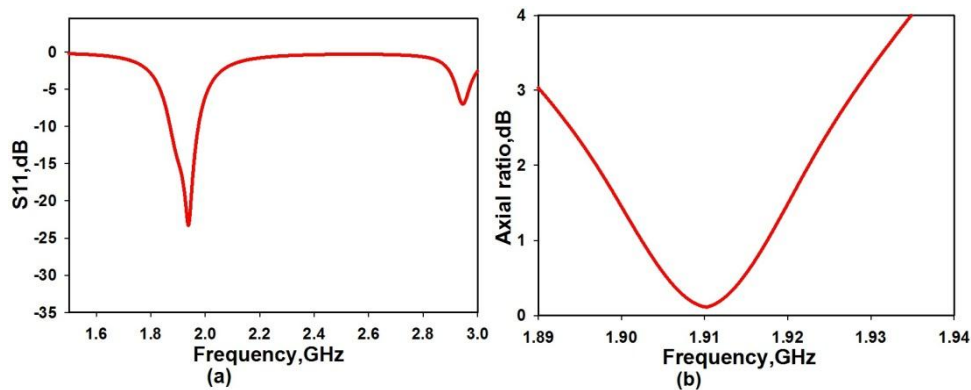


Fig. 6.8. Simulated characteristics of the modified coaxial probe fed circular disc patch antenna with tuning stub a) S_{11} b) Axial ratio ($L=50$, $W=60$, $R=21$, $w_3=1$, $l_3=11$, $h=1.6$ (all in mm), $A(7,7)$, $\epsilon_r=4.4$)

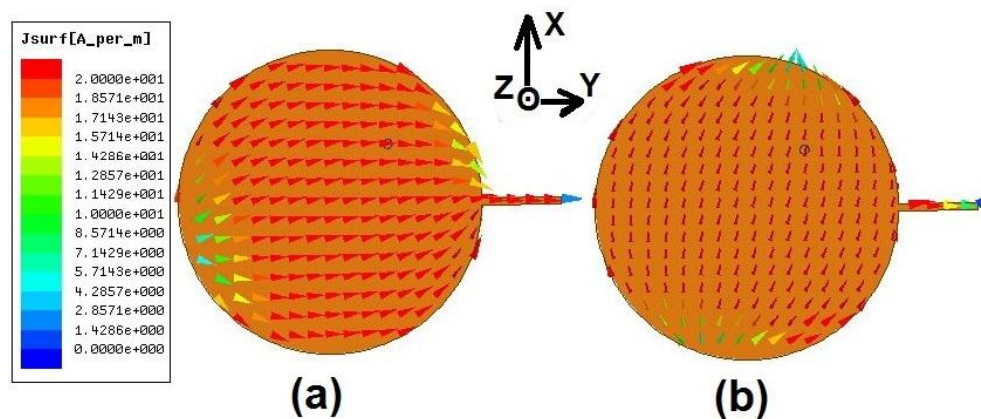


Fig. 6.9. Simulated current distributions on Antenna C at a) 1.88 GHz b) at 1.9375GHz ($L=50$, $W=60$, $R=21$, $w_3=1$, $l_3=11$, $h=1.6$ (all in mm), $A(7,7)$, $\epsilon_r=4.4$)

The simulated surface current distributions on Antenna C at the two near degenerate frequencies of 1.88 GHz and 1.9375 GHz are illustrated in

Fig.6.9. The mode in the direction parallel to the stub (TM_{01} in this case) has a lower resonance frequency than that of the mode in the direction perpendicular to the stub (TM_{10}). The drawback of this technique using stub is that the total antenna size becomes larger by 20%.

6.2.2 Parametric study of the circular patch antennas for CP

The three antennas Antenna A, Antenna B and Antenna C were investigated through software simulations to study the effects of the three modifications namely slits, centre slot and tuning stub on the input impedance and CP performance.

6.2.2.1 Effect of slit length and width on Antenna A

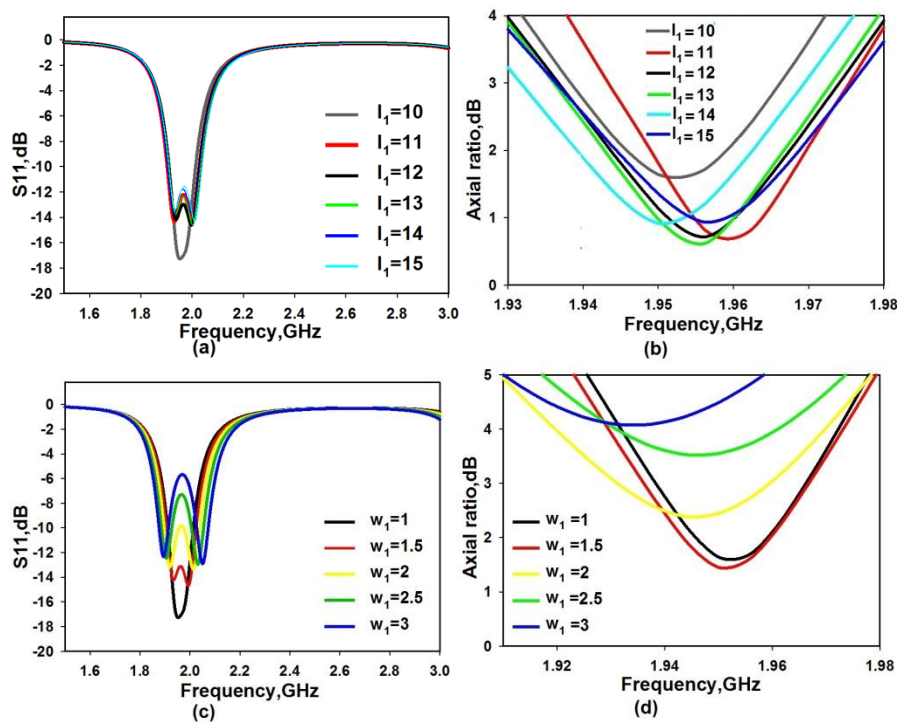


Fig. 6.10. Effect of slit length variation on a) S11 b) axial ratio and effect of slit width variation on c) S11 d) axial ratio of Antenna A ($L=W=50$, $R=21$, $h=1.6$ (all in mm), $A(7,7)$, $\epsilon_r=4.4$)

The variation in the slit lengths has very little effect on the reflection coefficient and matching of the antenna as seen from Fig.6.10a. However the axial ratio varies in terms of both the bandwidth and minimum AR value (Fig.6.10b). The variation of the slit width has a greater effect on both the reflection and CP characteristics of the antenna as understood from Figs.6.10c and 6.10d. The matching decreases with increase in the slit width when w_1 is varied from 1 to 3mm, keeping the length fixed at 12mm. The fundamental resonance band splits into two beyond $w_1=2$ mm. The ARBW decreases and ARmin value increases beyond $w_1= 2$ mm. The optimum values of $l_1=12$ mm and $w_1=1$ mm have been selected.

6.2.2.2 Effect of slot length and width on Antenna B

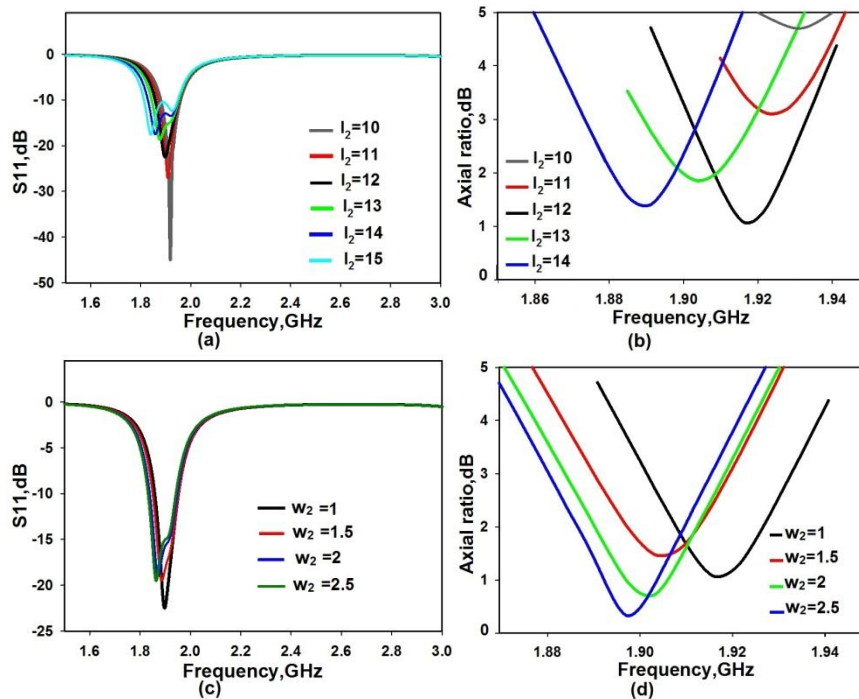


Fig. 6.11. Effect of slot length variation on a) S11 b) axial ratio and effect of slot width variation on c) S11 d) axial ratio of Antenna B ($L=W=50$, $R=21$, $h=1.6$ (all in mm), $A(7,7)$, $\epsilon_r=4.4$)

Keeping the width of the slot fixed at 1mm, the slot length l_2 is varied from 10 to 14mm. The impedance matching becomes poorer and the band shifts to lower frequencies with the increase in l_2 as is obvious from Figs.6.11a and 6.11b. When the slot width is varied keeping the length of the slot l_2 constant, the band shifts to lower side in frequency. The S11 value also becomes lower. Although the ARBW is not much changed, the band shifts by a large amount towards the left side in frequency. The optimum values which provide the best impedance matching, maximum ARBW and least ARmin value within the desired frequency band have been selected as $l_2=12\text{mm}$ and $w_2=1\text{mm}$.

6.2.2.3 Effect of the length and width of tuning stub on Antenna C

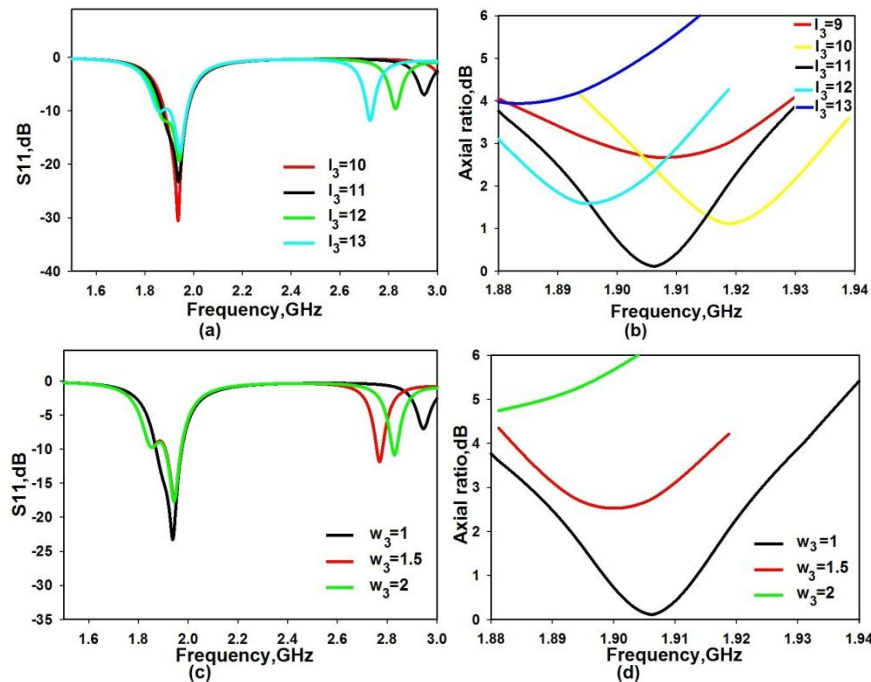


Fig. 6.12. Effect of stub length variation on a) reflection coefficient b) axial ratio and effect of stub width variation on c) reflection coefficient d) axial ratio of Antenna C ($L=50, W=60, R=21, h=1.6$ (all in mm), $A(7,7), \epsilon_r=4.4$)

Although the compactness of the structure is lost, the tuning stub offers a convenient and simple method to obtain circularly polarized radiation from the circular patch. By selecting the appropriate length and width for the rectangular stub, an appreciable ARBW and lowest ARmin value can be obtained. As can be seen from Figs.6.12a and 6.12b, increasing the length beyond 11mm degrades both the impedance matching and the ARBW. Similarly, the best results in terms of both S11 and ARBW are obtained at $l_3=11\text{mm}$ and $w_3=1\text{mm}$.

6.2.3 Experimental results

The prototypes of the three antennas Antenna A, B and C were fabricated according to the optimized dimensions $w_1= w_2= w_3= 1\text{mm}$, $l_1= l_2 =12\text{mm}$ and $l_3=11\text{mm}$ on FR4 substrates of $\epsilon_r = 4.4$ and thickness $h=1.6\text{mm}$. The measured and simulated S11 characteristics are shown in Fig.6.13 and are found to be in agreement with each other for all three structures.

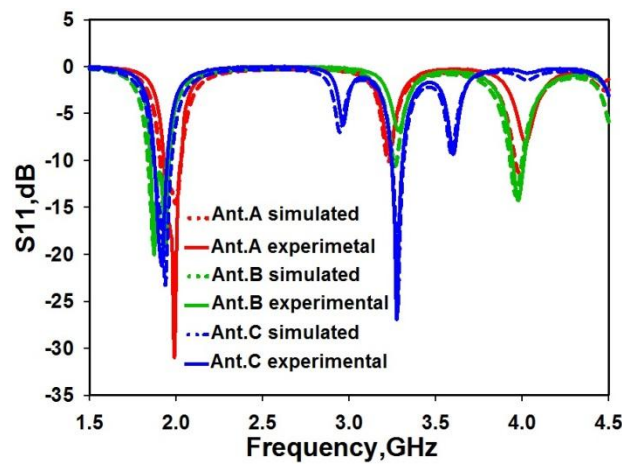


Fig. 6.13. Measured and simulated reflection coefficients of the Antennas A, B and C for circular polarization ($R=21$, $w_1=1$, $l_1=12$, $w_2=1$, $l_2=12$, $w_3=1$, $l_3=11$, $h=1.6$ (all in mm), A (7,7), $\epsilon_r=4.4$)

The three antennas exhibit fundamental resonance frequency near 2 GHz and two higher order resonance frequencies at 3.3 GHz and 4 GHz. However, these higher order resonances are found to be poorly matched in terms of the -10dB return loss and are hence not studied more in this section.

The axial ratio curves for all three prototypes are shown plotted in Fig.6.14. The CP centre frequencies are measured respectively as 1.95GHz, 1.92 GHz and 1.91GHz. CP bandwidths measured are respectively 2.5 %, 2.1 % and 3%. The reason for the ARBW being higher for Antenna C than the other two is based on the inverse relation between the CP bandwidth and Q factor of a single fed circularly polarized patch antenna [5]. The Q factor in turn is inversely dependent on the volume or size occupied by the antennas as proved by Wheeler [6-7]. Antenna C possesses the larger volume than the other two structures and hence enjoys a lower Q value. This lower Q is responsible for the higher CP bandwidth.

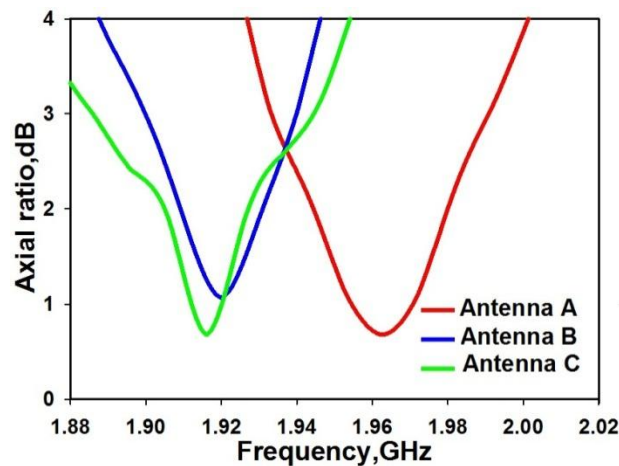


Fig. 6.14. Measured axial ratios of the Antennas A, B and C for circular polarization ($R=21$, $w_1=1$, $l_1=12$, $w_2=1$, $l_2=12$, $w_3=1$, $l_3=11$, $h=1.6$ (all in mm), A (7,7), $\epsilon_r=4.4$)

The measured RHCP radiation patterns for Antennas A, B and C at the respective CP centre frequencies in two orthogonal planes are shown in Fig.6.15, compared to the simulated patterns. A good agreement has been observed between the simulated and experimental sets of radiation patterns.

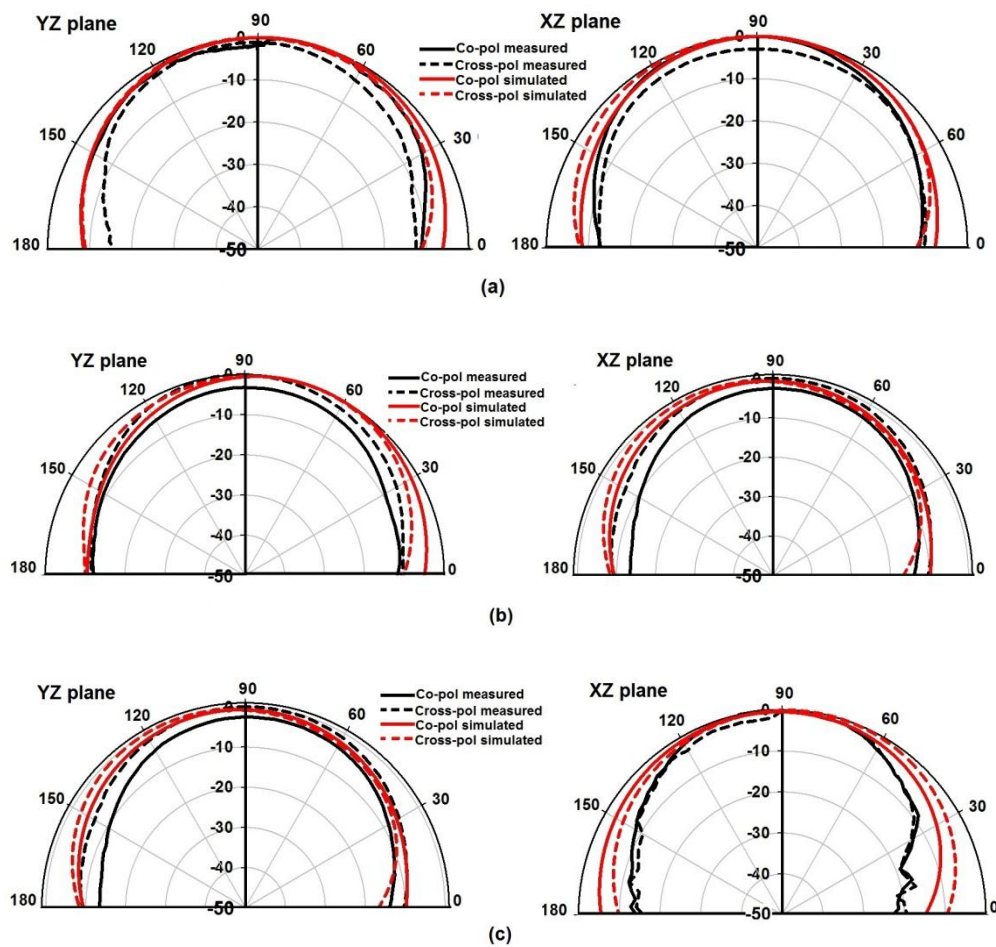


Fig. 6.15. Measured and simulated RHCP radiation patterns in two orthogonal planes of a) Antenna A at 1.95 GHz b) Antenna B at 1.92 GHz and c) Antenna C at 1.91 GHz ($R=21$, $w_1=1$, $l_1=12$, $w_2=1$, $l_2=12$, $w_3=1$, $l_3=11$, $h=1.6$ (all in mm), A (7,7), $\epsilon_r=4.4$)

With the double ridged horn antenna as reference, the gains of the three antennas were measured. The peak gains were obtained as 2.5 dBi, 1.9 dBi and 2.2 dBi respectively. Efficiencies of 48 %, 46% and 50 % respectively were evaluated for the three antennas using the Wheeler cap method.

Table 6.1 Comparison of measured characteristics of Antennas A, B and C

Structure	Imp.BW (%)	CP centre frequency (GHz)	ARBW (%)	ARmin (dB)	Beamwidth (deg)	Antenna size (cm ²)
Ant.A	6.35	1.96	2.5	0.7	70	25
Ant.B	6.6	1.92	2.1	1.01	75	25
Ant. C	6.3	1.91	3	0.67	80	30

A comparison of the three described techniques to obtain CP radiation from a circular patch antenna for the prototypes Antennas A, B and C is listed in Table 6.1. The performances show little variation except for Antenna C where the CP bandwidth is slightly higher which is attributed to the lower Q factor arising due to the larger volume of the antenna.

6.3 Slit embedded annular ring dual band patch antenna

The previous section described three techniques which could be utilized to produce CP radiation without degradation in radiation performance. The first two techniques have been combined here, with the shape of the slit embedded in Antenna B previously being changed to circular. This modification results in the annular ring shaped patch antenna with an edge slit and its characteristics are studied experimentally in this section. The dimensions of the basic circular geometry have been retained so that the fundamental resonance frequency remains the same.

6.3.1 Antenna geometry

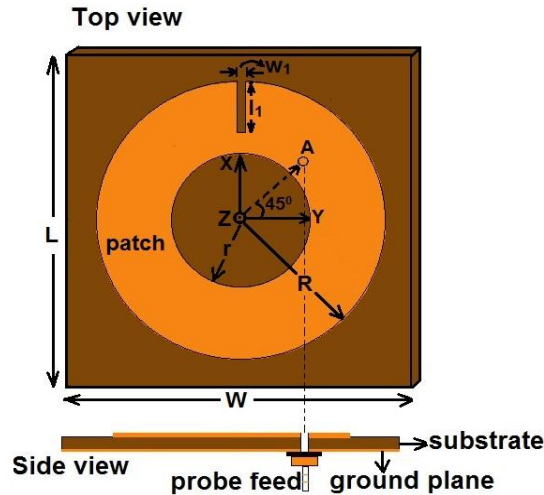


Fig. 6.16. Geometry of the coaxial probe fed slit embedded annular ring patch antenna ($L=W=50$, $R=21$, $r=10$, $l_1=7.5$, $w_1=1$, $h=1.6$ (all in mm), $A(7,7)$, $\epsilon_r=4.4$)

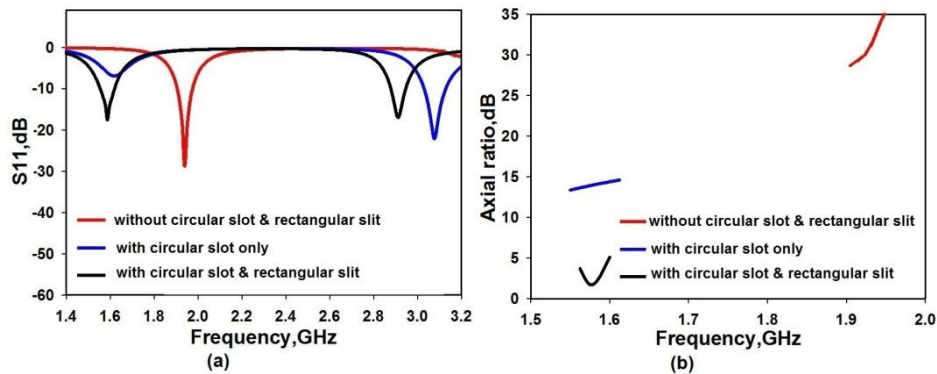


Fig. 6.17. Effect of the circular slot and rectangular slit on the simulated a) S_{11} b) Axial ratio characteristics in the slit embedded annular ring patch antenna ($L=W=50$, $R=21$, $r=10$, $l_1=7.5$, $w_1=1$, $h=1.6$ (all in mm), $A(7,7)$, $\epsilon_r=4.4$)

The geometry of the slit embedded annular ring patch antenna is shown in Fig.6.16. The centre slot has a radius of $r = 10$ mm and the rectangular slit along the X axis has dimensions $l_1=7.5$ mm and $w_1=1$ mm. The presence of the slot and the slit alters the S_{11} and axial ratio characteristics

of the circular patch as illustrated in Fig.6.17. Without both the slot and the slit, the geometry is a simple circular patch as described in the previous section with a single fundamental resonance at 2 GHz. When the geometry changes to annular ring with the addition of the circular slot, the response shows two resonances at 1.6 GHz and 3.1 GHz respectively. The fundamental resonance has been shifted down by about 400 MHz from 2 GHz. The excited surface currents under the patch are longer in the annular ring patch causing the fundamental frequency to be much lower than that of the corresponding circular patch. This corresponds to a compactness or area reduction of 53% when compared to standard circular patch designed for 1.6 GHz frequency. The second resonance at 3.1 GHz has been introduced due to the circular slot of radius r mm. The axial ratio value of the annular ring patch also decreases but the radiation is not yet circularly polarized. Upon adding the vertical rectangular slit on the patch edge, the axial ratio value falls below the 3 dB level confirming the occurrence of CP. This is further confirmed in the input impedance plot in Fig.6.18 which exhibits a kink that indicates the excitation of two orthogonal modes and consequent CP radiation.

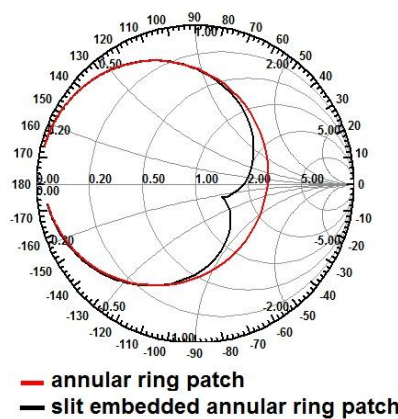


Fig. 6.18. Simulated input impedance plots of the annular ring patch antenna with and without rectangular slit
 ($L=W=50$, $R=21$, $r=10$, $l_1=7.5$, $w_1=1$, $h=1.6$ (all in mm), $A(7,7)$, $\epsilon_r=4.4$)

The first resonance shifts little more down to a centre frequency of 1.56 GHz and attains better reflection coefficient and improved impedance matching with the addition of the slit. The second resonance frequency is linearly polarized and experiences a shift from 3.1 GHz to 2.9 GHz.

6.3.2 Resonance modes

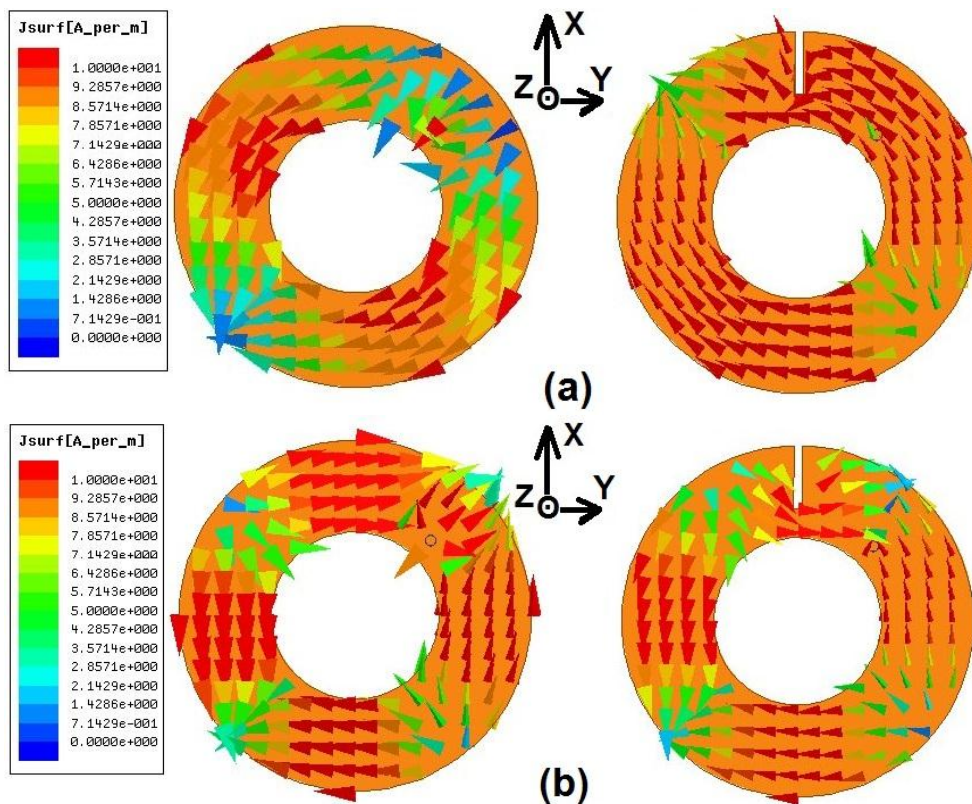


Fig. 6.19. Simulated current distribution on the annular patch antenna without and with rectangular slit at a) 1.56 GHz b) at 3 GHz. ($L=W=50$, $R=21$, $r=10$, $l_1=7.5$, $w_1=1$, $h=1.6$ (all in mm), $A(7,7)$, $\epsilon_r=4.4$)

The structure is further analyzed to study the resonance modes through the simulated current distribution on the patch. The path of the excited patch surface current in the annular patch is more elongated than that of a circular microstrip antenna causing the fundamental resonance to

occur at a much lower frequency. Examination of the surface current distribution in Fig.6.19 reveals that TM_{11} is the mode excited at the first resonance frequency as one half wave variation along each of the X and Y directions is observed. It is the presence of the slit that modifies the current distribution so that the Y directed currents are seen bending around the edge of the slit. Thus the slit causes the necessary perturbation needed to generate circularly polarized radiation. By properly selecting the slit dimensions, the fundamental TM_{11} mode is split into two orthogonal near degenerate modes with equal amplitude and 90° phase difference resulting in CP radiation. At the second frequency band, two half wave variations along each of the X and Y directions are occurring indicating that it is the TM_{22} mode that is excited at this band. The current distribution plot shows that this mode is linearly polarized along the Y direction.

6.3.3 Parametric study of the slit embedded annular ring patch antenna

To examine the effect of the various antenna parameters and feed point location on the performance characteristics, a thorough parametric analysis is performed. The resonant frequencies are determined by the outer and inner radii of the annular ring. The slit modifies the orthogonal dimensions so as to excite near degenerate orthogonal modes of equal amplitudes. This section describes the effect of these parameters and the conclusions obtained.

6.3.3.1 Effect of slot radius variation on the annular ring patch antenna

Keeping the feed point at (7,7) and outer radius R fixed at 21mm for a designed fundamental frequency of 1.9 GHz and without the rectangular slit, the radius of the inner circular slot is varied. As the radius of the circular slot r is increased from 2mm to 12mm, the first resonance shifts to a lower

value from the designed fundamental frequency as shown in Fig.6.20a. The input impedance locus only shrinks in size as can be seen from the smith chart in Fig.6.20b.

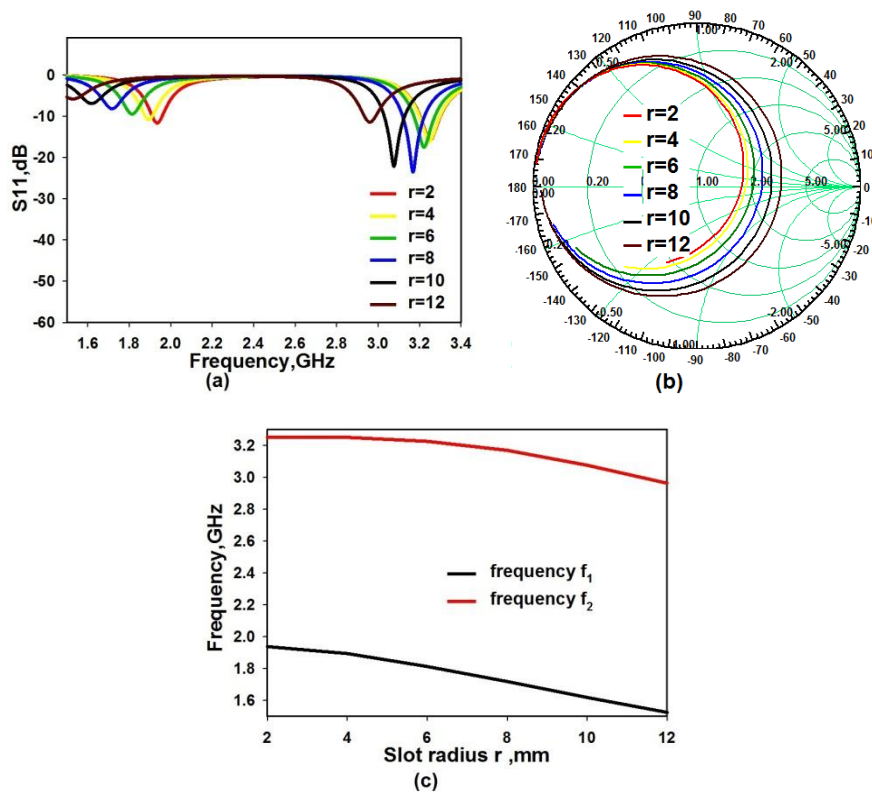


Fig. 6.20. Effect of inner radius variation on a) S_{11} b) input impedance c) resonant frequency of annular ring patch antenna without slit ($L=W=50$, $R=21$, $h=1.6$ (all in mm), $A(7,7)$, $\epsilon_r=4.4$)

No change in impedance matching at this frequency is observed due to the increase in the radius r . The second resonance frequency at the same time is affected in both frequency location and impedance matching as seen from Fig.6.20a. The slot radius is chosen as $r=10$ mm since at this dimension, the first resonance frequency falls in the GPS L2 range of 1.565-1.585 GHz and the second resonance frequency is maximum shifted to the lower side

with adequate impedance matching below the -10dB return loss level. Fig.6.20c shows the variation of the resonant frequencies f_1 and f_2 of the first and second resonant modes respectively with respect to the slot radius.

6.3.3.2 Effect of rectangular slit length variation on the annular ring patch antenna

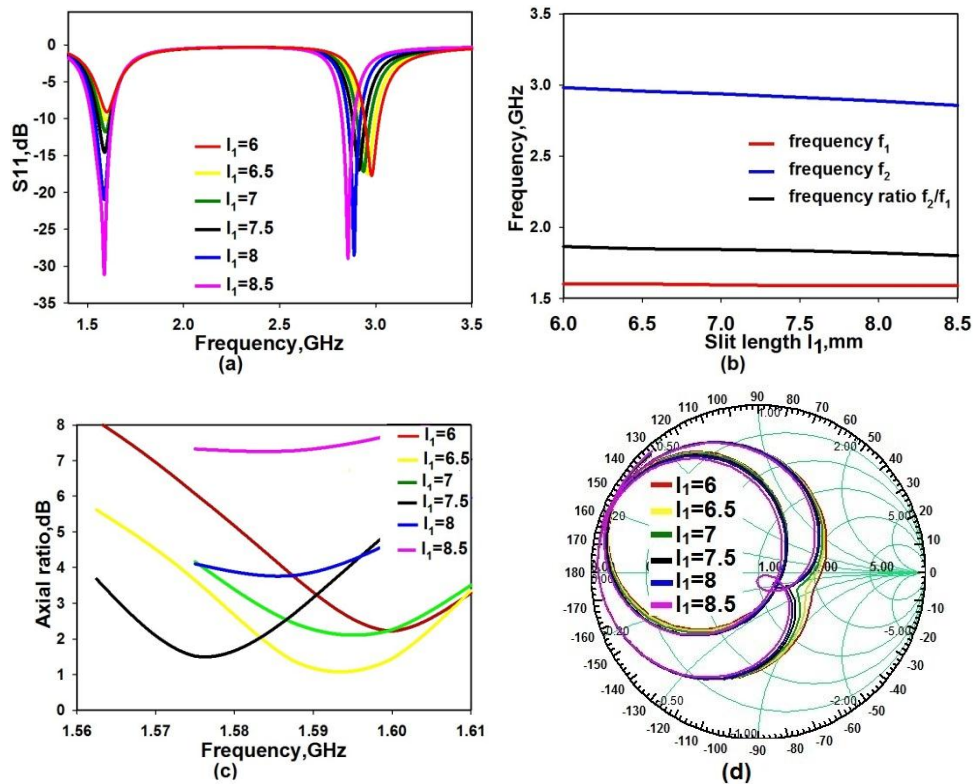


Fig. 6.21. Effect of slit length variation on a) S_{11} b) resonant frequencies c) input impedance d) axial ratio of slit embedded annular ring patch antenna ($L=W=50$, $R=21$, $r=10$, $h=1.6$ (all in mm), $A(7,7)$, $\epsilon_r=4.4$)

The effect of the rectangular slit on the annular ring patch antenna was studied in detail. The slit width w_1 is kept fixed at 1mm while the slit length l_1 was varied from 6mm to 8.5mm in steps of 0.5mm. The first resonance frequency experiences very little shift towards the lower side, while the second resonance frequency is shifted more to the lower side in frequency as

the slit length is increased as seen from Fig.6.21a. This is also clear from the graph in Fig.6.21b. Fig.6.21c displays that the CP performance is also optimum and falls within the GPS L2 band frequency range at $l_1=7.5\text{mm}$. This is because the dimensions of the patch are optimum at this slit dimension to excite near degenerate resonance modes. The input impedance curve in the smith chart in Fig.21d also indicates the presence of the kink in the outer circle which confirms CP radiation at $l_1=7.5\text{mm}$. The inner circle in the chart which represents the input impedance curve at the second resonance mode shrinks in size as l_1 is increased.

6.3.3.3 Effect of rectangular slit width variation on the annular ring patch antenna

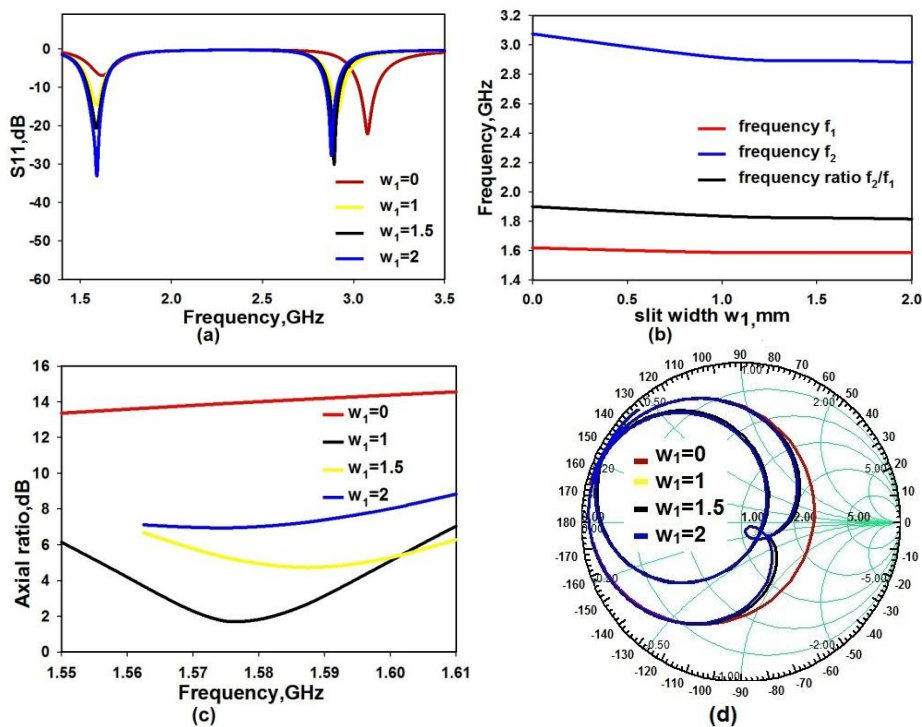


Fig. 6.22. Effect of slit width variation on a) S11 b) resonance frequency c) axial ratio d) input impedance on slit embedded annular ring patch antenna ($L=W=50$, $R=21$, $r=10$, $h=1.6$ (all in mm), $A(7,7)$, $\epsilon_r=4.4$)

The length l_1 was kept fixed at 7.5mm and the width of the slit w_1 was varied from 1mm to 2 mm and the effect on the reflection coefficient, axial ratio and the input impedance were observed. The variations in resonant frequencies of the two bands are illustrated in Figs.6.22a and 6.22b. Increasing the width does not cause much change with respect to shift in centre frequency and reflection coefficient in both frequency bands. However the CP performance is affected as obvious from Figs.6.22c and 6.22d. Axial ratio value below 3dB is obtained only at $w_1=1$ mm.

6.3.3.4 Effect of rectangular slit position on the annular ring patch antenna

The position of the slit was varied along the X, Y and diagonal axes and the impacts on the antenna performance were studied. When the slit is positioned along the positive and negative X and Y axes, the reflection and the CP characteristics of the antenna are identical except for the sense of circular polarization. This is represented in Figs.6.23A and 6.23B.

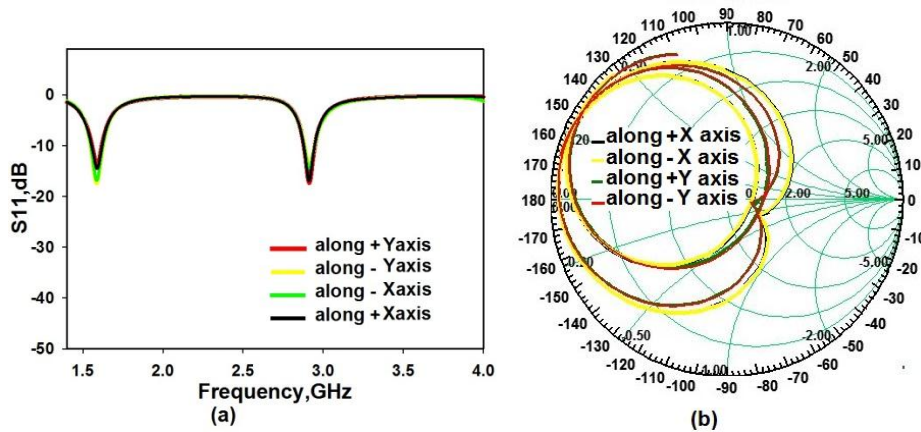


Fig. 6.23A. Effect of slit position variation along X and Y axes on a) S11 b) input impedance on slit embedded annular ring patch antenna (L=W=50, R=21, r=10, $l_1=7.5$, $w_1=1$, $h=1.6$ (all in mm), A (7,7), $\epsilon_r=4.4$)

The sense of polarization is left handed CP as the current vector rotates clockwise when the slit is along the X axis as seen from Fig.23B(c). When the slit is oriented along the Y axis, this sense changes to right handed CP with the current vectors following an anticlockwise rotation direction as shown in Fig.6.23B (d).

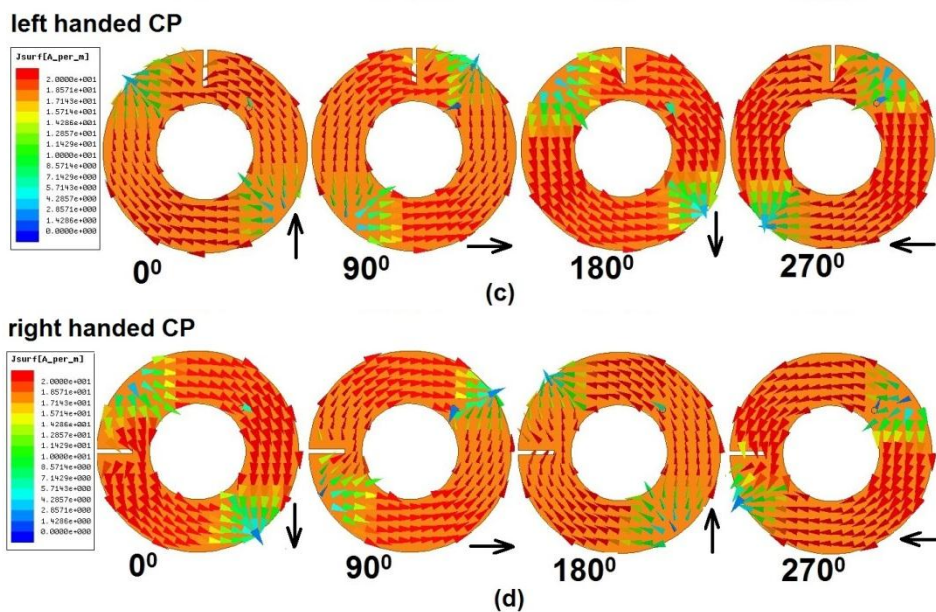


Fig. 6.23B. Effect of slit position variation on the sense of CP of annular ring patch antenna c) along X axis d) along Y axis ($L=W=50$, $R=21$, $r=10$, $l_1=7.5$, $w_1=1$, $h=1.6$ (all in mm), $A(7,7)$, $\epsilon_r=4.4$)

The slit was positioned along the diagonal axes also along the 45°, 135°, 225° and 315° directions also. It was observed that the first resonance frequency lost its impedance matching along all these four orientations as illustrated in Fig. 6.24. Thus the location of the slit determines the impedance matching and the circular polarization characteristics of the antenna in the first resonance band. The input impedance and matching in the second resonance band remain unaffected by the slit position variation.

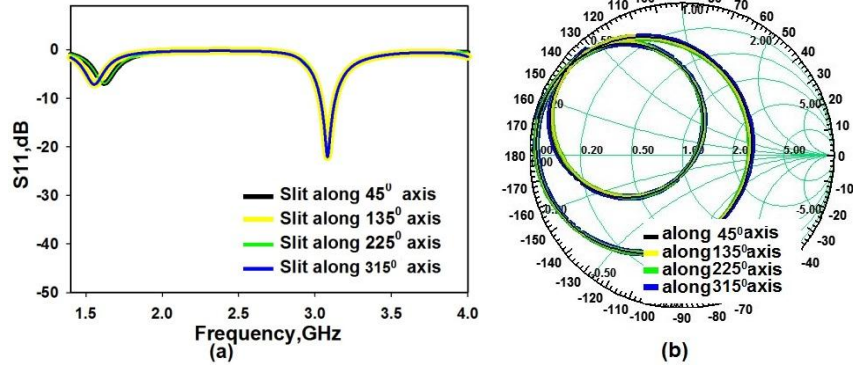


Fig. 6.24. Effect of slit position variation on a) S11 b) input impedance of annular ring patch antenna along the diagonal axes ($L=W=50$, $R=21$, $r=10$, $l_1=7.5$, $w_1=1$, $h=1.6$ (all in mm), $A(7,7)$, $\epsilon_r=4.4$)

From the above parametric study, it is concluded that depending on the desired sense of circular polarization, the rectangular slit has to be placed along the X or Y axes.

6.3.4 3D radiation patterns

The simulated three dimensional polar plots of the slit embedded annular ring patch antenna are shown in Fig.6.25. The pattern is broad side and directional at 1.57 GHz. The pattern shows omnidirectional properties at 2.9 GHz.

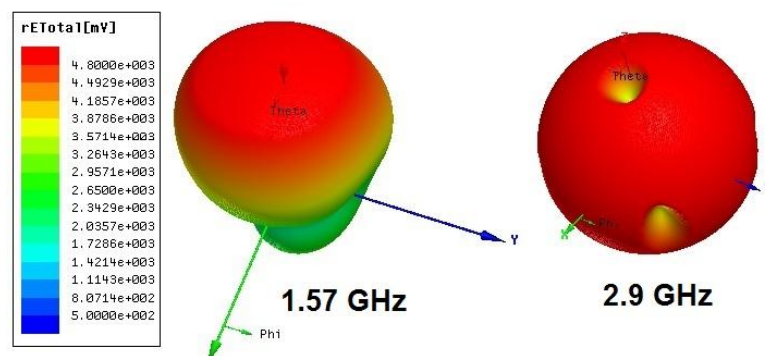


Fig. 6.25. Simulated radiation plots at the two bands of the slit embedded annular ring patch antenna ($L=W=50$, $R=21$, $r=10$, $w_1=1$, $l_1=7.5$, $h=1.6$ (all in mm), $A(7,7)$, $\epsilon_r=4.4$)

6.3.5 Experimental results

The proposed slit embedded annular ring patch antenna prototype was fabricated on FR4 substrate of $\epsilon_r=4.4$ and thickness $h=1.6\text{mm}$ with dimensions $L=W=50$, $R=21$, $r=10$, $l_1=7.5$, $w_1=1$ (all dimensions in mm) and the characteristics were experimentally obtained using the PNAE 8362B network analyzer. The measured and simulated reflection coefficient characteristics are compared in Fig.6.26a and are observed to be in good agreement.

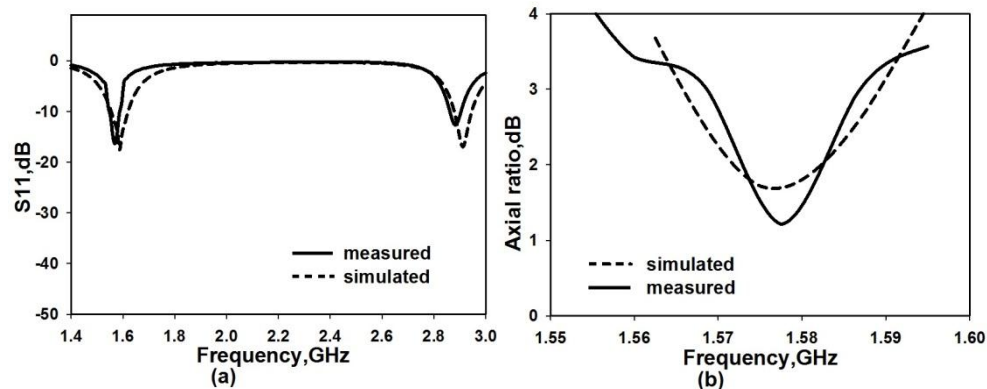


Fig. 6.26. Measured and simulated reflection coefficients of the slit embedded annular ring patch antenna ($L=W=50$, $R=21$, $r=10$, $w_1=1$, $l_1=7.5$, $h=1.6$ (all in mm), $A(7,7)$, $\epsilon_r=4.4$)

The -10dB impedance bandwidths of 3.1% at a centre frequency of 1.57GHz in the first band and 1.95% at a centre frequency of 2.87 GHz in the second resonance band were measured. The axial ratio characteristics in the first band was also experimentally measured and compared with the simulated results as shown in Fig.6.26b. 3dB axial ratio bandwidth of 1.27% at a centre frequency of 1.577 GHz is obtained. This indicates that the circularly polarized radiation obtained essentially covers the GPS L2 band.

The measured LHCP radiation patterns of the antenna at the CP centre frequency of 1.577 GHz in two orthogonal planes are shown in Fig.6.27a. Fig.6.27b represents the 2D radiation pattern at the second resonance frequency of 2.87 GHz. In this case the pattern is found to be nearly omnidirectional in YZ plane and figure of eight in the XZ plane.

The gains were also measured using gain comparison method and peak gains of 1.5 dBi and 1.1 dBi were obtained at the first and second bands respectively.

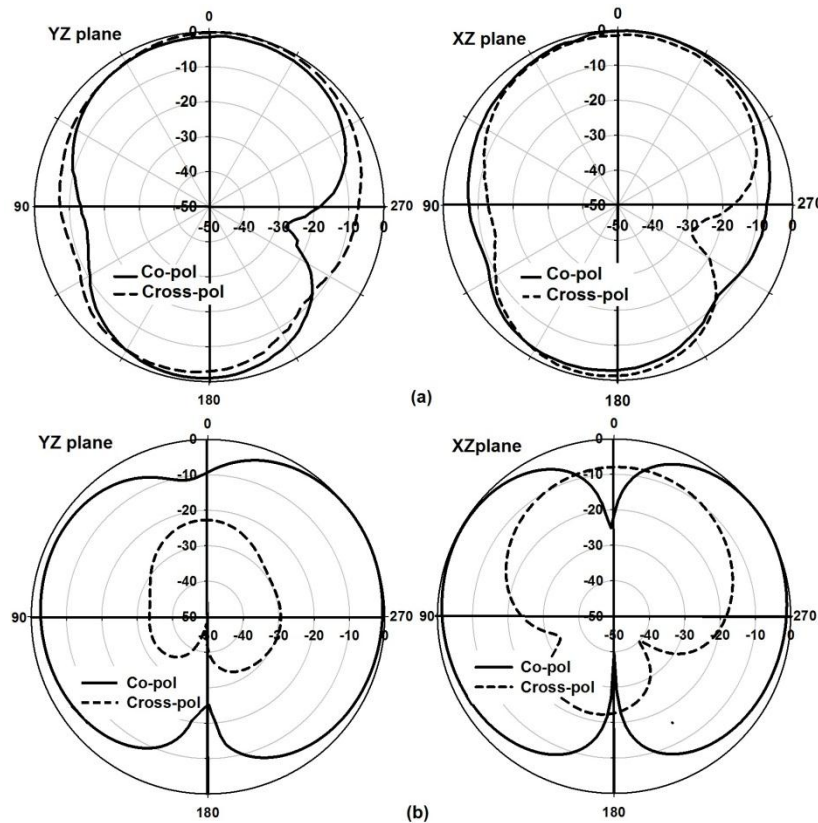


Fig. 6.27. Measured radiation patterns in two orthogonal planes of the slit embedded annular ring patch antenna a) LHCP at 1.57 GHz b) at 2.87 GHz ($L=W=50$, $R=21$, $r=10$, $w_1=1$, $l_1=7.5$, $h=1.6$ (all in mm), $A(7,7)$, $\epsilon_r=4.4$)

Radiation efficiencies of 30 % and 20% respectively were measured using the Wheeler cap method in the first and second bands. The low gain values are obtained as the radiating patch area is reduced by the circular slot. The currents along the patch circumference in the X direction are in opposite directions causing field cancellation which results in reduction of peak gain at the resonance frequency.

The slit embedded annular ring patch can be compared to a standard circular patch operating at the same dominant mode frequency. The area of the circular patch with $R= 21\text{mm}$ reduces by 23% when the slot and slit are etched. This reduces the fundamental resonance frequency by around 400 MHz which corresponds to an area reduction of 53% with respect to a standard circular patch designed with a fundamental resonance frequency of 1.56 GHz. Although the peak gain is low, the antenna provides good axial ratio bandwidth enough to cover the GPS L2 band and has nearly omnidirectional radiation with linear polarization at 2.9 GHz frequency.

6.4 Slit, slot and stub embedded circular triband patch antenna

The two previous sections in this chapter described the successful implementation of circularly polarized radiation in the fundamental mode of operation through utilization of slit, slot and stub techniques in the basic circular patch antenna. In the present section all these three methods have been efficiently combined so as to modify the circular patch and obtain triband dual polarized resonances in the UMTS, WiMAX and WLAN bands. The use of the three techniques achieves compactness for the antenna, good impedance matching and a better axial ratio bandwidth.

6.4.1 Antenna evolution and geometry

The geometry of the proposed antenna is shown in Fig.6.28. The steps leading to the final structure are shown in Fig.6.29. The initial basic circular patch is of radius $R=16.5$ mm which has a fundamental frequency of 2.5 GHz designed on an FR4 substrate of $\epsilon_r = 4.4$ and thickness $h= 1.6$ mm. At the centre of the patch, a circular slot of radius r mm is carved resulting in an annular ring shape. This is designated Antenna 1. On the outer circular patch boundary, two pairs of V shaped slits are etched in order to excite two orthogonal near degenerate modes for CP radiation. This forms Antenna 2. In the next step, two pairs of unequal V shaped stubs are added collinearly with the outer V shaped slits which is denoted as Antenna 3. These stubs are crucial to achieve optimum impedance matching. In the final step, the stubs are subjected to a rotation of 45° angle, to make the CP characteristics perfect. This is the proposed slit, slot and stub embedded Antenna 4.

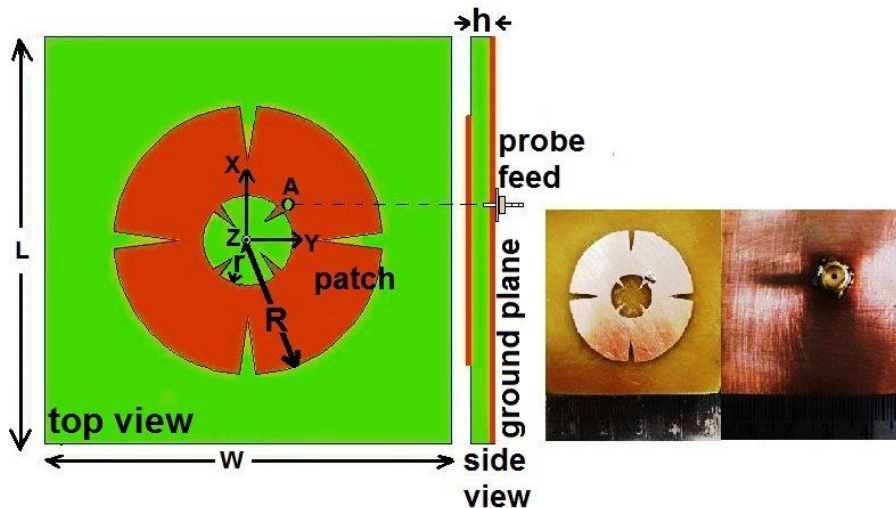


Fig. 6.28. Geometry and photograph of the coaxial probe fed slit, slot and stub embedded circular patch antenna ($L=W=50$, $R=16.5$, $r=5.5$, $w_1=2$, $l_{y1}=8$, $l_{x1}=7$, $w_2=1$, $l_{y2}=3.5$, $l_{x2}=3$ $h=1.6$ (all in mm), $A(5, 5)$, $\epsilon_r=4.4$)

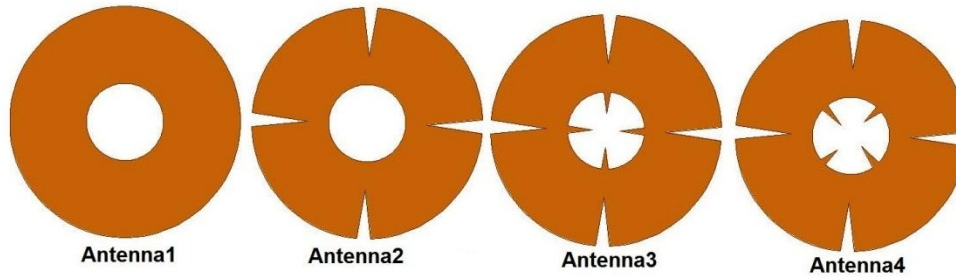


Fig. 6.29. Evolution of the coaxial probe fed slit, slot and stub embedded circular patch antenna

The interesting feature of the geometry is that the inner slot is a scaled down version of the outer patch. The feed is given coaxially along the 45° axis and is located at (5, 5) for best possible matching. The ground plane of size $W \times L \text{ mm}^2$ covers the bottom side of the antenna.

6.4.2 Antenna 1 characteristics

The simulated S11 and axial ratio characteristics of Antenna1 with circular slot of radius $r=5.5\text{mm}$ are shown in Fig.6.30. They are also compared to those of a regular circular patch of radius $R=16.5\text{mm}$ without the central circular slot. Antenna 1 shows triple band resonances at 2.3 GHz, 4 GHz and

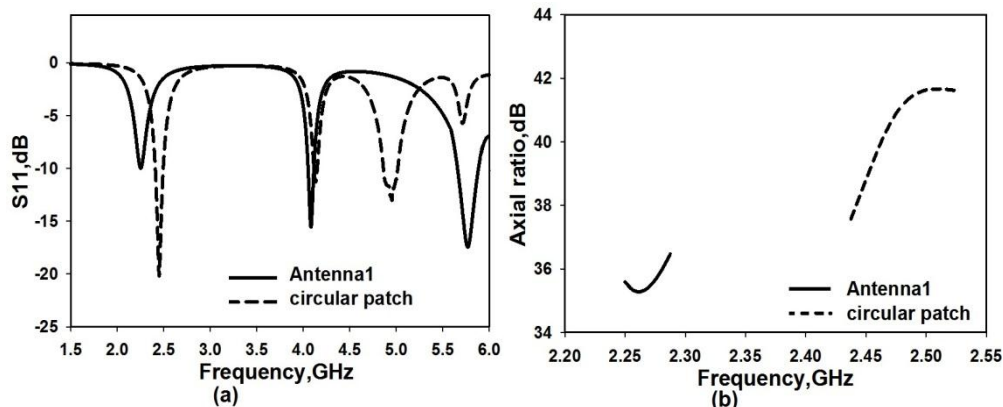


Fig. 6.30. Simulated a) S11 b) axial ratio characteristics of the Antenna1
($L=W=50$, $R=16.5$, $r=5.5$, $h=1.6$ (all in mm), $A(5, 5)$, $\epsilon_r=4.4$)

5.6 GHz respectively. The circular patch has a fundamental resonance frequency of 2.5 GHz which is shifted down to 2.3 GHz with the addition of the slot while becoming poorly matched in impedance. Both the structures do not possess circular polarization as is obvious from Fig.6.29b. The patch area reduces by 11 % while the frequency reduces by 200 MHz in Antenna 1 on comparison with the regular circular patch.

6.4.3 Antenna 2 characteristics

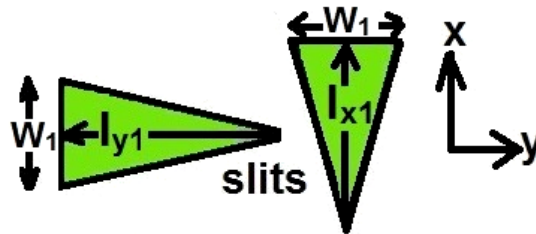


Fig. 6.31. Geometry of the V shaped slits in x and y directions
 (L=W=50, R=16.5, r=5.5, w₁=2, l_{y1}=8, l_{x1}=7, h=1.6 (all in mm),
 A (5, 5), ε_r=4.4)

As the fundamental resonance frequency was found to be poorly matched in Antenna1, an attempt is made to make this resonance properly matched in terms of return loss value while achieving circular polarization.

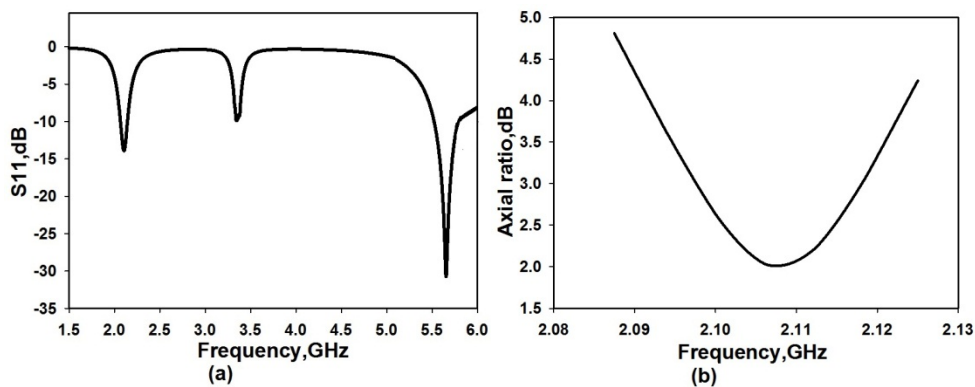


Fig. 6.32. Simulated a) S11 b) axial ratio characteristics of the Antenna2
 (L=W=50, R=16.5, r=5.5, h=1.6 (all in mm), A (5, 5), ε_r=4.4)

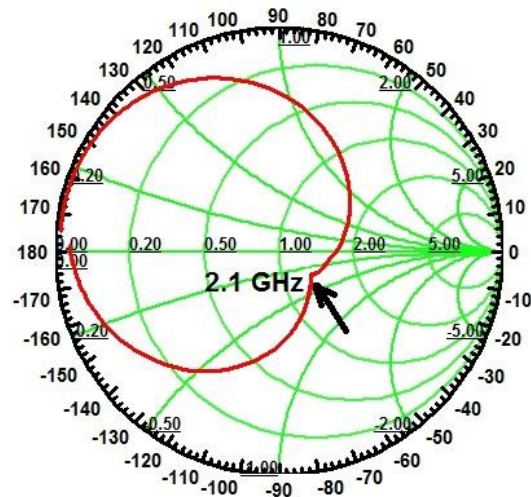


Fig. 6.33. Simulated input impedance plot of the Antenna2
 ($L=W=50$, $R=16.5$, $r=5.5$, $w_1=2$, $l_{y1}=8$, $l_{x1}=7$,
 $h=1.6$ (all in mm), $A(5, 5)$, $\epsilon_r=4.4$)

The orthogonal patch dimensions need to be modified such that they excite two near degenerate modes equal in amplitude and 90° out of phase. Two pairs of V shaped slits are etched on to the outer circumference. Different geometries of the slit were considered and finally the V shape was selected as it could introduce the required asymmetry in x and y directions. The geometry and dimensions of the V shaped slits shown in Fig.6.31 have the lengths l_{y1} and l_{x1} unequal while the widths are equal to w_1 . The reflection coefficient and axial ratio characteristics of the Antenna 2 are shown in Fig.6.32. The three resonances observed in the S11 plot are respectively at 2.1 GHz, 3.5 GHz and 5.6 GHz. The polarization is circular in the first band and linear in the second and third bands. The simulated input impedance plot of Antenna 2 is shown in Fig.6.33 which confirms the occurrence of good CP radiation by the presence of the small kink at 2.1 GHz. The fundamental frequency shifts to 2.1 GHz which is equivalent to 85% reduction from the

frequency of the unmodified circular patch i.e. 2.5 GHz. The second band undergoes a 15% reduction in frequency to 3.5 GHz. The resonance at the third band is less affected by these patch modifications and remain at 5.6 GHz. The resonance at 3.5 GHz is observed to have very poor matching. The next effort is to bring this resonance to have optimum return loss by introducing stubs.

6.4.4 Antenna 3 characteristics

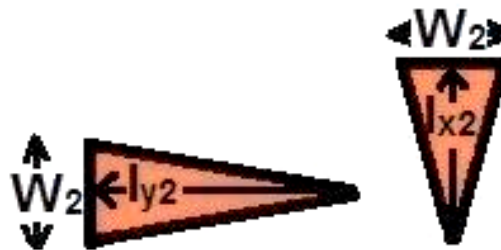


Fig. 6.34. Geometry of the V shaped stubs in x and y directions
 (L=W=50, R=16.5, r=5.5, w₁=2, l_{y1}=8, l_{x1}=7, w₂=1, l_{y2}=3.5, l_{x2}=3, h=1.6 (all in mm), A (5, 5), ε_r=4.4)

Two pairs of unequal length V shaped stubs are added to Antenna 2 geometry to form Antenna3. These stubs are placed such that their axes are collinear with those of the V shaped slits in Antenna 2. The geometry of the stubs are shown in Fig.6.34. The lengths of the stubs l_{y2} and l_{x2} are unequal while the widths are equal to w₂. The resonance at 3.5 GHz is now improved considerably in impedance matching as seen from Fig.6.35a. However, the drawback is that the CP characteristics have slightly deteriorated as can be seen from Fig.6.35b where the axial ratio values are above the 3dB level. The simulated impedance plot of Antenna 3 is also shown in Fig.6.36 where the dip at the centre frequency has become flatter further indicating the deviation from perfect CP radiation.

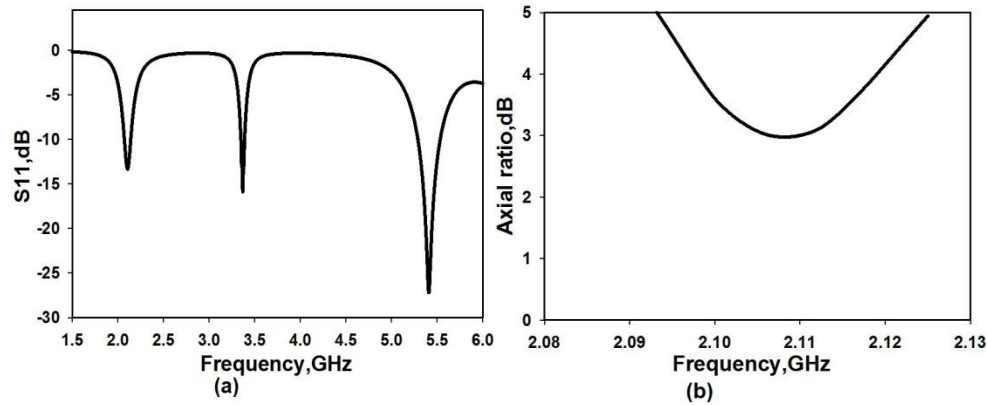


Fig. 6.35. Simulated a) S11 b) axial ratio characteristics of the Antenna3
 ($L=W=50$, $R=16.5$, $r=5.5$, $w_1=2$, $l_{y1}=8$, $l_{x1}=7$, $w_2=1$, $l_{y2}=3.5$, $l_{x2}=3$, $h=1.6$
 (all in mm), $A(5, 5)$, $\epsilon_r=4.4$)

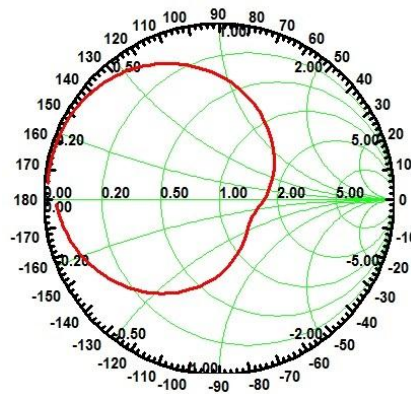


Fig. 6.36. Simulated input impedance plot of the Antenna3
 ($L=W=50$, $R=16.5$, $r=5.5$, $w_1=2$, $l_{y1}=8$, $l_{x1}=7$, $w_2=1$, $l_{y2}=3.5$,
 $l_{x2}=3$, $h=1.6$ (all in mm), $A(5, 5)$, $\epsilon_r=4.4$)

6.4.5 Antenna 4 characteristics

Antenna 4 is the final proposed antenna which results after modifications are applied to make the CP characteristics in the first band and the impedance matching in all the three bands optimum. To achieve this end, the stubs in Antenna 3 are given a 45° rotation in the clockwise direction which forms the slit, slot and stub embedded circular patch antenna. The most

noteworthy point about the antenna is that the inner slot is a downsized version of the outer patch. The S11 and axial ratio characteristics of the Antenna 4 are shown in Fig.6.37.

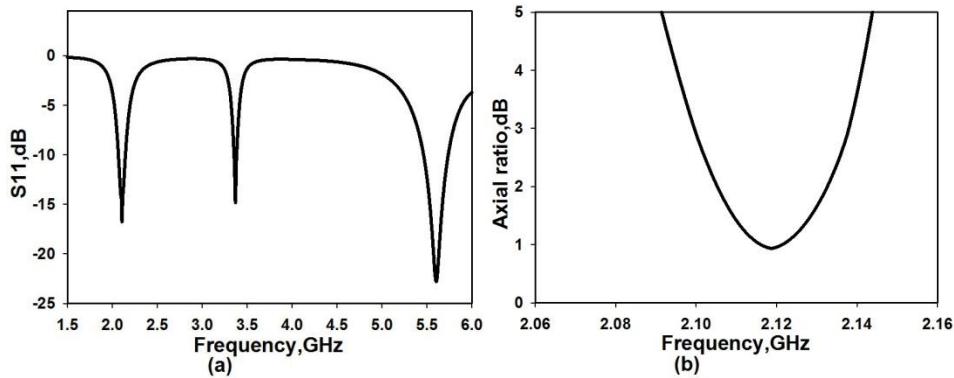


Fig. 6.37. Simulated a) S11 b) axial ratio characteristics of the Antenna4 (L=W=50, R=16.5, r=5.5, w₁=2, l_{y1}=8, l_{x1}=7, w₂=1, l_{y2}=3.5, l_{x2}=3, h=1.6 (all in mm), A (5, 5), ε_r=4.4)

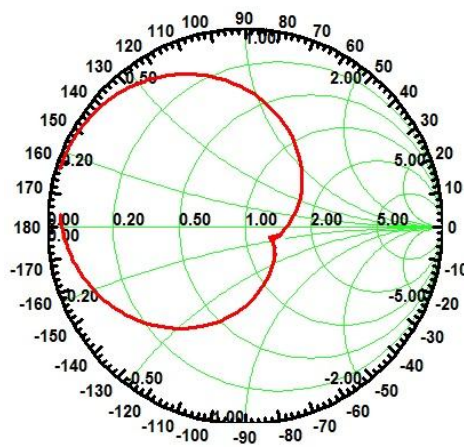


Fig. 6.38. Simulated input impedance plot of the Antenna 4 (L=W=50, R=16.5, r=5.5, w₁=2, l_{y1}=8, l_{x1}=7, w₂=1, l_{y2}=3.5, l_{x2}=3, h=1.6 (all in mm), A (5, 5), ε_r=4.4)

All the three bands now possess good impedance matching below the 10 dB return loss level. Adequate 3 dB ARBW is also obtained within the impedance bandwidth range of Band1. The simulated impedance

characteristics in the smith chart plot in Fig.6.38 exhibit the dip near 2.1 GHz confirming the occurrence of CP radiation.

6.4.6 Simulated current distributions and radiation plots on Antenna4

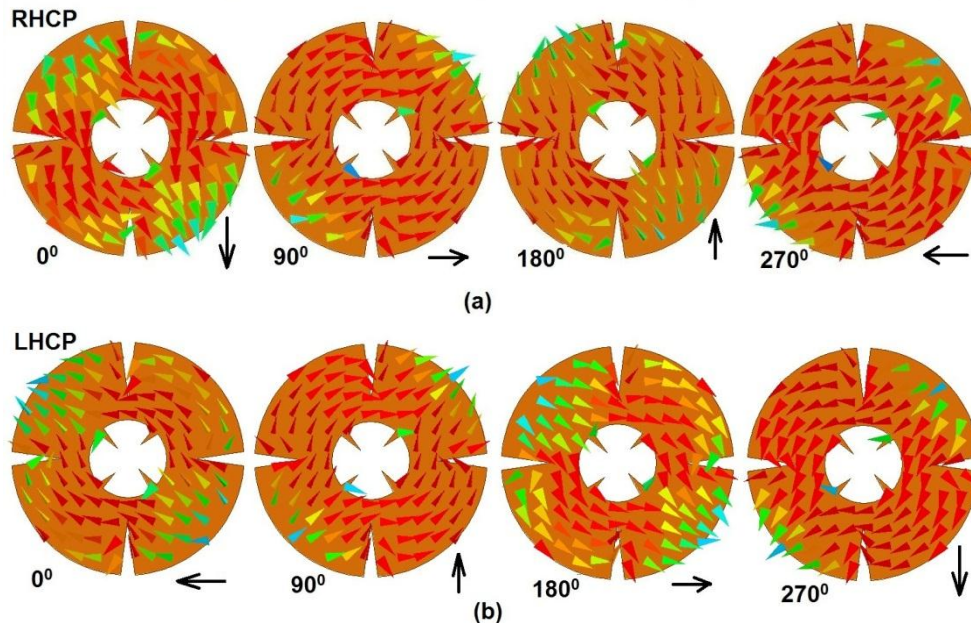


Fig. 6.39. Simulated vector surface current distribution at 2.1 GHz with a) $l_{y1} > l_{x1}$ b) $l_{y1} < l_{x1}$ of the Antenna4 ($L=W=50$, $R=16.5$, $r=5.5$, $w_1=2$, $l_{y1}=8$, $l_{x1}=7$, $w_2=1$, $l_{y2}=3.5$, $l_{x2}=3$, $h=1.6$ (all in mm), $A(5, 5)$, $\epsilon_r=4.4$)

The dimensions of the V shaped slits and stubs determine the sense of polarization in Band 1 as is illustrated in Fig.6.38. The widths of the two pairs of slits are equal to w_1 . The lengths (l_{y1}) of the y directed pair of slits are equal and those of the x directed pair (l_{x1}) are equal, with l_{x1} being less than l_{y1} . Similarly for the stubs, the corresponding lengths l_{y2} are equal and l_{x2} are equal with $l_{x2} < l_{y2}$. The sense of polarization is right handed CP in this case as observed from Fig.6.39a. When the dimensions are changed such that $l_{x1} > l_{y1}$ and $l_{x2} > l_{y2}$, the sense of polarization also reverses i.e., becomes left handed CP as can be seen from Fig.6.39b.

To facilitate a clear understanding of the dimensions which are the chief contributors to the excitation of the three bands, the surface current magnitude is pictorially represented once again in Fig.6.40 at three respective centre frequencies.

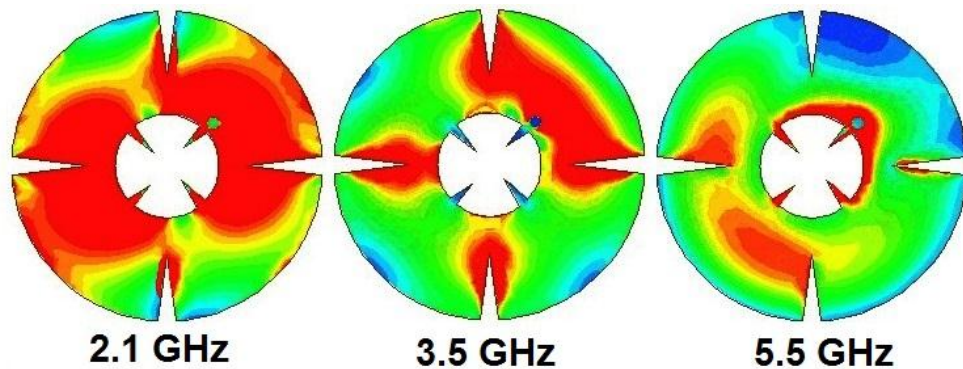


Fig. 6.40. Simulated surface current magnitude at the three bands in the Antenna4 ($L=W=50$, $R=16.5$, $r=5.5$, $w_1=2$, $l_{y1}=8$, $l_{x1}=7$, $w_2=1$, $l_{y2}=3.5$, $l_{x2}=3$, $h=1.6$ (all in mm), $A(5, 5)$, $\epsilon_r=4.4$)

The current distribution at 2.1GHz shows a strong concentration along the edges of the V slits on the outer patch boundary and along the inner slot boundary. Hence this resonance is generated by the combined effect of these two parameters. The resonance at 3.5 GHz is principally due to the V shaped slits alone as seen from the figure. The third resonance at 5.5 GHz is due to the current along the inner slot boundary. The simulated 3D radiation plots at the three centre frequencies are shown in Fig.6.41. It can be seen that the pattern is directional at 2.1 GHz. At 3.5 GHz, the pattern is flower shaped and is bidirectional. The 3D plot at 5.5 GHz appears to be approximately omnidirectional.

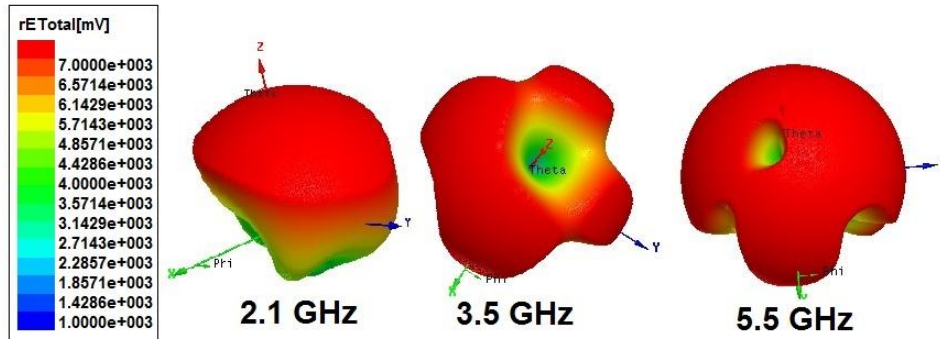


Fig. 6.41. Simulated 3D radiation patterns at the three bands in the Antenna4 ($L=W=50$, $R=16.5$, $r=5.5$, $w_1=2$, $l_{y1}=8$, $l_{x1}=7$, $w_2=1$, $l_{y2}=3.5$, $l_{x2}=3$, $h=1.6$ (all in mm), $A(5, 5)$, $\epsilon_r=4.4$)

6.4.7 Parametric analysis on Antenna 4

A detailed parametric analysis is conducted to examine the effect of the various antenna parameters and feed point location on the performance characteristics. The resonant frequencies are determined by the outer and inner radii of the proposed antenna. The V shaped slits modify the orthogonal dimensions so as to excite near degenerate orthogonal modes of equal amplitudes for CP radiation, while the V shaped stubs produce optimum impedance matching in the three bands. This section describes the effect of these parameters on the reflection and axial ratio characteristics.

6.4.7.1 Effect of inner circular slot radius (r) variation

Keeping the feed point fixed at (5, 5), the radius of the circular slot was varied from 3.5 mm to 6.5 mm. The effect on the S11 and axial ratio characteristics are shown in Fig.6.42. As the slot radius increases, the impedance matching in the first band decreases. The radiation is having linear polarization as seen from Fig.6.42b.

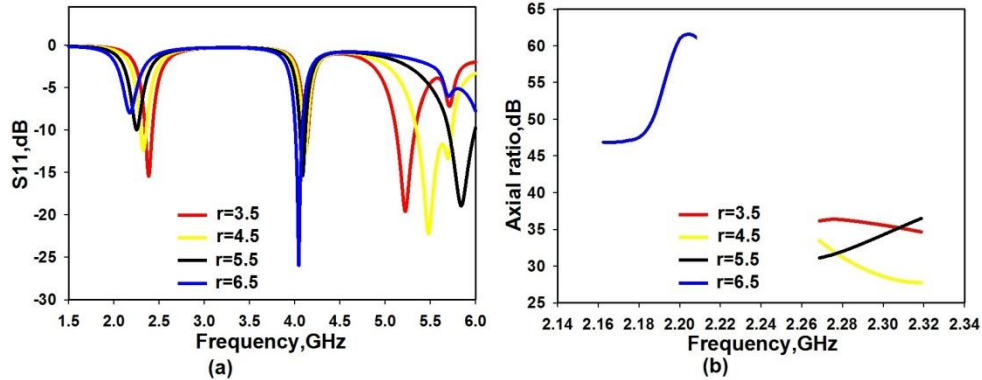


Fig. 6.42. Variation of a) S_{11} and b) Axial ratio with inner slot radius r in the Antenna4 ($L=W=50$, $R=16.5$, $w_1=2$, $l_{y1}=8$, $l_{x1}=7$, $w_2=1$, $l_{y2}=3.5$, $l_{x2}=3$, $h=1.6$ (all in mm), $A(5, 5)$, $\epsilon_r=4.4$)

6.4.7.2 Effect of length of y directed slits l_{y1}

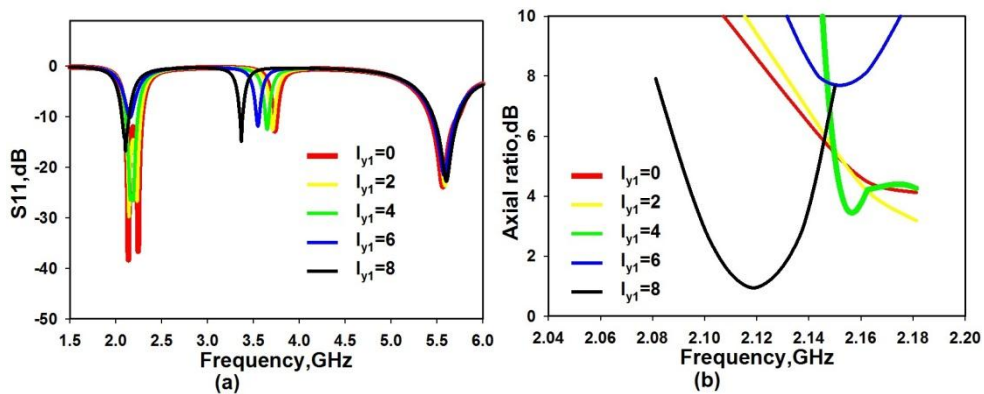


Fig. 6.43. Variation of a) S_{11} and b) Axial ratio with y directed slit length l_{y1} in the Antenna4 ($L=W=50$, $R=16.5$, $r=5.5$, $w_1=2$, $l_{x1}=7$, $w_2=1$, $l_{y2}=3.5$, $l_{x2}=3$, $h=1.6$ (all in mm), $A(5, 5)$, $\epsilon_r=4.4$)

Keeping the feed position same, length and width of x directed slits and width of y directed slits fixed, the length of the y directed slits are varied step by step and the effects on the impedance and CP characteristics are observed. The length of the y directed slits affect the impedance matching of both the first and second bands. The frequency ranges of both bands are

also tuned to the desired bands of UMTS and WiMAX respectively as seen in Fig.6.43a. The axial ratio characteristics are also optimum at the value $l_{y1}=8$ as understood from Fig.6.43b.

6.4.7.3 Effect of length of x directed slits l_{x1}

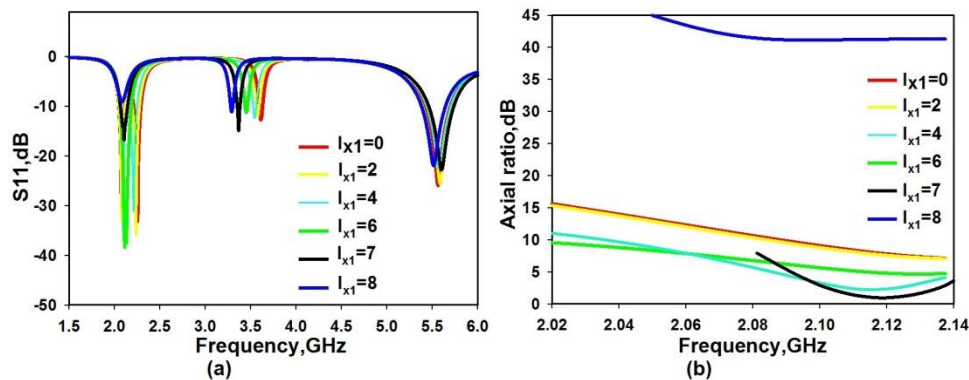


Fig. 6.44. Variation of a) S11 and b) Axial ratio with x directed slit length l_{x1} in the Antenna4 ($L=W=50$, $R=16.5$, $r=5.5$, $w_1=2$, $l_{y1}=8$, $w_2=1$, $l_{y2}=3.5$, $l_{x2}=3$, $h=1.6$ (all in mm), A (5, 5), $\epsilon_r=4.4$)

The length of the x directed slits are varied while keeping l_{y1} and w_1 fixed. At lower values of l_{x1} , the matching in Band 1 becomes better while that at Band 2 becomes poor. Band 2 also experiences a shift to the higher side in frequency. Band 3 is more or less unaffected by l_{x1} . Fig.6.44a shows the variation in S11 with l_{x1} . CP characteristics are poor at values of l_{x1} less than 7mm and beyond 7mm, they are completely degraded as seen from Fig.6.44b. Optimum S11 and axial ratio values are obtained at $l_{x1}=7$ mm.

6.4.7.4 Effect of width of y and x directed slits w_1

The widths w_1 of the x and y directed slits were varied while keeping the lengths fixed at $l_{y1}=8$ and $l_{x1}=7$. When the width is very small at 1mm, the impedance matching at all the three bands are poor as seen from Fig.6.45a. As shown in Fig.6.45b, the CP performance also is deteriorated at

values of w_1 lesser and higher than 2mm. The optimum performance is observed in terms of both S11 and axial ratio values at $w_1=2$ mm.

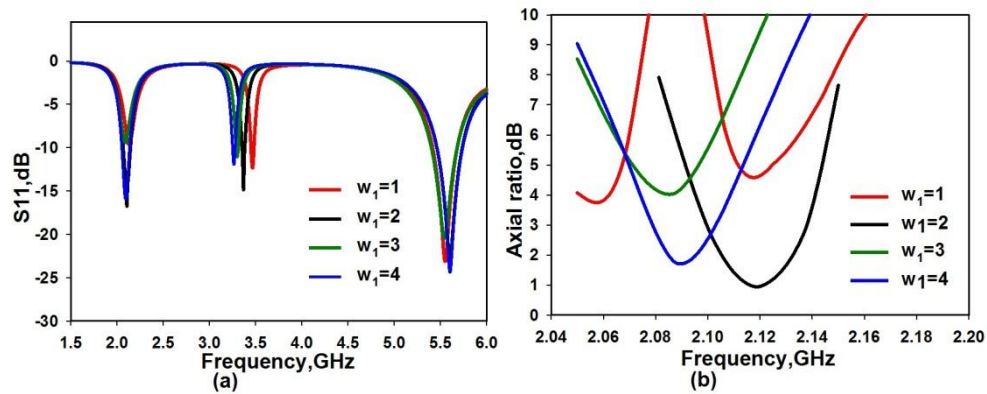


Fig. 6.45. Variation of a) S11 and b) Axial ratio with width w_1 of the x and y directed slits in the Antenna4 ($L=W=50$, $R=16.5$, $r=5.5$, $l_{y1}=8$, $l_{x1}=7$, $w_2=1$, $l_{y2}=3.5$, $l_{x2}=3$, $h=1.6$ (all in mm), $A(5, 5)$, $\epsilon_r=4.4$)

6.4.7.5 Effect of length of y directed stubs l_{y2}

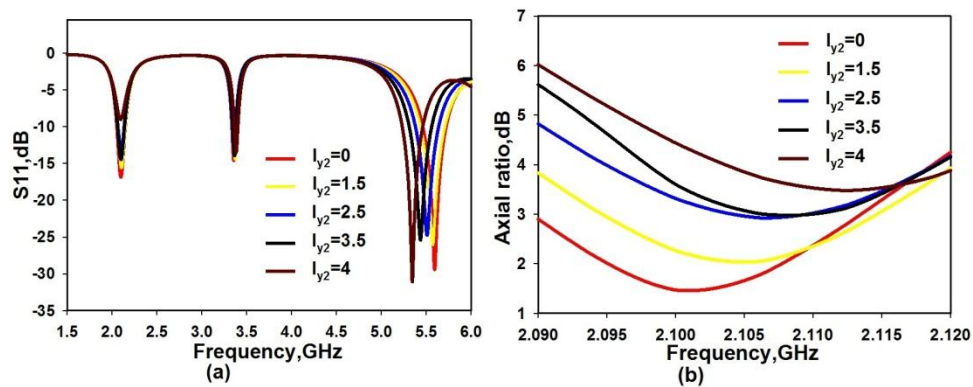


Fig. 6.46. Variation of a) S11 and b) Axial ratio with y directed stub length l_{y2} in the Antenna4 ($L=W=50$, $R=16.5$, $r=5.5$, $l_{y1}=8$, $l_{x1}=7$, $w_1=2$, $w_2=1$, $l_{x2}=3$, $h=1.6$ (all in mm), $A(5, 5)$, $\epsilon_r=4.4$)

The length l_{y2} of the y directed stubs is varied while keeping all other dimensions of the slits, length l_{x2} and width w_2 constant. The most notable effect of the presence of the stubs is on the third band which can be tuned to

the 5.5 GHz band by suitably adjusting the length. The matching at the second band also improves. Although the ARBW is below 3 dB level at $l_{y2}=0$, the matching is poor in the second band and the third band falls beyond the 5.5 GHz range. Hence by considering the best possible impedance matching in all three bands with an acceptable axial ratio level, $l_{y2}=3.5$ mm is selected as the optimum value. The variation in the reflection coefficient and axial ratio with l_{y2} are shown in Fig.6.46.

6.4.7.6 Effect of length of x directed stubs l_{x2}

The manner in which the S11 and the axial ratio characteristics change with the variation in the length of the x directed stubs was observed and is plotted in Fig.6.47a and 6.47b. In the absence of the x directed stubs, the first resonance has very poor matching and CP characteristics. The length l_{x2} is chosen as 3mm at which the matching is good in all the three bands and the axial ratio characteristics are acceptable.

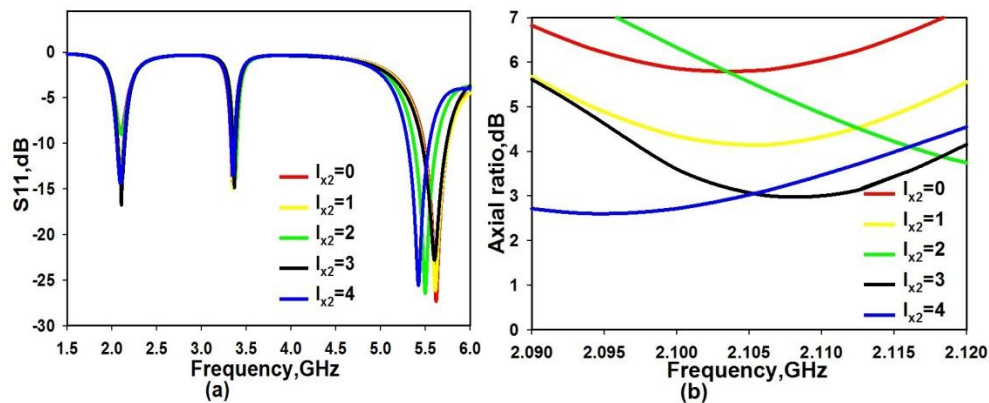


Fig. 6.47. Variation of a) S11 and b) Axial ratio with x directed stub length l_{x2} in the Antenna4 ($L=W=50$, $R=16.5$, $r=5.5$, $l_{y1}=8$, $l_{x1}=7$, $w_1=2$, $w_2=1$, $l_{y2}=3.5$, $h=1.6$ (all in mm), $A(5, 5)$, $\epsilon_r=4.4$)

6.4.7.7 Effect of width of x and y directed stubs w_2

The effect of the change in width of the x and y directed pairs of stubs are shown in Fig.6.48. In the absence of the stubs, the impedance matching becomes poor in Band 1 as seen from Fig.6.48a. The axial ratio also deteriorates as obvious from Fig.6.48b. As the width is increased beyond 1mm, although the matching is not affected, the axial ratio becomes poor. Hence $w_2=1\text{mm}$ is selected as the optimum width of the stubs.

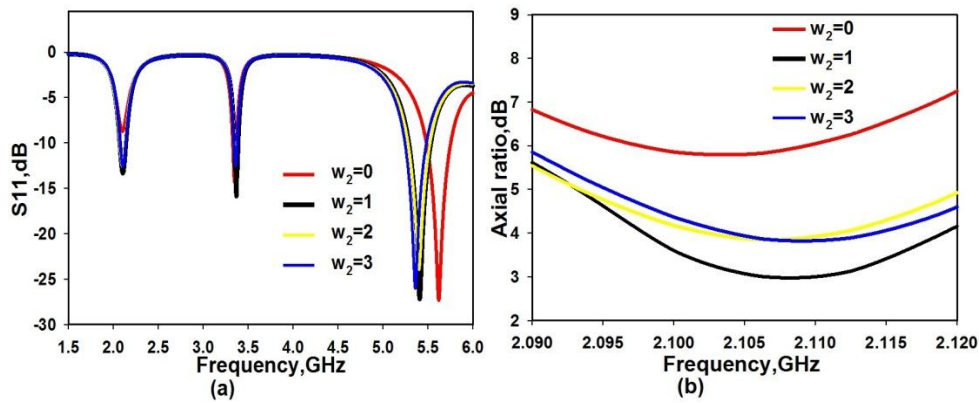


Fig. 6.48. Variation of a) S_{11} and b) Axial ratio with width w_2 of the x and y directed stubs in the Antenna4 ($L=W=50$, $R=16.5$, $r=5.5$, $l_{y1}=8$, $l_{x1}=7$, $w_1=2$, $l_{y2}=3.5$, $l_{x2}=3$, $h=1.6$ (all in mm), $A(5, 5)$, $\epsilon_r=4.4$)

6.4.7.8 Effect of angle of rotation of the inner slot α

Although the stubs improve the matching in all the three bands, the axial ratio was found to be degraded. The inner slot which contains the stubs was rotated through an angle α degrees w.r.t the Y axis to optimize the S_{11} and axial ratio characteristics. Parametric variations of α in the clockwise and counterclockwise directions were performed and the effects were analyzed to finalize the optimum rotation angle. The impedance matching in the three bands in terms of the reflection coefficient are found to improve

with increase in α . The axial ratio characteristics are also found to enhance. Although the CP performance is very good at $\alpha = 90^\circ$, the matching becomes poor at this level. It can also be observed that rotating the stubs also shifts the third resonance band significantly, confirming its dependence on the stub positioning. The value $\alpha = 45^\circ$ in clockwise direction is selected as the optimum value since both the reflection and the axial ratio characteristics yield the best possible results at this point. The effects of rotating the inner slot on the S11 and axial ratio are illustrated in Fig. 6.49A and 6.49B.

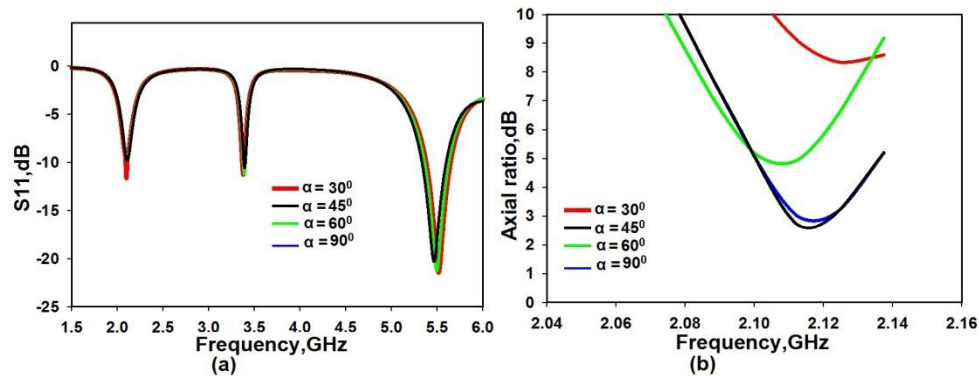


Fig. 6.49A. Effect of rotation of stubs in the anticlockwise direction on the a) S11 and b) Axial ratio of Antenna4 ($L=W=50$, $R=16.5$, $r=5.5$, $l_{y1}=8$, $l_{x1}=7$, $w_1=2$, $l_{y2}=3.5$, $l_{x2}=3$, $w_2=1$, $h=1.6$ (all in mm), A (5, 5), $\epsilon_r=4.4$)

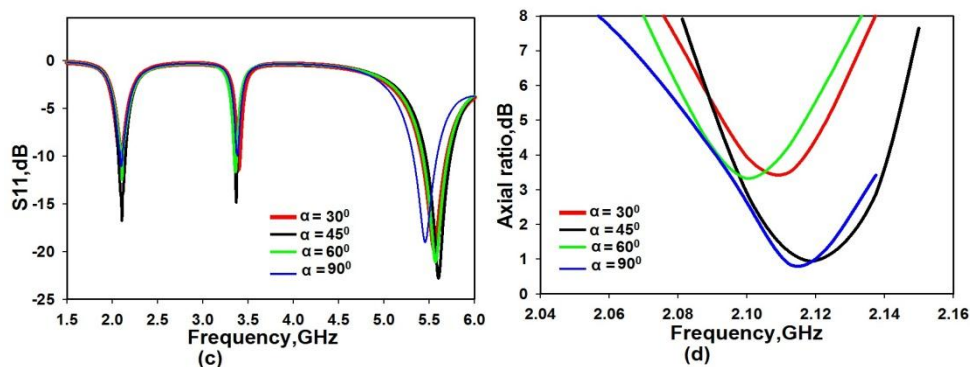


Fig. 6.49B. Effect of rotation of stubs in the clockwise direction on the c) S11 and d) Axial ratio of Antenna4 ($L=W=50$, $R=16.5$, $r=5.5$, $l_{y1}=8$, $l_{x1}=7$, $w_1=2$, $l_{y2}=3.5$, $l_{x2}=3$, $w_2=1$, $h=1.6$ (all in mm), A (5, 5), $\epsilon_r=4.4$)

6.4.8 Design

The simulation and parametric studies described in the earlier sections provide a clear perception about the radiation mechanism of the structure, dimensions which produce the three bands and the effect of the different parameters on the radiation characteristics. Based on these observations, the design equations of the antenna are derived which are the key factors necessary to extend the implementation on different substrates. The design equations are summed up in the following steps.

1. *Circular patch:* The basic circular patch is designed for a fundamental frequency of 2.5 GHz using the design equation from first principles given below [4].

$$f_{mn} = \frac{\chi_{mn} c}{2\pi a \sqrt{\epsilon_r}} \dots\dots\dots (6.1)$$

As TM₁₁ is the fundamental mode, m=n=1 and the Bessel coefficient χ_{mn} for this mode is 1.814. ‘a’ is the radius of the circular patch, λ_g , the guide wavelength is related to the free space wavelength by the relation,

$$\lambda_g = \frac{\lambda_0}{\sqrt{\epsilon_{eff}}} \dots\dots\dots (6.2)$$

Where ϵ_{eff} is the effective dielectric constant of the substrate given by

$$\epsilon_{eff} = \frac{\epsilon_r + 1}{4} \dots\dots\dots (6.3)$$

and is approximately equal to the circumference of the patch $C=2\pi R$ where $R=a$ is the radius of the patch is given by

$$R = \frac{\lambda_g}{2\pi} = 0.16\lambda_g \dots\dots\dots (6.4)$$

To account for the effect of the fringing fields on the edges of the patch the radius is modified with an effective radius a_e given by [4]

$$a_e = a \left\{ 1 + \frac{2h}{\pi a \epsilon_r} \left[\ln \frac{\pi a}{2h} + 1.7726 \right] \right\}^{1/2} \dots\dots\dots (6.5)$$

2. *Circular slot*: The inner circular slot is designed with radius r given by,

$$r = 0.33 * R = 0.053 \lambda_g \dots\dots\dots (6.6)$$

3. *V slits*: The y directed and x directed V shaped slits are designed with lengths l_{y1} and l_{x1} respectively and width w_1 such that

$$\begin{aligned} l_{y1} &= 0.077 * \lambda_g \\ l_{x1} &= 0.067 * \lambda_g \dots\dots\dots (6.7) \\ w_1 &= 0.02 \lambda_g \end{aligned}$$

4. *V stubs*: The dimensions of the y and x directed stubs are expressed in terms of λ_g as

$$\begin{aligned} l_{y2} &= 0.033 * \lambda_g \\ l_{x2} &= 0.028 * \lambda_g \dots\dots\dots (6.8) \\ w_2 &= 0.01 \lambda_g \end{aligned}$$

5. *Feed point*: The 50 ohm matched impedance point is located along the 45° diagonal at A whose coordinates are approximated as

$$x_p = y_p = 0.048 \lambda_g \dots\dots\dots (6.9)$$

with the centre of the patch as the origin.

6.4.9 Validation of the design

The above derived design equations were applied to substrates of different permittivity and the different parameters were computed. The results so obtained along with their calculated resonance frequencies are tabulated in Table 6.2. The dominant mode frequency values f_{11} of the

unmodified circular patch is computed for different substrates and are compared with the corresponding simulation results. They are found to be in good agreement. The centre frequency f_{c1} of Band1 of the slit, slot and stub embedded circular patch antenna is also obtained through simulation by applying the computed parameter values to the circular patch. It is observed that f_{c1} falls within the desired UMTS range for the modified structure in each case. Hence it is verified that the developed design equations hold good for substrates other than FR4 also.

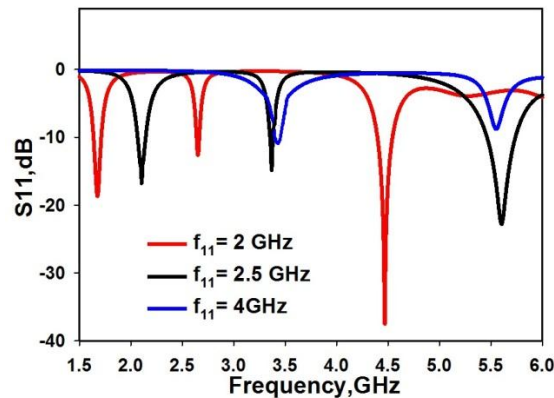


Fig. 6.50. Simulated reflection characteristics of Antenna4 designed for different fundamental frequencies (f_{11})

The design equations were applied to two other fundamental frequencies and were further validated. The reflection coefficients of the Antenna 4 designed for operation in other frequency bands shown in Fig. 6.50 indicate good impedance bandwidth in the respective bands. The frequency of the first resonance band (f_{c1}) shifts to the lower side from the fundamental frequency of design f_{11} . It can be seen from the simulated graph that f_{c1} falls down to around 1.5 GHz and 3.5 GHz respectively for $f_{11}= 2$ GHz and $f_{11}= 4$ GHz. This proves the suitability of the design equations to other frequency bands also.

6.4.10 Experimental Measurements

The antenna prototype was fabricated on an FR4 substrate with thickness $h = 1.6$ mm using the photolithographic process with the optimized dimensions of $L=W=50$, $R=16.5$, $r=5.5$, $l_{y1}=8$, $l_{x1}=7$, $w_1=2$, $l_{y2}=3.5$, $l_{x2}=3$, $w_2=1$. The measured S_{11} is shown compared with the simulated S_{11} in Fig.6.51a. The axial ratio performance was also experimentally obtained and are shown in Fig.6.51b. It is seen that there is good agreement between the measured and simulated values in the two characteristics.

Table 6.2. Validation on different substrates and comparison with simulation

Laminate	ϵ_r	h(mm)	R(mm)	Slits			Stubs			f_{11} (GHz) of unmodified circular patch		f_{c1} (GHz) simulated
				l_{y1}	l_{x1}	w_1	l_{y2}	l_{x2}	w_2	computed	simulated	
FR4	4.4	1.6	16.5	8	7	2	3.5	3	1	2.48	2.5	2.1
Rogers RO4003	3.38	1.57	18.4	8.8	7.7	2.3	3.8	3.2	1.15	2.43	2.475	2.1
Rogers RO3006	6.15	1.25	14.3	6.9	6	1.8	2.9	2.5	0.9	2.4	2.45	1.92
Rogers 6010LM	10.2	0.635	11.4	5.5	4.8	1.4	2.3	2	0.7	2.47	2.41	2.02

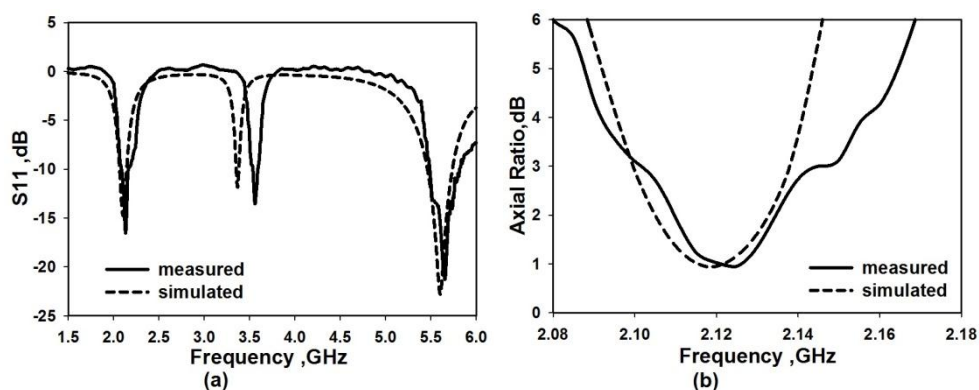


Fig. 6.51. Measured and simulated characteristics of Antenna4 a) S_{11} b) axial ratio ($L=W=50$, $R=16.5$, $r=5.5$, $l_{y1}=8$, $l_{x1}=7$, $w_1=2$, $l_{y2}=3.5$, $l_{x2}=3$, $w_2=1$, $h=1.6$ (all in mm), A (5, 5), $\epsilon_r=4.4$)

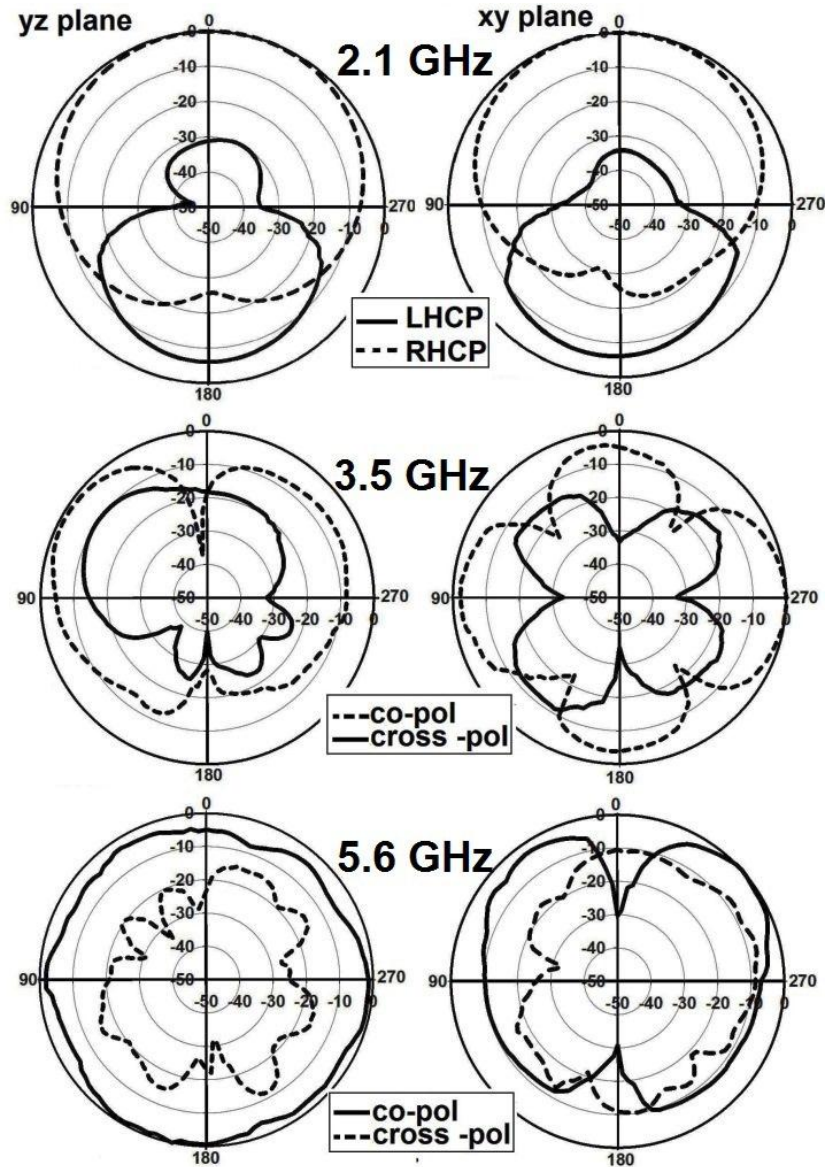


Fig. 6.52. Measured radiation patterns of Antenna4 in the three bands ($L=W=50$, $R=16.5$, $r=5.5$, $l_{y1}=8$, $l_{x1}=7$, $w_1=2$, $l_{y2}=3.5$, $l_{x2}=3$, $w_2=1$, $h=1.6$ (all in mm), $A(5, 5)$, $\epsilon_r=4.4$)

The triple band resonances of the antenna are in the bands UMTS, WiMAX and WLAN respectively. Impedance bandwidths measured are 4.2%, 2% and 6.2% at centre frequencies of 2.1 GHz, 3.5 GHz and 5.5 GHz

respectively. Measured ARBW is 2.3% at centre frequency of 2.12 GHz. The measured radiation patterns in two orthogonal planes at the three bands are depicted in Fig.6.52. At 2.1 GHz, good right hand circularly polarized radiation is observed in both planes of reference. The isolation from the corresponding LHCP is more than 30 dB. The pattern has a figure of eight shape in the y-z plane and flowerlike shape in the x-z plane at the 3.5 GHz centre frequency. More than 20dB isolation is obtained for the cross polarization. The radiation pattern is nearly omnidirectional at 5.5 GHz, with around 20 dB cross polar isolation.

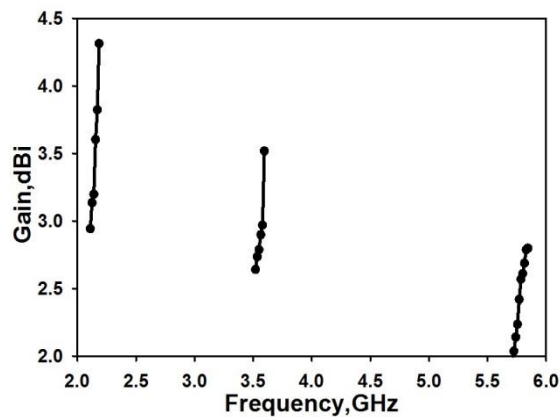


Fig. 6.53. Measured gain plot of Antenna4 in the three bands
 ($L=W=50$, $R=16.5$, $r=5.5$, $l_{y1}=8$, $l_{x1}=7$, $w_1=2$, $l_{y2}=3.5$,
 $l_{x2}=3$, $w_2=1$, $h=1.6$ (all in mm), $A(5, 5)$, $\epsilon_r=4.4$)

Using the gain comparison method, the gain at all three bands was also experimentally measured. From the gain plot shown in Fig.6.53, the peak gains are 4.4dBi, 3.5 dBi and 2.8dBi respectively in the three frequency bands of operation. The radiation efficiencies at the centre frequencies were measured using the Wheeler cap method and were obtained as 69%, 70% and 76% respectively at the three bands.

The proposed Antenna4 can be compared with a standard circular patch [1] designed for the same operating frequency. There is an area reduction of 48% and an improvement of 1.3 % in the ARBW. The frequencies at the fundamental and second resonances have been scaled down respectively by about 400 MHz and 500 MHz. Thus the proposed design achieves compactness. Hence it can be concluded that the antenna is a potential candidate for multi band applications with differing polarizations in the bands.

6.5 Summary of the chapter

Three different versions of the circular patch antenna have been analyzed in this chapter. The key inferences derived from the studies can be summarized below.

The circular patch antenna can be conveniently used to produce dual and triple band responses of different polarizations at the different bands. Three simple methods using slits at the boundary, slot at the centre and stub at appropriate position have been utilized to obtain circular polarization from the basic circular patch antenna. Circularly polarized radiation at the fundamental frequency is produced by the merging of near degenerate TM_{01} and TM_{10} modes. Lower Q factor and consequent higher ARBW than the other two methods is obtained when stub technique is used.

The annular ring patch with embedded slit generates a dual band response with different polarizations in the bands. The slit determines the CP characteristics of the antenna where the TM_{11} mode is split into two near degenerate modes to produce circular polarization in the first band. The

second band is linearly polarized where the higher order TM_{22} mode is excited. The ARBW efficiently covers the GPS L2 band and has omnidirectional pattern at the second resonance frequency. The structure achieves 53% area reduction compared to circular patch designed for the same fundamental frequency.

The three patch modifications of slits, slots and stubs have been efficiently combined to generate triple band response from the circular patch antenna with circular and linear polarizations in the bands. The slits determine the CP characteristics, the slot achieves compactness of the geometry and the stubs influence the impedance matching in the three bands. Area reduction of 48% and 1.3% improvement in the ARBW are obtained. Design equations developed have been validated for different substrates and also for various fundamental frequencies.

References

- [1] Lu, J.H., and Yang, K.P., “A simple design for single-feed circularly-polarized microstrip antennas”, Proc. Natl. Sci. Coun. Rep. China A, 2000, 24, (2), pp. 130–133.
- [2] Bokhari, S.A., Zurcher, J., Mosig, J.R., and Gardiol, F.E., “A small microstrip patch antenna with a convenient tuning option”, IEEE Trans. Antennas Propag., 1996, 44, (11), pp. 1521–1528.
- [3] Wong, K.L., and Lin, Y., “Circularly polarised microstrip antenna with a tuning stub”, Electron. Lett., 1998, 34, (9), pp. 8–9.
- [4] C. A. Balanis, “Antenna Theory: Analysis and Design”, Second Edition, John Wiley & Sons Inc. 1982.
- [5] W. F. Richards, Y. T. Lo, and P. Simon, “Design and theory of circularly polarized microstrip antennas”, IEEE APS Int. Symp. Dig., vol. 17, pp. 117–120, Jun. 1979.

- [6] H. A. Wheeler, Small Antennas, in H. Jasik (ed.), *Antenna Engineering Handbook*, 2nd edn., McGraw-Hill, 1984, chapter 6.
- [7] H. A. Wheeler, The Radian Sphere Around a Small Antenna, *Proceedings of IRE*, vol. 47, August 1959, pp. 1325–1331.

.....✂.....

CONCLUSIONS AND FUTURE PERSPECTIVE

Contents	7.1 <i>Thesis summary</i>
	7.2 <i>Inferences from the investigations on the various antennas described</i>
	7.3 <i>Suggestions for future work</i>

This chapter takes a quick look through the thesis and highlights the achievements of the research work carried out. The conclusions drawn from the numerical, simulated and experimental investigations on the different antennas portrayed are highlighted. Few suggestions relevant for future work are also presented.

7.1 Thesis summary

The aim of the thesis was to design and develop compact multi band antennas with different polarizations for multi frequency applications. Two different patch geometries were elaborated upon: sectoral and circular. The prime objective of the designs was to achieve circular polarization in the fundamental resonance band and linear polarization in the rest. The evolutions of the designed antennas were investigated in detail to have an insight into their multiband behavior.

All the geometrical parameters, upon which the various aspects of design are centered, were first investigated. The reflection, CP and current/field distribution simulation studies on the antenna at different resonances, confirm their dependence on the antenna dimensions. These parameters, which are decisive factors for determining the resonance frequencies, impedance matching and polarization of the antenna, were identified and simple relations were deduced. This enables the antenna designer to design the antenna on any chosen substrate for the desired frequency range of operation. The designs also incorporate technique within the structure to effectively reduce cross polarization.

An overview of the history of microstrip antenna technology with an emphasis to compactness and polarization diversity has been carried out in Chapter 1. A detailed review of the previous works in the concerned field, clearly conveys the relevance of the work and its novelty in chapter 2. Chapter 3 details the methodology adopted for the different stages of the work. Chapter 4 deals with the design and analysis of the dual band characteristics of the sectoral patch antenna. The triband performances of

the dual polarized sectoral patch antenna were investigated in Chapter 5. Chapter 6 extensively describes about combining the three different patch modification techniques and their influence on the tri band performance of the circular patch antenna.

7.2 Inferences from the investigations on the antennas described

The conjectures arrived at after investigating the different antennas are summarized below.

7.2.1 Dual band sectoral patch antenna with corner truncations

- Circularly polarized radiation could be obtained with the circular disc sector patch shape which is a specific fraction of a complete circular disc or a circular disc patch with a specific flare angle.
- The antenna produces dual band response with circular polarization in the first band and linear polarization in the second.
- Corner truncation method is effectively utilized to achieve compactness and improvement of the CP characteristics.
- The validity of the design equations developed are authenticated by actual fabrication at different commercial frequency bands.
- Null current positions occurring at the three corners of the sectoral patch can be utilized to shift the second resonance frequency without affecting the CP performance at the fundamental frequency.
- The technique of etching slits in the patch boundary can be successfully utilized to control the impedance matching and conveniently tune the operating frequency to the desired band.

7.2.2 Triband dual polarized corner truncated sectoral patch antenna

- Triple band operation of the sectoral patch is achieved in this antenna by the excitation of higher order degenerate modes.
- Polarizations in the three bands are different.
- A sectoral notch in the truncated boundary of the patch is utilized to control the frequency ratio tunability of the second and third bands.
- The overlapping of two higher order modes of the patch in Band 3 strengthens the current density in the patch resulting in a higher gain at Band 3.
- A higher value of axial ratio bandwidth has been obtained by the lowering of Q which results from the truncations.
- Optimization of ground plane in the proposed design produces a 64% reduction in the area of the structure.
- The antenna operates in the UMTS, WiMAX, and the ISM5.2 bands suitable for modern wireless communication systems where diverse polarizations are required.
- The simple technique of etching circular slots at precise locations reduces the cross polarization level in the third band by 5 dB. The gain in the third band is also improved by 1.5 dB. Sector shaped slots have also been used for enhancement of isolation.

7.2.3 Triband dual polarized circular patch antenna

- The single feed circular patch antenna can excite circularly polarized radiation without the use of an external polarizer. Moreover it is easier to obtain input matching by adjusting the

feed position. The feed position can be easily adjusted along the 45° axis to obtain optimum impedance matching.

- Circular polarization can be produced by exciting near degenerate modes through the etching of slits at the patch boundary and by slot at the patch centre. Compactness of the antenna is also preserved in these two modifications. The method of etching a rectangular stub or extension at the patch boundary can also produce circular polarization, though the structure has an increase in size. However the circular patch with a stub has better CP bandwidth than the other two. All the three patch modifications produce matched resonances at the fundamental frequency near 2 GHz.
- The coaxial probe fed slit embedded annular ring patch antenna is another geometry which produces dual band resonances at 1.5 GHz and 2.9 GHz with CP radiation characteristics in the first band and linear polarization in the second. The structure achieved an area reduction of 53% compared to the standard circular patch designed for the same fundamental frequency. TM_{11} and TM_{22} are the excited modes in the first and second bands respectively. The slit positioning along the X or Y axis determines the sense of circular polarization. With the patch modifications applied, the frequencies in the two bands reduce by 400 MHz and 200 MHz respectively. Good axial ratio bandwidth sufficient to cover the GPS L2 band is obtained in the first band.
- All three techniques of slit, slot and stub embedding in the patch were efficiently combined so as to modify the circular patch and

obtain triband dual polarized resonances in the UMTS, WiMAX and WLAN bands. The merger of the three techniques achieved antenna compactness, adequate impedance matching and an improved ARBW for the antenna. The structure is simple and could be easily realized. The sense of polarization in the first band is right handed when the length of y directed pair of slit is longer than that of the x directed pair. The sense reverses to LHCP when the x directed pair of slits are longer than the y directed pair. The dimensions which are responsible for the excitation of the three resonances were identified by analyzing the simulated current distributions on the patch.

- The antenna could achieve 48% size reduction and 1.3% improvement in ARBW on comparison with a standard circular patch for the same fixed design frequency.
- Design equations developed for the slit, slot and stub embedded circular patch antenna were proved to be valid for substrates other than FR4 and also for other frequencies of operation.

7.3 Suggestions for future work

Reconfigurable antennas are a class of antennas that have attained wide popularity with the ever increasing demand for multiband antennas. These antennas possess the ability to adapt to new operating scenarios thereby enhancing their performance. Reconfigurability in frequency, polarization and radiation pattern can be incorporated in the proposed structure described in the thesis. Investigations to implement this using varactor and PIN diodes may be carried out in future. RF-MEMS switches

are another option for achieving the switching function. Differential feeding arrangement can provide the tunability over a wide range. Attaining reconfigurability in frequency without affecting the radiation patterns is also a major challenge for the designer. The radiation pattern can be steered away from noise sources whose applications are in phased antenna array scanning. Shorting pins and in line open tuning elements are options to achieve this. Use of electrically tuned or switched parasitic elements makes this reconfigurability in radiation pattern independent of the frequency. The pattern can also be made more directive by the employment of parasitic slot in the ground plane.

The designs of the antennas described have been implemented on FR4 substrate only. Instead of using such lossy substrates, the design can be printed on low temperature co-fired ceramic (LTCC) substrates for enabling them to be directly integrated with monolithic microwave circuits.

Another future prospect is to explore the possibility towards achieving circular polarization in all the three bands. Further miniaturization of the existing structures can also be probed in detail. Time domain analysis of the antennas presented can also be carried out in future.

.....❧.....

**TRIBAND DUAL POLARIZED SECTORAL PATCH
ANTENNA FOR LOW CROSS POLARIZATION**

Contents	<i>A.1 Introduction</i>
	<i>A.2 Antenna design and simulations</i>
	<i>A.3 Parametric study of sectoral slots</i>
	<i>A.4 Experimental results</i>
	<i>A.5 Conclusion</i>

The detailed analysis of the triband performance of the sectoral patch antenna with slotted ground is carried out in this appendix. Sectoral shaped slots have been etched with the objective of attaining reduced cross polarization. Extensive simulation studies and finally experimental validations have been performed.

A.1 Introduction

Different broad banding techniques devised to overcome the prime limitation of narrow bandwidth of the microstrip antenna such as the use of a thick substrate[1], embedded reactive loading of the patch[2] and employing photonic band gap (PBG) structures[3], mentioned earlier in section 5.3 produce reduction in isolation between co-polar and cross polar radiation. Increased cross polarization can also result while achieving compactness through size reduction methods [4]. The method of etching of circular slots in the ground plane has been employed in the triband corner truncated sectoral patch antenna and its effects on the performance are explored in this appendix.

A.2 Antenna design and simulations

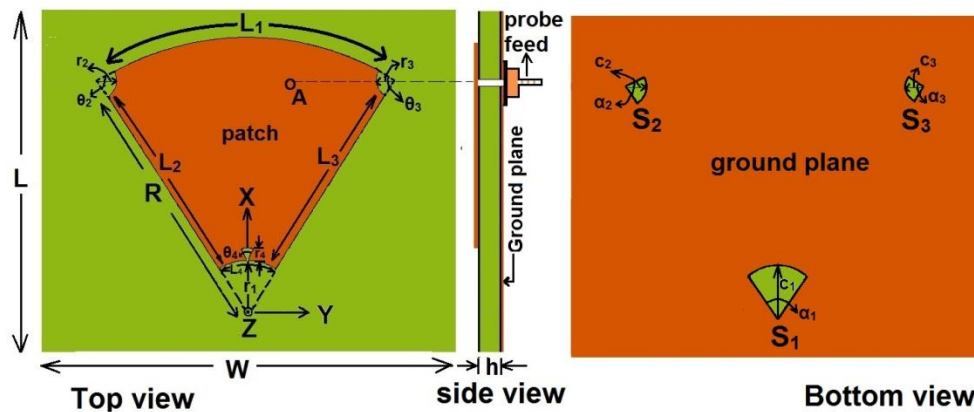


Fig. A.1. Geometry of the triband sectoral patch antenna with sectoral slots in ground plane ($L=45$, $W=52$, $R=45$, $L_1 = 51$, $r_1=9$, $r_2= r_3=3$, $c_1=9$, $c_2= c_3=3$, $h=1.6$ (all in mm) $\theta_1 =65^\circ$, $\theta_2 = \theta_3 = \theta_4=90^\circ$, $\alpha_1 =65^\circ$, $\alpha_2 = \alpha_3 =90^\circ$, $A(37,7)$, $\epsilon_r=4.4$)

Sector shaped slots are etched at most appropriate locations in the ground plane of the triband dual polarized corner truncated sectoral patch

antenna. The cross polarization levels are found to be significantly reduced in the third frequency band as observed from the radiation patterns.

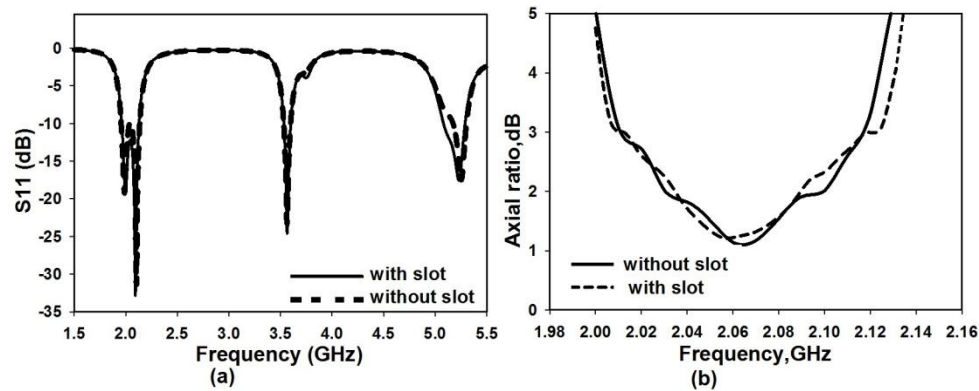


Fig. A.2. a) Reflection coefficient and b) axial ratio characteristics of the triband sectoral patch antenna with & without sectoral slots in ground plane ($L=45$, $W=52$, $R=45$, $L_1 = 51$, $r_1=9$, $r_2= r_3=3$, $c_1=9$, $c_2= c_3=3$, $h=1.6$ (all in mm) $\theta_1 =65^\circ$, $\theta_2 = \theta_3 = \theta_4=90^\circ$, $\alpha_1 =65^\circ$, $\alpha_2 = \alpha_3 =90^\circ$, $A(37,7)$, $\epsilon_r=4.4$)

The antenna geometry is shown in Fig.A.1. The antenna prototype is designed on an FR4 substrate of $\epsilon_r = 4.4$ and thickness $h=1.6$ mm. The dimensions of the sectoral patch on top of the substrate are kept same as those in the triband dual polarized sectoral patch antenna described in the section 5.2. The ground plane on the bottom side is modified by etching three sectoral slots s_1 , s_2 and s_3 precisely below the sectoral corner truncations on the patch on top side. These sectoral slots are identical in shape, indentation radius (c) and indentation angle (α) to the respective sectoral truncations in the patch. The slots are carved such that their circumferences are exactly aligned with the truncated edges above. The antenna shows circularly polarized radiation in the first band and linear polarization in the second and third bands. The reflection characteristics of the antenna in Fig.A.2a with and without the ground slots show that the resonances remain at the same frequency locations.

There is no change in the impedance bandwidth also. The CP characteristics in the first band are preserved. The simulated axial ratio graph also in Fig.A.2b shows a small increase in the 3dB ARBW with the slots applied.

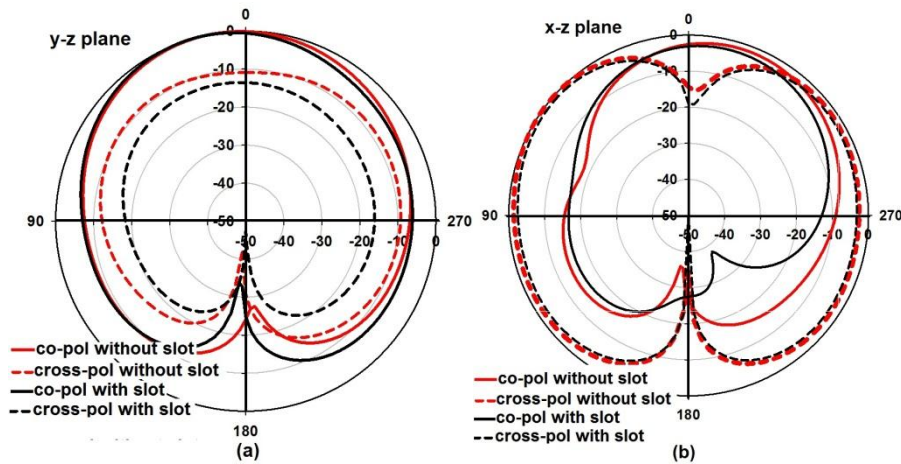


Fig. A.3. Simulated radiation patterns of the triband sectoral patch antenna with & without sectoral slots in ground plane in Band 2 a) yz plane b) xz plane ($L=45, W=52, R=45, L_1 = 51, r_1=9, r_2= r_3=3, c_1=9, c_2= c_3=3, h=1.6$ (all in mm) $\theta_1 =65^\circ, \theta_2 = \theta_3 = \theta_4=90^\circ, \alpha_1 =65^\circ, \alpha_2 = \alpha_3 =90^\circ, A(37,7), \epsilon_r=4.4$)

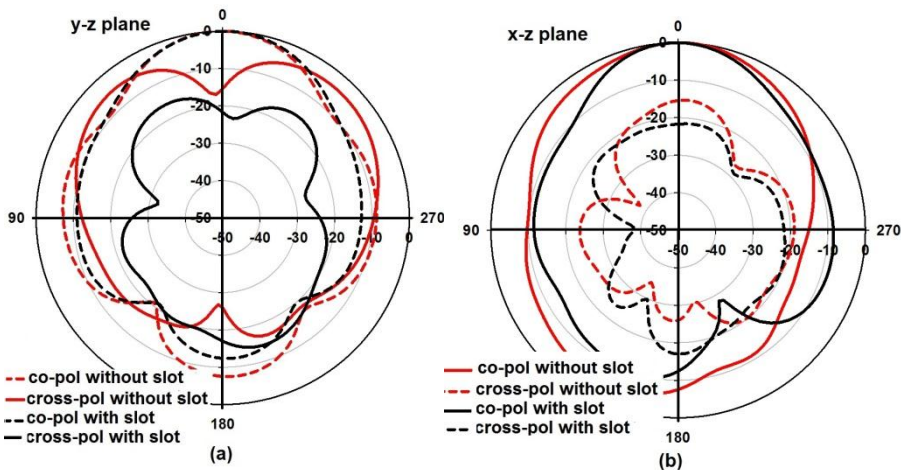


Fig. A.4. Simulated radiation patterns of the triband sectoral patch antenna with & without sectoral slots in ground plane in Band 3 a) yz plane b) xz plane ($L=50, W=40, R=45, L_1 = 51, r_1=9, r_2= r_3=3, c_1=9, c_2= c_3=3, h=1.6$ (all in mm) $\theta_1 =65^\circ, \theta_2 = \theta_3 = \theta_4=90^\circ, \alpha_1 =65^\circ, \alpha_2 = \alpha_3 =90^\circ, A(37,7), \epsilon_r=4.4$)

The simulated radiation patterns in the linearly polarized bands 2 and 3 are analyzed. The radiation patterns in Band 2 and Band 3 are shown respectively in Fig.A.3 and Fig.A.4. In Band 2, the cross polarization in the two orthogonal planes are reduced by only a very little amount and is not much affected by the presence of the sectoral slots in the ground plane. In Band 3, the cross polarization level is found to be lowered by around 5 dB in both planes of simulation.

A.3 Parametric study of sectoral slots

The impact of the sectoral slots in ground on the radiation pattern in Band 3, are studied by parametric variation of indentation radius and flare angle of the slots. The results are analyzed to conclusively select the optimum slot dimensions so as not to alter the CP radiation in the dominant mode. The reflection coefficient and axial ratio characteristics are examined. The cross polarization isolation level at each parametric step is tabulated.

A.3.1 Effect of presence/absence of slots

The three slots are etched in the ground plane in combinations of one, pairs and all three together. The S11 and axial ratio graph are shown in Fig.A.5. The reflection coefficient values are not at all affected by the presence or absence of the slots in the ground. However, the axial ratio graphs show that axial ratio below the 3dB standard level is obtained for more than one case. Hence to choose the structure with the optimum dimensions, the cross polarization isolation in Band 3 was also analyzed through simulation. This is listed in Table A.1. The optimum isolation level in both planes is observed only for the case with all three slots present together. This proves that all the three slots are essential for low cross polarization in Band 3.

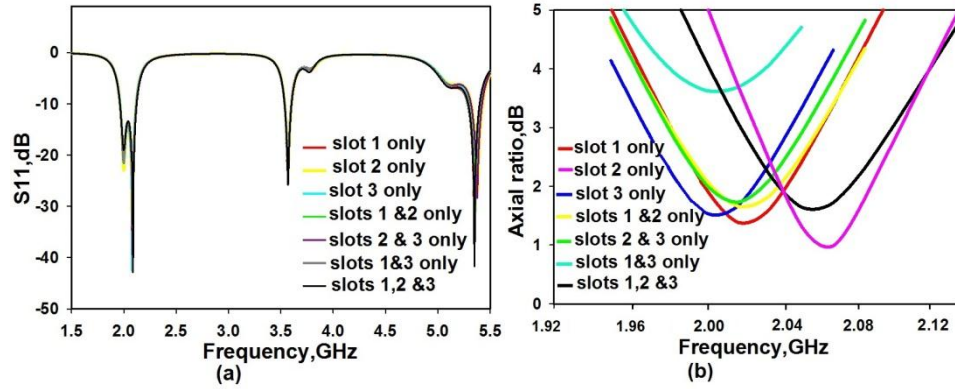


Fig. A.5. Simulated a) S11 b) axial ratio of the triband sectoral patch antenna with combinations of sectoral slots in ground plane ($L=50$, $W=40$, $R=45$, $L_1 = 51$, $r_1=9$, $r_2= r_3=3$, $c_1=9$, $c_2= c_3=3$, $h=1.6$ (all in mm) $\theta_1 =65^\circ$, $\theta_2 = \theta_3 = \theta_4=90^\circ$, $\alpha_1 =65^\circ$, $\alpha_2 = \alpha_3 =90^\circ$, $A(37,7)$, $\epsilon_r=4.4$)

Table A.1. Effect of combination of slots on cross polar level in Band 3

Slot	Slot radius(mm)			Cross polar isolation(dB)	
	c_1	c_2	c_3	YZ plane	XZ plane
1 only	9	0	0	21	21
2 only	0	3	0	2	2
3 only	0	0	3	16	17
1& 2 only	9	3	0	18	19
2 &3 only	0	9	3	21	22
1 & 3 only	9	0	3	18	19
All 1,2 & 3	9	3	3	23	23

A.3.2 Effect of variation of radius c_1 of slot 1

Since the effect of the slot 1 is more pronounced on the cross polar isolation, the radius c_1 of slot 1 is varied with radii c_2 & c_3 and the centre point of the sectoral slot are kept fixed and the impacts on the S11 and axial ratio characteristics are studied as depicted in Fig.A.6.

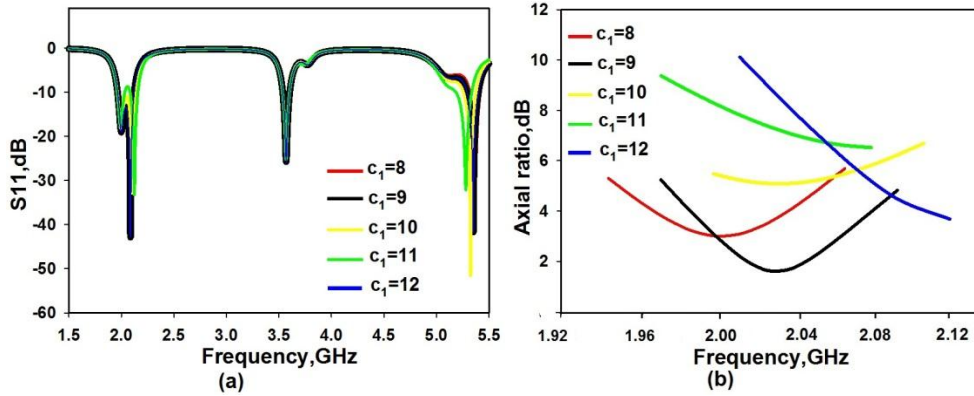


Fig. A.6. Simulated a) S11 b) axial ratio of the triband sectoral patch antenna with radius of slot 1 varied ($L=50$, $W=40$, $R=45$, $L_1 = 51$, $r_1=9$, $r_2= r_3=3$, $c_2= c_3=3$, $h=1.6$ (all in mm), $\theta_1 =65^\circ$, $\theta_2 = \theta_3 = \theta_4=90^\circ$, $\alpha_1 =65^\circ$, $\alpha_2 = \alpha_3 =90^\circ$, $A(37,7)$, $\epsilon_r=4.4$)

Table A.2. Effect of radius c_1 on cross polar level in Band 3

Slot radius(mm)			Cross polar isolation(dB)	
c_1	c_2	c_3	YZ plane	XZ plane
8	3	3	23	24
9	3	0	23	23
10	3	3	21	20
11	3	3	13	13
12	3	3	13	13

The variation in radius c_1 of slot1 has little or no effect on the reflection coefficient as observed from Fig.A.6a while it significantly affects the axial ratio characteristics as seen in Fig.A.6b. Table A.2 shows the cross polar isolation values obtained for each c_1 value. Although good isolation is obtained at $c_1 = 8$, the axial ratio value is above 3 dB which means that CP performance is degraded. Hence the optimum radius is selected as $c_1=9$.

A.3.3 Effect of variation of flare angle α_1 of slot 1

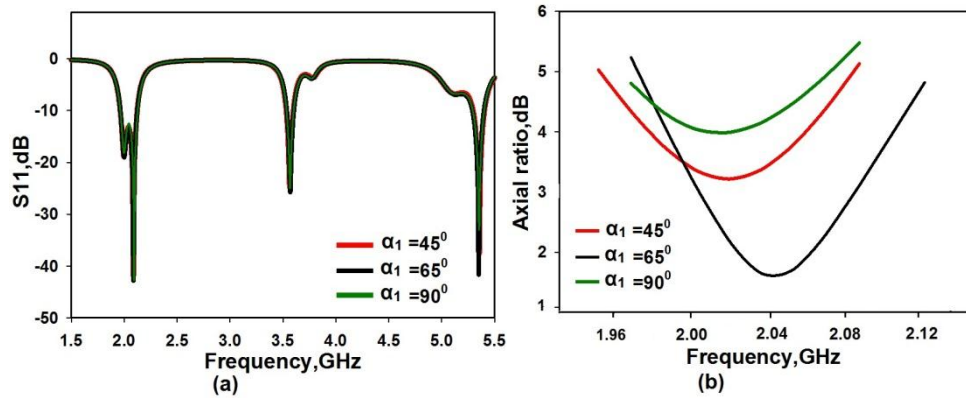


Fig. A.7. Simulated a) S11 b) axial ratio of the triband sectoral patch antenna with flare angle of slot 1 varied ($L=50$, $W=40$, $R=45$, $L_1 = 51$, $r_1=9$, $r_2=r_3=3$, $c_1=9$, $c_2=c_3=3$, $h=1.6$ (all in mm) $\theta_2 = \theta_3 = \theta_4=90^\circ$, $\alpha_2 = \alpha_3 =90^\circ$, $A(37,7)$, $\epsilon_r=4.4$)

Table A.3. Effect of flare angle α_1 on cross polar level in Band 3

Slot radius(mm)			Cross polar isolation(dB)	
α_1	α_2	α_3	YZ plane	XZ plane
45	3	3	23	24
65	3	0	23	23
90	3	3	23	23

The radii c_1 , c_2 and c_3 are kept fixed. Changing the flare angle α_1 does not affect the S11 characteristics whereas it has a major effect on axial ratio characteristics as is obvious from Fig.A.7. The cross polar isolation levels are not much affected by the variation in α_1 as seen from Table A.3.

A.4 Experimental results

The conventional photolithographic process was used to fabricate a prototype of the antenna on an FR4 substrate of $\epsilon_r =4.4$ and thickness

$h=1.6\text{mm}$ with the optimized dimensions of $L=50$, $W=40$, $R=45$, $L_1 = 51$, $r_1=9$, $r_2= r_3=3$, $c_1=9$, $c_2= c_3=3$, $h=1.6$ (all in mm) $\theta_1 =65^\circ$, $\theta_2 = \theta_3 = \theta_4=90^\circ$, $\alpha_1 =65^\circ$, $\alpha_2 = \alpha_3 =90^\circ$. The S_{11} and axial ratio characteristics were measured using the PNA E8362B network analyzer inside the anechoic chamber and are shown compared with the simulated results in Fig.A.8.

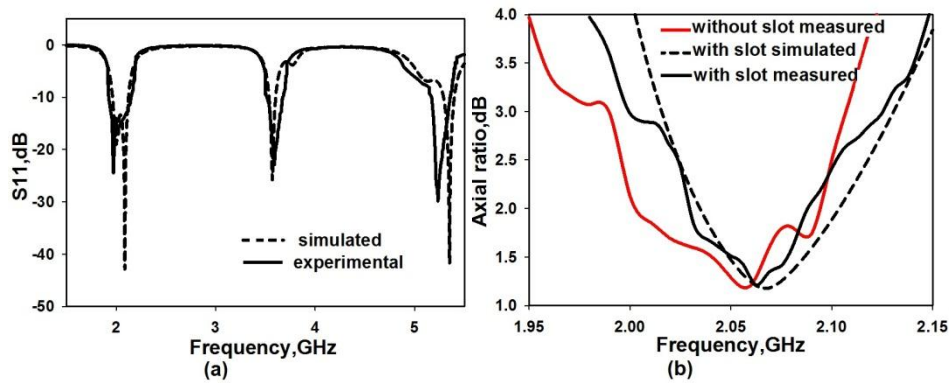


Fig. A.8. Measured and simulated a) S_{11} b) axial ratio of the triband sectoral patch antenna ($L=50$, $W=40$, $R=45$, $L_1 = 51$, $r_1=9$, $r_2= r_3=3$, $c_1=9$, $c_2= c_3=3$, $h=1.6$ (all in mm) $\theta_1=65^\circ$, $\theta_2 = \theta_3 = \theta_4=90^\circ$, $\alpha_2 = \alpha_3 =90^\circ$, $A(37,7)$, $\epsilon_r=4.4$)

From Fig.A.8a it is seen that the antenna covers the UMTS, WiMAX and WLAN 5.2 frequency bands with 9.8 %, 4.5 % and 4 % impedance bandwidths respectively. The measured axial ratio is shown compared with the simulated results and with the measured values without the slots in ground. The ARBW obtained is 6 % at a CP centre frequency of 2.072 GHz.

The measured radiation patterns in two orthogonal planes at the three centre frequencies clearly present the cross polar levels achieved through the etching of the slots. Fig.A.9 show the radiation patterns experimentally observed in Bands 1& 2 and Fig.A.10 illustrate the patterns in Band 3.

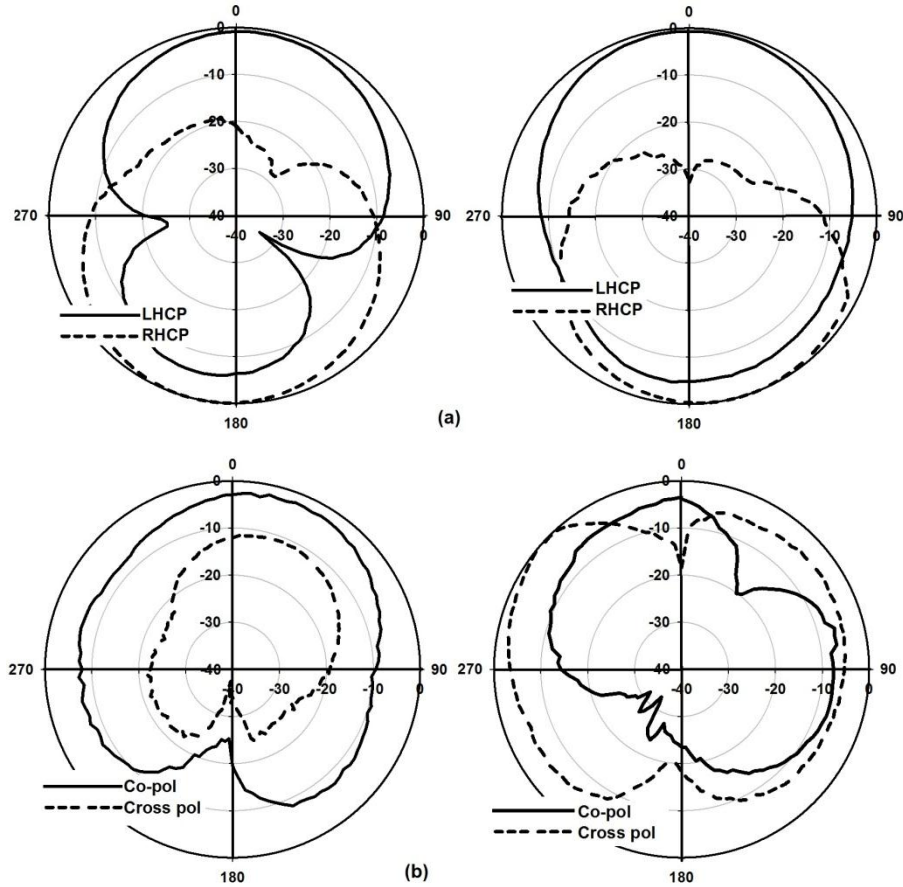


Fig. A.9. Measured radiation patterns of the triband sectoral patch antenna at a) 2.07 GHz b) 3.56 GHz ($L=50$, $W=40$, $R=45$, $L_1 = 51$, $r_1=9$, $r_2= r_3=3$, $c_1=9$, $c_2= c_3=3$, $h=1.6$ (all in mm) $\theta_1=65^\circ$, $\theta_2 = \theta_3 = \theta_4=90^\circ$, $\alpha_2 = \alpha_3 =90^\circ$, $A(37,7)$, $\epsilon_r=4.4$)

In Band 1 good left hand circularly polarized radiation is obtained. There is not much change in the cross polar levels in Band 2. In Band 3, the radiation patterns depicted in Fig.A.10 show a notable decrease in the cross polarization levels in both planes. The cross polar level has been decreased to 23 dB in both planes and are shown compared with those in Band 3 for the sectoral patch antenna without slots.

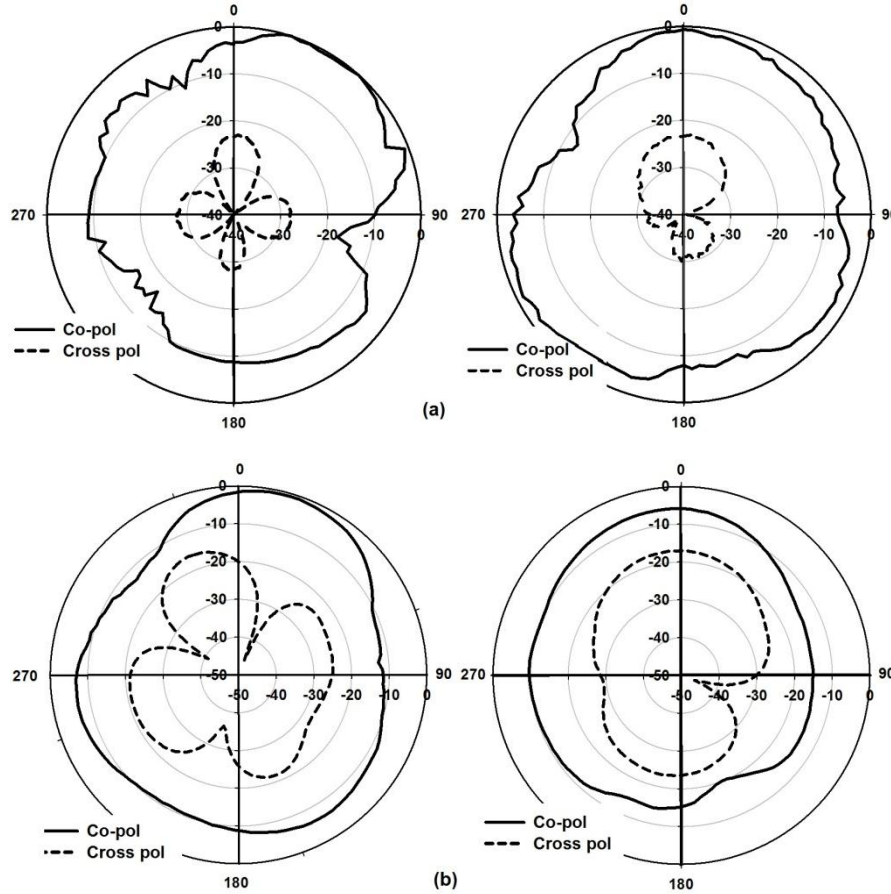


Fig. A.10. Measured radiation patterns of the triband sectoral patch antenna at 5.2 GHz a) with slot b) without slot ($L=50$, $W=40$, $R=45$, $L_1 = 51$, $r_1=9$, $r_2=r_3=3$, $c_1=9$, $c_2=c_3=3$, $h=1.6$ (all in mm) $\theta_1=65^\circ$, $\theta_2 = \theta_3 = \theta_4=90^\circ$, $\alpha_2 = \alpha_3 =90^\circ$, $A(37,7)$, $\epsilon_r=4.4$)

The radiation efficiencies were measured using the Wheeler cap method and were obtained as 62%, 53% and 60% respectively in the three bands. There is not much change in the values in Bands 1 and 2 when compared to the sectoral patch antenna without the ground slots. However the radiation efficiency improves by 20% in the third band. The quality factor is lowered by the addition of the slots in the ground which is the

reason for this increase. The performance characteristics of the sectoral patch antenna with ground slots is shown compared with those of the antenna without slots in Table A.4.

Table A.4. Comparison of Antennas with and without slot

Parameter	With slot			Without slot		
	Band1	Band2	Band3	Band1	Band2	Band3
Bandwidth (%)	9.8	4.5	4	11.2	5.1	3.9
ARBW (%)	6.	---	---	5.8	---	---
ARmin	1.3	---	---	1.2	---	---
Peak gain(dBi)	1.8	1.75	6.4	1.7	1.85	5.38
Rad. efficiency (%)	62	55	60	61	54	40
Cross polar level(dB)	---	12	23	----	10	18

Using the gain comparison method, the gain was measured and the peak gains were found as 1.8 dBi, 1.75 dBi and 6.4 dBi respectively in the three bands. From the simulated current distribution plots on the patch and the ground plane at Band 3 shown in Fig.A.11, the currents are found to be better enhanced by the addition of the slots. This results in the slight improvement in gain in Band 3.

A.5 Conclusion

A triband dual polarized sectoral patch antenna for reduced cross polarization is proposed. The method of embedding slots in the ground plane has been utilized to change the resonant condition in the y direction and thus reduce the level of cross polarization. The parameters on which the antenna performance is dependent upon are extensively studied and experimentally verified. Although the characteristics in Bands 1 & 2 are not affected, the radiation efficiency and gain in the third band has been

improved considerably. The method is found to be better effective than other gain enhancement techniques.

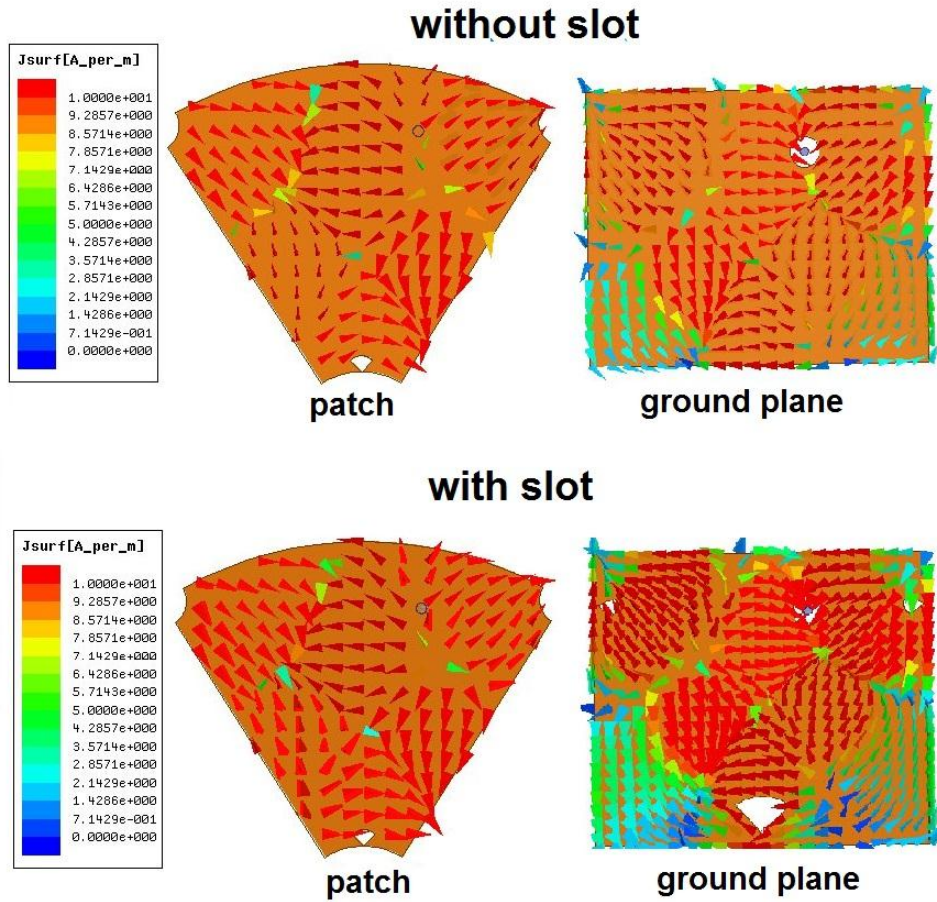


Fig. A.11. Simulated current distributions on the patch and ground planes with and without slot of the triband sectoral patch antenna at 5.2 GHz ($L=50$, $W=40$, $R=45$, $L_1 = 51$, $r_1=9$, $r_2= r_3=3$, $c_1=9$, $c_2= c_3=3$, $h=1.6$ (all in mm) $\theta_1=65^\circ$, $\theta_2 = \theta_3 = \theta_4=90^\circ$, $\alpha_2 = \alpha_3 =90^\circ$, $A(37,7)$, $\epsilon_r=4.4$)

References

- [1] Chang E, Long S.A, Richards W.F, “Investigation of electrically thick rectangular microstrip antennas”. IEEE Trans. Antennas Propag., vol.34, no.6, pp.767-772, 1986.
- [2] Kin-Lu Wong, Jen-Yea Jan, “Broadband circular microstrip antenna with embedded reactive loading”, Electronics Letters, 1998; vol.34, no.19, pp. 1804-1805,1998.
- [3] Coccioli R, Deal W.R, Itoh T, “Radiation characteristics of a patch antenna on a thin PBG substrate”, Proc. IEEE AP-S Int. Symp.; Atlanta, pp.21–26, 1998.
- [4] Wong K, Compact and Broadband Microstrip Antennas, New York, Wiley, 2002.

.....✉.....

**COMPACT GAP LOADED DUAL BAND ANNULAR RING PATCH
ANTENNA FOR WIMAX/WLAN APPLICATIONS**

Contents	B.1 Introduction
	B.2 Antenna geometry and simulations
	B.3 Experimental results
	B.4 Conclusion

The detailed analysis of the dual band performance of the annular ring patch antenna with partial ground is carried out in this chapter. The antenna is loaded with a horizontal gap to obtain maximum impedance matching. The antenna shows resonances in the WLAN band (2.4-2.484 GHz) and WiMAX frequency band (3.3-3.7GHz) with impedance bandwidths of 5.6% and 12 %. The structure radiates an omnidirectional pattern. Relevant simulation studies and experimental verifications have been performed.

B.1 Introduction

WLAN and WiMAX are two well known broadband wireless technologies around today which can deliver broadband access services to the common man in an economical way. WLAN enables portable devices such as laptops, computers, personal digital assistants and mobile phones to have wireless data connectivity for various business and personal applications. WiMAX provides wireless transfer of data from a single node to multi-node links for portable and fully mobile internet connectivity. Antennas which radiate with an omnidirectional pattern are highly desirable in this frequency range as they have the capability to cover a large service area and support a free alignment between the receiving and transmitting antennas. The annular ring patch is a much preferred low profile conformal geometry structure which can provide monopole like pattern for radiation. Studies by Mink[1] has shown that resonant frequency of the lowest order mode in an annular ring patch is much lower than a circular disk of approximately the same size. Also the annular ring has less stored energy and consequently a lower Q-factor which points to a wider bandwidth for the antenna [2]. The dominant mode TM_{11} in the annular ring patch is a poor radiation mode since the fields from the inner and outer edge interfere destructively. The resonant wavelength in the TM_{11} mode is approximately equal to the average circumferential length of the ring [3]. Stubs and notches have been employed to improve the matching at the dominant mode frequency [4-5]. The side effect of these techniques is the generation of new resonances around the dominant mode frequency[6].

In this section, a coaxial probe fed annular ring patch antenna loaded with a horizontal gap is presented. The patch loaded with a horizontal gap

radiates with horizontal polarization. Simulation and experimental results show that the impedance matching is influenced by the ground plane dimensions and the gap.

B.2 Antenna geometry and simulation

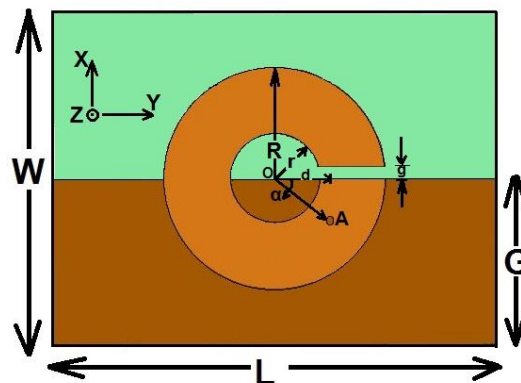


Fig. B.1. Geometry of the gap loaded annular ring patch antenna ($L=40$, $W=30$, $R=10$, $r=5$, $d=5$, $g= 1$, $G=15$, $h=1.6$ (all in mm), $\alpha= 45^\circ$, $\epsilon_r=4.4$)

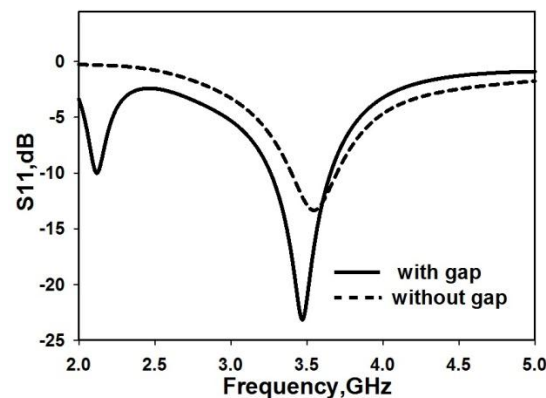


Fig. B.2. Reflection coefficients of the annular ring patch antenna with and without the gap loading and partial ground ($L=40$, $W=30$, $R=10$, $r=5$, $d=5$, $g= 1$, $G=15$, $h=1.6$ (all in mm), $\alpha= 45^\circ$, $\epsilon_r=4.4$)

The geometry of the proposed antenna shown in Fig.B.1 has a compact structure with dimensions $30\text{mm} \times 40\text{mm}$. The antenna is printed

on an FR4 substrate of thickness $h=1.6\text{mm}$ and $\epsilon_r = 4.4$ with the patch on the top which consists of two concentric circles of radii $R= 10\text{mm}$ and $r = 4\text{mm}$ and the partial ground plane of dimensions $15\text{mm} \times 40\text{mm}$ on the bottom side. The coaxial probe feed is located along the $\alpha = 45^\circ$ axis at a distance of $d=5\text{mm}$ from the centre. The gap of width $g=1\text{mm}$ is positioned along the y axis horizontally. The effect of the gap loading is to increase the impedance matching in the fundamental resonance band considerably as seen from Fig.B.2. Without the gap loading, the antenna shows a single resonance at 3.5 GHz frequency range. The gap loading also has the side effect of introducing a new resonance at a lower frequency much below the 3.5 GHz band. However this resonance is found to be poorly matched.

Fig.B.3 shows the reflection characteristics with feed point placed along different angles α . It is found that the desired value of resonance frequency and the best possible impedance matching are obtained when the feed point is located along $\alpha = 45^\circ$.

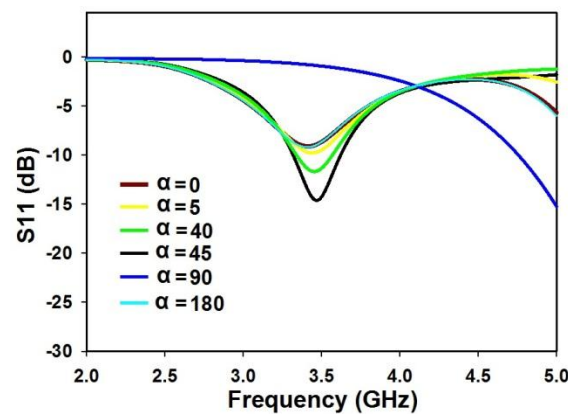


Fig. B.3. Reflection coefficients of the annular ring patch antenna without the horizontal gap loading for different feed positions ($L=40$, $W=30$, $R=10$, $r=5$, $d=5$, $g= 1$, $G=15$, $h=1.6$ (all in mm), $\epsilon_r=4.4$)

The effects of the ground plane width on the resonance, with the gap width fixed at $g=1\text{mm}$, are also studied through simulation and are shown in Fig.B.4a. With a full ground plane at the back side of the structure ($G=30$), the resonance has no matching. As the width G is increased, the matching also increases significantly. With the partial ground plane of width $G=15\text{ mm}$, the resonance is adequately matched in terms of return loss, while the occurrence of a new poorly matched resonance near 2 GHz is observed. Beyond $G=15\text{mm}$, the resonance shifts away from the desired frequency range while the resonance at 2 GHz increases in matching by a large amount.

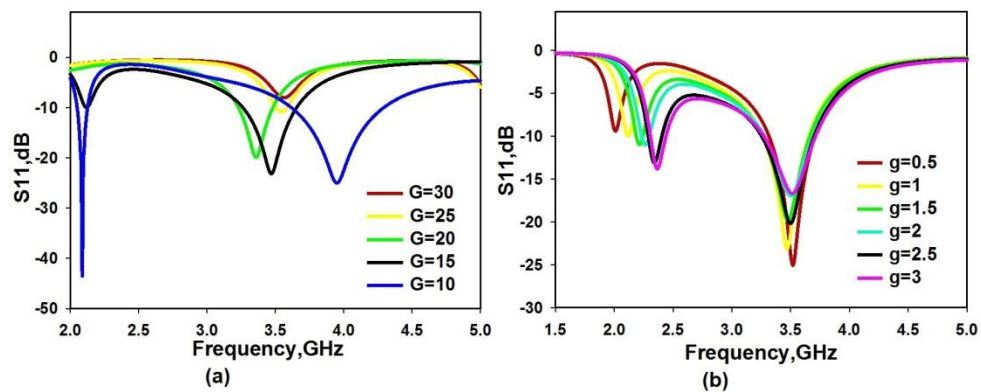


Fig. B.4. Reflection coefficients of the annular ring patch antenna with horizontal gap loading for a) varying ground plane widths b) varying gap widths ($L=40, W=30, R=10, r=5, d=5, h=1.6$ (all in mm), $\alpha= 45^\circ, \epsilon_r=4.4$)

The width of the horizontally loaded gap is varied and its effect on the resonance characteristics is studied next. Fig.B.4b shows the change in the two resonances with variation in g . The lower resonance gets shifted to the higher side in frequency as g is increased. The impedance matching also improves with increase in g . The fundamental resonance at 3.5 GHz is less affected by the gap except for a slight decrease in impedance matching level. At $g=2.5$ the two resonances are found to have adequate and optimum

matching. The lower resonance has the impedance bandwidth range 2.38-2.51 GHz which covers the WLAN 2.4 GHz commercial band. Thus the width of the gap can be varied to control the impedance matching of the new resonance.

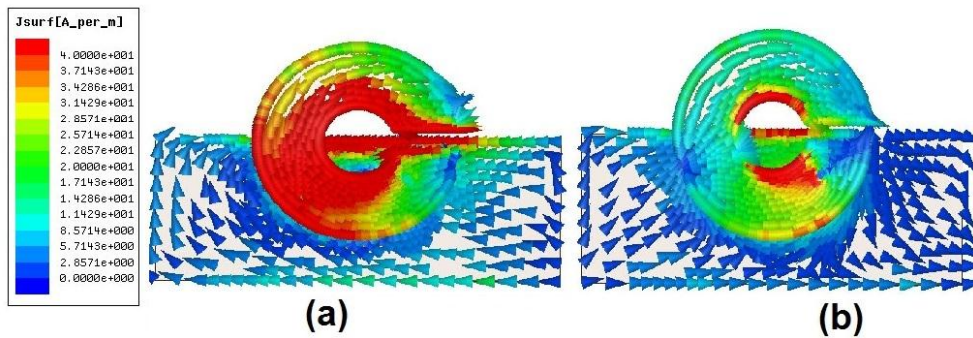


Fig. B.5. Simulated currents on the annular ring patch antenna with horizontal gap loading at a) 2.4GHz b) 3.5 GHz ($L=40$, $W=30$, $R=10$, $r=5$, $d=5$, $g=2.5$, $G=15$, $h=1.6$ (all in mm), $\alpha=45^\circ$, $\epsilon_r=4.4$)

The modes responsible for the excitation of the two resonances are determined by examining the simulated current distributions along the patch and ground plane as shown in Fig.B.5. The annular ring can be likened to a folded dipole which indicates a half wave variation along the circumference at 2.4 GHz frequency as seen in Fig.B.5a. Significant current distribution is observed along the gap and inner ring boundaries. At 3.5 GHz, one half wave variation each is observed along the x and y directions which confirms that the TM_{11} mode is excited at this frequency which is clear from Fig.B.5b.

The polarizations of the antenna at these two frequencies were deduced by plotting the simulated 2D radiation patterns as shown in Fig.B.6. At 2.4 GHz, E_θ is the co-polar component in the $\phi=0^\circ$ plane, indicating that the antenna is polarized in the x direction at this frequency (Fig.B.6a).

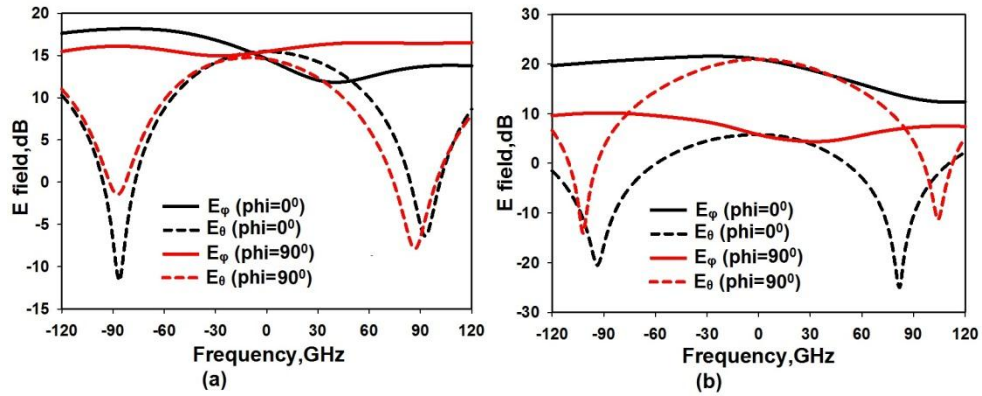


Fig. B.6. Simulated radiation patterns of the annular ring patch antenna with horizontal gap loading at a) 2.4GHz b) 3.5 GHz ($L=40$, $W=30$, $R=10$, $r=5$, $d=5$, $g=2.5$, $G=15$, $h=1.6$ (all in mm), $\alpha=45^\circ$, $\epsilon_r=4.4$)

At 3.5 GHz, in the $\phi=0^\circ$ plane, the co-polar component is E_ϕ which points that the antenna is y polarized at this frequency (Fig.B.6b). Moreover, there is a good margin of isolation between the copolar and cross polar components in the direction of maximum radiation. Thus it can be confirmed that the two bands are orthogonally linearly polarized. This deduction is later verified through actual experimental measurement of transmission coefficient.

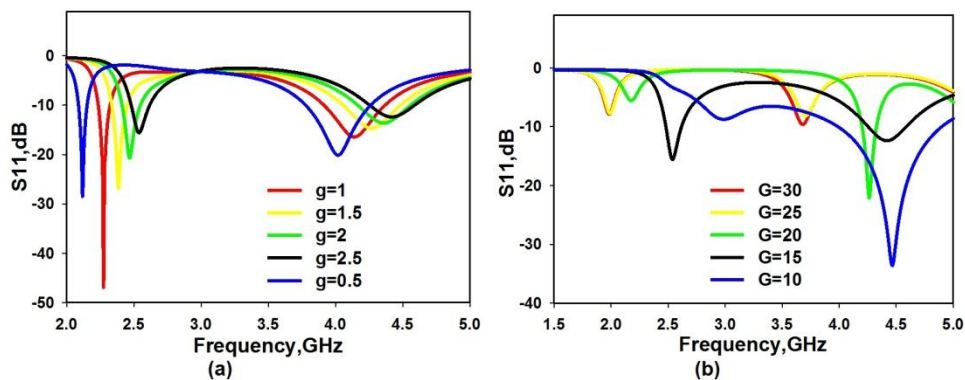


Fig. B.7. S11 characteristics of the annular ring patch antenna with vertical gap loading for a) varying gap widths b) varying ground plane widths ($L=40$, $W=30$, $R=10$, $r=5$, $d=5$, $h=1.6$ (all in mm), $\alpha=45^\circ$, $\epsilon_r=4.4$)

The gap was loaded vertically along the x axis and the reflection characteristics of the antenna were again observed and are shown in Fig.B.7. The gap width was varied to study the effects on the two resonances. It is observed that the unloaded resonance gets shifted to a frequency much beyond the desired WiMAX range, although the lower resonance with loading remains in the vicinity of 2 GHz. With gap width fixed at $g=2.5\text{mm}$, the ground plane width was varied to note the impact on impedance matching in both bands. From Fig.B.7b it is seen that, the ground plane dimension drastically affects the impedance matching in both resonances. A partial ground plane width of $G=15\text{ mm}$ is the case which has the nearest acceptable level of matching w.r.t. the -10dB return loss standard. However, this case of vertical gap was not further studied as the fundamental resonance after loading falls elsewhere from the desired band of $3.3\text{-}3.7\text{ GHz}$.

B.3 Experimental results

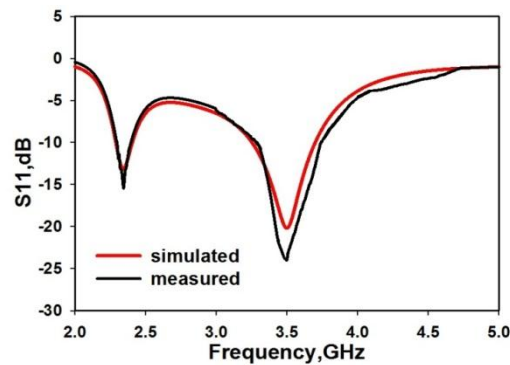


Fig. B.8. Measured and simulated S11 of the annular ring patch antenna with horizontal gap loading ($L=40$, $W=30$, $R=10$, $r=5$, $d=5$, $g=2.5$, $G=15$, $h=1.6$ (all in mm), $\alpha=45^\circ$, $\epsilon_r=4.4$)

The annular ring patch antenna loaded with horizontal gap was fabricated on FR4 substrate of $\epsilon_r = 4.4$ and thickness $h=1.6\text{mm}$. The

experimental reflection coefficients obtained are shown compared with the simulated values in Fig.B.8. A close agreement is noted between the two results. The first band of resonance has centre frequency 2.44 GHz with 5.6 % impedance bandwidth. The second band at 3.55 GHz centre frequency exhibits an impedance bandwidth of 12.3 %.

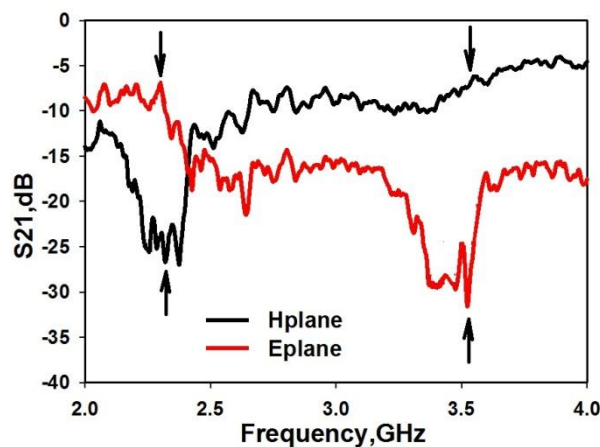


Fig. B.9. Measured S21 coefficient of the annular ring patch antenna with horizontal gap loading in two orthogonal planes. ($L=40$, $W=30$, $R=10$, $r=5$, $d=5$, $g= 2.5$, $G=15$, $h=1.6$ (all in mm), $\alpha= 45^\circ$, $\epsilon_r=4.4$)

The S21 transmission coefficient in two perpendicular planes was measured in order to verify the orthogonal polarization property of the two resonance bands and is depicted in Fig.B.9. The antenna prototype is configured as the receiver at port 1 and standard horn antenna is connected as the transmitter at port 2 of the network analyzer. In the E plane, when the 2.4 GHz band is at a maximum, a dip is correspondingly observed in the 3.5 GHz band. Similarly in the H plane, the first resonance band shows a minimum while Band 3 is at its peak value. Hence it is confirmed that the polarizations of the two bands are in mutually orthogonal planes.

The measured radiation patterns at the two centre frequencies are shown in Fig.B.10 and are found to be omnidirectional with more than 15 dB isolation between the co and cross polarizations. The gains at the two resonance bands were also measured using the gain comparison method and were found to be 2.8 dBi and 3 dBi respectively in the first and second bands.

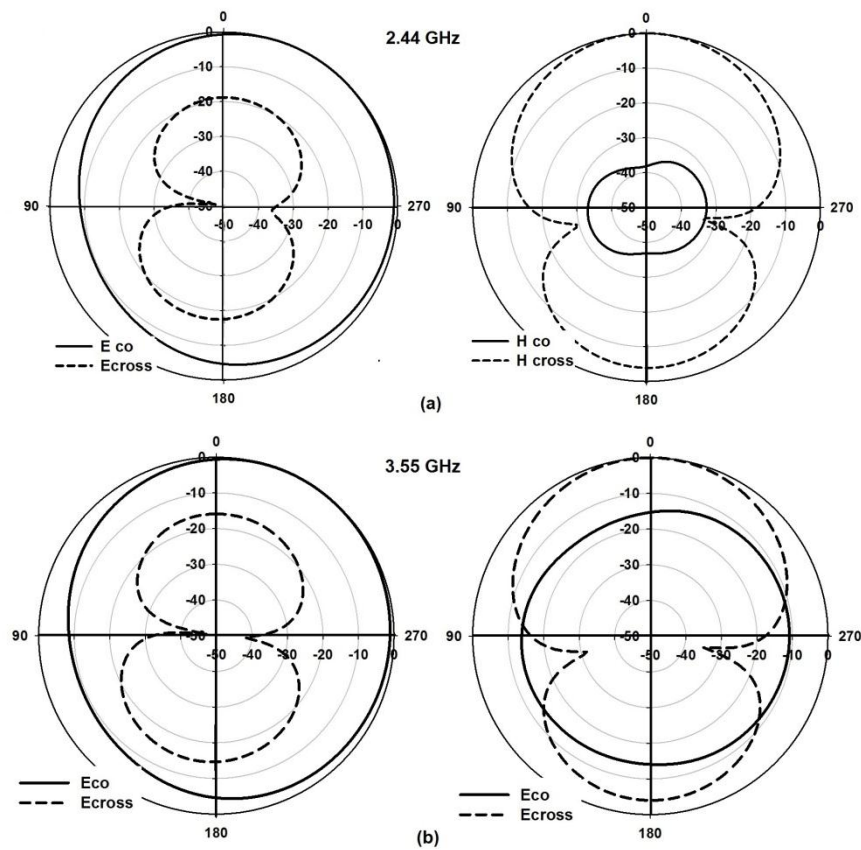


Fig. B.10. Measured radiation patterns of the annular ring patch antenna with horizontal gap loading in two orthogonal planes at a)2.44 GHz b) 3.55 GHz ($L=40$, $W=30$, $R=10$, $r=5$, $d=5$, $g=2.5$, $G=15$, $h=1.6$ (all in mm), $\alpha=45^\circ$, $\epsilon_r=4.4$)

B.4 Conclusion

A gap loaded annular ring patch antenna with partial ground plane exhibits dual resonances at the 2.4 GHz and 3.3 GHz frequency bands respectively with orthogonal linear polarizations and omnidirectional radiation patterns. The partial ground plane and the gap width play a significant role in the impedance matching of the two resonance bands.

References

- [1] J. W. Mink, "Circular ring microstrip antenna elements," IEEE AP-S Int. Symp. Digest, 1980, pp. 605408.
- [2] Weng Cho Chew "A Broad-Band Annular-Ring Microstrip Antenna," IEEE Transactions on Antennas and Propagation, vol. AP-30, no. 5, pp. 918–922, September 1982.
- [3] S. I. Latif and L. Shafai, "Polarization Characteristics of Multiband Loaded Microstrip Annular Ring Antennas," IEEE Transactions on Antennas and Propagation vol. 57, no. 9, pp. 2788–2793, 2009.
- [4] R. Garg and V. S. Reddy, "Edge feeding of microstrip ring antennas," IEEE Trans. Antennas Propag., vol. 51, pp. 1941–1946, 2003.
- [5] A. K. Bhattacharyya and L. Shafai, "A wider band microstrip antenna for circular polarization," IEEE Trans. Antennas Propag., vol. 36, no.2, pp. 157–163, Feb. 1988.
- [6] M. A. Sultan, "The mode features of an ideal-gap open-ring microstrip antenna," IEEE Trans. Antennas Propag., vol. 37, no. 2, pp. 137–142, Feb. 1989.

.....✂.....

||||| **List of Publications** |||||

International Journals

- [1] **Sumitha Mathew**, R. Anitha, T. K. Roshna, C. M. Nijas, C. K. Aanandan, P. Mohanan and K. Vasudevan, “A Fan-shaped circularly polarized patch antenna for UMTS band”, Progress in Electromagnetics Research C, Vol.52, 101-107, 2014.
- [2] **Sumitha Mathew**, R.Anitha, U. Deepak, C.K.Aanandan, P.Mohanan, and K.Vasudevan, “A Compact Tri-Band Dual Polarized Corner Truncated Sectoral Patch Antenna”, IEEE Transactions on Antennas and Propagation, Vol. 63, No. 12, pp.5842 – 5845, 2015.
- [3] **Sumitha Mathew**, M. Ameen, M. P. Jayakrishnan, P.Mohanan and K. Vasudevan , “Compact dual polarized V slit, stub and slot embedded circular patch antenna for UMTS/ WiMAX/ WLAN applications”, Electronics Letters, Vol. 52, No. 17, pp. 1425–1426, 18th August 2016.
- [4] Ramachandran Anitha, Puthiyapurayil V. Vinesh, **Sumitha Mathew**, Pezhohil Mohanan, and Kesavath Vasudevan, “Collocated MIMO Antenna with Reduced Mutual Coupling Using Square Ring DGS”, Progress In Electromagnetics Research C, Vol. 53, 119–125, 2014.
- [5] Anitha R , **Sumitha Mathew**, Vinesh P.V, P. Mohanan, Vasudevan K , “A Diversity Based Four-port MIMO Antenna Loaded with Interdigital Structure for High Isolation”, IET Microwaves, Antennas & Propagation, Vol.10, No.15, pp. 1633-1642, 2016.
- [6] K. C. Prakash, **S. Mathew**, R. Anitha, P. V. Vinesh, M. P. Jayakrishnan, P. Mohanan, and K. Vasudevan, “Circularly polarized dodecagonal patch antenna with polygonal slot for RFID applications”, Progress In Electromagnetics Research C, Vol. 61, pp. 9-15, 2016.
- [7] Anitha Ramachandran, **Sumitha Mathew**, Vivek Rajan and Vasudevan Kesavath, “A Compact Tri-Band Quad Element MIMO Antenna Using SRR Ring for High Isolation”, IEEE Antennas and Wireless Propagation Letters Volume: PP, Issue: 99 ,pp:1-1,2016.

International Conferences

- [8] **Sumitha Mathew**, R.Anitha, A.O.Lindo and K.Vasudevan, “A 2.4/5.1GHz Annular Ring Wideband Patch Antenna using Defected Ground Plane”, Proceedings of International Conference on Information Sciences (ICIS’14), College of Engineering, Cherthala, July 4-5, 2014.
- [9] **Sumitha Mathew**, Anitha Ramachandran, P.V. Vinesh and K. Vasudevan, “Circularly polarised sector- shaped patch antenna for WLAN applications”, Proceedings of the International Conference on Information and Communication Technologies(ICICT 2014), Kochi, December 3-5,2014.
- [10] **Sumitha Mathew**, Anitha Ramachandran, P. V. Vinesh, K. Vasudevan, “Sector-shaped dual-polarized Patch Antenna for UMTS/WiMAX Applications”, Proceedings of the International Microwave & RF Conference (IMaRC 2014), Bangalore ,December 15-17, 2014.
- [11] **Sumitha Mathew**, R. Anitha and K. Vasudevan “Wideband circularly polarized patch antenna for WiMax applications”, Proceedings of the International Symposium on Antennas and Propagation (APSYM 2014), Kochi December 17-19, 2014.
- [12] **Sumitha Mathew**, Prakash K.C., Vivek R Kurup and Vasudevan K, “Reduced crosspolarization using sectoral slots in the ground plane of a sectoral patch antenna”, Proceedings of the International conference on Computing, Communication and Signal Processing (ICCCSP-2016)’ organized by College of Engineering Karunagappally, July 8-9,2016, Kollam.
- [13] **Sumitha Mathew**, K.C.Prakash, Mohammed Ameen and K.Vasudevan “Annular ring patch antenna with omnidirectional radiation pattern for WiMAX applications”, Proceedings of the International Conference on Signal Processing and Advanced Communication (SPAAC 2016) organized by College of Engineering Cherthala, August 10-11, 2016.
- [14] **Sumitha Mathew**, R.Anitha, Vinesh P. V., Mohammed Ameen and K.Vasudevan “Dual Band Corner Truncated Sectoral Patch antenna with dual slits for GPS and WLAN”, Proceedings of the International Symposium on Antennas and Propagation (APSYM 2016), Kochi December 15-17, 2016.

- [15] **Sumitha Mathew**, Prakash K.C., Vinesh P.V., Mohammed Ameen, K.Vasudevan, “Slotted ground sectoral patch antenna with low cross polarization and enhanced gain”, Proceedings of the 12th International conference on Microwaves, Antenna, Propagation and Remote Sensing (ICMARS 2017) Feb 15-17, Jodhpur, India.
- [16] T. K. Roshna, U. Deepak, V. R. Sajitha, **Sumitha Mathew**, and P. Mohanan, “A Reflector Based Compact UWB MIMO Antenna”, Proceedings of the International Symposium on Antennas and Propagation (APSYM 2014), Kochi December 17-19, 2014.
- [17] A. Ramachandran, **S. Mathew**, V. P. Viswanathan, M. Pezholil, V. Kesavath, “Compact 4 Port MIMO Antennas using Polarization and Pattern Diversity”, Proceedings of the IEEE International Wireless and Microwave Technology Conference (WAMICON 2015), April 13-15 2015, Florida.
- [18] K.C Prakash, **Sumitha Mathew**, P.V Vinesh, Mohammad Ameen, K. Vasudevan “Circularly polarized tridecagonal patch antenna for power harvesting applications”, Proceedings of the International conference on Computing, Communication and Signal Processing (ICCCSP-2016) organized by College of Engineering Karunagappally, July 8-9, 2016, Kollam.
- [19] Mohammad Ameen, K.C Prakash, **Sumitha Mathew**, Manoj M. and K. Vasudevan, “A Compact ψ Shaped Microstrip Antenna for WLAN, TD-LTE and WiMAX Applications”, Proceedings of the International conference on Computing, Communication and Signal Processing (ICCCSP-2016) organized by College of Engineering Karunagappally, July 8-9, 2016, Kollam.
- [20] P. V Vinesh, R. Anitha, K. C. Prakash, **S. Mathew**, P. Mohanan, and K. Vasudevan, “A Compact L-slot loaded Planar Inverted F Antenna for GPS and WLAN Applications”, vol. 1, Proceedings of the Applied Electromagnetics Conference, AEMC 2015, pp. 6–7, India.
- [21] K. C. Prakash, V. R. Kurup, P. V Vinesh, M. Ameen, M. P. Jayakrishnan, R. Anitha, **S. Mathew**, and K. Vasudevan, “Dodecagonal Circularly Polarized Patch Antenna for RFID Applications”, Proceedings of the Applied Electromagnetics Conference, AEMC 2015, pp. 5–6, India.

- [22] M. Ameen, K. C. Prakash, **S. Mathew**, P. V Vinesh, R. Anitha, P. Mohanan, and K. Vasudevan, “A Compact S-Shaped 2x1 MIMO Antenna for WLAN / WiMAX Applications”, Proceedings of the Applied Electromagnetics Conference, AEMC 2015, vol. 3, no. c, pp. 5–6, India.
- [23] Vinesh P.V., Prakash K.C, Mohammed Ameen, **Sumitha Mathew**, Anitha R, Vivek R, and K.Vasudevan, “Compact wideband planar inverted F antenna for LTE applications”, Proceedings of the 12th International conference on Microwaves, Antenna, Propagation and Remote Sensing (ICMARS 2017) Feb 15-17, Jodhpur, India.
- [24] Mohammed Ameen, **Sumitha Mathew**, Prakash K.C ,Manoj M, Vinesh P.V. and K.Vasudevan, “Gain enhancement of a compact wideband antenna using hexagonal AMC ground plane”, Proceedings of the 12th International conference on Microwaves, Antenna, Propagation and Remote Sensing (ICMARS 2017) Feb 15-17, Jodhpur, India.

.....✉.....

||| ||| **Resume of Author** ||| |||

SUMITHA MATHEW	
DESIGNATION	Associate Professor (Electronics & Communication Engg.) Govt. College of Engg, Cherthala. sumithamathew@gmail.com, sumithamathew@cectl.ac.in
EDUCATION	
Pursuing Ph.D in the area of Microstrip Antennas	Cochin University of Science and Technology, India
M. Tech –Electronics Specialization-Microwave & Radar Engg.	Cochin University of Science and Technology, India, CGPA 9.24, 2003, I Rank.
B Tech – Electronics & Communication Engineering	NSS College of Engineering, Palakkad, University of Calicut, 76%, 1993
Pre-Degree	M.G. University, Kerala, 89.4%, 1989
SSC	Board of Public examinations, Kerala, 90%, 1987
IT SKILL AND COMPETENCY	
Operating Systems	Linux, Windows
Languages	C
Office Packages	MS Office '97
Software Simulators	MATLAB, HFSS
TEACHING EXPERIENCE	
Since JULY 1995	Worked as Lecturer, Assistant Professor and Associate Professor in various engineering Colleges under the Institute of Human Resources Development (IHRD), Govt. of Kerala.

PROFESSIONAL MEMBERSHIPS / REVIEWERSHIP	
<ul style="list-style-type: none">• Member, IEEE• Life Member, Indian Society of Technical Education (ISTE)• Reviewer, Progress in Electromagnetic Research (PIER) Journals.	
PERSONAL DETAILS	
Age & Date of Birth	45Years, 18 th January 1972 [Female]
Permanent Address	Nanthikattu House, Near St. Antonys Church, Thrikkakara Kerala, India, Pin-682021
Nationality	Indian
AREAS OF INTEREST	
Electromagnetic Field Theory, Microstrip Antennas, Radio Communication	
PUBLICATIONS	
International Journals	7
International Conferences	17
REFERENCES	
Dr. K .Vasudevan	Professor Emeritus, Department of Electronics, CUSAT, Pin -682021 Email: vasudevankdr@gmail.com Phone: +91 9447357328
Dr. P Mohanan	Professor Emeritus, Department of Electronics, CUSAT, 682021. Email: drmohan@cusat.ac.in Phone: +91 9447325765
Dr. P. Sureshkumar	Director, IHRD, Prajoe Towers, Thiruvananthapuram Phone: +91 8547005000 Email: director@ihrd.ac.in

.....✍.....

Index

A

Anechoic chamber 77
Antenna 2, 6,7,8
Aperture coupled 10, 11
Axial ratio 21, 83

B

Broadside 7, 8, 47

C

Cavity model 13, 14
Coaxial probe 10, 74
Circular Polarization 17
Compact 16, 17, 33
Co-polarization 12
Cross polarization 12
Current distribution 92, 122, 210

D

Deschamps 4, 8
Dielectric 8
Dipole 9
Dual band 18

E

Electromagnetic 98
Elliptical 12
Efficiency 82
Excitation 74

F

Finite element method 13, 15
FDTD 13, 16

G

GPS 5, 119

H

Hertz 2
HFSS 70

I

Impedance matching 10

L

Linear Polarization 12
LHCP 46

M

Marconi 2, 3, 24
Maxwell 2, 24
Method of moments 13, 14
Microstrip antenna 6, 8
Microstrip line 11
MMIC 7
Mobile communication 4
Multiport network model 13, 14

N

Numerical techniques 13

O

Orthogonal polarization 17

P

Patch antenna 8, 9
Perturbation 17
Photolithography 71, 72
Polarization 12, 82
Printed 9
Proximity 11

Q

Quality factor 156,157

R

Radar 3
Reflection coefficient 79
RFID 5
RHCP 46

S

Slit loading 21, 176
Slot 9, 19,161
SMA 10
Spectral domain analysis 13, 15
Stacking 19
Stub 182, 202, 207
Substrate 8, 71

T

TM mode 87
Transmission line 13
Transmitter 80
Truncation 21

U

UMTS 5, 18, 19

V

VNA 75
VSWR 79, 80

W

WiMAX 5
WLAN 5

X

XZ plane 106, 107

Y

YZ plane 106, 107
Yagi-Uda 3
Yee 16, 25

.....❧.....